SELECTED
TOPICS
IN

Identification Modelling and Control

Volume 6, 1993

Edited by O.H. Bosgra and P.M.J. Van den Hof

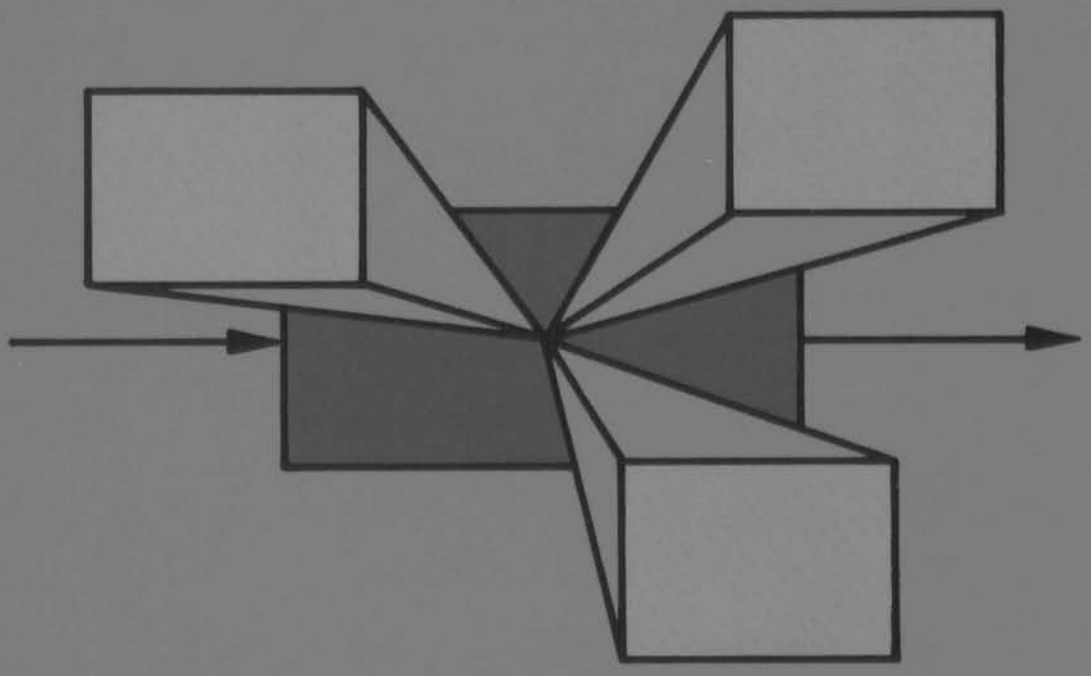

Delft University Press

IDENTIFICATION, MODELLING AND CONTROL

SELECTED TOPICS IN IDENTIFICATION, MODELLING AND CONTROL

Progress Report on Research Activities in the Mechanical Engineering Systems and Control Group

Edited by O.H. Bosgra and P.M.J. Van den Hof

Volume 6, December 1993

Mechanical Engineering Systems and Control Group
Delft University of Technology

Delft University Press/1993

Published and Distributed by

Delft University Press
Stevinweg 1
2628 CN Delft
The Netherlands
Tel.: (0)15 - 783254
Telefax: (0)15 - 781661

By order of

Mechanical Engineering Systems and Control Group
Delft University of Technology
Mekelweg 2, 2628 CD Delft
The Netherlands
Tel.: +31-15-786400; Telefax: +31-15-784717
email: arkesteijn @tudw03.tudelft.nl

CIP-GEGEVENS KONINKLIJKE BIBLIOTHEEK, DEN HAAG

Selected

Selected topics in identification, modelling and control:
progress report on research activities in the mechanical engineering
systems and control group. - Delft:Mechanical Engineering Systems and Control Group,
Delft University of Technology, Vol. 6-ed. by O.H. Bosgra and
P.M.J. Van den Hof.-ill. Met lit.opg.
ISBN 90-6275-930-0
SISO 656 UDC 531.7 + 681.5 NUGI 841

Cover design by Ruud Schrama

Contents

Volume 6, December 1993

Editorial

We are happy to present the sixth volume in our series *Selected Topics in Identification, Modelling and Control*, reporting on ongoing research in our *Mechanical Engineering Systems and Control Group* at Delft University of Technology. The current issue is the most voluminous one until now, containing seventeen papers. Some of them are reprints of papers that have appeared at the 1993 IEEE Conf. Decision and Control in San Antonio, Texas, or at the 2nd European Control Conference in Groningen last summer. Most of the material is only recently developed and is submitted or under review elsewhere.

Besides the people that regularly contribute to this magazine, we would like to mention a couple of newcomers.

First of all we would like to welcome Carsten Scherer who recently has entered the group as a new staff member. Carsten obtained the Ph.D.-degree in 1991 from the University of Würzburg, Germany, with a thesis on Riccati inequalities in $\mathcal{H}_\infty$ and robust control theory. We are happy that we have been able to attract Carsten to come to Delft. With this new staff position we intend to intensify our activities in the area of robust control theory and its applications. Carsten's contribution in the current issue is dealing with multiobjective $\mathcal{H}_2/\mathcal{H}_\infty$ control.

Raymond de Callafon is a Ph.D.-student in a research project that is sponsored by the Dutch Systems and Control Theory Network. His topic is the interplay between system identification and robust control design, employing model representations in terms of (normalized) coprime factorizations. The paper with Paul Van den Hof and Maarten Steinbuch that is incorporated in this issue, is a reflection of his M.Sc.-project that he finished at the end of 1992.

Hans Dötsch is a new Ph.D.-student in a research project that is performed in cooperation with the Philips Research Laboratories in Eindhoven. Hans will be involved in constructing appropriate models of the optical pick-up mechanism in CD-players, taking into account the high performance demands that are made on the control of this system, and the fact that the pieces of equipment are being mass-produced. His contribution in this issue is on a local structural identifiability test, being the result of his M.Sc.-project.

Gert van Schothorst is another new Ph.D.-student, whose participation in this issue reflects his M.Sc.-project, i.e. the modelling and control of an hydraulic rotary vane actuator. We expect to hear more from him in the future about his new project concerning motion control systems, which is performed in cooperation with the Aerospace Engineering Department.

Henk Huisman recently finished his Ph.D.-project with a thesis on design and control of electrical power converters. His present contribution is on control of a series-resonant converter.

There are a couple of former M.Sc.-students that contribute to this volume. Ilya Kraan, Taco Boerstra and Carel Ceton present the results of their projects in papers co-authored by their respective supervisors.

Finally we would like to mention our "external" colleagues and some products of our fruitful cooperation. Samir Bennani and Bob Mulder of the Department of Aerospace Engineering at Delft University; Maarten Steinbuch and Pepijn Wortelboer of the Philips Research Laboratories in Eindhoven; Peter Heuberger of the National Institue of Public Health and Environmental Protection (RIVM), and József Bokor of the Hungarian Academy of Sciences.

If you would like to react to any of the papers in this volume, please do not hesitate to contact us.

Okko Bosgra bosgra@tudw03.tudelft.nl
Paul Van den Hof vdhof@tudw03.tudelft.nl
Editors

Selected Topics in Identification, Modelling and Control
Vol. 6, December 1993

Identification of normalized coprime plant factors for iterative model and controller enhancement[‡]

Paul Van den Hof, Ruud Schrama[§], Okko Bosgra and Raymond de Callafon[♯]

Mechanical Engineering Systems and Control Group
Delft University of Technology, Mekelweg 2, 2628 CD Delft, The Netherlands.

Abstract. Recently introduced methods of iterative identification and control design are directed towards the design of high performing and robust control systems. These methods show the necessity of identifying approximate models from closed loop plant experiments. In this paper a method is proposed to approximately identify normalized coprime plant factors from closed loop data. The fact that *normalized* plant factors are estimated gives specific advantages both from an identification and from a robust control design point of view. It will be shown that the proposed method leads to identified models that are specifically accurate around the bandwidth of the closed loop system. The identification procedure fits very naturally into the iterative identification/control design scheme as presented in Schrama (1992).

1 Introduction

Recently it has been motivated that the problem of designing a high performance control system for a plant with unknown dynamics through separate stages of (approximate) identification and model based control design requires iterative schemes to solve the problem, Lee *et al.* (1992), Schrama (1992a, 1992b), Zang *et al.* (1991). In these iterative schemes each identification is based on new data collected while the plant is controlled by the latest compensator. Each new nominal model is used to design an improved compensator, which replaces the old compensator, in order to improve the performance of the controlled plant.

A few iterative schemes proposed in literature have been based on the prediction error identification method, together with LQG control design, Zang *et al.* (1991), Hakvoort *et al.* (1992). In Schrama (1992a), Schrama and Van den Hof (1992) and Lee *et al.* (1992) iterative schemes have been worked out, employing a Youla parametrization of the plant, and thus dealing with coprime factorizations in both identification and control design stage; as control design methods a robustness optimization procedure of McFarlane and Glover (1988), Bongers and Bosgra (1990) is applied in Schrama (1992), Schrama and Van den Hof (1992), while in Lee *et al.* (1992) the IMC-design method is employed. For a general background and a more extensive overview and comparison of different iterative schemes the reader is referred to Gevers (1993) and Bitmead (1993).

One of the central aspects in almost all iterative schemes is the fact that the identification of a control-relevant plant model has to be performed under closed loop experimental conditions. Standard identification methods have not been able to provide satisfactory models for plants operating in closed loop, except for the case that input/output dynamics and noise characterictics can be modelled exactly.

Recently introduced approaches to the closed loop identification problem, Hansen (1989), Schrama (1991), Lee *et al.* (1992), Schrama (1992a), Van den

[‡]This paper is presented at the 32nd IEEE Conf.Decision and Control, San Antonio, TX, December 15-17, 1993.

[§]Now with the Royal Dutch/Shell Company.

[♯]The work of Raymond de Callafon is sponsored by the Dutch "Systems and Control Theory Network".

Hof and Schrama (1993), show the possibility of also identifying approximate models, where the approximation criterion (if the number of data tends to infinity) becomes explicit, i.e. it becomes independent of the - unknown - noise disturbance on the data. This has opened the possibility to identify approximate models from closed loop data, where the approximation criterion explicitly can be "controlled" by the user, despite a lack of knowledge about the noise characteristics. In the corresponding iterative schemes of identification and control design this approximation criterion then is tuned to generate a control-relevant plant model. The identification methods considered in the iterative procedures presented in Schrama (1992a), Schrama and Van den Hof (1992), Lee *et al.* (1992) employ a plant representation in terms of a coprime factorization $P = ND^{-1}$, while in Schrama (1992) and Schrama and Van den Hof (1992) the two plant factors N, D are separately identified from closed-loop data.

Coprime factor plant descriptions play an important role in control theory. The parametrization of the set of all controllers that stabilize a given plant greatly facilitates the design of controllers, Vidyasagar (1985). The special class of *normalized* coprime factorizations has its applications in design methods (McFarlane and Glover, 1988; Bongers and Bosgra, 1990) and robustness margins (Vidyasagar, 1984; Georgiou and Smith, 1990; Schrama and Bongers, 1991). If we have only plant input-output data at our disposal, then a relevant question becomes how to model the normalized coprime plant factors as good as possible. In this paper we will focus on the problem of identifying normalized coprime plant factors on the basis of closed loop experimental data.

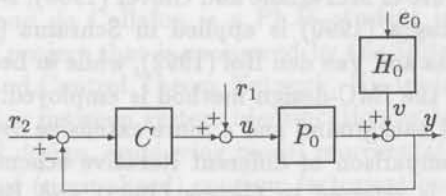

Fig. 1: Feedback configuration

As an experimental situation we will consider the feedback configuration as depicted in Fig. 1, where P_0 is an LTI-(linear time-invariant), possibly unstable plant, H_0 a stable LTI disturbance filter, e_0 a sequence of identically distributed independent random variables and C an LTI-(possibly unstable) controller. The external signals r_1,r_2 can either be considered as external reference (setpoint) signals, or as (unmeasurable) disturbances. In general we will assume to have available only measurements of the input and output signals u and y, and knowledge of the controller C that has been implemented. We will also regularly refer to the artificial signal $r(t) := r_1(t) + Cr_2(t)$.

First we will discuss some preliminaries about normalized coprime factorizations and their relevance in control design. In section 3 a generalized framework is presented for closed loop identification of coprime factorizations. Next we present a multistep algorithm for identification of normalized factors. In section 5 we briefly show the experimental results that were obtained when applying the algorithm to the radial servo-mechanism in a Compact Disc player.

$\mathcal{RH}_\infty$ will denote the set of real rational transfer functions in $\mathcal{H}_\infty$, analytic on and outside the unit circle; $\mathbb{R}[z^{-1}]$ is the ring of (finite degree) polynomials in the indeterminate z^{-1} and q is the forward shift operator: $qu(t) = u(t+1)$.

2 Normalized coprime factorizations

Consider a LTI system P, then P has a *right coprime factorization* (r.c.f.) (N, D) over $\mathcal{RH}_\infty$ if there exist $U, V, N, D \in \mathcal{RH}_\infty$ such that

$$P(z) = N(z)D^{-1}(z); \quad UN + VD = I. \quad (1)$$

In addition a right coprime factorization (N_n, D_n) of P is called *normalized* if it satisfies

$$N_n^T(z^{-1})N_n(z) + D_n^T(z^{-1})D_n(z) = I. \quad (2)$$

Dual definitions exist for left coprime factorizations (l.c.f.).

One of the properties of normalized coprime factors is that they form a decomposition of the system P in minimal order (stable) factors. In other words, if the plant has McMillan degree n_p, then normalized coprime factors of P will also have McMillan degree n_p[1]. Additionally there will always exist polynomials $a, b, f \in \mathbb{R}[z^{-1}]$ of degree n_p such that $N_n = f(z^{-1})^{-1}b(z^{-1})$ and $D_n = f(z^{-1})^{-1}a(z^{-1})$.

In robust stability analysis normalized coprime factors play an important role, reflected in the following robustness result (McFarlane and Glover, 1988; Bongers and Bosgra 1990).

Let $\hat{P}$ be a plant model that is stabilized by the controller C. Moreover let (N_n, D_n) be a normalized r.f.c. of $\hat{P}$, and let the real plant P_0 be such

[1] In the exceptional case that P contains all-pass factors, (one of) the normalized coprime factors will have McMillan degree $< n_p$, see Tsai *et al.* (1992).

that there exist stable perturbations Δ_N, Δ_D such that $P_0 = (N_n + \Delta_N)(D_n + \Delta_D)^{-1}$.
Then C stabilizes the plant P_0 for all Δ_N, $\Delta_D \in \mathcal{RH}_\infty$ satisfying $\left\| \begin{matrix} \Delta_N \\ \Delta_D \end{matrix} \right\|_\infty < \gamma$ if and only if $\gamma \leq \|T(\hat{P}, C_{\hat{P}})\|_\infty^{-1}$, with

$$T(\hat{P}, C) := \begin{bmatrix} \hat{P} \\ I \end{bmatrix} [I + C\hat{P}]^{-1} \begin{bmatrix} C & I \end{bmatrix}.$$

This result shows that when we would have access to the normalized coprime factors of the plant, together with an error bound on these (estimated) factors (in the form of error bounds on the mismatches Δ_N and Δ_D), then immediate results follow for the robust stability of the plant.
This result may not seem to be too striking, since a similar situation can be reached by any hard-bounded uncertainty on the system's transfer function, and application of the small gain theorem. However uncertainty decriptions in normalized coprime factor form have been shown to have some specific advantages, as the ability to deal with unstable plants and their close connection with uncertainty descriptions in the gap-metric, Georgiou and Smith (1990).
The control design method of Bongers and Bosgra (1990), McFarlane and Glover (1988) is directed towards optimizing this same robustness margin as discussed above. This control design method is employed in the iterative identification/control design scheme of Schrama (1992a), Schrama and Van den Hof (1992).

3 Closed loop identification of coprime factorizations

3.1 Closed loop identification

The closed loop identification problem is not straighforwardly solvable in the case that one is not sure that exact models of the plant and its disturbances can be obtained in the form of a consistent estimate of P_0 and H_0. What we would like to find - based on signal measurements - is a model $\hat{P}$ of the plant P_0 such that there exists an explicit approximation criterion $J(P_0, \hat{P})$ indicating the way in which P_0 has been approximated (at least asymptotically in the number of data), while $J(P_0, \hat{P})$ is independent of the unknown noise disturbance on the data.
Additionally one would like to be able to tune this approximation criterion to get an approximation of P_0 that is desirable in view of the control design to be performed. This explicit tuning of the approximation criterion is possible within the classical framework only when open-loop experiments can be performed.
Let's consider a few alternatives to deal with this closed-loop approximate identification problem, assuming the signal r is available from measurements[2]:

- If we know the controller C, we could do the following:
  Consider a parametrized model $P(\theta)$, $\theta \in \Theta$, and identify θ through:

  $$y(t) = \frac{P(\theta)}{1 + P(\theta)C} r(t) + \varepsilon(t) \qquad (3)$$

  by least squares minimization of the prediction error $\varepsilon(t)$.

  This first alternative leads to a complicatedly parametrized model set, and as a result it is not attractive, although it provides us with a consistent estimate of P irrespective of the noise modelling, and with an explicit approximation criterion.

- Identify transfer functions

  $$H_{yr} = \frac{P}{1 + PC} \quad \text{and} \quad H_{ur} = \frac{1}{1 + PC}$$

  as black box transfer functions $\hat{H}_{yr}, \hat{H}_{ur}$, then an estimate of P can be obtained as $\hat{P} = \hat{H}_{yr}\hat{H}_{ur}^{-1}$.

  This method shows a decomposition of the problem in two parts, actually decomposing the system into two separate (high) order factors, sensitivity function and plant-times-sensitivity function. In this setting it will be hard to "control" the order of the model to be identified, as the quotient of the two estimated transfer functions $\hat{H}_{yr}$, $\hat{H}_{ur}$ will generally not cancel the common dynamics that are present in both functions. As a result the model order will become unnecessarily high.

- As a third alternative we can first identify H_{ur} as a black box transfer function $\hat{H}_{ur}$, and consecutively identify P from:

  $$y(t) = P(\theta)\hat{u}_r(t) + \varepsilon(t) \quad \text{with } \hat{u}_r(t) := \hat{H}_{ur} r(t).$$

  This method is presented in Van den Hof and Schrama (1993). It also uses a decomposition

[2] Similar results follow if either r_1 or r_2 are available from measurements.

of the plant P in two factors as in the previous method, now requiring a very accurate estimate of H_{ur} in the first step. An explicit approximation criterion can be formulated.

If, as in the last two methods, the plant is represented as a quotient of two factors of which estimates can be obtained from data, it is advantageous to let these factors have the minimal order, thus avoiding the problem that the resulting plant model has an excessive order, caused by non-cancelling terms.

3.2 A generalized framework

We will now present a generalized framework for identification of coprime plant factors from closed loop data. It will be shown to have close connections to the Youla-parametrization, as employed in the identification schemes as proposed in Hansen (1989), Schrama (1991, 1992a), Lee *et al.* (1992).
Let us consider the notation[3]

$$S_0(z) = (I + C(z)P_0(z))^{-1} \quad \text{and} \tag{4}$$
$$W_0(z) = (I + P_0(z)C(z))^{-1}. \tag{5}$$

Then we can write the system's equations as[4]

$$y(t) = P_0(q)S_0(q)r(t) + W_0(q)H_0(q)e_0(t) \tag{6}$$
$$u(t) = S_0(q)r(t) - C(q)W_0(q)H_0(q)e_0(t). \tag{7}$$

Note also that

$$r(t) = r_1(t) + C(q)r_2(t) = u(t) + C(q)y(t). \tag{8}$$

Using knowledge of $C(q)$, together with measurements of u and y, we can simply "reconstruct" the reference signal r in (8) So in stead of a measurable signal r, we can equally well deal with the situation that y, u are measurable and C is known.
It can easily be verified from (6),(7) that the signal $\{u(t) + C(q)y(t)\}$ is uncorrelated with $\{e_0(t)\}$ provided that r is uncorrelated with e_0. This shows with equations (6),(7) that the identification problem of identifying the transfer function from signal r to $(y, u)^T$ is an "open loop"-type of identification problem, since r is uncorrelated with the noise terms dependent on e_0. The corresponding factorization of P_0 that can be estimated in this way is the factorization (P_0S_0, S_0), i.e. $P_0 = (P_0S_0) \cdot S_0^{-1}$, as also employed in e.g. Zhu and Stoorvogel (1992).

[3]The main part of the paper is directed towards multivariable systems, and so we distinguish between output and input sensitivity.

[4]Note that we have employed the relations $W_0P_0 = P_0S_0$ and $S_0C = CW_0$.

However this is only one of the many factorizations that can be identified from closed loop data in this way. By introducing an auxiliary signal

$$x(t) := F(q)r(t) = F(q)(u(t) + C(q)y(t)) \tag{9}$$

with $F(z)$ a fixed stable rational transfer function, we can rewrite the system's relations as

$$y(t) = P_0(q)S_0(q)F(q)^{-1}x(t) + W_0(q)H_0(q)e_0(t) \tag{10}$$
$$u(t) = S_0(q)F(q)^{-1}x(t) - C(q)W_0(q)H_0(q)e_0(t), \tag{11}$$

and thus we have obtained another factorization of P_0 in terms of the factors $(P_0S_0F^{-1}, S_0F^{-1})$. Since we can reconstruct the signal x from measurement data, these factors can also be identified from data, as in the situation considered above, provided of course that the factors themselves are stable. We will now characterize the freedom that is present in choosing this filter F.

Proposition 3.1 *Consider a data generating system according to* (6),(7), *such that C stabilizes P_0, and let $F(z)$ be a rational transfer function defining*

$$x(t) = F(q)(u(t) + C(q)y(t)). \tag{12}$$

Let the controller C have a left coprime factorization $(\tilde{D}_c, \tilde{N}_c)$. Then the following two expressions are equivalent

a. the mappings $col(r_2, r_1) \to x$ and $x \to col(y, u)$ are stable;

b. $F(z) = W\tilde{D}_c$ with W any stable and stably invertible rational transfer function. □

The proof of this Proposition is added in the appendix.
Note that stability of the mappings mentioned under (a) is required in order to guarantee that we obtain a bounded signal x as an input in our identification procedure, and that the factors to be estimated are stable, so we are able to apply the standard (open-loop) prediction error methods and analysis thereof.
Note that all factorizations of P_0 that are induced by these different choices of F reflect factorizations of which the stable factors can be identified from input/output data, cf. equations (10),(11).
The construction of the signal x is schematically depicted in Figure 2. Note that we have employed (8) which clearly shows that x is uncorrelated with e_0

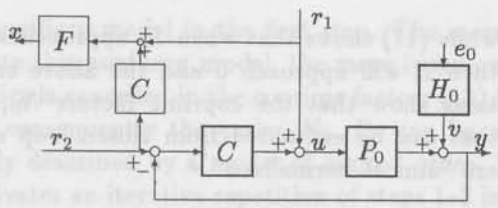

Fig. 2: Construction of auxiliary signal x from closed loop data.

provided the external signals are also uncorrelated with e_0.
For any choice of F satisfying the conditions of Proposition 3.1 the induced factorization of P_0 is right coprime, as shown next.

Proposition 3.2 *Consider the situation of Proposition 3.1. For any choice of $F = W\tilde{D}_c$ with W stable and stably invertible, the induced factorization of P_0, given by $(P_0S_0F^{-1}, S_0F^{-1})$ is right coprime.*

Proof: Let (X, Y) be right Bezout factors of (N, D), and denote $[X_1 \;\; Y_1] = W(\tilde{D}_cD + \tilde{N}_cN)[X \;\; Y]$. Then by employing (A.1) it can simply be verified that X_1, Y_1 are stable and are right Bezout factors of $(P_0S_0F^{-1}, S_0F^{-1})$. □

We will employ the freedom in the filter F, in order to tune the specific coprime factors that can be estimated from closed loop data. Similar to the Youla parametrization, we will use an auxiliary model P_x that is required to be stabilized by C.

Proposition 3.3 *Consider the situation of Propositions 3.1,3.2. Let P_x be an auxiliary model with r.c.f. (N_x, D_x) that is stabilized by C, which has l.c.f. $(\tilde{D}_c, \tilde{N}_c)$. Then a valid choice of W (satisfying (b) in Proposition 3.1) is given by $(\tilde{D}_cD_x + \tilde{N}_cN_x)^{-1}$, and the induced right coprime factorization of P_0 is given by*

$$N_0 = P_0(I + CP_0)^{-1}(I + CP_x)D_x \quad (13)$$
$$D_0 = (I + CP_0)^{-1}(I + CP_x)D_x. \quad (14)$$

Proof: With Lemma A.1 it follows that $\tilde{D}_cD_x + \tilde{N}_cN_x$ is stable and stably invertible, and thus it is an appropriate choice for W^{-1}. The resulting N_0 and D_0 follow by simple substitution of $F = W\tilde{D}_c = (\tilde{D}_cD_x + \tilde{N}_cN_x)^{-1}\tilde{D}_c = (D_x + CN_x)^{-1}$. □

Note that for any given controller C, and any stable and stably invertible W, there always exists an auxiliary model P_x that satisfies $(\tilde{D}_cD_x + \tilde{N}_cN_x)^{-1} = W$. This implies that the freedom that is present in W, as shown in Proposition 3.1, is not restricted by the specific choice of W in Proposition 3.3.
The representation of P_0 in terms of the coprime factorization above, shows great resemblance with the dual Youla-parametrization, i.e. the parametrization of all plants that are stabilized by a given controller. This connection is shown next.

Proposition 3.4 *Schrama (1992). Let C be a controller with r.c.f. (N_c, D_c), and let P_x with r.c.f. (N_x, D_x) be any system that is stabilized by C. Then*

(a) A system P_0 is stabilized by C if and only if there exists a stable R satisfying

$$N_x + D_cR = P_0(I + CP_0)^{-1}(I + CP_x)D_x \quad (15)$$
$$D_x - N_cR = (I + CP_0)^{-1}(I + CP_x)D_x. \quad (16)$$

(b) The stable matrix R in (a) is uniquely determined by

$$R = D_c^{-1}(I + P_0C)^{-1}(P_0 - P_x)D_x. \quad (17)$$

The proposition shows that the dual Youla-parametrization induces a set of coprime factorizations (15),(16) that have exactly the same structure as the coprime factorizations that can be identified from closed loop data, with an appropriate choice of the data filter F.
In the next section we will show how we can exploit the freedom in choosing F, N_x and D_x in order to arrive at an estimate of *normalized* coprime factors of the plant.

4 An algorithm for identification of normalized coprime factors

The idea of arriving at normalized coprime factorizations of P_0 is based on the following observation. Consider the coprime factors (13),(14) that are accessible from closed loop data as discussed before. Suppose we can find an auxiliary model P_x that is an accurate (possibly high order) approximation of the plant P_0, and we construct a normalized r.c.f. (N_n, D_n) of P_x. Using these normalized r.c.f.'s as N_x and D_x in (13),(14), it follows with (15),(16) that $N_0 = N_n + D_cR$ and $D_0 = D_n - N_cR$. Employing $P_x \approx P_0$ which leads to $R \approx 0$ then shows that (N_0, D_0) (approximately) equals a normalized r.c.f. of P_0. This line of thought is formalized in the following algorithm

1. Let there be available a nominal model P_{nom} of the plant P_0, such that P_{nom} is stabilized by C. Set $P_x = P_{nom}$ and construct a r.c.f. $P_x = N_x D_x^{-1}$. Construct the data filter F according to Proposition 3.3:

$$F = D_x^{-1}(I + CP_x)^{-1} \tag{18}$$

and use this data filter to construct an auxiliary signal $x = F(u + Cy)$. The corresponding closed loop system equations become

$$y(t) = N_0 x(t) + W_0 H_0 e_o(t) \tag{19}$$
$$u(t) = D_0 x(t) - C W_0 H_0 e_0(t) \tag{20}$$

with N_0, D_0 given by (13),(14).

2. Use the signals (y, u, x) in a (least squares) identification algorithm with a output error model structure (Ljung, 1987):

$$\varepsilon(t,\theta) = \begin{pmatrix} y(t) \\ u(t) \end{pmatrix} - \begin{bmatrix} N(\theta) \\ D(\theta) \end{bmatrix} x(t) \tag{21}$$

considering (y, u) as output signals and x as input signal.

Use this parametrization to identify the coprime factors N_0, D_0 as accurately as possible through high-order modelling, e.g. by employing orthogonal basis functions in a linear regression scheme. In this respect the new method of constructing orthogonal basis functions that contain system dynamics shows very promissing results, see Heuberger *et al.* (1992), as also applied for identification purposes in De Callafon *et al.* (1993).

This step is comparable to the first step in the so-called two-stage identifcation procedure in Van den Hof and Schrama (1993). The identified coprime factors are denoted as $\hat{N}$, $\hat{D}$.

3. Denote $P_n := \hat{N}\hat{D}^{-1}$ and construct a normalized right coprime factorization (N_n, D_n) such that $P_n = N_n D_n^{-1}$. A procedure for constructing this normalized r.c.f. can be found in Vidyasagar (1988), Bongers and Heuberger (1990). Set $P_x = P_n$, $D_x = D_n$, $N_x = N_n$.

4. Construct a new data filter F according to (18) and generate a new auxiliary signal $x = F(u + Cy)$. The corresponding system's equations are again given by (19),(20).

Employing the results of Proposition 3.4 it follows that

$$N_0 = N_n + D_c R \tag{22}$$
$$D_0 = D_n - N_c R, \tag{23}$$

while (17) shows that when P_n approaches P_0, then R will approach 0 and the above equations show that the coprime factors N_0, D_0 that can be estimated from closed loop data are "almost normalized".

5. Now again identify coprime plant factors as in Step 2, using measurement signals (y, u, x) and an output error model structure (21) where $N(\theta)$ and $D(\theta)$ are parametrized as

$$N(\theta) = f(q^{-1},\theta)^{-1} b(q^{-1},\theta) \tag{24}$$
$$D(\theta) = f(q^{-1},\theta)^{-1} a(q^{-1},\theta) \tag{25}$$

with a, b and f (matrix) polynomials of specified degree, having coefficients that are collected in the parameter vector θ. This parametrization, where N and D have a common denominator, guarantees that the McMillan degree of the ultimately identified model is equal to the McMillan degree of the estimated coprime factors.

The parameter estimate is obtained by

$$\hat{\theta}_N = \arg\min_{\theta} \frac{1}{N} \sum_{t=1}^{N} \varepsilon_f^T(t,\theta)\varepsilon_f(t,\theta), \tag{26}$$

with
$\varepsilon_f(t,\theta) = L\varepsilon(t,\theta)$, and $L \in \mathcal{RH}_\infty^{(n_y+n_u)\times(n_y+n_u)}$, decomposed as $L = diag(L_y, L_u)$.

6. The result of the algorithm is composed of estimated (almost normalized) right coprime plant factors $(N(\hat{\theta}_N), D(\hat{\theta}_N))$ and a resulting plant model $P(\hat{\theta}_N) = N(\hat{\theta}_N)D(\hat{\theta}_N)^{-1}$.

As shown in the previous section, the plant coprime factorizations that are accessible from closed experimental data are determined by the specific choice of filter F and signal x that are chosen. The coprime factorizations that can be obtained in this way can be made exactly normalized only in the situation that we have exact knowledge of the plant P_0. In the algorithm presented above, we have replaced this exact knowledge of P_0 by a (very) high order accurate estimate of P_0. This knowledge is used to shape the specific set of coprime factors that is accessible from data.
The nominal model P_{nom} that the algorithm is started by, can be obtained from previous experiments on the plant, or from the previous iteration step in an iterative identification/control design procedure. Note that the order of the "high order" estimate of P_0 in step 2 may be strongly dependent on the nominal model P_{nom} that is used as

an auxiliary model in the first step. The more accurate this auxiliary model, the more common dynamics is cancelled in the coprime factors (13),(14), and consequently the easier N_0, D_0 can be accurately described by a model of limited order. This motivates an iterative repetition of steps 1–3 in the algorithm presented above, in which the high order normalized r.c.f.'s in step 3 are used as auxiliary factors again in step 1 of the procedure, thus generating a new signal x to be used again for identification. Such an iterative procedure has also been applied in the application example discussed in the next section.

In order to explicitly write down the asymptotic identification criterion that has been minimized in the last step, note that we can write

$$\varepsilon(t,\theta) = \begin{bmatrix} L_y(N_0 - N(\theta)) \\ L_u(D_0 - D(\theta)) \end{bmatrix} x(t) + \\ + \begin{bmatrix} W_0 H_0 \\ -C W_0 H_0 \end{bmatrix} e_0(t) \qquad (27)$$

with N_0, D_0 given by (22),(23). As a result the asymptotic parameter estimate $\theta^* = \text{plim}_{N\to\infty} \hat{\theta}_N$ is characterized by

$$\theta^* = \arg\min_{\theta} \int_{-\pi}^{\pi} [|N_0(e^{i\omega}) - N(e^{i\omega},\theta)|^2 |L_y(e^{i\omega})|^2 \\ + |D_0(e^{i\omega}) - D(e^{i\omega},\theta)|^2 |L_u(e^{i\omega})|^2] \Phi_x(\omega) d\omega \qquad (28)$$

with $x(t) = D_n^{-1}(I + CP_n)^{-1}[u(t) + C(q)y(t)]$ and N_0, D_0 given by (22),(23).

If the first identification step (Step 1) of identifying (N, D) is accurately enough ($P_n \to P_0$), then N_n, D_n tend to be normalized right coprime factorizations of the plant. Since $P_x = P_n$, applying (17) shows that $R \to 0$, and the R-dependent terms in (22),(23) will vanish. The resulting frequency-domain expression shows that we obtain a (frequency-weighted) LS-approximation of normalized rcf's of the plant. The type of frequency-weighting can be influenced by designing the spectrum of the reference signal r and by appropriate prefilter L.

Note that in this identification method there is no additional problem if the plant and/or controller are unstable.

5 Application to a mechanical servo system

We will illustrate the proposed identification algorithm by applying it to data obtained from experiments on the radial servo mechanism in a CD (compact disc) player. For a more extensive description of this servo mechanism we refer to Steinbuch *et al.* (1992) and De Callafon *et al.* (1993). The radial servo mechanism concerns an unstable system, due to a double integrator. In the present configuration the radial control loop has been realized by a controller which consists of a lead–lag element and proportional and integrating action.

This experimental set up is used to gather time sequences of $u(t)$ and $y(t)$ in the radial control loop, exciting the signal $r_1(t)$. The signals were sampled at 25kHz and the reference signal $r_1(t)$ was chosen to be a bandlimited white noise signal in the frequency domain of interest (100Hz–10kHz).

Results of applying the algorithm presented in section 4 are shown in a couple of figures. Figure 3 shows the result of the estimated coprime factors $\hat{N}$, $\hat{D}$ at step 2 of the algorithm. This is the high-order estimate, being the result of a number of iterations over steps 1–3 as mentioned before. Order of the models is 24. The results are compared with non-parametric spectral estimates of the corresponding plant factors.

Figure 4 shows the final result, estimated low-order coprime factors, with model order 10. In Figure 5 it is checked whether the finally obtained estimates $N(\hat{\theta}_N), D(\hat{\theta}_N)$ indeed are normalized. To this end we have plotted the frequency response of $N^T(z^{-1},\hat{\theta}_N)N(z,\hat{\theta}_N) + D^T(z^{-1},\hat{\theta}_N)D(z,\hat{\theta}_N)$ and the same response of the high order (unnormalized) estimates.

Note that the control-relevant frequency region, i.e. the area of the cross-over frequency, is very well represented in both normalized coprime factors. I.e. the dynamics that is related to this frequency region is relatively easy to be identified from these factors.

Conclusions

In this paper it is shown that it is possible to identify (almost) normalized coprime plant factors based on closed loop experiments. A general framework is given for closed loop identification of coprime factorizations, and it is shown that the freedom that is present in generating appropriate signals for identification can be exploited to obtain (almost) normalized coprime plant factors from closed loop data. The resulting multi-step algorithm is illustrated with results that are obtained from closed loop experiments on an open loop unstable mechanical servo system.

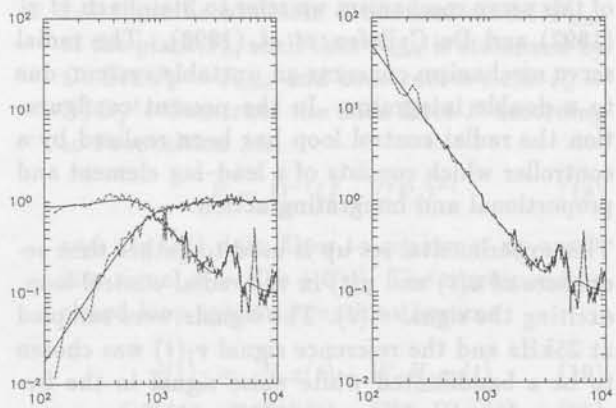

Fig. 3: Bode magnitude plots of high order model (step 2).
a: Identified coprime plant factors $\hat{N}$, $\hat{D}$ of 24th order model (solid line), and spectral estimates of the same factors (dashed line).
b: Estimated plant model $\hat{N}\hat{D}^{-1}$ (solid line) and spectral estimate (dashed line).

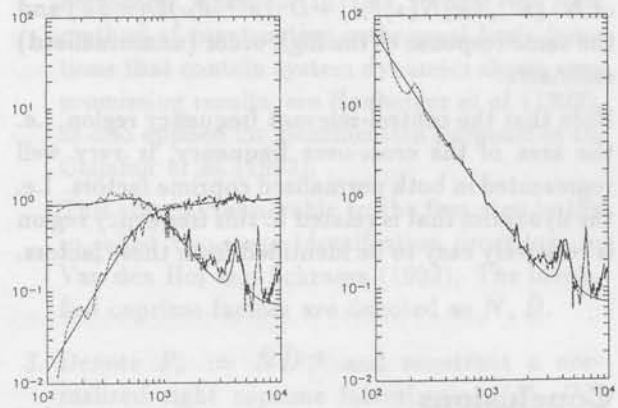

Fig. 4: Bode magnitude plots of final 10-th order model.
a: Identified coprime plant factors $N(\hat{\theta}_N)$, $D(\hat{\theta}_N)$ (solid line), and spectral estimates of the same factors (dashed line).
b: Estimated plant model $N(\hat{\theta}_N)D(\hat{\theta}_N)^{-1}$ (solid line) and spectral estimate (dashed line).

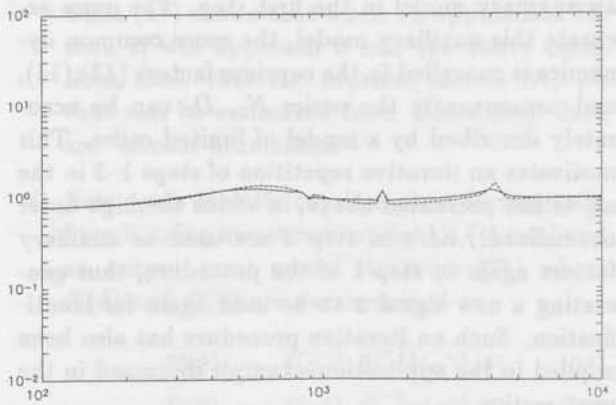

Fig. 5: Bode magnitude plot of $\hat{N}^T(z^{-1})\hat{N}(z) + \hat{D}^T(z^{-1})\hat{D}(z)$ (solid line) and $N^T(z^{-1},\hat{\theta}_N)N(z,\hat{\theta}_N) + D^T(z^{-1},\hat{\theta}_N)D(z,\hat{\theta}_N)$ (dashed line).

Acknowledgement

The authors are grateful to Douwe de Vries and Hans Dötsch for their contributions to the experimental part of the work, and to Gerrit Schootstra and Maarten Steinbuch of the Philips Research Laboratory for their help and support and for access to the CD-player experimental setup.

Appendix

Lemma A.1 *Vidyasagar (1985). Consider rational transfer functions $G_0(z)$ with right coprime factorization (N, D) and $C(z)$ with left coprime factorization $(\tilde{D}_c, \tilde{N}_c)$. Then* $T(G_0, C) = \begin{bmatrix} G_0 \\ I \end{bmatrix}(I + CG_0)^{-1}\begin{bmatrix} C & I \end{bmatrix}$ *is stable if and only if $\tilde{D}_c D + \tilde{N}_c N$ is stable and stably invertible.* □

Proof of Proposition 3.1.

$(a) \Rightarrow (b)$. By writing $\begin{bmatrix} G_0 S_0 \\ S_0 \end{bmatrix} = \begin{bmatrix} G_0 \\ I \end{bmatrix}(I + CG_0)^{-1}$ and substituting a right coprime factorization (N, D) for G_0, and a left coprime factorization $(\tilde{D}_c, \tilde{N}_c)$ for C we get, after some manipulation, that

$$\begin{bmatrix} G_0 S_0 \\ S_0 \end{bmatrix} = \begin{bmatrix} N \\ D \end{bmatrix}(\tilde{D}_c D + \tilde{N}_c N)^{-1}\tilde{D}_c \qquad \text{(A.1)}$$

and stability of $\begin{bmatrix} G_0 S_0 F^{-1} \\ S_0 F^{-1} \end{bmatrix}$ is equivalent with stability of $\begin{bmatrix} N \\ D \end{bmatrix}(\tilde{D}_c D + \tilde{N}_c N)^{-1}\tilde{D}_c F^{-1}$. Premultiplication of the latter expression with the stable transfer function $(\tilde{D}_c D + \tilde{N}_c N)\begin{bmatrix} X & Y \end{bmatrix}$ with (X, Y)

right Bezout factors of (N, D) shows that $\tilde{D}_c F^{-1}$ is implied to be stable. As a result, $\tilde{D}_c F^{-1} = W$ with W any stable transfer function.
Now stability of F and FC implies stability of $W^{-1} \begin{bmatrix} \tilde{D}_c & \tilde{N}_c \end{bmatrix}$, which after postmultiplication with the left Bezout factors of $(\tilde{D}_c, \tilde{N}_c)$ implies that W^{-1} is stable. This proves that $F = W^{-1}\tilde{D}_c$ with W a stable and stably invertible transfer function.
$(b) \Rightarrow (a)$. Stability of F and FC is straightforward. Stability of $S_0 F^{-1}$ and $G_0 S_0 F^{-1}$ follows from (A.1), using the fact that $(\tilde{D}_c D + \tilde{N}_c N)^{-1}$ is stable (lemma A.1). □

References

R.R. Bitmead (1993). Iterative control design approaches. *Proc. 12th IFAC World Congress*, 18-23 July 1993, Sydney, Australia, vol. 9, pp. 381-384.

P.M.M. Bongers and P.S.C. Heuberger (1990). Discrete normalized coprime factorization and fractional balanced reduction. Proc. 9th INRIA Conf. Analysis and Optimiz. Systems. *Lecture Notes in Control and Inform. Sciences, Vol. 144*. Springer Verlag, pp. 307-313.

P.M.M. Bongers and O.H. Bosgra (1990). Low order robust H_∞ controller synthesis. *Proc. 29th IEEE Conf. Decision and Control*, Honolulu, HI, pp. 194-199.

R.A. de Callafon, P.M.J. Van den Hof and M. Steinbuch (1993). Control relevant identification of a compact disc pick-up mechanism. *Proc. 32nd IEEE Conf. Decision and Control*, San Antonio, TX, USA.

T.T. Georgiou and M.C. Smith (1990). Optimal robustness in the gap metric. *IEEE Trans. Automat. Contr., AC-35*, pp. 673-686.

M. Gevers (1993). Towards a joint design of identification and control? In: H.L. Trentelman and J.C. Willems (Eds.), *Essays on Control: Perspectives in the Theory and its Applications*. Birkhäuser, Boston, 1993, pp. 111-151.

R.G. Hakvoort, R.J.P. Schrama and P.M.J. Van den Hof (1992). Approximate identification in view of LQG feedback design. *Proc. 1992 Amer. Control Conf.*, pp. 2824-2828.

F.R. Hansen (1989). *Fractional Representation Approach to Closed-Loop System Identification and Experiment Design*. Ph.D.-thesis, Stanford University, Stanford, CA, USA.

P.S.C. Heuberger, P.M.J. Van den Hof and O.H. Bosgra (1992). *A Generalized Orthonormal Basis for Linear Dynamical Systems*. Report N-404, Mech. Engin. Systems and Control Group, Delft Univ. Techn. Short version in CDC'93.

W.S. Lee, B.D.O. Anderson, R.L. Kosut and I.M.Y. Mareels (1992). On adaptive robust control and control-relevant system identification. *Proc. 1992 American Control Conf.*, June 26-28, 1992, Chicago, IL, pp. 2834-2841.

L. Ljung (1987). *System Identification - Theory for the User*. Prentice-Hall, Englewood Cliffs.

D. McFarlane and K. Glover (1988). An H_∞ design procedure using robust stabilization of normalized coprime factors. *Proc. 27th IEEE Conf. Decis. Control*, Austin, TX, pp. 1343-1348.

R.J.P. Schrama and P.M.M. Bongers (1991). Experimental robustness analysis based on coprime factorizations. In O.H. Bosgra and P.M.J. Van den Hof (Eds.), *Sel. Topics in Identif., Modelling and Contr.*, Vol. 3. Delft Univ. Press, pp. 1-8.

R.J.P. Schrama (1991). An open-loop solution to the approximate closed-loop identification problem. *Proc. 9th IFAC/IFORS Symposium Identification and System Param. Estim.*, July 1991, Budapest, Hungary, pp. 1602-1607.

R.J.P. Schrama (1992a). *Approximate Identification and Control Design with Application to a Mechanical System*. Dr. Dissertation, Delft University of Technology, May 1992.

R.J.P. Schrama and P.M.J. Van den Hof (1992). An iterative scheme for identification and control design based on coprime factorizations. *Proc. 1992 American Control Conf.*, June 24-26, 1992, Chicago, IL, pp. 2842-2846.

R.J.P. Schrama (1992b). Accurate models for control design: the necessity of an iterative scheme. *IEEE Trans. Automat. Contr., AC-37*, pp. 991-994.

M. Steinbuch, G. Schootstra and O.H. Bosgra (1992). Robust control of a compact disc player. *Proc. 31st IEEE Conf. Decision and Control*, Tucson, Az, pp. 2596-2600.

M.C. Tsai, E.J.M. Geddes and I. Postlethwaite (1992). Pole-zero cancellations and closed-loop properties of an H∞ - mixed sensitivity design problem. *Automatica, 28*, 519-530.

P.M.J. Van den Hof and R.J.P. Schrama (1993). An indirect method for transfer function estimation from closed loop data. *Automatica, Vol. 28*, No. 6, November 1993.

M. Vidyasagar (1984). The graph metric for unstable plants and robustness estimates for feedback stability. *IEEE Trans. Automat. Contr., AC-29*, pp. 403-417.

M. Vidyasagar (1985). *Control Systems Synthesis: A Factorization Approach*. M.I.T. Press, Cambridge, MA, USA.

M. Vidyasagar (1988). Normalized coprime factorizations for nonstrictly proper systems. *IEEE Trans. Automat. Contr., AC-33*, pp. 300-301.

Z. Zang, R.R. Bitmead and M. Gevers (1991). *Iterative Model Refinement and Control Robustness Enhancement.* Report 91.137, CESAME, Univ. Louvain-la-Neuve, November 1991.

Y.C. Zhu and A.A. Stoorvogel (1992). Closed loop identification of coprime factors. *Proc. 31st IEEE Conf. Decision and Control*, Tucson, AZ, pp. 453-454.

Selected Topics in Identification, Modelling and Control
Vol. 6, December 1993

Control relevant identification of a compact disc pick–up mechanism[‡]

Raymond A. de Callafon[§♯], Paul M.J. Van den Hof[♯] and Maarten Steinbuch[♭]

[♯]*Mechanical Engineering Systems and Control Group*
Delft University of Technology, Mekelweg 2, 2628 CD Delft, The Netherlands.
[♭]*Philips Research Laboratories, P.O. Box 80.000, 5600 JA Eindhoven, The Netherlands.*

Abstract. This paper discusses the control relevant parametric identification of a servo system present in a Compact Disc player. In this application an approximate closed loop identification problem is solved in order to come up with a linear multivariable discrete time model, suitable for control design. This identification problem is handled by a recently introduced two stage method. It yields an explicit and tunable expression for the bias distribution of the model being estimated, clearly showing the dynamics of the closed loop system in the (asymptotic) approximation criterion. This result will be exploited to identify the model in a control relevant way by additional data filtering. The recently introduced method in de Vries and Van den Hof (1993) for model uncertainty quantification is used to construct an upper bound for the corresponding model error.

Keywords. compact disc player; closed loop identification; two stage method; control relevant identification; model uncertainty.

1 Introduction

Compact Disc players use an optical decoding device to reproduce high quality audio from a digitally coded signal, recorded as a spiral track on a reflective disc, see also Bouwhuis *et al.* (1985). An increasing amount of equivalent optical devices will be used in portable applications, having severe shock disturbances. The track following properties of a CD player, operating in these conditions, could be improved by designing an enhanced multivariable controller. The intention of this paper is to estimate a (nominal) multivariable FDLTI (Finite Dimensional Linear Time Invariant) dynamical model, obtained from closed loop experiments, which can be used for control design. Additionally, the procedure presented in de Vries and Van den Hof (1993) is used for a quantification of the resulting model error by estimating a non–parametric additive model uncertainty.

There is a growing interest in merging the problems of control design and identification. On the one hand this is caused by the fact that from a robust control design point of view we require expressions for model uncertainty that have to be used in robust control design procedures. On the other hand the (nominal) models used to design control systems very often will have to be gathered by experimental methods.

Practically it is impossible to exactly characterize all phenomena that describe the dynamical behaviour of a physical system and the corresponding models will necessarily be approximative. Furthermore, control design methods can get unmanageable if they are applied to models of high complexity. Since the validity of any approximate model hinges on its intended use, the identification procedure being applied will be subjected to several requirements, in order to provide estimated models that are suitable for control design. These considerations have resulted in the statement that the best model for control design cannot be derived from

[‡]This paper is presented at the 32nd IEEE Conference on Decision and Control, San Antonio, TX, USA, December 15–17, 1993. Copyright of this paper remains with IEEE.

[§]The work of Raymond de Callafon is sponsored by the Dutch "Systems and Control Theory Network".

open loop experiments alone, Bitmead *et al.* (1990), Schrama (1990).

A control relevant identification requires that the relevant dynamical behaviour of the system is estimated while it operates in a closed loop configuration with the controller to be designed. Since the controller obtained from the control design is (yet) unknown, this will generally lead to an iterative scheme of identification and control design, using the controller of step $i-1$ to estimate a model for step i. This has led to study several different types of iterative schemes of identification and control design, see Hakvoort *et al.* (1992), Lee *et al.* (1992), Liu and Skelton (1990), Schrama (1992), Schrama and Van den Hof (1992), Zang *et al.* (1991).

In this paper we concentrate on one identification step in such an iterative procedure. Within the framework of prediction error identification (Ljung (1987)) we will identify a multivariable control relevant approximate model, employing a number of recently introduced methods. An indirect (two-stage) method (Van den Hof and Schrama (1993)) will be employed to perform the approximate closed loop identification. The basic advantage of this approach is that an overall approximate identification results, in which the asymptotic bias distribution of the identified model becomes an explicit and tunable expression that is independent of the (unknown) noise disturbance on the data. Additional data filtering is applied to tune the approximation criterion to become a control relevant criterion.

The outline of this paper is as follows. First a concise description of the Compact Disc pick–up mechanism and the experimental set up is given in section 2. Next some preliminary notation is discussed. In section 4 we pay attention to the specific two-stage identification procedure, while in section 5 we discuss the use of orthonormal basis functions that are employed in the first stage of the procedure. Next, the control relevance of the identification approach is given attention and in section 6 we will present the experimental results.

2 Compact Disc Mechanism

The CD mechanism consists of a turn table DC–motor for the rotation of the Compact Disc and a radial arm in order to follow the track of the disc. Furthermore, an OPU (Optical Pick–up Unit) is mounted on the end of the balanced radial arm to read the digitally coded signal, recorded on the disc. Schematically the CD mechanism is given in figure 1.

A diode generates a laser beam that passes through a series of optical lenses in the OPU to give a spot on the disc surface. The light reflected from the disc is measured on an array of photo diodes,

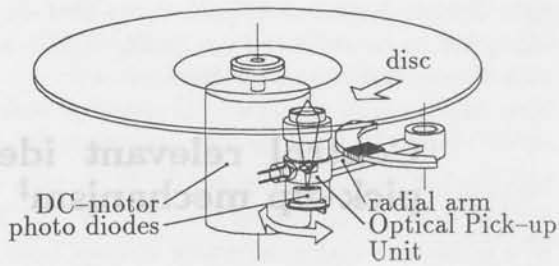

Fig. 1: Schematic view of CD mechanism

mounted in the bottom of the OPU, yielding the signals required for position error information of the laser spot on the Compact Disc, see also Draijer *et al.* (1992).

Following the track on the Compact Disc involves basically two control loops. First a radial control loop using a permanent magnet/coil system mounted on the radial arm, in order to position the laser spot in the direction orthogonal to the track. Secondly a focus control loop using an objective lens suspended by two parallel leaf springs and a permanent magnet/coil system, with the coil mounted in the top of the OPU to focus the laser spot on the disc. In the present configuration, both the radial and focus control loops have been realized by a SISO (Single Input Single Output) controller, which consists of a lead–lag element and a proportional and integrating action. The closed loop bandwidth is approximately 500 Hz, which is a compromise between several conflicting factors, see Draijer *et al.* (1992) and Steinbuch *et al.* (1992).

In figure 2 a block diagram of the two control loops is shown. In here $P_a(q)$ denotes the transfer function of radial and focus actuator, C_{opu} the OPU, $C(q)$ the controller and $P_0(q) = -C_{opu}P_a(q)$. The variable q is the forward shift operator, yielding $x(t+1) = qx(t)$.

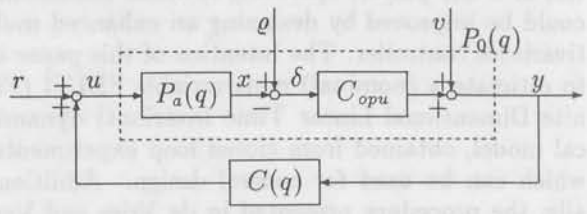

Fig. 2: Block diagram of the Compact Disc mechanism

The signals have the following interpretation. The spot position error $\delta(t)$, which is the difference between the track position $\varrho(t)$ and actuator posi-

tion $x(t)$ in radial and focus direction, generates a (disturbed) error signal $y(t)$ via C_{opu}. This error signal $y(t)$ is led into the controller $C(q)$ and feeds the system $P_a(q)$ with the input $u(t)$. The signal $v(t)$ reflects the disturbance on the error signal $y(t)$.

The absolute track position $\varrho(t)$ and actuator position $x(t)$ cannot be measured directly and used for identification. Only the error signal $y(t)$ and the input $u(t)$ are available. Therefore an additional and known reference signal $r(t)$, uncorrelated with the additive noise $v(t)$ will be injected into the control loops, as illustrated in figure 2.

3 Preliminaries

Given figure 2, the system $P_0(q)$ will be described by the following FDLTI data generating system **S** throughout this paper.

$$\mathbf{S}: \quad \begin{aligned} y(t) &= P_0(q)u(t) + H_0(q)e(t) \\ u(t) &= r(t) + C(q)y(t) \end{aligned} \tag{1}$$

In (1) the disturbance $v(t) + C_{opu}\varrho(t)$ is described by a filtered white noise signal $H_0(q)e(t)$. Using the input sensitivity $S_0(q)$ and output sensitivity $W_0(q)$ of the closed loop system

$$\begin{aligned} S_0(q) &= [I - C(q)P_0(q)]^{-1} \\ W_0(q) &= [I - P_0(q)C(q)]^{-1} \end{aligned} \tag{2}$$

we can rewrite (1) into the following equations.

$$u(t) = S_0(q)r(t) + C(q)W_0(q)H_0(q)e(t) \tag{3}$$

$$y(t) = P_0(q)S_0(q)r(t) + W_0(q)H_0(q)e(t) \tag{4}$$

Throughout this paper we will consider model sets $\mathcal{M}$ that are parametrized in an OE (Output Error) structure, Ljung (1987). For a general input/output system with input u and output y this model structure is reflected by the equation:

$$\mathcal{M}: \quad y(t) = P(q,\rho)u(t) + \varepsilon(t), \quad \rho \in D_{\mathcal{M}} \tag{5}$$

where $\varepsilon(t)$ is the one step ahead prediction error. The parameter ρ will be estimated by employing a least squares criterion, see also Ljung (1987),

$$\begin{aligned} \hat{\rho} &= \arg\min_{\rho} V_N(\rho, Z^N), \quad \rho \in D_{\mathcal{M}} \\ V_N(\rho, Z^N) &= \frac{1}{2N}\sum_{t=0}^{N-1} \mathrm{tr}\left\{\varepsilon_l^T(t,\rho)\, Q\, \varepsilon_l(t,\rho)\right\} \\ \varepsilon_l(t,\rho) &= L(q)\varepsilon(t,\rho) \end{aligned} \tag{6}$$

where Q is a symmetric weighting matrix, Z^N reflects the observed data of length N and $L(q)$ is an additional filter on the prediction error $\varepsilon(t,\rho)$.

4 Two Stage Method

The major problem arising from an approximate identification using closed loop experiments, is the correlation of the additive noise with the input of the system, see also figure 2. Most important in identification for control design is to estimate $P_0(q)$ given in (1). Furthermore, an explicit expression of the approximation of $P_0(q)$ is needed, to tune the bias distribution of the model $P(q,\hat{\rho}_N)$ being estimated in a feedback relevant way. The method to handle the closed loop situation in this paper, is based on the two stage identification method given in Van den Hof and Schrama (1993). The two steps are recapitulated in the following.

The external reference signal $r(t)$ given in (3) is uncorrelated with the additive noise $v(t)$ acting on the closed loop system. By using an OE model structure, similar as in (5)

$$u(t) = S(q,\alpha)r(t) + \varepsilon(t) \tag{7}$$

and the least squares criterion given in (6) to estimate α, it is possible to identify the input sensitivity $S_0(q)$ in an open loop way. In this step we take $L(q) = 1$. This is the *first* step in the two stage identification strategy. It is even possible to consistently estimate $S_0(q)$, provided a sufficiently high model order has been selected.

Given the estimate $S(q,\hat{\alpha}_N)$ of the input sensitivity $S_0(q)$, a noise free input signal $\hat{u}_r(t)$ can be simulated from the observations of the reference signal $r(t)$.

$$\hat{u}_r(t) = S(q,\hat{\alpha}_N)r(t) \tag{8}$$

which in the *second* step of the procedure is employed, again using an OE model structure

$$y(t) = P(q,\rho)\hat{u}_r(t) + \varepsilon(t) \tag{9}$$

and the least squares criterion given in (6) to estimate the parameter $\hat{\rho}_N$ in $P(q,\hat{\rho}_N)$.

A result for the asymptotic bias distribution of the estimate $P(q,\hat{\rho}_N)$ in the SISO case is given in the following theorem (Van den Hof and Schrama (1993)):

Theorem 4.1 *Consider the two-stage identification discussed above, resulting in a parameter estimate $\hat{\rho}_N$. Then, under weak conditions,*

$$\begin{aligned} \hat{\rho}_N \to \rho^\star = \arg\min_{\rho} \frac{1}{4\pi}\int_{-\pi}^{\pi} \Big| &[P_0(e^{i\omega}) - P(e^{i\omega},\rho)]\cdot \\ &\cdot S_0(e^{i\omega}) + P(e^{i\omega},\rho)[S_0(e^{i\omega}) - S(e^{i\omega},\alpha^\star)]\Big|^2 \cdot \\ &\cdot \Phi_r(\omega)|L(e^{i\omega})|^2\, d\omega, \quad w.p.\ 1 \ as\ N \to \infty \end{aligned} \tag{10}$$

and

$$\alpha^* = \arg\min_{\alpha} \frac{1}{4\pi} \int_{-\pi}^{\pi} |S_0(e^{i\omega}) - S(e^{i\omega}, \alpha)|^2 \Phi_r(\omega)\, d\omega \tag{11}$$

where $L(q)$ denotes the filter on the prediction error $\varepsilon(t)$, used in the second step and $\Phi_r(\omega)$ denotes the (auto)spectrum of the reference signal $r(t)$.

The frequency representation (10) in theorem 4.1 shows the influence of a model error in the estimated sensitivity function on the final result of the identification. If in the first step of the procedure a very accurate (high order) model of the sensitivity function is identified, then the second term in the integrand expression in (10) will vanish. For the multivariable case, this will result in the following expression, where $\Delta P(e^{i\omega}, \rho)$ is used to denote the difference $P_0(e^{i\omega}) - P(e^{i\omega}, \rho)$.

$$\begin{aligned} \rho^* = \arg\min_{\rho} \frac{1}{4\pi} \int_{-\pi}^{\pi} \mathrm{tr}\{ & L(e^{-i\omega})^T Q L(e^{i\omega}) \cdot \\ & \cdot \Delta P(e^{i\omega}, \rho) S_0(e^{i\omega}) \Phi_r(\omega) \cdot \\ & \cdot S_0(e^{-i\omega})^T \Delta P(e^{-i\omega}, \rho)^T \}\, d\omega \end{aligned} \tag{12}$$

Clearly, (12) is an explicit and tunable expression for the bias distribution of the asymptotic model $P(q, \rho^*)$. In this expression the prediction error filter $L(q)$, the input spectrum $\Phi_r(\omega)$ and the weighting matrix Q can been seen as design variables, see also Hakvoort *et al.* (1992) and Wahlberg and Ljung (1986). Therefore, we define the design variables $\mathcal{D}_c$ to be:

$$\mathcal{D}_c \stackrel{\text{def}}{=} \{L(q), \Phi_r(\omega), Q\}. \tag{13}$$

The usage of the design variables $\mathcal{D}_c$ will be scrutinized in section 6.

5 Linear Regression using Orthonormal Basis Functions

In the first step of the identification procedure we need an output error type algorithm in order to arrive at the results as presented in theorem 4.1. Moreover the identified sensitivity $S(q, \hat{\alpha}_N)$ has to be very accurate, which asks for high model orders to be applied. Since OE model structures in general require non-linear optimization algorithms to solve the least squares identification problem given in (6), high model orders are very unattractive from a computational point of view. Moreover the occurrence of local minima in the optimization may heavily influence the parameter estimate that is obtained.

In our procedure we will apply a linear regression identification that also has an output error structure, and that exploits the recently obtained results on system-based orthonormal basis functions as presented in Heuberger (1990) and Heuberger *et al.* (1992). This model structure is given by:

$$\varepsilon(t, \alpha) = u(t) - \sum_{k=0}^{n} L_k(\alpha) V_k(q) r(t-1) \tag{14}$$

where $\{L_k(\alpha)\}_{k=1,\cdots,n}$ is a sequence of expansion coefficients of the parametrized model of the sensitivity function $S(q, \alpha)$ with respect to the basis functions $\{V_k(z)\}_{k=1,\cdots,\infty}$. It is based on the fact that any stable, strictly proper FDLTI system $S(z)$ has a unique expansion

$$S(z) = \sum_{k=0}^{\infty} L_k V_k(z) \tag{15}$$

In the case $V_k(z) = z^{-k}$, this model structure matches a Finite Impulse Representation (FIR), while in that case L_k represent the impulse response coefficients of the model.

By choosing appropriate basis functions $V_k(z)$, the convergence rate of a series expansion as in (15) can become very fast, which means that a very accurate model can be identified by only incorporating a restricted number of coefficients $L_k(\alpha)$.

In Heuberger (1990), Heuberger *et al.* (1992) it is shown how dynamical systems themselves can induce orthonormal basis functions $V_k(z)$, pointing to an iterative scheme of identifying expansion coefficients and rebuilding basis functions. In our application we have iteratively constructed such basis functions that were found from the estimated model in the previous iteration step. For more details the reader is referred to the references.

6 Control Relevant Identification

6.1 Finding the right weight

The validity of any approximate model hinges on its intended use and therefore the identification procedure being applied will be subjected to several requirements to estimate a model suitable for control design. Since the "quality" of a model actually is dependent on the controller that is designed on the basis of the model, this future controller actually should be incorporated in a control relevant identification criterion.

Since the controller obtained from the control design is (yet) unknown, a minimization of the model error using the *current* feedback, provided by the present controller, is generally used to estimate a model for subsequent control design. In the literature a number of many techniques can be found to perform such an identification, see for example Bitmead *et al.* (1990), Hakvoort *et al.* (1992), Liu

and Skelton (1990), Schrama (1992). In this paper a 2–norm minimization will be used, see (6), which is related to a LQG control paradigm, see also Hakvoort *et al.* (1992), Zang *et al.* (1991).

The (input) sensitivity $S_0(q)$ given in (2) is found to be of considerable importance in posing performance requirements of the closed loop system. The sensitivity, based on the (nominal) model $P(q,\hat{\rho}_N)$ being estimated will be denoted as

$$S(q,\hat{\rho}_N) = [I - C(q)P(q,\hat{\rho}_N)]^{-1} \tag{16}$$

Clearly, the difference between the sensitivities $S_0(q)$ and $S(q,\hat{\rho}_N)$ reflects a *feedback–relevant mismatch*, caused by the difference between the nominal model $P(q,\hat{\rho}_N)$ and the system $P_0(q)$. Considering any norm or distance function $\|\cdot\|$ and applying the triangle inequality to $\|S_0(q) - S(q,\hat{\rho}_N)\|$ yields:

$$\|S_0(q)\| \leq \|S(q,\hat{\rho}_N)\| + \|S_0(q) - S(q,\hat{\rho}_N)\| \tag{17}$$

$$\|S_0(q)\| \geq \Big|\|S(q,\hat{\rho}_N)\| - \|S_0(q) - S(q,\hat{\rho}_N)\|\Big| \tag{18}$$

From (17) and (18) we see that by posing the following requirement

$$\|S_0(q) - S(q,\hat{\rho}_N)\| \ll \|S(q,\hat{\rho}_N)\| \tag{19}$$

similar performances of the controller $C(q)$ applied to the model $P(q,\hat{\rho}_N)$ and the system $P_0(q)$ can be derived, see also (Schrama (1992)). Therefore, minimizing the difference $\|S_0(q) - S(q,\rho)\|$ on the basis of measurement data can be seen as a control relevant identification. By rewriting the difference between $S_0(q)$ and $S(q,\hat{\rho}_N)$, omitting the use of the forward shift operator q for ease of notation, we may write

$$\begin{aligned} &\|[I - CP_0]^{-1} - [I - CP(\rho)]^{-1}\| = \\ &\|[I - CP(\rho)]^{-1}C\,[P_0 - P(\rho)]\,[I - CP_0]^{-1}\| \end{aligned} \tag{20}$$

From (20) it can been seen that minimizing the difference between $S_0(q)$ and $S(q,\hat{\rho}_N)$ is equal to a weighted norm applied to $[P_0(q) - P(q,\rho)]$, where $S_0(q)$ is used as input weighting and $S(q,\rho)C(q)$ as an output weighting. By replacing the norm operator $\|\cdot\|$ in (20) by the H_2–norm, see (Maciejowski (1989), pp. 99), the difference term in (20) matches the following closed loop performance criterion $J_c(\lambda)$

$$\begin{aligned} J_c(\lambda) \stackrel{\text{def}}{=} \frac{1}{4\pi}\int_{-\pi}^{\pi} \mathrm{tr}\{&[S(e^{-i\omega},\rho)C(e^{-i\omega})]^T \cdot \\ &\cdot[S(e^{i\omega},\rho)C(e^{i\omega})][P_0(e^{i\omega}) - P(e^{i\omega},\rho)] \cdot \\ &\cdot S_0(e^{i\omega})S_0(e^{-i\omega})^T[P_0(e^{-i\omega}) - P(e^{-i\omega},\rho)]^T\}\,d\omega \end{aligned} \tag{21}$$

The way this minimization will be carried out for the identification of the Compact Disc pick–up mechanism, is discussed in the following section.

6.2 Prefiltering

The weighted minimization of $\|P_0(q) - P(q,\rho)\|_2$ given in (21) can be accomplished during the identification, by modifying the design variables $\mathcal{D}_c$ given in (13). The prediction error filter $L(q)$, the symmetric weighting matrix Q and the spectrum Φ_r can be exploited to 'shape' the model $P(q,\hat{\rho}_N)$ being estimated in the approximate identification. To achieve a minimization of the closed loop performance criterion given in (21) the design variables have to be chosen as follows.

Proposition 6.1 *Given a consistent estimate of the input sensitivity $S_0(q) = [I - C(q)P_0(q)]^{-1}$ used to simulate the noise free input $\hat{u}_r(t)$ given in (8), then with the choice of the design variables,*

$$\mathcal{D}_c = \begin{cases} L(q,\rho) &= [I - C(q)P(q,\rho)]^{-1}C(q) \\ \Phi_r(\omega) &= c_1 I \\ Q &= c_2 I \end{cases}$$

where c_1, c_2 are arbitrarily chosen real constants, the least squares criterion given in (6) will converge to the closed loop performance criterion defined in (21), under weak conditions as $N \to \infty$.

A proof of proposition 6.1 can be found in Hakvoort *et al.* (1992), since basically an equivalent closed loop performance criterion is used in this paper. The choice of the design variables given in proposition 6.1 can also be seen directly, by comparing a constant c_1c_2 times the closed loop performance criterion defined in (21) with the equivalent frequency domain representation of the least square identification algorithm given in (12).

Clearly, the consistent estimate of the input sensitivity used to simulate the noise free input signal $\hat{u}_r(t)$, given in (8) can be a strong requirement. An approximate identification of $S_0(q)$ can lead to a biased closed loop performance criterion, see theorem 4.1. As stated before, linear regression models using system based orthonormal functions are used to model the input sensitivity and can be used to substantially reduce this effect.

Furthermore, the following notes on proposition 6.1 should be given.

- Firstly, it should be noted that the input weighting with the 'real' sensitivity $S_0(q)$ can *only* be achieved when performing closed loop experiments. Note that this weighting factor is already present in the asymptotic identification criterion (12).
- Instead of $L(q,\rho) = [I - C(q)P(q,\rho)]C(q)^{-1}$ given in proposition 6.1, a fixed filter will generally be used to filter the prediction error,

as to avoid very complicatedly parametrized nonlinear optimization problems. An iterative scheme using the model $P(q, \hat{\rho}_N)$ from step $i-1$, for constructing a filter $L(q, \hat{\rho}_N)$ used in step i to filter the prediction error can be used to overcome this problem. The control relevant model $P(q, \hat{\rho}_N)$ and the matching filter $L(q, \hat{\rho}_N)$ will be found when the iterative scheme converges.

- Finally it should be noted that the iterative scheme mentioned above, is performed in a SISO configuration. In this way the filtering of the prediction error $\varepsilon(t)$ can be replaced by filtering the input and output of the system to be identified.

7 Application to the CD Player

7.1 Data acquisition

Measurements of the CD mechanism have been obtained from an experimental set up of a Compact Disc player at Philips' Research Laboratories. This experimental set up is used to gather time sequences of $r(t)$, $u(t)$ and $y(t)$, see figure 2, in radial and focus control loops simultaneously. Matching software is used to control the sample frequency, anti aliasing filter, data storage and input generation.

The signals have been sampled at 25 kHz and the reference signal $r(t)$ injected in the closed loop was chosen to be a white noise signal, to fulfil the choice of the second design variable $\Phi_r(\omega)$ given in proposition 6.1. The white noise reference signal was chosen to be bandlimited in the frequency domain of interest (100 Hz - 10 kHz). A 5^{th} order Butterworth filter, with a cut off frequency at 9.5 kHz was used to reduce the effects of aliasing.

The two-stage identification procedure previously discussed is applied to this experimental data. Furthermore, a non parametric estimate of the input sensitivity $S_0(\omega)$ and the system $P_0(\omega)$ is obtained by a spectral analysis (Priestly (1981)) and given by

$$\hat{S}^T(\omega) = \hat{\Phi}_r(\omega)^{-1}\hat{\Phi}_{ru}(\omega), \ \det\{\hat{\Phi}_r(\omega)\} \not\equiv 0 \quad (22)$$

$$\hat{P}^T(\omega) = \hat{\Phi}_{ru}(\omega)^{-1}\hat{\Phi}_{ry}(\omega), \ \det\{\hat{\Phi}_{ru}(\omega)\} \not\equiv 0. \quad (23)$$

The estimates of the spectra in (22) and (23) have been carried out by using 100 averages over 409600 time samples. The results will be used only as a (additional) validation tool for the parametric models $S(q, \hat{\alpha}_N)$ and $P(q, \hat{\rho}_N)$ being estimated, which is based only on 2000 time samples.

7.2 Estimate of sensitivity function

As mentioned in section 5, a linear regression scheme based on orthonormal functions has been used. Firstly, a relatively rough (low order) estimate is computed by a multivariable Output Error minimization using the DUMSI[1]–package. Secondly, an iterative scheme using the model from step $i-1$ for constructing a set of orthonormal functions $V_k(z)$ used in step i will be utilized. The results of this identification procedure can be found in figure 3 and 4. The model $S(q, \hat{\alpha}_N)$ is constructed by estimating 4 coefficients $L_k(\alpha)$ based on an 12-th order model inducing the basis functions. This results in a model with state space dimension 48.

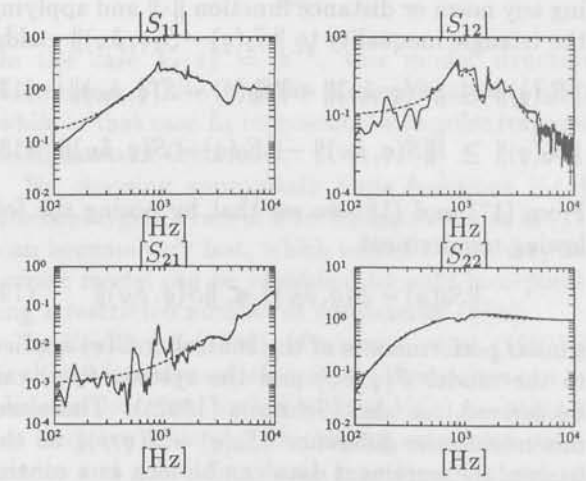

Fig. 3: Amplitude of spectral estimate $\hat{S}(\omega)$ (—) and parametric model $S(e^{i\omega}, \hat{\alpha}_N)$ (- -)

Figure 3 presents the amplitude plots of the spectral estimate $\hat{S}(\omega)$ and the parametric model $S(e^{i\omega}, \hat{\alpha}_N)$. The input sensitivity has been estimated reasonably well, which has been emphasized by comparing a part of the simulation of the input $\hat{u}_r(t)$ and the actual input $u(t)$ measured in closed loop, given in figure 4. This data is taken from a data set, not used for identification. Furthermore, it can been seen from figure 4 that the amount of noise on the input $u(t)$ in closed loop is relatively small.

7.3 Towards a low order model

This section discusses the second step of the two stage identification algorithm, where an approximate identification will be performed, using the reconstructed input $\hat{u}_r(t)$ and output $y(t)$. For the sake of completeness it should be mentioned that the input $\hat{u}_r(t)$ cannot be used directly. This is

[1] Delft University Multivariable System Identification

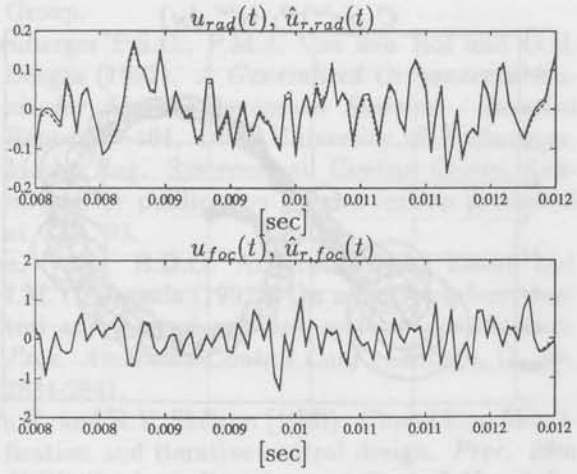

Fig. 4: Measured input $u(t)$ (—) and simulated input $\hat{u}_r(t)$ (- -) of *rad*ial and *foc*us loop

caused by the fact that the radial and focus actuators act like double integrators in the frequency domain of interest.

The properties of the prediction error methods, like the results given in proposition 6.1, are valid only for a stable prediction error mapping, see Ljung (1987), Van den Hof and Schrama (1993). Hence, identifying a double integrator will inevitably lead to undesirable results. In order to omit the identification of the (known) double integrator, the input $\hat{u}_r(t)$ will be put through a zero order hold equivalent of a continues time double integrator. In this way the *remaining* dynamics of the system $P_0(q)$ has to be identified only.

As mentioned before, the iterative scheme of filtering and identification, discussed in section 6.2, is performed on the radial $P_{0,11}(q)$ and focus $P_{0,22}(q)$ transfer functions in a SISO configuration. In this way filtering of the prediction error $\varepsilon(t)$ now can be replaced by filtering of input $\hat{u}_r(t)$ and output $y(t)$ of the system to be identified.

Finally, the filters $L_{11}(q)$ and $L_{22}(q)$ arising from the iterative scheme mentioned above, are used to estimate a multivariable Output Error model, using the DUMSI–package. This multivariable model has a 16^{th} order (without the double integrators) and is parametrized using a pseudo canonical (observability) form (Ljung (1987), pp. 119–123), with structure indices (7,9). It should be mentioned that the multivariable model being estimated now, will not be optimal in the sense of the closed loop criterion given in (21), since the choice of the filter $L(q,\rho)$ does not exactly meet the requirements of proposition 6.1. However, the results of this control relevant scheme can be quite illuminating. The results of the multivariable model being estimated can be found in figure 5 and 6.

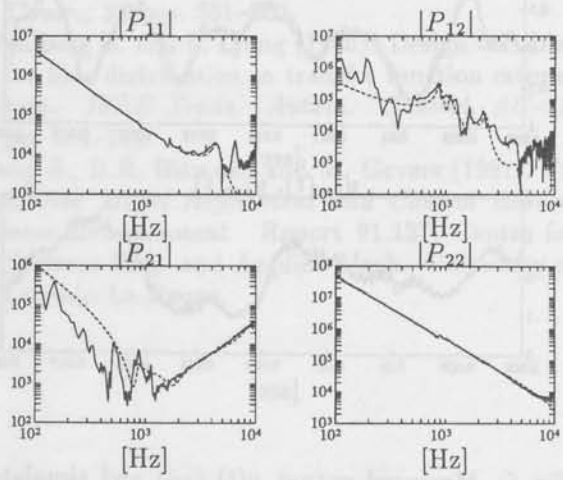

Fig. 5: Amplitude of spectral estimate $\hat{P}(\omega)$ (—) and parametric model $P(e^{i\omega}, \hat{\rho}_N)$ (- -)

Figure 5 presents the amplitude Bode plots of the spectral estimate $\hat{P}(\omega)$, see (23), and the model $P(e^{i\omega}, \hat{\rho}_N)$ being estimated. It can be seen from this figure that there is some parasitic dynamics in the radial transfer function $P_{0,11}(e^{i\omega})$, around 0.9, 1.7, 4 and 6 kHz. Some of these parasitic dynamics only have a small contribution in the *open loop* behaviour of the system and therefore should not have to be estimated. On the other hand, in the closed loop behaviour of the system these parasitic dynamics play an significant role. This is illustrated in figure 3, where one can recognize peaks in the sensitivity function. Clearly, this discussion illustrates the use of a control relevant identification scheme. A part of the simulations, based on closed loop data that has not been used for identification, has been depicted in figure 6. It illustrates that the model $P(e^{i\omega}, \hat{\rho}_N)$ predicts the closed loop data very well.

Given the nominal model $P(q, \hat{\rho}_N)$, the procedure presented in de Vries and Van den Hof (1993) can be used to quantify an additive model error. Using a partly periodic input signal $\hat{u}_r(t)$ and additional information about the decay rate of the impulse response of the system under consideration, an additive model error can be estimated using an Empirical Transfer Function Estimate, see de Vries and Van den Hof (1993) for further details. The results of this procedure, applied to the radial transfer function only, can be found in figure 7.

In figure 7 a part of the Nyquist contour of $C_{11}(q)P_{11}(q, \hat{\rho}_N)$ is depicted, based on the given controller $C_{11}(q)$ of the radial servo loop and the nominal model $P_{11}(q, \hat{\rho}_N)$ of the radial transfer function being estimated. Furthermore, the addi-

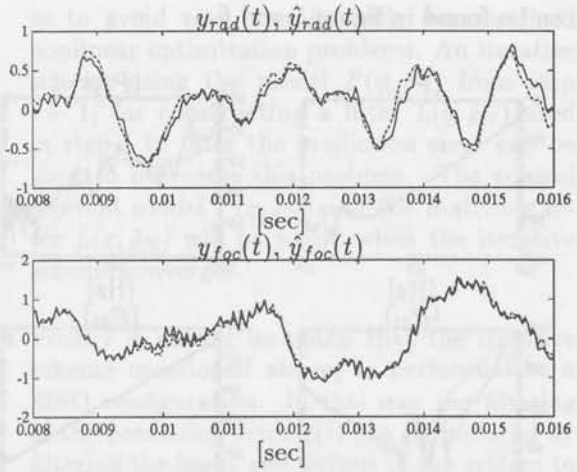

Fig. 6: Measured output $y(t)$ (—) and simulated output $\hat{y}(t)$ (- -) of *rad*ial and *foc*us loop

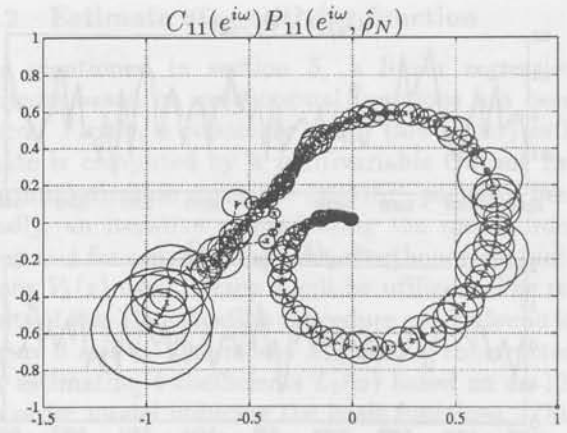

Fig. 7: Nyquist contour of radial servo loop, based on the nominal model $P_{11}(q, \hat{\rho}_N)$ (- -) and uncertainty bounds (—)

tive error bounds on the nominal model are characterized by circles in the complex plane for several frequency points. From figure 7 it can also be seen that the additive model error has been kept small in the closed loop frequency domain of interest (around the bandwidth).

8 Conclusions

In this paper a control relevant parametric identification scheme is applied to a Compact Disc servo system, using the well known Prediction Error methods, wherein the problems of approximate and closed loop identification have been merged. This is done by using a two stage identification algorithm, wherein a simulation of the input signal is used to estimate the system. The two stage algorithm requires an accurate estimate of the input sensitivity of the closed loop system. This can be achieved by employing a linear regression scheme using system based orthonormal functions. The resulting expression for the bias distribution of the model being estimated, is tuned in a control relevant way by choosing appropriate design variables. Using closed loop time domain observations of a Compact Disc pick–up mechanism, this has led to a multivariable discrete time model that can be used for designing an enhanced controller.

9 Acknowledgement

The authors are grateful to Douwe de Vries for his contribution to the experimental part and the estimation of the additive model uncertainty. Furthermore we like to thank Gerrit Schootstra and Jos Mooren of the Philips Research Laboratory for their help and support.

References

Bitmead R.R., M. Gevers and V. Wertz (1990). Interplay between control law selection and closed loop adaption. *Preprints of 11th IFAC World Congress,* Tallin, Estonia USSR, Vol. 4, pp. 202–207.

Bouwhuis, G et al. (1985). *Principles of Optical Disc Systems.* Adam Hilger Ttd.

Dailey R.L. and M.S. Lukich (1988). Recent results in identification and control of a flexible truss structure. *Proc. American Cont. Conf.,* Atlanta, Georgia, USA, pp. 1468–1473.

Draijer W., M. Steinbuch and O.H. Bosgra (1992). Adaptive control of the Radial Servo System of a Compact Disc Player. *Automatica,* Vol. 28, pp. 455–462.

Gevers M.R. and L. Ljung (1986). Optimal experiment design with respect to the intended model application. *Automatica,* Vol. 22, pp. 543–554.

Hakvoort R.G., R.J.P. Schrama and P.M.J. Van den Hof (1992). Approximate Identification in view of LQG Feedback Design. *Proc. Amer. Cont. Conf.,* Chicago, pp. 2824–2828.

Heuberger P.S.C. and O.H. Bosgra (1990). Approximate system identification using system based orthonormal functions. *Proc. 29th IEEE Conf. on Decision and Control,* Honolulu, Hawaii, pp. 1086–1092.

Heuberger P.S.C. (1990). *On Approximate System Identification with System Based Orthonormal Functions.* PhD. Thesis, Delft University of Technology, Mech. Eng. Systems and Control

Group.

Heuberger P.S.C., P.M.J. Van den Hof and O.H. Bosgra (1992). *A Generalized Orthonormal Basis for Linear Dynamical Systems.* Internal Report N–404, Delft University of Technology, Mech. Eng. Systems and Control Group, Submitted for publication. Short version presented at CDC'93.

Lee, W.S., B.D.O. Anderson, R.L. Kosut and I.M.Y. Mareels (1992). On adaptive robust control and control relevant system identification. *Proc. American Control Conf.*, Chicago, IL, pp. 2834-2841.

Liu K. and R.E. Skelton (1990). Closed loop identification and iterative control design. *Proc. 29th IEEE Conf. on Decision and Control,* Honolulu, USA, pp. 482–487.

Ljung L. (1987). *System Identification: Theory for the User.* Prentice Hall Inc., Information and System Sciences Series, Englewood Cliffs.

Maciejowski J.M. (1989). *Multivariable Feedback Design.* Addison–Wesley Publishing Company Inc.

Priestly M.B. (1981). *Spectral Analysis and Time Series.* Academic Press, New York.

Schrama R.J.P. (1992). *Approximate Identification and Control Design with application to a mechanical system.* PhD. Thesis, Delft University of Technology, Mech. Eng. Systems and Control Group.

Schrama R.J.P. (1990). Accurate models for control design: the necessity of an iterative scheme. *IEEE Trans. Automat. Contr.,* AC–37, pp. 991–994.

Schrama R.J.P. and P.M.J. Van den Hof (1992). An iterative scheme for identification and control design based on coprime factorizations. *Proc. American Control Conf.*, Chicago, IL, pp. 2842-2846.

Steinbuch M., G. Schootstra and O.H. Bosgra (1992). Robust Control of a Compact Disc Player. *Proc. 31st IEEE Conf. on Decision and Control,* pp. 2596–2600, Tucson, Arizona.

Van den Hof, P.M.J and R.J.P. Schrama (1993). An Indirect Method for Transfer Function Estimation from Closed Loop Data. *Automatica,* Vol. 28, no. 6, November 1993.

Vries de D.K. and P.M.J. Van den Hof (1993). Quantification of Uncertainty in Transfer Function Estimation: a mixed deterministic–probabilistic approach. *Proc. 12th IFAC World Congress*, Sydney, Australia, Vol. 8, pp. 157-160.

Wahlberg, B. (1990). *On the Use of Orthogonalized Exponentials in System Identification.* Report LiTH-ISY-1099, Dept. Electr. Eng., Linköping University, Sweden.

Wahlberg, B. (1991). System Identification using Laguerre Models. *IEEE Trans. Automat. Contr., 36.* pp. 551–562.

Wahlberg B. and L. Ljung (1986). Design variables for bias distribution in transfer function estimation. *IEEE Trans. Autom. Control, AC–31,* pp. 134–144.

Zang Z., R.R. Bitmead and M. Gevers (1991). *Iterative Model Refinement and Control Robustness Enhancement.* Report 91.137, Centre for Systems Eng. and Applied Mech., University of Louvain-La-Neuve.

Selected Topics in Identification, Modelling and Control
Vol. 6, December 1993

Consistent parameter bounding identification for linearly parametrized model sets

Richard G. Hakvoort and Paul M.J. Van den Hof

Mechanical Engineering Systems and Control Group
Delft University of Technology, Mekelweg 2, 2628 CD Delft, The Netherlands.

Abstract. In parameter bounding identification, a time–domain bound on the noise signal is the basic prior that determines the resulting feasible parameter set. One of the properties of this approach is that no consistency occurs if the noise bound is chosen conservative.
By introducing alternative bounds on the noise signal, it is shown that parameter bounding identification methods result that under fairly general conditions exhibit the property of consistency, i.e. asymptotically in the number of data samples the feasible parameter set converges to the true parameter.
As alternative prior, a bound on the cross–covariance between the noise and some instrumental (input) signal is introduced. The noise bound is represented by a small number of linear inequalities, which can be employed in parameter bounding by linear programming. It is shown that consistency is achieved even when the bound is chosen conservative. Additionally a procedure is presented to estimate the cross–covariance bound from data.
Similar consistency results are shown for another type of noise prior: a bound on the discrete Fourier transform of the noise, in combination with sinusoidal excitation.

Keywords. system identification, discrete time systems, linear programming, convergence analysis, probability

1 Introduction

The literature on set membership, bounded error or parameter bounding identification is quite extensive by now. See Walter and Piet–Lahanier (1990) and Milanese and Vicino (1991) for overviews on this topic. The idea is to calculate a parameter set of minimal size using measurement data and certain deterministic bounds on the noise. To clarify the discussion consider the discrete–time linear regression model

$$y(t) = \phi^T(t)\theta + e(t),\ t = 1, \ldots, N,$$

where $y(t)$ is the measured output at time t, $\phi(t)$ the $n \times 1$ regression vector, θ the $n \times 1$ parameter vector, $e(t)$ the equation error or residual and N the number of samples. This linear regression model can describe a large class of systems, including multi input single output and nonlinear systems. The observations are assumed to be generated by

$$y(t) = \phi^T(t)\theta_0 + e_0(t),\ t = 1, \ldots, N, \qquad (1)$$

with $\{e_0(t)\}$ an unknown stochastic noise process. It is emphasized that $\{e_0(t)\}$ is not assumed to be white noise or uncorrelated to the regression vector $\{\phi(t)\}$. Hence the data may be generated in closed loop and the regression vector may contain samples of the output signal $\{y(t)\}$. Basically $\{e_0(t)\}$ may also account for undermodelling, however in this paper undermodelling will not be considered.

In parameter bounding identification the param-

eter vector θ is bounded on the basis of certain bounds on $\{e(t)\}$. The most common procedure is to bound the amplitude of the residuals in the time domain,

$$e_l(t) \leq e(t) \leq e_u(t),\ t = 1, \ldots, N, \qquad (2)$$

see e.g. Walter and Piet–Lahanier (1990). The feasible parameter set is then defined as

$$\Theta_N = \Big\{\theta \mid e_l(t) \leq y(t) - \phi^T(t)\theta \leq e_u(t),$$

$$t = 1, \ldots, N\Big\}.$$

Next an orthotopic outer bounding parameter set can be constructed by calculating

$$\theta_k^{(l)} = \min_{\theta \in \Theta_N} \theta_k,\ \theta_k^{(u)} = \max_{\theta \in \Theta_N} \theta_k, \qquad (3)$$

for $k = 1, \ldots, n$, which requires solving $2n$ linear programming problems with n unknowns subject to $2N$ linear inequality constraints, see Milanese and Belforte (1982) for details. If $\{e_0(t)\}$ also satisfies the residual bounds (2), then the parameter vector θ_0 is guaranteed to be in the identified set.

Fogel and Huang (1982) and Veres and Norton (1991) have shown that under certain conditions the outer bounding parameter set converges to θ_0 if $N \to \infty$, provided the noise $\{e_0(t)\}$ is at sufficiently many time instants arbitrarily close to the specified noise bounds, without exceeding them. However it seems impossible to meet this requirement in many practical situations. In practice the noise bounds have to be chosen conservative in order to guarantee their correctness. Therefore in general there is no consistency in parameter bounding identification. A similar situation is encountered in the field of robust identification in H_∞, see e.g. Helmicki *et al.* (1991) and Gu and Khargonekar (1992). There deterministic bounds on the noise are assumed, and basically only consistency is established under the condition that the noise level tends to zero. This highlights the demerit of only using the bounds (2). The explanation for this lack of consistency in the presence of noise is that the noise is assumed to be able to take a worst–case realization within the noise bounds, i.e. heavily correlated with the input signal.

For prediction error type of identification procedures it is known that if the number of data samples tends to infinity the parameter estimate converges to the true parameter vector θ_0 under fairly general conditions, also for nonzero noise, see e.g. Ljung (1987). This is due to the fact that stochastic or averaging properties are present in this identification setting. The objective of this paper is to adjust the parameter bounding identification such that a similar consistency property is obtained in the presence of noise. This is achieved by introducing alternative noise bounds, which have a stochastic interpretation. A basic motivation for using the noise bounds (2) is that for small data sets, N small, stochastic assumptions on the noise may not be justifiable. However if large data sets are available stochastic noise assumptions often can be justified, in which case the noise characterization (2) is overly pessimistic.

Stochastics have already been introduced into parameter bounding identification by Fogel and Huang (1982), where basically a stochastic interpretation is given for the noise bounds (2). In Veres and Norton (1989) the situation is considered that the noise has a bounded auto–covariance, or cross–covariance with a specified signal, but only for the purpose of model structure selection. Fogel (1979) considers bounds on the energy of the noise, but this neither leads to consistency.

In this paper a cross–covariance bound on the noise is introduced into parameter bounding identification as an alternative for the standard time–domain bound on the noise (2). The sample covariance between the residuals and some given signal is bounded. Typically this signal is chosen such that it is correlated to the input signal, but uncorrelated to the noise process. In an open loop experimental situation the (filtered) input signal meets the specifications. In closed loop operation some external reference signal can be taken. The cross–covariance noise bounds can be represented by a small number of linear inequalities, which can be used to calculate an outer bounding parameter set by means of linear programming, similar to (3). Sufficient conditions are derived which make the feasible parameter region converge to the parameter vector θ_0. These conditions are very general, basically only persistence of excitation is required, and it is not required that the specified bounds are tight. A stochastic interpretation is given of the cross–covariance bounds on the noise. Also a procedure is presented to estimate correct bounds from measurement data.

Similar consistency results appear obtainable with other types of noise bounds, which also give rise to linear constraints usable in parameter bounding identification with linear programming techniques. A frequency–domain bound on the noise is introduced into parameter bounding identification. More specifically the amplitude of the discrete Fourier transform of the residuals, the square–root of its periodogram, is bounded for a set of specified frequencies. This bound is also utilized

in frequency–domain identification procedures, see Lamaire *et al.* (1991) and De Vries and Van den Hof (1992). As parameter bounding identification adopts a time–domain setting, the bound requires a translation into linear constraints in the time domain, which is presented in this paper. A stochastic analysis of the noise bound is presented, as well as sufficient conditions for consistency.

Finally similar results appear obtainable for a time–domain bound on the noise in combination with measurement averaging and periodic excitation. However, due to space limitations this will not be discussed in this paper. The interested reader is referred to Hakvoort and Van den Hof (1993).

The outline of the paper is as follows. In Section 2 the cross–covariance bound on the noise is elaborated and consistency results are derived. In Section 3 it is discussed how to estimate noise bounds from data in a statistically reliable way. In Section 4 the frequency–domain bound on the noise is considered. In Section 5 a simulation example is shown. Finally in Section 6 conclusions are drawn.

This paper is a version of Hakvoort *et al.* (1993). Due to space limitations all proofs are omitted. These can be found in Hakvoort and Van den Hof (1993).

2 Cross–Covariance Constraints on the Noise

First the cross–covariance constraints on the noise are introduced into parameter bounding identification. Consider the following linear constraints,

$$c_l(p) \leq \frac{1}{\sqrt{N}} \sum_{t=1}^{N} r_p(t) e(t) \leq c_u(p), \; p = 1, \ldots, s, \tag{4}$$

yielding the feasible parameter set,

$$\Theta_N = \left\{ \theta \,|\, c_l(p) \leq \frac{1}{\sqrt{N}} \sum_{t=1}^{N} r_p(t)(y(t) - \phi^T(t)\theta) \leq \right.$$
$$\left. \leq c_u(p), \; p = 1, \ldots, s \right\}, \tag{5}$$

where $c_l(p)$ and $c_u(p)$ are specified bounds, and $\{r_p(t)\}$ is some specified signal, typically equal to a delayed and/or filtered signal that is correlated to the regression vector $\{\phi(t)\}$ but uncorrelated to the noise process $\{e_0(t)\}$, as explained later. The constraints (4) restrict the set of accepted residuals, and therefore the feasible parameter set. As the constraints in (5) are linear in the parameter vector θ they can easily be included in the linear programming problems (3).

Of course it is desirable to specify the bounds $c_l(p)$ and $c_u(p)$ on the sample covariance of the residuals with the signals $\{r_p(t)\}$ such that they are satisfied by the true noise process $\{e_0(t)\}$. Analogously to the noise bounds (2) it is possible to consider the bounds (4) as being entirely deterministic, which then does not require the noise being looked upon as a stochastic process. However it appears that a nice probabilistic interpretation of the bounds (4) exists if the noise process $\{e_0(t)\}$ has some stochastic properties, which can often be justified in practical situations. In fact (4) then boils down to the assumption that the noise process $\{e_0(t)\}$ is uncorrelated to the signals $\{r_p(t)\}$. For the analysis some technical assumptions on the signals $\{e_0(t)\}$, $\{r_p(t)\}$ and $\{\phi(t)\}$ are needed. The assumptions about $\{e_0(t)\}$ are:

Assumption 2.1 *The noise process $\{e_0(t)\}$ is stationary, satisfying $e_0(t) = H_0(q)w_0(t)$ for some stable $H_0(q)$, and where $\{w_0(t)\}$ is a sequence of independent random variables with zero mean values, variances λ_0, and bounded fourth moments.*

The assumptions about $\{r_p(t)\}$ are:

Assumption 2.2 *Each signal $\{r_p(t)\}$ is quasi–stationary, i.e. its auto–covariance function*

$$R_{r_p}(\tau) = \lim_{N\to\infty} \frac{1}{N} \sum_{t=1}^{N} E r_p(t+\tau) r_p(t)$$

exists $\forall \tau$. Moreover $\{r_p(t)\}$ satisfies

$$r_p(t) = \bar{r}_p(t) + R_p(t,q)\tilde{r}_p(t),$$

where $\{\bar{r}_p(t)\}$ is a bounded deterministic signal, $\{R_p(t,q),\ t = 1,2,\ldots\}$ is a uniformly stable family of filters, and $\{\tilde{r}_p(t)\}$ is a sequence of independent random variables with zero mean values, variances $\lambda_{p,t}$, and bounded fourth moments.

The assumptions about $\{\phi(t)\}$ are:

Assumption 2.3 *Each signal $\{\phi_k(t)\}$, this is element k of vector $\phi(t)$, is quasi–stationary and it satisfies*

$$\phi_k(t) = \bar{\phi}_k(t) + S_k(t,q)\tilde{\phi}_k(t),$$

where $\{\bar{\phi}_k(t)\}$ is a bounded deterministic signal, $\{S_k(t,q),\ t = 1,2,\ldots\}$ is a uniformly stable family of filters, and $\{\tilde{\phi}_k(t)\}$ is a sequence of independent random variables with zero mean values, variances $\mu_{k,t}$, and bounded fourth moments.

And the assumptions about joint properties of $\{r_p(t)\}$ and $\{\phi_k(t)\}$ are:

Assumption 2.4 *For each p and k the signals $\{r_p(t)\}$ and $\{\phi_k(t)\}$ are jointly quasi-stationary, i.e. they are both quasi-stationary, and the cross-covariance function*

$$R_{r_p\phi_k}(\tau) = \lim_{N\to\infty} \frac{1}{N}\sum_{t=1}^{N} Er_p(t+\tau)\phi_k(t)$$

exists. Moreover the signal $\begin{bmatrix} \tilde{r}_p(t) \\ \tilde{\phi}_k(t) \end{bmatrix}$ *has covariances $\nu_{p,k,t}$ and bounded fourth moments.*

Using these assumptions a stochastic interpretation of the constraints (4) can be established. In this interpretation the notion of uncorrelation is strengthened to independence.

Theorem 2.5 *Suppose that $\{e_0(t)\}$ and $\{r_p(t)\}$ are independent and that they satisfy the assumptions 2.1 and 2.2 respectively. Denote*

$$\Lambda_p^N := E\left(\frac{1}{\sqrt{N}}\sum_{t=1}^{N} r_p(t)e_0(t)\right)^2,$$

$$\Lambda_p := \lim_{N\to\infty} \Lambda_p^N,$$

and

$$R_{r_p}^N(\tau) := \frac{1}{N-|\tau|}\sum_{t=1}^{N-|\tau|} Er_p(t)r_p(t+|\tau|),$$

$$\tau = -N+1,\ldots,N-1.$$

Then

$$\text{(i)}\ \ \Lambda_p^N = \sum_{\tau=-N+1}^{N-1} \frac{N-|\tau|}{N} R_{r_p}^N(\tau)R_{e_0}(\tau),$$

$$\text{(ii)}\ \ \Lambda_p = \sum_{\tau=-\infty}^{\infty} R_{r_p}(\tau)R_{e_0}(\tau),$$

$$\text{(iii)}\ \ \frac{1}{\sqrt{N}}\sum_{t=1}^{N} r_p(t)e_0(t) \overset{N\to\infty}{\longrightarrow} \mathcal{N}(0,\Lambda_p),$$

where $\mathcal{N}(0,\Lambda_p)$ denotes the normal distribution with mean 0 and variance Λ_p.

On the one hand the bound (4) is a hard or deterministic bound, on the other hand a probabilistic interpretation has been given in the above theorem. Note that due to the normalization factor $\frac{1}{\sqrt{N}}$ in (iii) the asymptotic distribution is independent of N. For example asymptotically in N a 0.9995 probability region is obtained by choosing $c_u(\tau) = -c_l(\tau) = 3.5\sqrt{\Lambda_p}$. The theorem also states that Λ_p can be evaluated by considering the second order statistics of $\{r_p(t)\}$ and $\{e_0(t)\}$ separately. The second order statistics of the signals $\{r_p(t)\}$ will generally be known exactly, the statistics of the noise process $\{e_0(t)\}$ have to be estimated from data. How to estimate these statistics is the subject of Section 3. Note that the parts (ii) and (iii) of Theorem 2.5 have been stated in Ljung (1987, Pr. 16T.1) without proof.

The covariance bound (4) is especially useful if $\{r_p(t)\}$ is a signal that is correlated to the regression vector sequence $\{\phi(t)\}$, but uncorrelated to the noise $\{e_0(t)\}$. This follows from the following consistency result.

Theorem 2.6 *Suppose that the signal $\{e_0(t)\}$ satisfies the constraints (4) for given signals $\{r_p(t)\}$, $p = 1,\ldots,s$, and given and finite $c_l(p)$ and $c_u(p)$. Suppose that $\{r_p(t)\}$ and $\{\phi_k(t)\}$ satisfy the assumptions 2.2, 2.3 and 2.4. If the matrix*

$$R = \begin{bmatrix} R_{r_1\phi_1}(0) & \cdots & R_{r_1\phi_n}(0) \\ \vdots & & \vdots \\ R_{r_s\phi_1}(0) & \cdots & R_{r_s\phi_n}(0) \end{bmatrix}$$

has full column rank, then the feasible parameter region (5) converges to the true parameter vector θ_0,

$$\lim_{N\to\infty} \max_{\theta\in\Theta_N} |\theta - \theta_0| = 0.$$

This theorem thus provides a consistency result for bounded error identification without requiring tight error bounds. If the values $c_u(p)$ and $c_l(p)$ in (4) are chosen too large, convergence will still take place. The cross-covariance noise bounds possess a certain averaging property which is not present in standard parameter bounding identification with time-domain noise bounds.

Though the bounds may be chosen conservative, they are required to be correct for the convergence result to hold. Theorem 2.5 shows that the bounds in (4) can be chosen such that they will be correct with any prespecified probability. For this theorem to be applicable it is necessary that the signals $\{r_p(t)\}$ are independent of the noise $\{e_0(t)\}$. The other conditions of Theorem 2.6 are not very restrictive. Generally the matrix R will have full column rank provided the signals $\{r_p(t)\}$ have been chosen suitably, i.e. correlated with the regression vector $\{\phi(t)\}$. If identification takes place in open loop the (filtered and/or delayed) input signal is a suitable choice. If identification takes place in closed loop a (filtered and/or delayed) external reference signal has the desired properties. Moreover a necessary condition for the matrix R to have full column rank is that the identification experiment was sufficiently informative. Note that no assumptions on the distribution or colour of the noise

$\{e_0(t)\}$ have been made. However for Theorem 2.5 to be applicable it has to be stationary and independent of the signal $\{r_p(t)\}$.

Remark 2.7 *Note that the use of cross–covariance bounds is closely related to the instrumental variable identification method, see Söderström and Stoica (1989, Ch. 8). In fact the signals $\{r_p(t)\}$ can be regarded as instrumental variables. Also note the close connection of the consistency result of Theorem 2.6 to consistency for instrumental variable identification techniques, see Ljung (1987, Ch. 8). In the present parameter bounding identification setting as well as the instrumental variable identification setting, consistency has been shown under fairly general conditions. For example in both cases there is still consistency if the input signal is correlated to the noise process (closed loop identification), or in case the true system has an output error structure whereas the model is parametrized as a linear regression.*

3 Estimating the Cross–Covariance Bounds from Data

In bounded error identification an a priori specification of noise bounds is required. In case time–domain noise constraints (2) are used the bounds $e_l(t)$ and $e_u(t)$ need to be specified. In case cross–covariance noise constraints (4) are used the bounds $c_l(p)$ and $c_u(p)$ need to be specified. It may be possible that these bounds are known a priori, e.g. from physical laws. However it is not at all imaginary that this is not the case, and that measurement data have to be used to establish the noise bounds. Unfortunately, in the parameter bounding literature very little attention is paid to the problem of estimating the noise bounds from data.

In this section the problem is considered of estimating appropriate cross–covariance bounds from data. Theorem 2.5 shows that this boils down to estimating Λ_p^N, which is related to the second order noise statistics. If knowledge of the noise statistics is not available from physical contemplations about the process, measurements have to be used to estimate these. This is a valid procedure if the noise is stationary, i.e. the statistical properties do not change in time. In that case any measurement sequence may be used to estimate the noise statistics. The estimated statistics will then remain to hold for the measurement sequence used in the parameter bounding identification procedure.

Notice that if an exact value for Λ_p^N is not obainable, an upper bound is still of use. If Λ_p^N is overestimated, the resulting noise bounds $c_l(p)$ and $c_u(p)$ are conservative but correct (with a certain specified probability), and the resulting feasible parameter region will be correct, i.e. will contain the true parameter vector. Even if the noise bounds are chosen conservative, the consistency result given in Theorem 2.6 remains valid.

Suppose that there is available a measurement sequence generated by (1). As mentioned above this need not be the same measurement sequence as the one used in the parameter bounding identification procedure, it may be an independent data set. In this section it is assumed that the regression process $\{\phi(t)\}$ is uncorrelated to the noise process $\{e_0(t)\}$. This implies that measurements have to take place in open loop and that the regression vector may only contain filtered and/or delayed samples of the input signal, as the output signal is disturbed by noise. This does not necessarily imply a restriction to FIR identification. Also identification with Laguerre polynomials (Wahlberg, 1991), and identification with generalized orthonormal polynomials (Heuberger and Bosgra, 1990; Heuberger *et al.*, 1992) fit in this setting. Let there be available a nominal model $\hat{\theta}$, which has been obtained independently of the given data set, but for example by physical modelling or identification based on another dataset. The prediction or output error $\hat{e}(t)$ for this nominal model $\hat{\theta}$ is given by

$$\hat{e}(t) := y(t) - \phi^T(t)\hat{\theta} = \psi(t) + e_0(t), \qquad (6)$$

with

$$\psi(t) := \phi^T(t)(\theta_0 - \hat{\theta}).$$

The idea is to use this prediction error in order to estimate the second order statistics of the noise process. First some technical assumptions are made with respect to the signal $\psi(t)$.

Assumption 3.1 *The signal $\{\psi(t)\}$ is quasi–stationary and it satisfies*

$$\psi(t) = \bar{\psi}(t) + P(t,q)\bar{\psi}(t),$$

where $\{\bar{\psi}(t)\}$ is a bounded deterministic signal, $\{P(t,q),\ t = 1,2,\ldots\}$ is a uniformly stable family of filters, and $\{\tilde{\psi}(t)\}$ is a sequence of independent random variables with zero mean values, variances μ_t, and bounded fourth moments. Moreover the auto–covariance function of the signal $\{\psi(t)\}$ is exponentially decaying, i.e. $R_\psi(\tau) \leq M\rho^\tau$, $\forall\tau$, for certain finite M and $\rho < 1$.

Next denote

$$\hat{R}_{\hat{e}}^N(\tau) := \frac{1}{N - |\tau|} \sum_{t=1}^{N-|\tau|} \hat{e}(\tau)\hat{e}(t + |\tau|),$$

and consider the following estimate for Λ_p^N,

$$\hat{\Lambda}_p^N = \sum_{\tau=-w(N)}^{w(N)} c_w(\tau)\frac{N-|\tau|}{N} R_{r_p}^N(\tau)\hat{R}_{\hat{e}}^N(\tau), \quad (7)$$

where $c_w(\tau)$ is a window–function, similar to the ones used in spectral analysis, see Ljung (1987, Ch. 6). In the analysis use will be made of the so–called Tukey–window (Brillinger, 1981, p. 55), given by

$$c_w(\tau) =$$

$$\begin{cases} 1, & 0 \le |\tau| \le fw(N) \\ \frac{1}{2}+\frac{1}{2}\cos\left(\frac{\pi}{1-f}\left(\frac{|\tau|}{w(N)}-f\right)\right), & fw(N) < |\tau| < w(N) \\ 0, & |\tau| \ge w(N) \end{cases} \quad (8)$$

for some constants $0 < f < 1$ and $0 < w(N) < N$, such that

$$\lim_{N\to\infty} w(N) = \infty, \ \lim_{N\to\infty} \frac{w(N)}{N} = 0. \quad (9)$$

Notice that the quantities $R_{r_p}^N(\tau)$ appearing in the estimate $\hat{\Lambda}_p^N$ are assumed to be known precisely. This is a realistic situation, as the signals $\{r_p(t)\}$ are generally user–determined. These signals may be deterministic, and completely known, or stochastic, with known second order statistics, or mixed deterministic–stochastic, with given auto–covariance function. The following theorem states that the given estimate $\hat{\Lambda}_p^N$ asymptotically over-bounds Λ_p^N.

Theorem 3.2 *Consider Λ_p^N as given in part (i) of Theorem 2.5, and the estimate $\hat{\Lambda}_p^N$ defined in (7) with the window specified by (8) and (9). Suppose that $\{e_0(t)\}$ satisfies assumption 2.1, $\{r_p(t)\}$ assumption 2.2, and $\{\psi(t)\}$ assumption 3.1. Moreover suppose that the regression process $\{\phi(t)\}$ is uncorrelated to $\{e_0(t)\}$, and that the estimate $\hat{\theta}$ used in (6) has been established independently of the noise process $\{e_0(t)\}$. Then,*

$$\text{(i)} \ \lim_{N\to\infty} \hat{\Lambda}_p^N = \Lambda_p + \sum_{\tau=-\infty}^{\infty} R_{r_p}(\tau)R_\psi(\tau),$$

with probability 1.

$$\text{(ii)} \ \sum_{\tau=-\infty}^{\infty} R_{r_p}(\tau)R_\psi(\tau) \ge 0,$$

Hence, asymptotically correct cross–covariance bounds $c_l(p)$ and $c_u(p)$ can be established as the estimated variance $\hat{\Lambda}_p^N$ is overbiased. The conservatism decreases if the nominal model $\hat{\theta}$ becomes a more accurate description of the true system θ_0.

In the special case that the system had not been excited, implying $\phi(t)$ to be equal to zero, the signal $\psi(t)$ vanishes, and $\hat{e}(t)$ equals $e_0(t)$, yielding an asymptotically unbiased estimate for the noise statistics.

Remark 3.3 *For finite N the estimate $\hat{\Lambda}_p^N$ has a nonzero variance as well. In fact it is a kind of spectral estimate, for which it has been shown in Ljung (1987, p. 160) that the variance is asymptotically linearly proportional to $\frac{w(N)}{N}$, which tends to zero. Hence the variance becomes negligible for N large enough.*

Remark 3.4 *The most severe restriction in Assumption 3.1 is that $R_\psi(\tau)$ is exponentially decaying. This means that $\psi(t)$, and hence $\hat{e}(t)$, may not contain undecaying deterministic components such as sinusoids. If they are present in the prediction error, they can be detected and removed from the signal, e.g. by taking the DFT of the prediction error, removing the peak–values, and taking the inverse DFT of the remaining part. Notice that asymptotically this will not influence the contribution of $\{e_0(t)\}$ to $\{\hat{e}(t)\}$.*

Remark 3.5 *It is desirable to introduce as little conservatism as possible when establishing the noise bounds $c_l(p)$ and $c_u(p)$, in order to avoid that unnecessarily large parameter sets are identified in the parameter bounding identification procedure. Part (ii) of Theorem 3.2 shows that asymptotically the estimate $\hat{\Lambda}_p^N$ upper bounds Λ_p^N. As mentioned only in the special case that $\hat{e}(t)$ equals $e_0(t)$ the estimate is unbiased, yielding minimal conservatism. However there is another special situation where it is possible to derive a non–conservative estimate of the noise statistics, with a procedure different from the one described above. This is the case if a repeated experiment has been performed, i.e. if*

$$\phi(t+T) = \phi(t), \ t = 1, \ldots, T,$$

for some period time T. If the regression vector only contains (filtered) samples of the input, this is realized by applying a periodic input signal. Now consider the signal

$$\epsilon(t) := (y(t+T) - y(t))/\sqrt{2}, \ t = 1, \ldots, T,$$

which with (1) can be written as

$$\epsilon(t) = (\phi(t+T)-\phi(t))\theta_0/\sqrt{2}+(e_0(t+T)-e_0(t))/\sqrt{2}$$
$$= (e_0(t+T) - e_0(t))/\sqrt{2}.$$

The signal $\varepsilon(t)$ actually appears to have second order statistics identical to those of the noise process $e_0(t)$ (in the asymptotic case $T \to \infty$). Also if the regression process is not perfectly periodic, e.g. due to different initial conditions, the given signal $\varepsilon(t)$ can still be used to estimate the second order noise statistics of $e_0(t)$. Using an argument similar to the one used in Theorem 3.2 it can be shown that the estimate $\hat{\Lambda}_p^N$ will then be overbiased, yielding correct bounds $c_l(p)$ and $c_u(p)$.

4 Frequency–Domain Constraints on the Noise

It appears that consistency results in parameter bounding identification, similar to those of Theorem 2.6, can be obtained with another type of noise constraint. This concerns a frequency–domain bound on the noise. Consider the function $E(\omega_j)$ defined by

$$E(\omega_j) := \frac{1}{\sqrt{N}} \sum_{t=1}^{N} e(t) e^{-i\omega_j t}, \qquad (10)$$

which for $\omega_j = 2\pi j/N$, $j = 1, \ldots, N$, is the discrete Fourier transform of the sequence $\{e(1), \ldots, e(N)\}$. With some abuse of terminology $E(\omega_j)$ will be called the discrete Fourier transform of the signal $\{e(t)\}$, no matter what ω_j is, and keeping in mind that it is dependent on N. By bounding its amplitude, the square root of the so–called periodogram, the residuals are bounded in the frequency domain. Consider the constraints,

$$|E(\omega_j)| \leq f(\omega_j), \ \omega_j \in [0, \pi], \ j = 1, \ldots, l,$$

for some specified bounds $f(\omega_j)$. This type of noise constraint is also used in Lamaire *et al.* (1991) and De Vries and Van den Hof (1992) in a frequency–domain identification setting. Substituting $e(t) = y(t) - \phi^T(t)\theta$ gives the feasible parameter set,

$$\Theta_N = \left\{ \theta \,|\, \left| \frac{1}{\sqrt{N}} \sum_{t=1}^{N} (y(t) - \phi^T(t)\theta) e^{-i\omega_j t} \right| \leq f(\omega_j), \right.$$
$$\left. \omega_j \in [0, \pi], \ j = 1, \ldots, l, \right\}.$$

If parameter outer bounding by linear programming is carried out, linear constraints are required. However, the constraints given above are nonlinear due to the fact that the DFT is a complex quantity. Fortunately it appears possible to approximate each nonlinear constraint by a number of linear constraints. Consider the following linear constraints,

$$f_l(\omega_j, \alpha_{k'}) \leq \frac{1}{\sqrt{N}} \sum_{t=1}^{N} e(t) \cos(\omega_j t - \alpha_{k'}) \leq f_u(\omega_j, \alpha_{k'}), \qquad (11)$$

$\omega_j \in [0, \pi]$, $j = 1, \ldots, l$, $\alpha_{k'} \in [0, \pi]$, $k' = 1, \ldots, m$, yielding the feasible parameter set,

$$\Theta_N = \left\{ \theta \,|\, f_l(\omega_j, \alpha_{k'}) \leq \right.$$
$$\leq \frac{1}{\sqrt{N}} \sum_{t=1}^{N} \cos(\omega_j t - \alpha_{k'})(y(t) - \phi^T(t)\theta) \leq$$
$$f_u(\omega_j, \alpha_{k'}), \ \omega_j \in [0, \pi], \ j = 1, \ldots, l,$$
$$\left. \alpha_{k'} \in [0, \pi], \ k' = 1, \ldots, m \right\}, \qquad (12)$$

where $f_l(\omega_j, \alpha_{k'})$ and $f_u(\omega_j, \alpha_{k'})$ are specified bounds, ω_j specified frequencies and $\alpha_{k'}$ specified phase shifts. As the constraints in (12) are linear in the parameter vector θ they can easily be included in linear programming problems like the ones in (3).

The relation of the constraints (11) to the amplitude of the DFT of $\{e(t)\}$ is investigated. This amplitude can be written as

$$\begin{aligned} |E(\omega_j)| &= \left| \frac{1}{\sqrt{N}} \sum_{t=1}^{N} e(t) e^{-i\omega_j t} \right| = \\ &= \max_{\alpha \in [0, 2\pi]} \mathrm{Re} \left(e^{i\alpha} \frac{1}{\sqrt{N}} \sum_{t=1}^{N} e(t) e^{-i\omega_j t} \right) = \\ &= \max_{\alpha \in [0, 2\pi]} \frac{1}{\sqrt{N}} \sum_{t=1}^{N} e(t) \mathrm{Re} \left(e^{-i\omega_j t + \alpha} \right) = \\ &= \max_{\alpha \in [0, 2\pi]} \frac{1}{\sqrt{N}} \sum_{t=1}^{N} e(t) \cos(\omega_j t - \alpha), \end{aligned}$$

which shows that the bound (11) approximates the bound on $|E(\omega_j)|$. The approximation improves if more phase shifts $\alpha_{k'}$ are used. This is formalized in the next proposition.

Proposition 4.1 *Let $E(\omega_j)$ be defined by (10) and $\alpha_{k'}$ be given by $\alpha_{k'} = \pi k'/m$, $k' = 1, \ldots, m$, then*

$$\max_{k'} \left| \frac{1}{\sqrt{N}} \sum_{t=1}^{N} e(t) \cos(\omega_j t - \alpha_{k'}) \right| \leq |E(\omega_j)| \leq$$
$$\leq \frac{\max_{k'} \left| \frac{1}{\sqrt{N}} \sum_{t=1}^{N} e(t) \cos(\omega_j t - \alpha_{k'}) \right|}{\cos(\frac{\pi}{2m})}.$$

Hence this proposition states that (11) bounds the amplitude of the residuals $\{e(t)\}$ in the frequency domain. This apparently boils down to excluding the residuals to contain sinusoids with the specified frequencies ω_j, $j = 1, \ldots, l$. For $\omega_j = 0$ (11) is a bound on the mean value of the residuals.

The frequency–domain bounds on the noise are especially useful if the system is excited by sinusoids. This follows from the following consistency result.

Theorem 4.2 *Suppose that the signal $\{e_0(t)\}$ satisfies the constraints (11) for given and finite $f_l(\omega_j, \alpha_{k'})$ and $f_u(\omega_j, \alpha_{k'})$, $j = 1, \ldots, l$, $\alpha_{k'} = \pi k'/m$, $k' = 1, \ldots, m \geq 2$. Suppose that $\{\phi_k(t)\}$ satisfies assumption 2.3. Denote for each j and k,*

$$\Psi_k(\omega_j) := \lim_{N\to\infty} \frac{1}{N} \sum_{t=1}^{N} E\phi_k(t) e^{-i\omega_j t}.$$

If the matrix

$$\Psi = \begin{bmatrix} \mathrm{Re}\,(\Psi_1(\omega_1)) & \cdots & \mathrm{Re}\,(\Psi_n(\omega_1)) \\ \vdots & & \vdots \\ \mathrm{Re}\,(\Psi_1(\omega_l)) & \cdots & \mathrm{Re}\,(\Psi_n(\omega_l)) \\ \mathrm{Im}\,(\Psi_1(\omega_1)) & \cdots & \mathrm{Im}\,(\Psi_n(\omega_1)) \\ \vdots & & \vdots \\ \mathrm{Im}\,(\Psi_1(\omega_l)) & \cdots & \mathrm{Im}\,(\Psi_n(\omega_l)) \end{bmatrix}$$

has full column rank, then the feasible parameter region (12) converges to the true parameter vector θ_0,

$$\lim_{N\to\infty} \max_{\theta\in\Theta_N} |\theta - \theta_0| = 0.$$

Again this is a consistency result for bounded error identification without requiring tight error bounds. If the values $f_l(\omega_j, \alpha_{k'})$ and $f_u(\omega_j, \alpha_{k'})$ are chosen too large, convergence will still take place under the conditions given.

Remark 4.3 *In general $\Psi_k(\omega_j)$ is unequal to zero if $\{\phi_k(t)\}$ contains a sinusoid with frequency ω_j. A sinusoid $s(t) = a\sin(\omega_j t + \phi)$ namely has the well-known property that its periodogram is unbounded, as the following relation holds,*

$$\lim_{N\to\infty} \frac{1}{N} \sum_{t=1}^{N} s(t) e^{-i\omega_j t} =$$

$$= \begin{cases} \frac{a}{2}(\sin(\phi) - i\cos(\phi)), & \omega_j \in (0, \pi), \\ a\sin(\phi), & \omega = 0, \pi. \end{cases}$$

Hence the consistency result of Theorem 4.2 will only hold if the system has been excited by a sum of at least $n/2$ sinusoids. This type of excitation has also been exploited by De Vries and Van den Hof (1992) and Bayard (1992).

It is desirable to specify the bounds $f_l(\omega_j, \alpha_{k'})$ and $f_u(\omega_j, \alpha_{k'})$ such that they are satisfied by the true noise process $\{e_0(t)\}$. The bounds (11) may be regarded as entirely deterministic, which does not require any stochastic assumptions about the noise. However analogously to the bounds (4) a nice probabilistic interpretation exists in case the noise has some stochastic properties. In the following proposition probabilistic properties of the periodogram of the noise are evaluated.

Proposition 4.4 *Suppose that $\{e_0(t)\}$ satisfies assumption 2.1. Let $E_0(\omega_j)$ be the DFT of $\{e_0(t)\}$, defined analogously to (10), then*

$$|E_0(\omega_j)|^2 \xrightarrow{N\to\infty} \begin{cases} \frac{1}{2}\Phi_{e_0}(\omega_j)\chi^2(2), & \omega_j \in (0, \pi), \\ \Phi_{e_0}(\omega_j)\chi^2(1), & \omega_j = 0, \pi, \end{cases}$$

where $\Phi_{e_0}(\omega_j)$ denotes the auto-spectrum of the process $\{e_0(t)\}$, defined by

$$\Phi_{e_0}(\omega_j) = \sum_{\tau=-\infty}^{\infty} R_{e_0}(\tau) e^{-i\tau\omega_j},$$

and $\chi^2(n)$ denotes the chi-squared distribution with n degrees of freedom.

Proof: See Brillinger (1981, Theorem 5.2.6). □

Again note that the bound (11) is a hard or deterministic bound, which however enables a probabilistic interpretation. For example asymptotically in N a 0.999 probability region is obtained by choosing $f_u(\omega_j, \alpha_{k'}) = -f_l(\omega_j, \alpha_{k'}) = c\sqrt{\Phi_{e_0}(\omega_j)}$, $k' = 1, \ldots, m$, with $c = 2.63$ if $\omega_j \neq 0, \pi$ and $c = 3.29$ if $\omega_j = 0, \pi$.

Remark 4.5 *The information required to establish the frequency-domain bounds on the noise consists of $\Phi_{e_0}(\omega_j)$, see Proposition 4.4. Analogously to the procedure of Section 3 it is possible to use the prediction error to (conservatively) estimate the noise spectrum. With the definitions and assumptions of Section 3 it follows that*

$$\Phi_{\tilde{e}}(\omega_j) = \Phi_{\psi}(\omega_j) + \Phi_{e_0}(\omega_j) \geq \Phi_{e_0}(\omega_j),$$

where the latter inequality follows from the fact that an auto-spectrum is nonnegative. The spectrum of the prediction error can be estimated with standard techniques for spectral estimation, see Brillinger (1981).

5 Example

Consider the data generating system

$$y(t) = \theta_0^{(1)}u(t) + \theta_0^{(2)}u(t-1) + \theta_0^{(3)}u(t-2) + e_0(t),$$

$$\theta_0^{(1)} = 2,\ \theta_0^{(2)} = 1,\ \theta_0^{(3)} = 0.6,$$

with the noise process given by

$$e_0(t) = n(t) + 0.8n(t-1) + 0.2n(t-2) + 0.1n(t-3),$$

where $\{n(t)\}$ is a white noise process uniformly distributed between -0.25 and 0.25. The input signal $\{u(t)\}$ is chosen to be

$$u(t) = \begin{cases} 0, & t \leq 0, \\ \sin(\frac{\pi t}{4}) + \sin(\frac{\pi t}{2}), & t = 1, \ldots, N = 800. \end{cases}$$

The following parameter bounding identification procedures have been carried out.

1. Parameter bounding with bounds on the amplitude of the noise as in (2). As $|e_0(t)| \leq 0.25(1+0.8+0.2+0.1) = 0.525$, the bounds have been chosen $e_u(t) = -e_l(t) = 0.525, \forall t$. Altogether 6 linear programming problems had to be solved each with 3 unknowns subject to 1600 inequality constraints.

2. Parameter bounding with bounds on the cross–covariance of the noise as in (4). The signals $\{r_p(t)\}$ have been chosen $r_p(t) = u(t+\tau_p)$, $\tau_p = 1-p$, $p = 1,\ldots,8$, which with Theorem 2.5 yields $\Lambda_p = 0.0388$, $p = 1,\ldots,8$. The bounds $c_u(p) = -c_l(p) = 3\sqrt{\Lambda_p}$, $p = 1,\ldots,8$ have been chosen, hence each bound is satisfied with probability 0.997. Altogether 6 linear programming problems had to be solved each with 3 unknowns and 16 constraints. According to the rule of Bonferroni (Manoukian, 1986) the resulting parameter region is correct with a probability larger than or equal to $1-8(1-0.997) = 0.98$.

3. Parameter bounding with bounds on the periodogram of the noise as in (11). The frequencies $\omega_1 = \pi/4$ and $\omega_2 = \pi/2$ were selected, and $\alpha_{k'} = \pi k'/m$, $k' = 1,\ldots,4$. Straighforward calculations show that $\Phi_{e_0}(\omega_1) = 0.2473$ and $\Phi_{e_0}(\omega_2) = 0.1534$. The bounds $f_u(\omega_j,\alpha_{k'}) = -f_l(\omega_j,\alpha_{k'}) = 2.146\sqrt{\Phi_{e_0}(\omega_j)}$, $j = 1,2$, $k' = 1,\ldots,4$ have been chosen, which corresponds to a 0.99 confidence interval for each frequency seperately. Hence 6 linear programming problems with each 3 unknowns subject to 16 constraints had to be solved. The resulting parameter region is correct with probability larger than or equal to $1-2(1-0.99) = 0.98$.

The resulting upper and lower bounds on the parameters are shown in Table 1. It is concluded

	$\theta_1^{(l)}$	$\theta_1^{(u)}$	$\theta_2^{(l)}$	$\theta_2^{(u)}$	$\theta_3^{(l)}$	$\theta_3^{(u)}$
Pr. 1	1.890	2.117	0.862	1.127	0.468	0.707
Pr. 2	1.964	2.044	0.963	1.046	0.557	0.637
Pr. 3	1.954	2.048	0.981	1.028	0.554	0.648

Table 1: Results parameter bounding identification.

that for the first and third parameter the tightest bounds are obtained with the cross–covariance bounds on the noise, for the second parameter this is the case with the frequency–domain bounds on the noise. The parameter uncertainty intervals estimated with cross–covariance noise constraints, procedure 2, are a factor 3 smaller than the ones estimated with time–domain noise constraints, procedure 1. The uncertainty interval for the second parameter estimated with the frequency–domain noise constraints, procedure 3, is even a factor 5.7 smaller than the corresponding interval for procedure 1. The new parameter bounding identification methods 2 and 3 appear to outperform the standard parameter bounding identification procedure 1. Much smaller parameter uncertainty intervals are estimated with these new methods compared to the result of identification with bounds on the amplitude of the noise in the time domain.

Remark 5.1 *For simplicity exact knowledge of the second order noise statistics has been used to establish the bounds on the noise. The procedure of Section 3 may be used to estimate these statistics. In particular the method indicated in Remark 3.5 is applicable as the input is periodic.*

6 Conclusions

Valuable alternatives have been presented for time–domain bounds on the noise in parameter bounding identification by linear programming. Especially cross–covariance bounds on the noise are powerful as consistency has been proven for an arbitrary persistently exciting input signal. Frequency–domain bounds on the noise are powerful if the input signal contains sinusoids, in which case consistency has been proven as well. In both cases the number of constraints does not increase with an increasing number of measurements, hence the identification problem remains tractable for large N. The example showed a considerable reduction of parameter uncertainty in case the new types of noise constraints are utilized.

A stochastic analysis has been presented of the new types of noise bounds. The basic assumptions needed to justify this analysis are that the number of samples is large enough, and that the noise is stationary, i.e. its stochastic properties do not change in time. The analysis showed that the bounds for the noise can be specified such that they are correct with a certain probability. This means that a parameter set estimate is calculated which contains the true parameter vector with a certain probability. It is emphasized that the probability density function of the noise is arbitrary and need not be known. Only knowledge of the second order statistics of the noise process is required. A procedure

has been presented to estimate these statistics from data.

In Hakvoort (1992, 1993a, 1993b) bounded error identification with linear programming techniques is applied to identification in ℓ_1 and H_∞. The alternative noise bounds presented here can be fruitfully applied in those settings. In those papers also the problem of undermodelling is considered.

References

Bayard, D.S. (1992). Statistical plant set estimation using Schroeder–phased multisinusoidal input design. *Proc. Am. Contr. Conf.*, Chicago, pp. 2988–2995.

Brillinger, D.R. (1981). *Time Series: Data Analysis and Theory*, Holden–Day, San Francisco.

De Vries, D.K. and P.M.J. Van den Hof (1992). Quantification of model uncertainty from data: input design, interpolation and connection with robust control design specifications. *Proc. Am. Contr. Conf.*, Chicago, U.S.A., pp. 3170–3175.

Fogel, E. (1979). System identification via membership set constraints with energy constrained noise. *IEEE Trans. Autom. Contr.*, Vol. AC–24, pp. 752–758.

Fogel, E. and Y.F. Huang (1982). On the value of information in system identification — bounded noise case. *Automatica*, Vol. 18, pp. 229–238.

Gu, G., and P.P. Khargonekar (1992). Linear and nonlinear algorithms for identification in H_∞ with error bounds. *IEEE Trans. Autom. Contr.*, Vol. AC–37, pp. 953–963.

Hakvoort, R.G. (1992). Worst–case system identification in ℓ_1: error bounds, optimal models and model reduction. *Proc. 31st IEEE Conf. Dec. and Contr.*, Tucson, U.S.A., pp. 499–504.

Hakvoort, R.G. (1993a). Worst–case system identification in H_∞: error bounds and optimal models. Proc. 12th IFAC World Congress, Sydney, Australia.

Hakvoort, R.G. (1993b). A linear programming approach to the identification of frequency domain error bounds. *Internal Report N–455*, Mech. Eng. Syst. and Contr. Group, Delft Univ. of Techn., The Netherlands.

Hakvoort, R.G. and P.M.J. Van den Hof (1993). Consistent parameter bounding identification for linearly parametrized model sets. *Internal Report N–427*, Mech. Eng. Syst. and Contr. Group, Delft Univ. of Techn., The Netherlands.

Hakvoort, R.G., P.M.J. Van den Hof and O.H. Bosgra (1993). Consistent parameter bounding identification using cross–covariance constraints on the noise. *Proc. 32nd IEEE Conf. Dec. and Contr.*, San Antonio, U.S.A.

Helmicki, A.J., C.A. Jacobson, and C.N. Nett (1991). Control–oriented system identification: a worst–case/deterministic approach in H_∞. *IEEE Trans. Autom. Contr.*, Vol. 36, pp. 1163–1176.

Heuberger, P.S.C. and O.H. Bosgra (1990). Approximate system identification using system based orthonormal functions. *Proc. 29th IEEE Conf. Dec. and Contr.*, Honolulu, U.S.A., pp. 1086–1092.

Heuberger, P.S.C., P.M.J. Van den Hof and O.H. Bosgra (1992). A generalized orthonormal basis for linear dynamical systems. *Internal Report N–404*, Mech. Eng. Syst. and Contr. Group, Delft Univ. of Techn., The Netherlands. Short version in *Proc. 32nd IEEE Conf. Dec. and Contr.*, San Antonio, U.S.A., 1993.

Lamaire, R.O., L. Valavani, M. Athans and G. Stein (1991). A frequency domain estimator for use in adaptive control systems. *Automatica*, Vol. 27, pp. 23–38.

Ljung, L. (1987). *System Identification: Theory for the User*, Prentice–Hall, Englewood Cliffs, N.J.

Manoukian, E.B. (1986). *Modern Concepts and Theorems of Mathematical Statistics*, Springer Verlag, New York.

Milanese, M. and G. Belforte (1982). Estimation theory and uncertainty intervals evaluation in presence of unknown but bounded errors: linear families of models and estimators. *IEEE Trans. Autom. Contr.*, Vol. AC–27, pp. 408–414.

Milanese, M. and A. Vicino (1991). Optimal estimation theory for dynamic systems with set membership uncertainty: an overview. *Automatica*, Vol. 27, pp. 997–1009.

Söderström, T. and P. Stoica (1989). *System Identification*, Prentice–Hall, U.K.

Veres, S.M. and J.P. Norton (1989). Structure identification of parameter bounding models by use of noise structure bounds. *Int. J. Contr.*, Vol. 50, pp. 639–649.

Veres, S.M. and J.P. Norton (1991). Structure selection for bounded parameter models: consistency conditions and selection criterion. *IEEE Trans. Autom. Contr.*, Vol. AC–36, pp. 474–481.

Walter, E. and H. Piet–Lahanier (1990). Estimation of parameter bounds from bounded error data: a survey. *Math. and Comp. in Sim.*, Vol. 32, pp. 449–468.

Wahlberg, B. (1991). System identification using Laguerre models. *IEEE Trans. Autom. Contr.*, Vol. AC–36, pp. 551–562.

Selected Topics in Identification, Modelling and Control
Vol. 6, December 1993

Frequency domain curve fitting with maximum amplitude criterion and guaranteed stability ‡

Richard G. Hakvoort

Mechanical Engineering Systems and Control Group
Delft University of Technology, Mekelweg 2, 2628 CD Delft, The Netherlands.

Abstract. The problem is considered of fitting a stable rational transfer function to complex frequency response data minimizing a weighted maximum amplitude criterion. A solution for this problem is provided in both discrete and continuous time by parametrizing the transfer function and solving a nonlinear constrained optimization problem. The denominator is parametrized as a product of first and second order polynomials. By adding some linear constraints on the denominator parameters to the nonlinear programming problem the poles of the curve fit model are restricted to the stability region in the complex plane, i.e. the unit disc or the left half plane. To provide an initial estimate for the nonlinear optimization problem an iterative procedure is proposed where in each step a linear programming problem has to be solved.

Keywords. curve fitting, frequency domain, ℓ_∞–norm, stability, linear and nonlinear programming

1 Introduction

The problem is considered of fitting a discrete or continuous time stable rational transfer function of a specified order to a set of complex frequency response data. In literature reasonable attention has been paid to curve fit problems, however without restricting the model set to the set of stable models. Levy (1959) introduced a curve fit problem with a sum of squares (ℓ_2) criterion function and provided a solution for it. Sanathanan and Koerner (1963) proposed an iterative weighting in order to improve on the estimate. The asymptotic behaviour of this and other iterative linear schemes has been investigated by Whitfield (1987). Payne (1970) already noticed that if high order models are used in the curve fit procedure, the resulting estimate tends to be unstable.

Alternative criteria (other than ℓ_2) are used in Spanos (1991) and Sidman *et al.* (1991). In the first paper an iteration of weighted least squares problems is used to solve an unweighted least maximum amplitude (ℓ_∞) optimization problem. In the latter paper the ℓ_2–criterion is adjusted such that it is well suited for logarithmically spaced frequency response data.

In the present paper a weighted ℓ_∞–criterion is considered. An advantage of an ℓ_∞–criterion compared to an ℓ_2–criterion is that in the ℓ_∞–case each frequency is basically equally important. The frequency distribution (linearly or logarithmically, etc.) does not influence the resulting estimate as much as it does in the ℓ_2–case. Moreover the weighting allows for an easy and effective shaping of the model error. A final motivation for a maximum amplitude criterion is that in many applications, for example robust control design, it is desirable that the maximum (weighted) distance between system and model is minimal, in order to have maximum robustness.

The ℓ_∞–optimization problem is solved by trans-

‡This paper has also been presented at the 2nd European Control Conference, Groningen, The Netherlands, June 28 – July 1, 1993.

forming it into a smooth nonlinear constrained optimization problem, which is a different approach from the one followed by Spanos (1991). The transfer function is guaranteed to be stable by parametrizing the denominator as a product of first and second order polynomials and adding certain linear constraints on the denominator parameters to the optimization problem. In fact in the discrete time case a bound can be specified for the amplitude of the transfer function poles. In the continuous time case a bound can be specified for the real part of the poles. The nonlinear programming problem can be solved using standard software, but requires the specification of a good initial estimate. A procedure is presented to arrive at such an initial estimate. It involves a Sanathanan–Koerner iteration in ℓ_∞–setting, where in each step one linear programming problem has to be solved.

A completely different approach for frequency domain identification is taken in the field of identification in H_∞, see e.g. Gu and Khargonekar (1992). There the primary interest is in finding a stable transfer function with some worst–case optimality properties using frequency response data. For that purpose standard curve fit procedures do not apply as they do not guarantee stability of the resulting estimate. However the algorithms for identification in H_∞ generally do not restrict the model order, extremely high order nominal models may result. The present curve fit procedure seems to be an attractive alternative as both stability is guaranteed and the model order is user–defined. Also note that the maximum amplitude criterion is closely related to the H_∞–norm.

The outline of the paper is as follows. In Section 2 the curve fit problem is formulated and a solution is derived in the form of a nonlinear programming problem. In Section 3 a procedure is derived to provide an initial estimate for the nonlinear programming problem. Section 4 discussed some practical implementation aspects of the linear and nonlinear programming problems involved. Section 5 contains a simulation example which shows the applicability of the curve fit procedure. Finally in Section 6 conclusions are drawn.

The present paper only treats the SISO case. Extensions of the curve fit procedure to the MIMO case are presented in Hakvoort and Van den Hof (1993).

2 The Curve Fit Procedure

Consider complex–valued frequency response data $G(\omega_j)$, $j = 1, \ldots, l$ and a positive real–valued frequency dependent weight $W(\omega_j)$, $j = 1, \ldots, l$. The objective is to find a stable rational transfer function $\hat{G}(\xi)$ in a certain model set $\mathcal{M}$ that optimally describes the frequency response data in a weighted ℓ_∞–sense,

$$\hat{G}(\xi) = \arg \min_{\hat{G}' \in \mathcal{M}} \max_{j=1,\ldots,l} \left| \left(G(\omega_j) - \hat{G}'(\xi(\omega_j)) \right) W(\omega_j) \right|. \tag{1}$$

Following the notation in Bayard (1992) the complex variable ξ is used to present the continuous and discrete time case in a unified way. Hence ξ can be thought of as the Laplace operator s or the z–transform operator z. And $\xi(\omega)$ represents the evaluation of the complex variable ξ as a function of frequency, hence $\xi(\omega) = i\omega$, $\xi(\omega) = e^{i\omega}$ respectively.

For $\mathcal{M}$ the model set is chosen consisting of all rational transfer functions with numerator and denominator of specified degrees and the roots of the denominator in some a priori specified (stability) region $\mathcal{R}$ in the complex plane.

$$\mathcal{M}: \ \hat{G}'(\xi) = \frac{n(\xi)}{d(\xi)}, \ n(\xi) = \sum_{k=0}^{n} n_k \xi^k,$$

$$d(\xi) = \xi^d + \sum_{k=0}^{d-1} d_k \xi^k, \ \xi_{d,k} \in \mathcal{R}, \ k = 1, \ldots, d,$$

where $\xi_{d,k}$, $k = 1, \ldots, d$, are the roots of the polynomial $d(\xi)$, i.e. all solutions to the equation $d(\xi) = 0$. In the discrete time case the region $\mathcal{R}$ is defined by $\mathcal{R} = \mathcal{R}_\rho$ with

$$\mathcal{R}_\rho = \{ \xi_{d,k} \text{ s.t. } |\xi_{d,k}| \leq \rho, \ k = 1, \ldots, d \},$$

which corresponds to an upper bound ρ on the amplitude of the poles of the transfer function. In the continuous time case this region is defined by $\mathcal{R} = \mathcal{R}_r$ with

$$\mathcal{R}_r = \{ \xi_{d,k} \text{ s.t. } \mathrm{Re}\,(\xi_{d,k}) \leq r, \ k = 1, \ldots, d \},$$

which corresponds to an upper bound r on the real part of the poles of the transfer function. Here ρ and r are user–defined constants. The choice $\rho = 1$ corresponds to stability in the discrete time case. The choice $r = 0$ corresponds to stability in the continuous time case.

Now the objective (1) can be written as

$$\min_{\hat{G}' \in \mathcal{M}} \max_{j=1,\ldots,l} \left| \left(G(\omega_j) - \hat{G}'(\xi(\omega_j)) \right) W(\omega_j) \right| =$$

$$= \min_{h_\infty, \hat{G}' \in \mathcal{M}} h_\infty \text{ s.t.}$$

$$\left| \left(G(\omega_j) - \hat{G}'(\xi(\omega_j)) \right) W(\omega_j) \right| \leq h_\infty, \ j = 1, \ldots, l$$

$$= \min_{h_\infty, n(\xi), d(\xi)} h_\infty^2 \text{ s.t.}$$

$$\left|\left(G(\omega_j)-\frac{n(\xi(\omega_j))}{d(\xi(\omega_j))}\right)W(\omega_j)\right|^2 \le h_\infty^2,\ j=1,\dots,l,$$
$$\xi_{d,k}\in\mathcal{R},\ k=1,\dots,d$$
$$= \min_{h_\infty, n(\xi), d(\xi)} h_\infty^2 \text{ s.t.}$$
$$W^2(\omega_j)\,|G(\omega_j)d(\xi(\omega_j))-n(\xi(\omega_j))|^2 \le h_\infty^2 |d(\xi(\omega_j))|^2,$$
$$j=1,\dots,l,\ \xi_{d,k}\in\mathcal{R},\ k=1,\dots,d. \qquad (2)$$

In order to cope with the region $\mathcal{R}$ for the roots of the denominator polynomial in a computationally attractive way an alternative parametrization is introduced for the denominator by representing the polynomial as a product of first and second order polynomials.

$$d(\xi)=\begin{cases}\prod_{k=1}^{d/2}\left(\xi^2+a_k\xi+b_k\right), & d \text{ even}\\ (\xi+c)\prod_{k=1}^{(d-1)/2}\left(\xi^2+a_k\xi+b_k\right), & d \text{ odd}\end{cases} \qquad (3)$$

where the parameters a_k, b_k and c are real–valued. Then the following Lemma gives necessary and sufficient conditions for the location of the roots of $d(\xi)$ by means of simple linear constraints on the parameters.

Lemma 2.1 *Let $\xi_{d,k}$, $k=1,\dots,d$, be the roots of $d(\xi)$, i.e. all solutions to $d(\xi)=0$, then for any $\rho\ge 0$, $r\in\mathbb{R}$,*

(i) $|\xi_{d,k}|\le\rho,\ \forall k \Leftrightarrow$
$$\begin{cases} b_k\le\rho^2, & \forall k\\ a_k\rho\le\rho^2+b_k, & \forall k\\ -a_k\rho\le\rho^2+b_k, & \forall k\\ -\rho\le c\le\rho, & d \text{ odd}\end{cases}$$

(ii) $\mathrm{Re}(\xi_{d,k})\le r,\ \forall k \Leftrightarrow$
$$\begin{cases} b_k+a_kr+r^2\ge 0, & \forall k\\ a_k\ge -2r, & \forall k\\ c\ge -r, & d \text{ odd}\end{cases}$$

Proof: (i) First notice that $\xi+c=0$ has a solution $|\xi|\le\rho$ if and only if $|c|\le\rho$. Next consider a second order term $\xi^2+a\xi+b$.

($\Rightarrow$) Assume $\xi^2+a\xi+b=0$ has solutions ξ_1, ξ_2 which satisfy $|\xi_{1,2}|\le\rho$.
Case 1 $a^2-4b\ge 0 \Rightarrow \xi_{1,2}=-\frac{a}{2}\pm\sqrt{\left(\frac{a}{2}\right)^2-b}$. Hence $|\xi_{1,2}|\le\rho \Rightarrow \frac{|a|}{2}+\sqrt{\left(\frac{a}{2}\right)^2-b}\le\rho \Rightarrow 2\rho-|a|\ge\sqrt{a^2-4b} \Rightarrow 4\rho^2-4\rho|a|+a^2\ge a^2-4b \Rightarrow \boxed{\rho^2+b\ge\rho|a|}$. Also $\boxed{b}\le\left(\frac{a}{2}\right)^2\le\left(\rho-\sqrt{\left(\frac{a}{2}\right)^2-b}\right)^2\boxed{\le\rho^2}$.
Case 2 $a^2-4b\le 0 \Rightarrow \xi_{1,2}=-\frac{a}{2}\pm i\sqrt{b-\left(\frac{a}{2}\right)^2}$. Hence $|\xi_{1,2}|\le\rho \Rightarrow \left(\frac{a}{2}\right)^2+b-\left(\frac{a}{2}\right)^2\le\rho^2 \Rightarrow \boxed{b\le\rho^2}$. And $\boxed{\rho^2+b-|a|\rho}\ge\rho^2+\left(\frac{a}{2}\right)^2-|a|\rho=\left(\rho-\frac{|a|}{2}\right)^2\boxed{\ge 0}$.

($\Leftarrow$) Assume that $b\le\rho^2$, $\rho^2+b\ge|a|\rho$.
Case 1 $a^2-4b\ge 0$. Using the fact that $-b\le\rho^2-|a|\rho$ and $\rho-\frac{|a|}{2}\ge\frac{\rho^2-b}{2\rho}\ge 0$, this gives $\boxed{|\xi_{1,2}|\le}\ \frac{|a|}{2}+\sqrt{\left(\frac{a}{2}\right)^2-b}\le\frac{|a|}{2}+\sqrt{\left(\frac{a}{2}\right)^2+\rho^2-|a|\rho}=\frac{|a|}{2}+\sqrt{\left(\rho-\frac{|a|}{2}\right)^2}=\frac{|a|}{2}+\rho-\frac{|a|}{2}=\boxed{\rho}$.
Case 2 $a^2-4b\le 0 \Rightarrow \boxed{|\xi_{1,2}|}=\sqrt{\left(\frac{a}{2}\right)^2+b-\left(\frac{a}{2}\right)^2}=\sqrt{b}\boxed{\le\rho}$.

(ii) First notice that $\xi+c=0$ has a solution $\mathrm{Re}(\xi)\le r$ if and only if $\mathrm{Re}(c)=c\ge -r$. Next consider a second order term $\xi^2+a\xi+b$.

($\Rightarrow$) Assume $\xi^2+a\xi+b=0$ has solutions ξ_1, ξ_2, which satisfy $\mathrm{Re}(\xi_{1,2})\le r$.
Case 1 $a^2-4b\ge 0 \Rightarrow \mathrm{Re}(\xi_{1,2})=-\frac{a}{2}\pm\sqrt{\left(\frac{a}{2}\right)^2-b}\le r \Rightarrow -\frac{a}{2}+\sqrt{\left(\frac{a}{2}\right)^2-b}\le r \Rightarrow r+\frac{a}{2}\ge\sqrt{\left(\frac{a}{2}\right)^2-b} \Rightarrow r^2+ar+\left(\frac{a}{2}\right)^2\ge\left(\frac{a}{2}\right)^2-b \Rightarrow \boxed{r^2+ar+b\ge 0}$. Also $r+\frac{a}{2}\ge\sqrt{\left(\frac{a}{2}\right)^2-b}\ge 0 \Rightarrow \boxed{a\ge -2r}$.
Case 2 $a^2-4b\le 0 \Rightarrow \mathrm{Re}(\xi_{1,2})=-\frac{a}{2}\le r \Rightarrow \boxed{a\ge -2r}$. And $\boxed{b+ar+r^2}\ge\left(\frac{a}{2}\right)^2+ar+r^2=\left(\frac{a}{2}+r\right)^2\boxed{\ge 0}$.

($\Leftarrow$) Assume that $b+ar+r^2\ge 0$, $a\ge -2r$.
Case 1 $a^2-4b\ge 0$. Using the fact that $-b\le ar+r^2$ and $\frac{a}{2}+r\ge 0$, this yields $\boxed{\mathrm{Re}(\xi_{1,2})\le}-\frac{a}{2}+\sqrt{\left(\frac{a}{2}\right)^2-b}\le-\frac{a}{2}+\sqrt{\left(\frac{a}{2}\right)^2+ar+r^2}=-\frac{a}{2}+\sqrt{\left(\frac{a}{2}+r\right)^2}=$

$-\frac{a}{2} + \frac{a}{2} + r = \boxed{r}$.

Case 2 $a^2 - 4b \leq 0 \Rightarrow \boxed{\mathrm{Re}(\xi_{1,2})} = -\frac{a}{2}\boxed{\leq r}$.

□

Note that the first part of the Lemma has a straightforward application in restricting the roots of the denominator to the region $\mathcal{R}_\rho$ by means of simple linear parameter constraints. The second part of the Lemma can obviously be applied in restricting the roots of the denominator to the region $\mathcal{R}_r$ by means of simple linear parameter constraints. The conditions given in Lemma 2.1 are necessary and sufficient conditions, which implies that any polynomial $d(\xi)$ with roots in the specified regions in the complex plane can be parametrized in such a way that the parameter constraints of Lemma 2.1 are satisfied.

The optimization problem (1) has been translated into a smooth nonlinear constrained optimization problem (2) extended with some linear constraints in order to restrict the location of the roots of the denominator polynomial (Lemma 2.1). This nonlinear optimization problem can be tackled by applying standard software for nonlinear constrained optimization. In Section 4 some aspects of the practical implementation will be discussed.

3 The Initial Estimate

In the previous Section the frequency domain curve fitting problem with maximum absolute value objective function and guaranteed stability of the resulting model has been translated into a nonlinear constrained optimization problem. Such a nonlinear optimization problem can generally only be solved satisfactorily if a good initial estimate is available. Here an iterative procedure is proposed using linear programming techniques to arrive at such an initial estimate. The following model structure is considered,

$$\mathcal{M} : \hat{G}'(\xi) = \frac{n(\xi)}{d(\xi)},$$

$$n(\xi) = \sum_{k=0}^{n} n_k \xi^k, \; d(\xi) = \xi^d + \sum_{k=0}^{d-1} d_k \xi^k,$$

hence stability of the initial estimate is not required. For some positive, real valued weight $\tilde{W}(\omega_j)$ the following optimization problem is considered,

$$\min_{n(\xi),d(\xi)} \max_{j=1,\ldots,l} \left| \left(G(\omega_j)d(\xi(\omega_j)) - n(\xi(\omega_j))\right) \tilde{W}(\omega_j) \right|, \tag{4}$$

or equivalently,

$$\min_{h_\infty, n(\xi), d(\xi)} h_\infty \text{ s.t.}$$

$$\left| \left(G(\omega_j)d(\xi(\omega_j)) - n(\xi(\omega_j))\right) \tilde{W}(\omega_j) \right| \leq \tag{5}$$
$$\leq h_\infty, \; j = 1, \ldots, l.$$

Before continuing first an auxiliary Lemma is presented.

Lemma 3.1 *Consider the function* $f_{m'}(x) : \mathbb{C} \to \mathbb{R}$, *defined by*

$$f_{m'}(x) = \max_{k'=1,\ldots,m'} \mathrm{Re}\,(c_{m',k'}x),$$

with $c_{m',k'} = e^{2\pi \frac{k'}{m'} i}$, $k' = 1, 2, \ldots, m' \geq 3$, *where* $\mathrm{Re}\,(\cdot)$ *denotes the real part of* $\cdot$, *then*

$$\textbf{(i)} \;\; f_{m'}(x) \leq |x| \leq \frac{f_{m'}(x)}{\cos\left(\frac{\pi}{m'}\right)},$$

$$\textbf{(ii)} \;\; \lim_{m' \to \infty} f_{m'}(x) = |x|.$$

Proof: For any x and any $c_{m',k'}$ with $|c_{m',k'}| = 1$, $\mathrm{Re}\,(c_{m',k'}x) \leq |c_{m',k'}x| \leq |c_{m',k'}||x| = |x|$, which proves the left–hand inequality of (i). Further for any x there exist an integer l' and $\delta \in [-\frac{\pi}{m'}, \frac{\pi}{m'})$ such that $x = |x|e^{(2\pi \frac{l'}{m'} + \delta)i}$, yielding

$$\mathrm{Re}\,(c_{m',k'}x) = \mathrm{Re}\left(e^{2\pi \frac{k'}{m'} i}|x|e^{(2\pi \frac{l'}{m'} + \delta)i}\right) =$$

$$= |x|\mathrm{Re}\left(e^{(2\pi \frac{k'+l'}{m'} + \delta)i}\right) = |x|\cos\left(2\pi \tfrac{k'+l'}{m'} + \delta\right).$$

If $k' = k^*$ is chosen such that $k^* + l' = n'm'$ for some integer n', this gives

$$\mathrm{Re}\,(c_{m',k^*}x) = |x|\cos(2\pi n' + \delta) = |x|\cos(\delta) \geq$$

$$\geq |x|\cos(\pi/m') \Leftrightarrow |x| \leq \frac{\mathrm{Re}\,(c_{m',k^*}x)}{\cos(\frac{\pi}{m'})},$$

which proves the right–hand inequality of part (i). Finally part (ii) immediately follows from part (i) for $m' \to \infty$. □

Moreover it is easy to show that the bounds in (i) are tight in the sense that there exists an x such that the lower bound becomes equality, and there is an x such that the upper bound becomes equality. The Lemma in fact says that the amplitude of a

complex number can be calculated approximately by checking a number of different directions in the complex plane.

Using the $c_{m',k'}$ defined in Lemma 3.1 the optimization problem (5) can be approximated by the optimization problem

$$\min_{h_\infty, n(\xi), d(\xi)} h_\infty \text{ s.t.}$$

$$\operatorname{Re}\left(c_{m',k'}\left(G(\omega_j)d(\xi(\omega_j)) - n(\xi(\omega_j))\right)\tilde{W}(\omega_j)\right) \le h_\infty,$$

$$j = 1,\ldots,l,\ k' = 1,\ldots,m',$$

which is equivalent to the linear programming problem

$$\min_{h_\infty, n_k, d_k} h_\infty \text{ s.t.}$$

$$\begin{aligned}
&\tilde{W}(\omega_j)\operatorname{Re}\left(c_{m',k'}G(\omega_j)\xi^d(\omega_j)\right) + \\
&+\sum_{k=0}^{d-1} d_k\tilde{W}(\omega_j)\operatorname{Re}\left(c_{m',k'}G(\omega_j)\xi^k(\omega_j)\right) + \qquad (6)\\
&-\sum_{k=0}^{n} n_k\tilde{W}(\omega_j)\operatorname{Re}\left(c_{m',k'}\xi^k(\omega_j)\right) - h_\infty \le 0,\\
&\qquad j = 1,\ldots,l,\ k' = 1,\ldots,m'.
\end{aligned}$$

The following Theorem quantifies the accuracy of the approximation.

Theorem 3.2 *Denote the optimal solution of (4) by h'_∞, $n'(\xi)$, $d'(\xi)$ and the optimal solution of (6) by h''_∞, $n''(\xi)$, $d''(\xi)$, then*

$$\text{(i) } h''_\infty \le$$

$$\max_{j=1,\ldots,l}\left|\left(G(\omega_j)d'(\xi(\omega_j)) - n'(\xi(\omega_j))\right)\tilde{W}(\omega_j)\right| \le$$

$$\max_{j=1,\ldots,l}\left|\left(G(\omega_j)d''(\xi(\omega_j)) - n''(\xi(\omega_j))\right)\tilde{W}(\omega_j)\right| \le$$

$$\frac{h''_\infty}{\cos\left(\frac{\pi}{m'}\right)},$$

$$\text{(ii) } \lim_{m'\to\infty}\frac{n''(\xi)}{d''(\xi)} = \frac{n'(\xi)}{d'(\xi)}.$$

Proof: The second inequality in part (i) arises from the definition of $n'(\xi)$, $d'(\xi)$. Next it is noticed that the optimal solution to problem (6) has the property

$$h''_\infty =$$

$$\max_{j=1,\ldots,l} f_{m'}\left(\left(G(\omega_j)d''(\xi(\omega_j)) - n''(\xi(\omega_j))\right)\tilde{W}(\omega_j)\right),$$

which yields the third inequality by applying Lemma 3.1. Finally optimality of of $n''(\xi)$, $d''(\xi)$ implies that for some j',

$$f_{m'}\left(\left(G(\omega_{j'})d'(\xi(\omega_{j'})) - n'(\xi(\omega_{j'}))\right)\tilde{W}(\omega_{j'})\right) \ge h''_\infty,$$

which yields the first inequality of part (i) by again applying Lemma 3.1. For $m' \to \infty$ the right–hand side in (i) converges to the left–hand side, which proves part (ii). □

The optimization problem (6) can be solved exactly using standard linear programming software available. See Luenberger (1984) for an extensive treatment of the linear programming problem and algorithms to solve it. According to Theorem 3.2 the solution to the optimization problem (6) is an arbitrarily good approximation to problem (4) for m' sufficiently large.

Now to obtain a good initial estimate for the nonlinear programming problem (1) an iteration is proposed analogously to the Sanathanan–Koerner iteration for ℓ_2–curve fitting (Sanathanan and Koerner, 1963). In each iteration the weight $\tilde{W}(\omega_j)$ is chosen such that

$$\tilde{W}(\omega_j) = W(\omega_j)\left|d_{\text{prev}}(\xi(\omega_j))\right|^{-1},\ j = 1,\ldots,l,$$

where $d_{\text{prev}}(\xi)$ denotes the denominator that resulted in the previous iteration. The idea is that the optimization problem (4) more and more resembles the nonlinear problem (1). It is emphasized that on the one hand convergence of the iterative procedure is not guaranteed and on the other hand if it converges the ultimate outcome will generally not be equal to the optimal result of the non–linear problem (1). However Sanathanan and Koerner reported good results obtained with this iteration in an ℓ_2–setting and the simulation in Section 5 show that the procedure also works adequately in the ℓ_∞–setting adopted here, i.e. the resulting model is in general a suitable initial estimate for the nonlinear optimization problem. Finally it is mentioned that the initial estimate need not be stable, as no constraints of the kind of those in Lemma 2.1 are imposed on the denominator.

4 Implementation Aspects

The curve fit problem (1) appears solvable by using linear and nonlinear programming routines. In practice things like numerical accuracy play an important role. Therefore some modifications to the programming problems (2) and (6) may be necessary to get well–conditioned optimization problems.

From equation (2) it is apparent that in the continuous time case, $\xi(\omega_j) = i\omega_j$, the expressions on the left– and right–hand side can be very large if $\omega_j > 1$. This may cause numerical problems. The problem is dealt with by introducing a scaling

factor. A proper scaling is achieved by multiplying all constraints corresponding to $\omega_j > 1$ in the continuous time case with the factor $f^2(\omega_j)$ where $f(\omega_j) = \omega_j^{-\max(n,d)}$. Hence one such constraint is given by

$$f^2(\omega_j)W^2(\omega_j)\,|G(\omega_j)d(\xi(\omega_j)) - n(\xi(\omega_j))|^2 \leq \leq h_\infty^2 f^2(\omega_j)|d(\xi(\omega_j))|^2.$$

Analogously the constraints in the linear programming problem (6) need to be scaled. In the continuous time case for $\omega_j > 1$ all terms appearing in these constraints should be multiplied with the factor $f(\omega_j)$ as given above. In the discrete time case and in the continuous time case for frequencies smaller than or equal to 1 no scaling is required.

A slight improvement of the nonlinear programming problem (2) is obtained by replacing h_∞^2 by a new parameter $h_{\infty,2}$. A consequence of this is that the objective function becomes linear, which is in general preferable to a nonlinear objective function.

For the simulation in Section 5 the sequential quadratic programming method implemented in the FORTRAN NAG–library has been used, see Gill *et al.* (1981) for details about this method. This method requires the first partial derivatives of the nonlinear constraints to the unknowns. To compute these the fact can be used that for any complex–valued function $y(x_1,\ldots,x_n)$ of the real variables $x_1,\ldots,x_n$ the first (partial) derivative of the squared magnitude is given by

$$\frac{\partial|y(x_1,\ldots,x_n)|^2}{\partial x_k} = \frac{\partial y'y}{\partial x_k} = y'\frac{\partial y}{\partial x_k} + \frac{\partial y'}{\partial x_k}y = \\ = y'\frac{\partial y}{\partial x_k} + \left(y'\frac{\partial y}{\partial x_k}\right)' = \\ = 2\,\mathrm{Re}\left(y'(x_1,\ldots,x_n)\frac{\partial y(x_1,\ldots,x_n)}{\partial x_k}\right),$$

where y' is the complex conjugate of y and $\mathrm{Re}\,(y)$ is the real part of y. Then the first partial derivatives of the constraints in (2) to the parameters $h_{\infty,2}$, n_k, a_k, b_k and c can straightforwardly be computed. The results can be found in Hakvoort and Van den Hof (1993).

It has already been noted that the initial estimate resulting from the linear programming problem need not have all its poles in the specified region $\mathcal{R}$. If such a model is found it will not be a feasible solution to the nonlinear programming problem. It may then be advisable to first change the poles of the initial model, for example by mirroring, in order to ensure feasibility of the initial estimate, which will generally improve the performance of the nonlinear optimization algorithm.

Finally it is noticed that the parametrization (3) is not unique as there is freedom in the ordering of the second order terms. It depends on the specific nonlinear programming routine that is used if this nonuniqueness in the solution space will cause trouble. The routine applied for the simulation in Section 5 has no difficulties with it. If a routine is used that has difficulties with the nonuniqueness, uniqueness may be enforced by specifying additional constraints which correspond to ordering the second order terms uniquely. These constraints may for example be the following linear constraints,

$$a_1 > a_2 > \cdots > a_p,\ p = d/2 \text{ or } p = (d-1)/2,$$

yielding a unique parametrization, which however excludes the possibility of identical a–parameters in two second order polynomials.

5 Example

For the simulation example consider the 5th order discrete time SISO system given by

$$G(z) = \frac{0.8z^5 - 0.9z^4 + 0.24z^3 + 0.52z^2 - 0.9z + 0.4}{z^5 - 2.47z^4 + 2.89z^3 - 1.98z^2 + 0.83z - 0.18},$$

from which noisy frequency response measurements $G(\omega_j)$ have been taken at 100 frequencies logarithmically distributed between $10^{-1.5}$ and π. At each frequency the noise was the sum of a real and imaginary part which were realizations of independent gaussian stochastic processes with zero mean and variance 0.1. The weighting $W(\omega_j)$ was chosen to be equal to $|W(e^{i\omega_j})|$, with $W(z) = (z-0.4)/(z-0.7)$.

Third order models have been estimated. The initial estimate has been calculated using the procedure of Section 3 with $m' = 4$. The iteration was started with $d_{\mathrm{prev}}(q)$ set to 1 and was stopped when the maximum parameter change in both numerator and denominator was smaller than 0.1. Altogether 6 iterations were sufficient to reach the final result. The transfer function of the initial estimate is given by

$$\hat{G}_{\mathrm{init}}(z) = \frac{0.821z^3 - 0.914z^2 + 0.216z - 0.0723}{z^3 - 2.30z^2 + 2.04z - 0.709},$$

which happens to be stable. After this the nonlinear problem was solved with $\rho = 1$. The result is given by

$$\hat{G}(z) = \frac{0.865z^3 - 0.478z^2 + 0.345z - 0.199}{z^3 - 1.53z^2 + 0.968z - 0.125},$$

which is also stable, as expected. In Fig. 1 a Nyquist diagram is shown of the noisy frequency response data, the fit of the initial estimate and the fit of the ultimate ℓ_∞–optimal model. In Fig. 2 an amplitude Bode diagram is presented of the frequency dependent weighted fit error for the optimal model. The maximum error is achieved 7 times. From this plot it is very clear that the optimization objective has been to minimize the maximum amplitude over all frequencies.

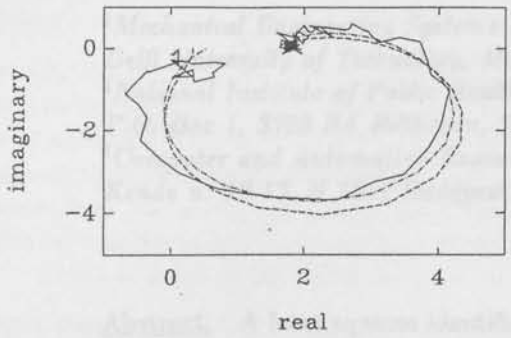

Fig. 1: Nyquist diagram frequency response data $G(\omega_j)$ (solid), initial estimate $\hat{G}_{\text{init}}(e^{i\omega_j})$ (dashed) and ℓ_∞–optimal model $\hat{G}(e^{i\omega_j})$ (dash–dotted)

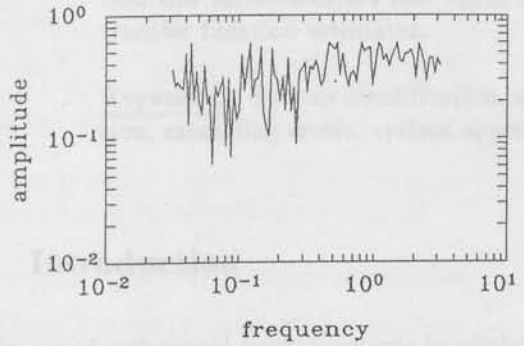

Fig. 2: Amplitude Bode diagram weighted fit error $\left(G(\omega_j) - \hat{G}(e^{i\omega_j})\right) W(e^{i\omega_j})$

6 Conclusions

A procedure has been developed to fit a discrete or continuous time rational transfer function to a set of frequency response data minimizing a weighted ℓ_∞–criterion. The procedure consists of two steps. First an initial estimate is calculated using linear programming techniques. Then the optimal model is estimated by solving a smooth nonlinear constrained optimization problem. An important feature of the present curve fit procedure is that the resulting nominal model has its poles in a user–defined region in the complex plane. It is for example straightforward to restrict the model set to the set of stable models. The consequence of this then is that the resulting curve fit model will always be stable.

The example in the previous Section showed the applicability of the proposed curve fit procedure. The weighting $W(\omega_j)$ can be tuned in order to shape the model error as a function of frequency. The curve fit procedure can be used to construct a parametric model from frequency response measurements taken from some system. However this is not the only application that one may think of. Because of the close connection of the ℓ_∞–norm and the H_∞–norm the curve fit procedure may for example also be applied to perform model reduction in H_∞–norm. Moreover it can also be used to perform a transformation from discrete to continuous time or vice versa in a weighted H_∞–optimal way. The only problem that remains in these cases is the intersample behaviour of the curve fit model. As only a finite number of frequencies is used in the curve fit criterion function, the model may theoretically be arbitrarily bad between two subsequent frequencies. In Hakvoort (1992) some conditions are given which guarantee that the intersample behaviour is not arbitrarily bad, but bounded. In practice it is often a matter of taking enough frequencies compared to the curve fit model order, and afterwards checking if the frequency response of the estimated model is satisfactory for all frequencies.

References

Bayard, D.S. (1992). Multivariable frequency domain identification via 2–norm minimization. *Proc. Am. Contr. Conf.*, Chicago, pp. 1253–1257.

Gill, P.E., W. Murray and M.H. Wright (1981). *Practical Optimization,* Academic Press, London.

Gu, G. and P.P. Khargonekar (1992). A class of algorithms for identification in H_∞. *Automatica,* Vol. 28, pp. 299–312.

Hakvoort, R.G. (1992). Worst–case system identification in H_∞: error bounds and optimal models. *Sel. Top. Id., Mod. and Contr.,* Vol. 5, eds. O.H. Bosgra and P.M.J. Van den Hof, Delft University Press, The Netherlands, pp. 73–84. Also in *Proc. IFAC World Congress,* Sydney, Australia, 1993.

Hakvoort, R.G. and P.M.J. Van den Hof (1993). Frequency domain curve fitting with maximum amplitude criterion and guaranteed stability. *To appear in Int. Journal of Contr.*

Levy, E.C. (1959). Complex curve fitting. *IRE Trans. Autom. Contr.*, Vol. 4, pp. 37–43.

Luenberger, D.G. (1984). *Linear and Nonlinear Programming,* Addison Wesley, U.K., 2nd edition.

Payne, P.A. (1970). An improved technique for transfer function synthesis from frequency response data. *IEEE Trans. Autom. Contr.*, Vol. AC–15, pp. 480–483.

Sanathanan, C.K. and J. Koerner (1963). Transfer function synthesis as a ratio of two complex polynomials. *IEEE Trans. Autom. Contr.*, Vol. AC–8, pp. 56–58.

Sidman, M.D., F.E. DeAngelis and G.C. Verghese (1991). Parametric system identification on logarithmic frequency response data. *IEEE Trans. Autom. Contr.*, Vol. AC–36, pp. 1065–1070.

Spanos, J.T. (1991). Algorithms for ℓ_2 and ℓ_∞ transfer function curve fitting. *Proc. AIAA Guid., Navig. and Contr. Conf.*, New Orleans, LA.

Whitfield, A.H. (1987). Asymptotic behaviour of transfer function synthesis methods. *Int. J. Contr.*, Vol. 45, pp. 1083–1092.

Selected Topics in Identification, Modelling and Control
Vol. 6, December 1993

Identification with generalized orthonormal basis functions - statistical analysis and error bounds

Paul Van den Hof [‡], Peter Heuberger [§] and József Bokor [♯]

[‡]*Mechanical Engineering Systems and Control Group*
Delft University of Technology, Mekelweg 2, 2628 CD Delft, The Netherlands.
[§]*National Institute of Public Health and Environmental Protection (RIVM),*
P.O. Box 1, 3720 BA Bilthoven, The Netherlands.
[♯]*Computer and Automation Research Institute, Hungarian Academy of Sciences,*
Kende u. 13-17, H 1502 Budapest, Hungary.

Abstract. A least squares identification method is studied that estimates a finite number of expansion coefficients in the series expansion of a transfer function, where the expansion is in terms of recently introduced generalized basis functions. The basis functions are orthogonal in $\mathcal{H}_2$ and generalize the pulse, Laguerre and Kautz bases. One of their important properties is that when chosen properly they can substantially increase the speed of convergence of the series expansion. This leads to accurate approximate models with only few coefficients to be estimated. Explicit bounds are derived for the bias and variance errors that occur in the parameter estimates as well as in the resulting transfer function estimates.

Keywords. System identification, orthogonal basis functions, FIR models, linear regression, modelling errors, system approximation.

1 Introduction

The use of orthogonal basis functions in modelling and identification of dynamical systems has a long history. Recently, renewed attention has been given to the problem of chosing basis functions that are in some sense suitable for accurately modelling a given dynamical system. The use of Laguerre functions (King et al., 1979; Nurges and Yaaksoo, 1981; Nurges, 1987; Wahlberg, 1991) shows the ability to choose a scalar design variable in a range that matches the dominating (first order) dynamics of the process to be modelled. An optimal choice of this design variable is given attention in Fu and Dumont (1993). For moderately damped systems, Kautz functions have been introduced, which actually are basis functions based on second order dynamics, see e.g. Kautz (1954), Wahlberg (1990, 1994).

Recently a generalized set of orthonormal basis functions has been developed that is generated by inner (all pass) transfer functions of any prechosen order, Heuberger and Bosgra (1990), Heuberger (1991), Heuberger *et al.* (1992, 1993). This type of basis functions generalizes the Laguerre and Kautz-type bases, which actually occur as special cases when choosing first order and second order inner functions. Given any inner transfer function (with any set of eigenvalues), an orthonormal basis for the signal space ℓ_2 (and similarly for the operator space $\mathcal{H}_2$) can be constructed.

Using basis functions that contain dynamics can have important advantages in identification and approximation problems. It has been shown in Heuberger et al. (1992), that if the dynamics of the basis generating system and the dynamics of the system to be modelled approach each other, the convergence rate of a series expansion of the

system becomes very fast. Needless to say that the identification of expansion coefficients in a series expansion benefits very much from a fast convergence rate; the number of coefficients to be determined to accurately model the system becomes smaller.
In this paper, we will focus on the properties of the identification scheme that estimates expansion coefficients in such series expansions, by using simple (least squares) linear regression algorithms. In a stochastic framework, similar to Ljung (1987), we will derive expressions for bias and variance errors that affect the (asymptotic) parameter and transfer function estimates.

Concerning notation, a transfer function is called inner if it is stable and it additionally satisfies $G^T(z^{-1})G(z) = 1$. $\ell_2[0,\infty)$ is the space of squared summable sequences on the time-interval $\mathbf{Z} \cap [0,\infty)$. $\mathcal{H}_2$ is the Hilbert space of stable linear systems, that are squared integrable on the unit circle. $\delta(t)$ is the Kronecker delta function, i.e. $\delta(t) = 1$, $t = 0$; $\delta(t) = 0$, $t \neq 0$.

We consider the following problem set-up.
Let there be a data generating system:

$$y(t) = G_0(q)u(t) + v(t) \tag{1}$$

with $G_0(z) = \sum_{k=1}^{\infty} g_0(k)q^{-k}$ a scalar, stable and strictly proper linear, time-invariant discrete-time system; $y(t)$ and $u(t)$ scalar-valued output and input signal; v a zero-mean stationary stochastic process with rational spectral density, and q^{-1} the delay operator. We will write $v(t)$ as

$$v(t) = H_0(q)e_0(t) \tag{2}$$

with e_0 a unit variance, zero mean white noise process, and H_0 a stable rational transfer function.
When given a sequence of orthonormal basis functions $\{V_k(z)\}_{k=0,\cdots,\infty}$, we will accordingly write:

$$G_0(z) = z^{-1}\sum_{k=0}^{\infty} L_0(k)V_k(z) \tag{3}$$

Given data $\{u(t), y(t)\}_{t=0,\cdots,N}$ that is taken from experiments on this system, a model will be identified using a model structure

$$\varepsilon(t,\theta) = y(t) - \sum_{k=0}^{n-1} L(k,\theta)V_k(q)u(t-1) \tag{4}$$

with $\varepsilon(t,\theta)$ referring to the one-step-ahead prediction error of the model given by parameter θ (see Ljung, 1987). The estimated parameter is determined by the least squares method:

$$\hat{\theta}_N = \arg\min_{\theta} \frac{1}{N}\sum_{t=1}^{N} \varepsilon(t,\theta)^2 \tag{5}$$

where θ varies over some appropriate parameter space.

2 Generalized orthonormal basis functions

The basic result from Heuberger et al. (1992) concerning generalized basis functions is reflected in the following proposition.

Proposition 2.1 *Let $G_b(z)$ be a scalar inner function with McMillan degree $n_b > 0$, having a minimal balanced realization (A, B, C, D).*
Denote

$$V_k(z) := z(zI - A)^{-1}BG_b^k(z) \tag{6}$$

Then the sequence of scalar rational functions $\{e_i^T V_k(e^{i\omega})\}_{i=1,\cdots,n_b;k=0,\cdots,\infty}$ forms an orthonormal basis for the set $\mathcal{H}_2$ of all stable rational functions that are squared integrable on the unit circle. □

As a result, for any such $V_k(z)$, any strictly proper transfer function $G(z) \in \mathcal{H}_2$ has a unique series expansion

$$G(q) = q^{-1}\sum_{k=0}^{\infty} L(k)V_k(q) \tag{7}$$

with $L(k) \in \mathbb{R}^{1\times n_b}$.

Remark 2.2 *Note that for specific choices of $G_b(z)$ well known classical basis functions can be generated, such as the pulse functions $V_k(z) = z^{-k}$ which originate from $G_b(z) = z^{-1}$, and the Laguerre functions*

$$V_k(z) = \sqrt{1-a^2}\,z\frac{(1-az)^k}{(z-a)^{k+1}} \tag{8}$$

that originate from the inner function $G_b(z) = \dfrac{1-az}{z-a}$, with some real-valued a, $|a| < 1$, and balanced realization

$$(A, B, C, D) = (a, \sqrt{1-a^2}, \sqrt{1-a^2}, -a).$$

The Kautz functions (Kautz, 1954; Wahlberg, 1990,1994), can be shown to be generated by a second order inner function, see Heuberger et al. (1992).

This orthonormal basis for $\mathcal{H}_2$ also induces a similar basis for the signal space $\ell_2[0,\infty)$ of squared summable sequences, through inverse z-transformation to the signal-domain. Let

$$V_k(z) = \sum_{\ell=0}^{\infty} \phi_k(\ell)z^{-\ell} \tag{9}$$

then $\{e_i^T\phi_k(\ell)\}_{i=1,\cdots,n_b;k=0,\cdots,\infty}$ is an orthonormal basis for the signal space $\ell_2[0,\infty)$.

3 Orthogonal transformations of signals and systems

The orthonormal basis for $\ell_2/\mathcal{H}_2$ induces a transformation of signals and systems to an "orthogonal" domain. Next to the intrinsic importance of signal and systems analysis in this transform-domain (for some of these results see Heuberger (1991)), we can fruitfully use these transformations in the analysis of statistical properties of the identified models, as well as in the derivation of bias and variance error bounds.

Let $\{V_k(z)\}_{k=0,\cdots\infty}$ be an orthonormal basis, as defined in the previous section, and let $\{\phi_k(t)\}_{k=0,\cdots\infty}$ be as defined in (9), then for any signal $x(t) \in \ell_2^m$ there exists a unique transformation

$$\mathcal{X}(k) := \sum_{t=0}^{\infty} \phi_k(t) x^T(t) \tag{10}$$

and we denote the corresponding λ-transform of $\mathcal{X}(k)$ as:

$$\tilde{x}(\lambda) := \sum_{k=0}^{\infty} \mathcal{X}(k)\lambda^{-k} \tag{11}$$

We will refer to $\tilde{x}(\lambda)$ as the *Hambo*-transform of the signal $x(t)$. Note that $x \in \ell_2^m$, and $\tilde{x}(\lambda) \in \mathcal{H}_2^{n_b \times m}$.
Now consider a scalar system $y(t) = G(q)u(t)$ with $G \in \mathcal{H}_2$ with u, y signals in ℓ_2. Then there exists a Hambo-transformed system $\tilde{G}(\lambda) \in \mathcal{H}_2^{n_b \times n_b}$ such that

$$\tilde{y}(\lambda) = \tilde{G}(\lambda)\tilde{u}(\lambda). \tag{12}$$

In terms of the sequence of expansion coefficients, this can also be written as

$$\mathcal{Y}(k) = \tilde{G}(q)\mathcal{U}(k) \quad \text{for all } k \tag{13}$$

where the shift operator q operates on the sequence index k. The construction of this transformed system is given in the following proposition.

Proposition 3.1 *Consider a scalar system $G \in \mathcal{H}_2$ relating input and output signals according to $y(t) = G(q)u(t)$ with $u, y \in \ell_2$, with $G(z) = \sum_{k=0}^{\infty} g(k)z^{-k}$.*
Consider an orthonormal basis $\{V_k(z)\}_{k=0,\cdots\infty}$ as defined in the previous section, generated by a scalar inner transfer function $G_b(z)$ with input-balanced realization (A, B, C, D).
Denote:

$$N(\lambda) := A + B(\lambda I - D)^{-1}C \tag{14}$$

Then

$$\tilde{y}(\lambda) = \tilde{G}(\lambda)\tilde{u}(\lambda) \tag{15}$$

with

$$\tilde{G}(\lambda) := \sum_{k=0}^{\infty} g(k)N(\lambda)^k. \tag{16}$$

Proof: See Appendix. □

The interpretation of this proposition is that the Hambo-transform of any system G can be obtained by a simple variable-transfomation on the original transfer function, where the variable transformation concerned is given by $z^{-1} = N(\lambda)$.
Note that this result generalizes the situation of a corresponding Laguerre transformation, where it concerns the variable-transformation $z = \dfrac{\lambda + a}{1 + a\lambda}$ (see also Wahlberg, 1991). However due to the fact that the McMillan degree of the inner function generating the basis in this generalized case is $n_b \geq 1$, the Hambo-transformed system decription $\tilde{G}$ increases in input/output-dimension to $\tilde{G} \in \mathcal{H}_2^{n_b \times n_b}$. Note that G is scalar. $N(\lambda)$ is an $n_b \times n_b$ rational transfer function matrix of order 1 (since D is scalar).
The previous Proposition considers scalar ℓ_2 signals and scalar systems. There exists a straightforward extension of these results to a particularly structured multivariable system that will appear to be fruitful in the sequel of this paper.

Proposition 3.2 *Consider a scalar transfer function $G \in \mathcal{H}_2$ relating m-dimensional input and output signals $y, u \in \ell_2^m$, according to* [1]

$$y(t) = [G(z)I_m]u(t) \tag{17}$$

Then

$$\tilde{y}(\lambda) = \tilde{G}(\lambda)\tilde{u}(\lambda) \tag{18}$$

with $\tilde{G}(\lambda)$ as defined in (16). □

Proof: For $m = 1$ the result is shown in Proposition 3.1. If we write the relation between y and u componentwise, i.e. $y_i(t) = G(z)u_i(t)$ it follows from the mentioned Proposition that $\tilde{y}_i(\lambda) = \tilde{G}(\lambda)\tilde{u}_i(\lambda)$, where $\tilde{y}_i, \tilde{u}_i \in \mathbb{R}^{n_b \times 1}(\lambda)$. It follows directly that

$$\begin{aligned}\tilde{y}(\lambda) &= [\tilde{y}_1(\lambda) \mid \cdots \mid \tilde{y}_m(\lambda)] = \\ &= \tilde{G}(\lambda)[\tilde{u}_1(\lambda) \mid \cdots \mid \tilde{u}_m(\lambda)] = \tilde{G}(\lambda)\tilde{u}(\lambda).\end{aligned}$$

□

One of the results that we will need in the analysis of least squares related block Toeplitz matrices is formulated in the following Proposition.

[1] Since $G(z)$ is scalar we allow the notation $G(z)I_m$, which more formally should be denoted as $G(z) \otimes I_m$.

Proposition 3.3 *Consider a scalar inner transfer function $G_b(z)$ generating an orthogonal basis as discussed before. Then*

$$\tilde{G}_b(\lambda) = \lambda^{-1} I_{n_b}. \tag{19}$$

Proof: It can simply be verified that for all k, $G_b(q)\phi_k(t) = \phi_{k+1}(t)$. With Proposition 3.1 it follows that $\tilde{\phi}_{k+1}(\lambda) = \tilde{G}_b(\lambda)\tilde{\phi}_k(\lambda)$.
Since for each k, $\tilde{\phi}_k(\lambda) = \sum_{t=0}^{\infty} I_{n_b}\delta(t-k)\lambda^{-t}$, it follows that for all k,

$$I_{n_b}\lambda^{-k-1} = \tilde{G}_b(\lambda) I_{n_b}\lambda^{-k}. \tag{20}$$

Since this holds for all k it follows that $\tilde{G}_b(\lambda) = I_{n_b}\lambda^{-1}$. □

The basis generating inner function transforms to a simple shift in the Hambo-domain.
The following lemma relates quadratic signal properties to properties of the transformed signals.

Lemma 3.4 *Let $x_j, x_\ell \in \ell_2^m$ and consider a Hambo-transform induced by an orthonormal basis $V_k(z)$ generated by an inner function $G_b(z)$ with McMilland degree $n_b \geq 1$. Then*

$$\sum_{t=0}^{\infty} x_j(t)x_\ell^T(t) = \sum_{k=0}^{\infty} \mathcal{X}_j^T(k)\mathcal{X}_\ell(k) = \frac{1}{2\pi}\int_{-\pi}^{\pi} \tilde{x}_\ell^T(e^{-i\omega})\tilde{x}_j(e^{i\omega})d\omega.$$

Proof: This Lemma is a direct consequence of the fact that due to the fact that the basis is orthonormal, it induces a transformation that is an isomorphism. □

The transformation that is discussed in this section refers to ℓ_2-signals and the corresponding transformation of systems actually concerns the transformation of the ℓ_2-behaviour of a dynamical system. However, this same orthogonal basis for ℓ_2 can also be employed to induce a transformation of (quasi-) stationary stochastic processes to an orthogonal domain.

4 Orthogonal transformations and stochastic processes

Let v be a scalar valued stochastic process or quasi-stationary signal (Ljung, 1987), having a rational spectral density $\Phi_v(\omega)$. Let $H_v(e^{i\omega})$ be a stable spectral factor of $\Phi_v(\omega)$, and let $h_v(k)$ be its ℓ_2 impulse response, satisfying $H_v(z) = \sum_{k=0}^{\infty} h_v(k)z^{-k}$.
Then

$$h_v(t) = H(q)\delta(t) \tag{21}$$

and consequently with Proposition 3.1

$$\tilde{h}_v = \tilde{H}\tilde{\delta}. \tag{22}$$

Similarly, let $w(t) = P_{wv}(q)v(t)$ with P_{wv} a stable scalar transfer function, then

$$\tilde{h}_w = \tilde{P}_{wv}\tilde{h}_v \tag{23}$$

with $h_w, h_v \in \ell_2$, the impulse responses of stable spectral factors of $\Phi_w(\omega)$, $\Phi_v(\omega)$, respectively.
Similarly to Lemma 3.4 we can now formulate some properties of stochastic processes.

Lemma 4.1 *Let w, z be m-dimensional stationary stochastic processes, satisfying $w(t) = \sum_{k=0}^{\infty} h_w(k)e(t-k)$ and $z(t) = \sum_{k=0}^{\infty} h_z(k)e(t-k)$, with e a scalar-valued unit variance white noise process. Then*

$$\bar{E}[w(t)z^T(t)] = \frac{1}{2\pi}\int_{-\pi}^{\pi} \tilde{h}_w^T(e^{-i\omega})\tilde{h}_z(e^{i\omega})d\omega. \tag{24}$$

Lemma 4.2 *Let w, z, and v be m-dimensional stationary stochastic processes, satisfying*

$$w(t) = P_{wv}(q)I_m v(t) \tag{25}$$

$$z(t) = P_{zv}(q)I_m v(t), \tag{26}$$

with $P_{wv}, P_{zv} \in \mathcal{H}_2$, and $v(t) = \sum_{k=0}^{\infty} h_v(k)e(t-k)$, with e a scalar-valued unit variance white noise process. Then

$$\bar{E}w(t)z^T(t) = \frac{1}{2\pi}\int_{-\pi}^{\pi} \tilde{h}_v^T(e^{-i\omega})\tilde{P}_{wv}^T(e^{-i\omega})\tilde{P}_{wv}(e^{i\omega})\tilde{h}_v(e^{i\omega})d\omega.$$

The previous two lemma's can simply be shown to hold also in the case of quasi-stationary signals. To this end we already used the operator $\bar{E} := \lim_{N\to\infty} \frac{1}{N}\sum_{t=0}^{N-1} E$, where E stands for expectation.

5 Identification with linear regression models

As mentioned in the introduction, we will consider a least squares identification scheme applied to the model structure

$$\varepsilon(t,\theta) = y(t) - q^{-1}\sum_{k=0}^{n-1} L(k)V_k(q)u(t), \tag{27}$$

where we will assume that the input signal $u(t)$ is a realization of some stationary stochastic process, and we will denote

$$\theta := [L(0) \cdots L(n-1)]^T \quad \in \mathbb{R}^{n_b \cdot n}. \tag{28}$$

We will further denote

$$x_k(t) := q^{-1}V_k(q)u(t) \tag{29}$$

$$\psi(t) := \begin{bmatrix} x_0(t) \\ x_1(t) \\ \vdots \\ x_{n-1}(t) \end{bmatrix} \tag{30}$$

and consequently

$$\varepsilon(t,\theta) = y(t) - \psi^T(t)\theta. \tag{31}$$

Following Ljung (1987) under weak conditions the parameter estimate $\hat{\theta}_N(n)$ (5) will converge with probability 1 to the asymptotic estimate

$$\theta^*(n) = R(n)^{-1}F(n) \tag{32}$$

with

$$R(n) = \bar{E}\psi(t)\psi^T(t) \qquad F(n) = \bar{E}\psi(t)y(t) \tag{33}$$

For the analysis of bias and variance errors of this identification scheme, we will further use the following notation:

$$\begin{aligned} G_0(z) &= z^{-1}\sum_{k=0}^{\infty} L_0(k)V_k(z) \\ \theta_0 &= [L_0(0)\cdots L_0(n-1)]^T \\ \theta_e &= [L_0(n)\ L_0(n+1)\cdots]^T \\ \psi_e(t) &= [x_n^T(t)\ x_{n+1}^T(t)\cdots]^T \\ \Omega_n(e^{i\omega}) &:= e^{-i\omega}[V_0^T(e^{i\omega})\ V_1^T(e^{i\omega})\ \cdots V_{n-1}^T(e^{i\omega})]^T \\ \Omega_e(e^{i\omega}) &:= e^{-i\omega}[V_n^T(e^{i\omega})\ V_{n+1}^T(e^{i\omega})\ \cdots]^T \end{aligned}$$

leading to the following alternative description of the data generating system:

$$y(t) = \psi^T(t)\theta_0 + \psi_e^T(t)\theta_e + v(t), \tag{34}$$

$$G_0(e^{i\omega}) = \Omega^T(e^{i\omega})\theta_0 + \Omega_e^T(e^{i\omega})\theta_e. \tag{35}$$

We will further assume that the input signal u has a rational spectral density function $\Phi_u(\omega)$, with a stable spectral factor $H_u(e^{i\omega})$.

6 Asymptotic analysis of bias and variance errors

6.1 Introduction

First we will present a couple of results concerning the properties of the block-Toeplitz matrix $R(n)$.

Lemma 6.1 *The block-Toeplitz matrix $R(n)$ defined in (33) is the covariance matrix related to the spectral density function*

$$\Phi_{\tilde{x}_0}(\omega) = \tilde{h}_{x_0}^T(e^{-i\omega})\tilde{h}_{x_0}(e^{i\omega}),$$

where $h_{x_0}(t) := q^{-1}V_0(q)H_u(q)\delta(t)$.

Proof: The matrix $R(n)$ has a block-Toeplitz structure with the (j,ℓ) block-element given by $\bar{E}x_j(t)x_\ell^T(t)$. Since $x_j(t) = G_b^j(q)I_{n_b} \cdot x_0(t)$ it follows with Lemma 4.2 that

$$\bar{E}x_j(t)x_\ell^T(t) = \frac{1}{2\pi}\int_{-\pi}^{\pi} \tilde{h}_{x_0}^T(e^{-i\omega})[\tilde{G}_b^T(e^{-i\omega})]^j[\tilde{G}_b(e^{i\omega})]^\ell \tilde{h}_{x_0}(e^{i\omega})d\omega.$$

With Proposition 3.3 it follows that

$$\bar{E}x_j(t)x_\ell^T(t) = \frac{1}{2\pi}\int_{-\pi}^{\pi} e^{i\omega(j-\ell)}\Phi_{\tilde{x}_0}(\omega)d\omega, \tag{36}$$

with $\Phi_{\tilde{x}_0}(\omega) := \tilde{h}_{x_0}^T(e^{-i\omega})\tilde{h}_{x_0}(e^{i\omega})$, and this proves the result. □

Lemma 6.2 *Let H_u be a stable spectral factor of the spectral density function $\Phi_u(\omega)$. Then*

$$\Phi_{\tilde{x}_0}(\omega) = \tilde{H}_u^T(e^{-i\omega})\tilde{H}_u(e^{i\omega}). \tag{37}$$

Proof: Since $x_0(t) = q^{-1}V_0(q)u(t)$ we can write $h_{x_0}(t) = q^{-1}V_0(q)H_u(q)\delta(t)$. Since H_u is scalar, we can write $h_{x_0}(t) = H_u(q)q^{-1}V_0(q)\delta(t) = H_u(q)h_{v_0}(t)$, with $h_{v_0}(t)$ the impulse response of the transfer function $q^{-1}V_0(q)$.
Applying Proposition 3.1 now shows $\tilde{h}_{x_0} = \tilde{H}_u\tilde{h}_{v_0} = \tilde{H}_u$. The latter equality follows from $\tilde{h}_{v_0} = I_{n_b}$, as the impulse response of $q^{-1}V_0(q)$ exactly matches the first n_b basis functions in the Hambo-domain. □

Remark 6.3 *Note that in Wahlberg (1991) for the (first order) Laguerre case, the corresponding Toeplitz matrix is the covariance matrix related to the spectral density*

$$\Phi_u\left(\frac{e^{i\omega}+a}{1+ae^{i\omega}}\right). \tag{38}$$

This implies that in that case a variable transformation

$$e^{i\omega} \to \frac{e^{i\omega}+a}{1+ae^{i\omega}} \tag{39}$$

is involved, or equivalently

$$e^{-i\omega} \to \frac{1+ae^{i\omega}}{e^{i\omega}+a}. \tag{40}$$

Note that in this Laguerre case we can write $G_b(z) = \dfrac{1-az}{z-a}$, *which can be realized by the minimal balanced realization* $(A,B,C,D) = (a, \sqrt{1-a^2}, \sqrt{1-a^2}, -a)$.
In the setting of this paper, the variable transformation involved is given by $e^{-i\omega} \rightarrow N(e^{i\omega})$, *while* N *has a minimal balanced realization*

$$(D,C,B,A) = (-a, \sqrt{1-a^2}, \sqrt{1-a^2}, a).$$

This directly leads to the variable transformation (40).

The following Proposition bounds the eigenvalues of the Toeplitz matrix $R(n)$.

Proposition 6.4 *Let the Toeplitz matrix* $R(n)$ *defined in* (33) *have eigenvalues* $\lambda_j(R(n))$. *Then*

(a) For all n, *the eigenvalues of* $R(n)$ *are bounded by*

$$ess \inf_{\omega} \Phi_u(\omega) \leq \lambda_j(R(n)) \leq ess \sup_{\omega} \Phi_u(\omega).$$

(b) $\lim_{n\rightarrow\infty} \max_j \lambda_j(R(n)) = ess \sup_{\omega} \Phi_u(\omega)$.

Proof: See Appendix. □

6.2 Asymptotic bias error

We will analyse upper bounds for the asymptotic bias errors $\theta^* - \theta_0$ and $|G(e^{i\omega},\theta^*) - G_0(e^{i\omega})|$.
Combining equations (32),(33) and (34) shows that

$$\theta^* - \theta_0 = R(n)^{-1} \bar{E}[\psi(t)\psi_e^T(t)\theta_e] \qquad (41)$$

consequently

$$\| \theta^* - \theta_0 \|_2 \leq \| R(n)^{-1} \|_2 \cdot \| \bar{E}[\psi(t)\psi_e^T(t)] \|_2 \cdot \|\theta_e\|_2, \qquad (42)$$

where for a (matrix) operator T, $\|T\|_2$ refers to the induced operator 2-norm. For simplicity of notation we have skipped the dependence of θ^* (and θ_0) on n. This leads to the following result.

Proposition 6.5 *Consider the identification setup as discussed in the previous section. Then*

$$\|\theta^* - \theta_0\|_2 \leq \frac{ess \sup_{\omega} \Phi_u(\omega)}{ess \inf_{\omega} \Phi_u(\omega)} \cdot \|\theta_e\|_2, \qquad (43)$$

where $\|\theta_e\|_2 = \sqrt{\sum_{k=n}^{\infty} L_0^T(k) L_0(k)}$. □

The Proof of the Proposition is added in the Appendix.
For the bias in the transfer function estimate the corresponding result is as follows.

Proposition 6.6 *Consider the identification setup as discussed in the previous section. Then*
Part (a). For all $\omega_1 \in \mathbb{R}$,

$$|G(e^{i\omega_1},\theta^*) - G_0(e^{i\omega_1})| \leq$$
$$\leq \|V_0(e^{i\omega_1})\|_\infty [\|\theta_0 - \theta^*\|_1 + \|\theta_e\|_1] \leq$$
$$\|V_0(e^{i\omega_1})\|_\infty \{\sqrt{n_b n} \frac{\text{ess sup}_\omega \Phi_u(\omega)}{\text{ess inf}_\omega \Phi_u(\omega)} \|\theta_e\|_2 + \|\theta_e\|_1\}, \quad (44)$$

where $\|V_0(e^{i\omega_1})\|_\infty$ is the ℓ_∞-induced operator norm of the matrix $V_0(e^{i\omega_1}) \in \mathbb{C}^{n_b \times 1}$, i.e. the maximum absolute value over the elements in $V_0(e^{i\omega_1})$.
Part (b). The $\mathcal{H}_2$-norm of the model error is bounded by:

$$\|G(z,\theta^*) - G_0(z)\|_{\mathcal{H}_2} \leq$$
$$\leq \sqrt{\|\theta_0 - \theta^*\|_2^2 + \|\theta_e\|_2^2},$$
$$\leq \{1 + \frac{ess \sup_\omega \Phi_u(\omega)}{ess \inf_\omega \Phi_u(\omega)}\} \|\theta_e\|_2.$$

The proof is added in the Appendix. □

Note that this latter bound on the bias in the transfer function estimate as well as the previously derived bound, are dependent on the basis functions chosen.
Note that the factor $\|\theta_e\|_2^2$ is determined by the convergence rate of the series expansion of G_0 in the generalized basis. The closer the dynamics of the system G_0 will be to the dynamics of the inner transfer function G_b, the faster the convergence rate will be. Upper bounds for the convergence rate in terms of the eigenvalues of G_0 and G_b are derived in Heuberger et al. (1992).

The results in (43), (45) show that we achieve consistency of the parameter and transfer function estimates as $n \rightarrow \infty$ provided that the input spectrum is bounded away from 0 and $\|\theta_e\|_2 \rightarrow 0$ for $n \rightarrow \infty$. The latter condition is guaranteed if $G_0 \in \mathcal{H}_2$.

For the FIR case, corresponding with $G_b(z) = z^{-1}$, we know that under specific experimental conditions also the finite number of expansion coefficients can be estimated consistently, irrespective of the tail. This situation can also be formulated for the generalized case.

Corollary 6.7 *Consider the identification setup as discussed in the previous section.*
If $\tilde{H}_u$ *is an inner transfer function, then for any value of* n, $\theta^* = \theta_0$ *and the transfer function error bounds become*

(a) $|G(e^{i\omega_1},\theta^*) - G_0(e^{i\omega_1})| \leq \|V_0(e^{i\omega_1})\|_\infty \|\theta_e\|_1$, *for each* ω_1;

(b) $\|G(z,\theta^*) - G_0(z)\|_{\mathcal{H}_2} \leq \|\theta_e\|_2^2$.

Proof: Under the given condition it can simply be verified that $\Phi_{\tilde{x}_0}(\omega) = cI_{n_b}$. This implies that the block-Toeplitz matrix $R(n) = I$, and that for all $n \geq 1$, $R_{12}(n) = 0$. Employing this relation in the proofs of Propositions 6.5, 6.6 shows the results. □

Note that a special case of the situation of an inner $\tilde{H}_u$ is obtained if the input signal u is uncorrelated (white noise). In that situation $H_u = 1$ and consequently $\tilde{H}_u = I_{n_b}$, being inner.

6.3 Asymptotic variance error

For an analysis of the asymptotic variance of the estimated transfer function, we can generalize the results as obtained for the case of Laguerre functions in Wahlberg (1991).
From classical analysis of prediction error identification methods, Ljung (1987), we know that under fairly weak conditions

$$\sqrt{N}(\hat{\theta}_N(n) - \theta^*) \to \mathcal{N}(0, Q_n) \quad \text{as } N \to \infty, \tag{45}$$

where $\mathcal{N}(0, Q_n)$ denotes a Gaussian distribution with zero mean and covariance matrix Q_n. For output error identification schemes, as applied in this paper, the asymptotic covariance matrix satisfies:

$$Q_n = [\bar{E}\psi(t)\psi^T(t)]^{-1}[\bar{E}\bar{\psi}(t)\bar{\psi}^T(t)][\bar{E}\psi(t)\psi^T(t)]^{-1} \tag{46}$$

with $\bar{\psi}(t) = \sum_{i=0}^{\infty} h_0(i)\psi(t+i)$, and $h_0(i)$ the impulse response of the corresponding transfer function H_0.
Note that according to Lemma 6.1, $R(n) = \bar{E}\psi(t)\psi^T(t)$ is a finite part of an infinite covariance block-Toeplitz matrix with spectral density $\Phi_{\tilde{x}_0}(\omega) = \tilde{H}_u^T(e^{-i\omega})\tilde{H}_u(e^{i\omega})$.
For ease of notation we will introduce the following transformed spectrum for any (quasi-stationary) stochastic process $s(t)$:

$$\tilde{\Phi}_s(\omega) := \tilde{H}_s^T(e^{-i\omega})\tilde{H}_s(e^{i\omega}), \tag{47}$$

where H_s is a stable spectral factor of the spectrum of s.
This notation implies that $\Phi_{\tilde{x}_0}(\omega) = \tilde{\Phi}_u(\omega)$.
In our evaluation of the asymptotic covariance matrix Q_n, this brings us to the following result for the block-Toeplitz matrix $P(n) = \bar{E}\bar{\psi}(t)\bar{\psi}^T(t)$.

Lemma 6.8 *The spectral density function related to the block Toeplitz matrix $P(n) = \bar{E}\bar{\psi}(t)\bar{\psi}^T(t)$ is given by*

$$\tilde{\Phi}_u(\omega) \cdot \tilde{\Phi}_v(\omega). \tag{48}$$

Proof: The proof follows along similar lines as followed in the proofs of Lemma's 6.1 and 6.2. □

From the asymptotic covariance of the parameter estimate, we can derive the expression for the transfer function estimate:

$$\sqrt{\frac{N}{n}} cov(\hat{G}(e^{i\omega_1}), \hat{G}(e^{i\omega_2})) \to \frac{1}{n}\Omega_n^T(e^{i\omega_1})Q_n\Omega_n(e^{-i\omega_2}) \tag{49}$$

as $N \to \infty$, while $cov(\cdot,\cdot)$ refers to the cross-covariance matrix in the joint asymptotic distribution of

$$[G(e^{i\omega_1}, \hat{\theta}_N) - G(e^{i\omega_1}, \theta^*), G(e^{i\omega_2}, \hat{\theta}_N) - G(e^{i\omega_2}, \theta^*)].$$

Now we have the ingredients for formulating an expression for the asymptotic covariance ($n \to \infty$, $N \to \infty$) of the estimated transfer functions.

Theorem 6.9 *Assume the spectral density $\Phi_u(\omega)$ to be bounded away from zero and sufficiently smooth.*
Then for $N \to \infty$ and $n \to \infty$:

$$\sqrt{\frac{N}{n}} cov(G(e^{i\omega_1}, \hat{\theta}_N), G(e^{i\omega_2}, \hat{\theta}_N)) \to \begin{cases} 0 & \text{for } G_b(e^{i\omega_1}) \neq G_b(e^{i\omega_2}), \\ V_0^T(e^{i\omega_1})V_0(e^{-i\omega_1}) \cdot \dfrac{\Phi_v(\omega_1)}{\Phi_u(\omega_1)} & \text{for } \omega_1 = \omega_2. \end{cases}$$

The proof is added in the Appendix.

Theorem 6.9 gives a closed form expression for the asymptotic covariance. Note that it implies that the variance of the transfer function estimate for a specific ω_1 is given by

$$V_0^T(e^{i\omega_1})V_0(e^{-i\omega_1}) \cdot \frac{\Phi_v(\omega_1)}{\Phi_u(\omega_1)} \tag{50}$$

which is the noise to input signal ratio weighted with an additional weighting factor that is determined by the basis functions. This additional weighting, which is not present in the case of FIR estimation again generalizes the weighting that is also present in the case of Laguerre basis functions, see Wahlberg (1991). Since the frequency function $V_0(e^{i\omega})$ has a low pass character, it ensures that the variance will have a roll-off at high frequencies. This is unlike the case of FIR estimation, where the absolute variance generally increases with increasing frequency.
The role of V_0 in this variance expression clearly shows that there is a design variable involved that can be chosen also from a point of view of variance reduction. In that case V_0 has to be chosen

in such away that it reduces the effect of the noise ($\Phi_v(\omega)$) in those frequency regions where the noise is dominating.

The result of the theorem also shows that - in general - the transfer function estimates will be asymptotically uncorrelated. An exception has to be made for thoses frequencies $\omega_1 \neq \omega_2$ for which holds that $G_b(e^{i\omega_1}) = G_b(e^{i\omega_2})$. This situation will occur in the situation that $n_b > 1$, where it becomes possible that the covariance of the two estimates becomes unequal to zero.

Conclusions

In this paper we have analysed some asymptotic properties of linear estimation schemes that identify a finite number of expansion coefficients in a series expansion of a linear stable transfer function, employing recently developed generalized orthogonal basis functions. These basis functions generalize the well known pulse, Laguerre and Kautz basis functions and are shown to provide flexible design variables, that when properly chosen provide fast convergence of the series expansion. In an identification context this implies that only few coefficients have to be estimated to obtain accurate estimates, while simple linear regression schemes can be used. Both bias and variance errors are analysed and error bounds are established.

Acknowledgement

The authors would like to thank Douwe de Vries for his contributions to this project, and the Dutch Systems and Control Theory Network for its financial support.

Appendix

Proof of Proposition 3.1.

Let us consider the situation for $G(z) = z^{-1}$. In this situation $y(t) = u(t-1)$. Consequently $\mathcal{Y}(k) := \sum_{t=0}^{\infty} \phi_k(t) y(t) = \sum_{t=0}^{\infty} \phi_k(t) u(t-1)$. From Heuberger *et al.* (1992), we now that for each $k \in \mathbf{Z}$:

$$\begin{bmatrix} \phi_0(t) \\ \phi_1(t) \\ \vdots \\ \phi_k(t) \end{bmatrix} = A_{k+1} \begin{bmatrix} \phi_0(t-1) \\ \phi_1(t-1) \\ \vdots \\ \phi_k(t-1) \end{bmatrix} \tag{A.1}$$

with the matrix $A_k \in \mathbb{R}^{kn_b \times kn_b}$ given by

$$A_k = \begin{bmatrix} A & 0 & \cdots & \cdot & 0 \\ BC & A & 0 & \cdot & 0 \\ BDC & BC & \cdot & \cdot & 0 \\ \vdots & \vdots & \cdot & \ddots & 0 \\ BD^{k-2}C & BD^{k-1}C & \cdots & BC & A \end{bmatrix}. \tag{A.2}$$

Using this in the expression for $\mathcal{Y}(k)$ shows that

$$\mathcal{Y}(k) = \sum_{t=0}^{\infty} \phi_k(t) u(t-1) \tag{A.3}$$

$$= [0\ 0\ \cdots\ I_{n_b}] A_{k+1} \sum_{t=0}^{\infty} \begin{bmatrix} \phi_0(t-1) \\ \phi_1(t-1) \\ \vdots \\ \phi_k(t-1) \end{bmatrix} u(t-1)$$

$$= [0\ 0\ \cdots\ I_{n_b}] A_{k+1} \begin{bmatrix} \mathcal{U}(0) \\ \mathcal{U}(1) \\ \vdots \\ \mathcal{U}(k) \end{bmatrix}.$$

As a result, for each k,

$$\mathcal{Y}(k) = A\mathcal{U}(k) + BC\mathcal{U}(k-1) + BDC\mathcal{U}(k-2) + \\ + \cdots + BD^{k-1}C\mathcal{U}(0).$$

This immediately shows that

$$\tilde{y}(\lambda) = [A + B(\lambda - D)^{-1}C]\tilde{u}(\lambda), \tag{A.4}$$

leading to $\tilde{G}(\lambda) = [A + B(\lambda - D)^{-1}C]$.
Putting several time delay transfer functions in cascade, it follows straightforwardly that $G(z) = z^{-k}$ leads to $\tilde{G}(\lambda) = N(\lambda)^k$, which proves the result. □

Proof of Proposition 6.4.

Part (a).

Denote the vector $\mu(n) := [\mu_0^T\ \mu_1^T\ \cdots\ \mu_{n-1}^T]^T$, $\mu_i \in \mathbb{R}^{n_b}$. Then

$$\mu(n)^T R(n) \mu(n) = \sum_{k=0}^{n-1} \sum_{\ell=0}^{n-1} \mu_k^T c_{k\ell} \mu_\ell \tag{A.5}$$

with

$$c_{k\ell} = \frac{1}{2\pi} \int_{-\pi}^{\pi} V_k(e^{i\omega}) V_k^T(e^{-i\omega}) \Phi_u(\omega) d\omega. \tag{A.6}$$

Denoting $\eta^T(e^{i\omega}) := \sum_{k=0}^{n-1} \mu_k^T V_k(e^{i\omega})$, it follows that

$$\mu(n)^T R(n) \mu(n) = \frac{1}{2\pi} \int_{-\pi}^{\pi} \eta^T(e^{i\omega}) \Phi_u(\omega) \eta(e^{-i\omega}) d\omega, \tag{A.7}$$

while the orthonormality of the basis functions implies that

$$\frac{1}{2\pi}\int_{-\pi}^{\pi}\eta^T(e^{i\omega})\eta(e^{-i\omega})d\omega = \mu(n)^T\mu(n). \quad (A.8)$$

Since
$ess\inf_\omega \Phi_u(\omega)\cdot\mu(n)^T\mu(n) \le \mu(n)^T R(n)\mu(n) \le$
$\le ess\sup_\omega \Phi_u(\omega)\cdot\mu(n)^T\mu(n)$, it follows that

$$ess\inf_\omega \Phi_u(\omega) \le \|R(n)\|_2 \le ess\sup_\omega \Phi_u(\omega). \quad (A.9)$$

The latter equation can be verified by realizing that, since $R(n)$ is symmetric, there exists $Q(n)$ satisfying $R(n) = Q(n)Q(n)^T$ leading to

$$ess\inf_\omega \Phi_u(\omega) \le \|Q(n)\|_2^2 \le ess\sup_\omega \Phi_u(\omega).$$

Part (b).
The Hermitian form $T_n := \mu^T(n)R(n)\mu(n)$ can be written as

$$T_n = \nu^T(n)diag\{\lambda_1^{(n)},\cdots,\lambda_{n_b n}^{(n)}\}\nu(n)$$

through unitary transformation preserving the norm, i.e. $\nu^T(n)\nu(n) = \mu^T(n)\mu(n)$. Consequently

$$\frac{\mu(n)^T R(n)\mu(n)}{\mu^T(n)\mu(n)} \le \max_i \lambda_i^{(n)}, \quad (A.10)$$

which is known to be bounded by $ess\sup_\omega \Phi_u(\omega)$. Since the Hermitian form T_n is related to the Toeplitz form (A.7), Theorem 5.2.1 in Grenander and Szegö (1958) directly leads to the result that

$$\lim_{n\to\infty}\max_i \lambda_i^{(n)} = ess\sup_\omega \Phi_u(\omega).$$

Proof of Proposition 6.5.
With Proposition 6.4(a) it follows that $\|R(n)^{-1}\|_2 \le (ess\inf_\omega \Phi_u(\omega))^{-1}$.
For constructing a bound on the second term on the right hand side of (42), we first consider the following notation.
Denote $R_{12}(n) := \bar{E}[\psi(t)\psi_e^T(t)]$; then we can write

$$R := \bar{E}\left[\begin{bmatrix}\psi(t)\\ \psi_e(t)\end{bmatrix}\begin{bmatrix}\psi^T(t) & \psi_e^T(t)\end{bmatrix}\right] = \begin{bmatrix}R(n) & R_{12}(n)\\ R_{21}(n) & R_{22}(n)\end{bmatrix},$$

which is an infinite block-Toeplitz matrix, of which $R(n)$ is a finite part.

As $R_{12}(n) = \begin{bmatrix} I_{n_b n} & 0\end{bmatrix} R \begin{bmatrix} 0_{n_b n\times\infty}\\ I\end{bmatrix}$ it follows that

$$\|R_{12}(n)\|_2 \le \|\begin{bmatrix} I_{n_b n} & 0\end{bmatrix}\|_2\|R\|_2\|\begin{bmatrix} 0_{n_b n\times\infty}\\ I\end{bmatrix}\|_2, \le \|R\|_2. \quad (A.11)$$

As a result

$$\|R_{12}(n)\|_2 \le \lim_{n\to\infty}\max_j \lambda_j(R(n)),$$

which
by Proposition 6.4(b) is equal to $ess\sup_\omega \Phi_u(\omega)$. This proves the result. □

Proof of Proposition 6.6.
Writing

$$G(e^{i\omega},\theta^*) - G_0(e^{i\omega}) = [\,\Omega^T(e^{i\omega})\;\Omega_e^T(e^{i\omega})]\begin{bmatrix}\theta^*-\theta_0\\ \theta_e\end{bmatrix} \quad (A.12)$$

it follows that for each ω_1:

$$|G(e^{i\omega_1},\theta^*) - G_0(e^{i\omega_1})| \le \le \|\begin{bmatrix}\Omega^T(e^{i\omega_1}) & \Omega_e^T(e^{i\omega_1})\end{bmatrix}\|_1\cdot\|\begin{bmatrix}\theta^*-\theta_0\\ \theta_e\end{bmatrix}\|_1,$$

where $\|\cdot\|_1$ refers to the induced ℓ_1 matrix norm and the ℓ_1-norm, respectively. It follows from the fact that G_b is inner that

$$\begin{aligned}|G(e^{i\omega_1},\theta^*) - G_0(e^{i\omega_1})| &\le\\ &\le \|V_0^T(e^{i\omega_1})\|_1\cdot\|\begin{bmatrix}\theta^*-\theta_0\\ \theta_e\end{bmatrix}\|_1,\\ &= \|V_0^T(e^{i\omega_1})\|_1\cdot[\|\theta^*-\theta_0\|_1 + \|\theta_e\|_1],\\ &= \|V_0(e^{i\omega_1})\|_\infty\cdot[\|\theta^*-\theta_0\|_1 + \|\theta_e\|_1]. \quad (A.13)\end{aligned}$$

Part (a) of the Proposition now follows by substituting the error bound obtained in Proposition 6.5, and using the inequality $\|\theta^*-\theta_0\|_1 \le \sqrt{n_b n}\|\theta^*-\theta_0\|_2$.

Because of the orthonornality of the basis functions on the unit circle, it follows that

$$\|G(z,\theta^*) - G_0(z)\|_{\mathcal{H}_2} = \|\begin{bmatrix}\theta^*-\theta_0\\ \theta_e\end{bmatrix}\|_2,$$

which together with Proposition 6.5 proves the result of (b). □

Proof of Theorem 6.9.
Using (49), and substituting $\Omega_n(e^{i\omega})$ shows that

$$\frac{1}{n}\Omega_n^T(e^{i\omega_1})Q_n\Omega_n(e^{-i\omega_2}) = \frac{1}{n}[V_0^T(e^{i\omega_1})\;V_1^T(e^{i\omega_1})\;\cdots V_{n-1}^T(e^{i\omega_1})]\cdot Q_n\cdot \cdot[V_0^T(e^{-i\omega_2})\;V_1^T(e^{-i\omega_2})\;\cdots V_{n-1}^T(e^{-i\omega_2})]^T.$$

Note that this latter expression can be written as

$$\frac{1}{n}([1\ G_b(e^{i\omega_1})\ \cdots\ G_b^{n-1}(e^{i\omega_1})] \otimes V_0^T(e^{i\omega_1}))Q_n \cdot$$
$$([1\ G_b(e^{-i\omega_2})\ \cdots\ G_b^{n-1}(e^{-i\omega_2})] \otimes V_0^T(e^{-i\omega_2}))^T,$$

and this equals

$$\frac{1}{n}[1\ G_b(e^{i\omega_1})\ \cdot\ G_b^{n-1}(e^{i\omega_1})]S_n \cdot$$
$$\cdot[1\ G_b(e^{-i\omega_2})\ \cdot\ G_b^{n-1}(e^{-i\omega_2})]^T$$

where

$$S_n = [I_n \otimes V_0^T(e^{i\omega_1})]Q_n[I_n \otimes V_0^T(e^{-i\omega_2})]. \quad \text{(A.14)}$$

Since G_b is an inner function we can consider the variable transformation

$$e^{-i\bar{\omega}} := G_b(e^{i\omega}). \quad \text{(A.15)}$$

Employing this transformation in the derived expression for the covariance matrix provides:

$$\frac{1}{n}\Omega_n^T(e^{i\omega_1})Q_n\Omega_n(e^{-i\omega_2}) =$$
$$= \frac{1}{n}[1\ e^{i\bar{\omega}_1}\ \cdot\ e^{i\bar{\omega}_1(n-1)}]S_n[1\ e^{-i\bar{\omega}_2}\ \cdot\ e^{-i\bar{\omega}_2(n-1)}]^T.$$

The convergence result of Hannan and Wahlberg (1989) and Ljung and Yuan (1985) now show that for $n \to \infty$, this expression converges to

$$\begin{matrix} 0 & \text{if } \bar{\omega}_1 \neq \bar{\omega}_2, \\ S(\bar{\omega}_1), & \text{if } \bar{\omega}_1 = \bar{\omega}_2. \end{matrix} \quad \text{(A.16)}$$

where $S(\omega)$ is the spectral density related to the Toeplitz matrix S_n in the limit as $n \to \infty$.
It can be verified that

$$S(\omega) = V_0^T(e^{i\omega_1}) \cdot \tilde{\Phi}_v(\omega)\tilde{\Phi}_u(\omega)^{-1} \cdot V_0(e^{i\omega_2}). \quad \text{(A.17)}$$

However note that in (A.16) this spectrum has to be evaluated under the variable transformation (A.15). Consider the variable transformtion (A.15) applied to $\tilde{H}_v(e^{i\omega})$. Note that

$$\tilde{H}_v(e^{i\bar{\omega}}) = \tilde{H}_v(G_b(e^{i\omega})) = H_v(e^{i\omega}), \quad \text{(A.18)}$$

the latter equality following from Proposition 3.1. As a result, the expression in (A.16) becomes

$$S(\bar{\omega}_1) = V_0^T(e^{i\omega_1})\Phi_v(\omega_1)\Phi_u(\omega_1)^{-1}V_0(e^{-i\omega_2}),$$

which proves the result. □

References

Y. Fu and G.A. Dumont (1993). An optimum time scale for discrete Laguerre network. *IEEE Trans. Autom. Control, AC-38*, pp. 934-938.

G.C. Goodwin, M. Gevers and D.Q. Mayne (1991). Bias and variance distribution in transfer function estimation. *Preprints 9th IFAC/IFORS Symp. Identification and Syst. Param. Estim.*, July 1991, Budapest, Hungary, pp. 952-957.

U. Grenander and G. Szegö (1958). *Toeplitz Forms and Their Applications.* Univ. California Press, Berkeley, 1958.

E.J. Hannan and B. Wahlberg (1989). Convergence rates for inverse Toeplitz matrix forms. *J. Multiv. Analysis, 31*, no. 1, pp. 127-135.

P.S.C. Heuberger and O.H. Bosgra (1990). Approximate system identification using system based orthonormal functions. *Proc. 29th IEEE Conf. Decision and Control*, pp. 1086-1092.

P.S.C. Heuberger (1991). *On Approximate System Identification with System Based Orthonormal Functions.* Dr. Dissertation, Delft University of Technology, The Netherlands, 1991.

P.S.C. Heuberger, P.M.J. Van den Hof and O.H. Bosgra (1992). *A Generalized Orthonormal Basis for Linear Dynamical Systems.* Report N-404, Mech. Eng. Systems and Control Group, Delft Univ. Techn. Abbreviated version in *Proc. 32nd IEEE Conf. Decision and Control, 1993.*

W.H. Kautz (1954). Transient synthesis in the time domain. *IRE Trans. Circ. Theory, CT-1*, 29-39.

L. Ljung and Z.D. Yuan (1985). Asymptotic properties of black-box identification of transfer functions. *IEEE Trans. Autom. Control, AC-30*, pp. 514-530.

L. Ljung (1987). *System Identification - Theory for the User.* Prentice Hall, Englewood Cliffs, NJ.

Y. Nurges (1987). Laguerre models in problems of approximation and identification of discrete systems. *Autom. and Remote Contr., 48*, 346-352.

Y. Nurges and Y. Yaaksoo (1981). Laguerre state equations for a multivariable discrete system. *Autom. and Remote Contr., 42*, 1601-1603.

B. Wahlberg (1990). *On the Use of Orthogonalized Exponentials in System Identification.* Report LiTH-ISY-1099, Dept. Electr. Eng., Linköping University, Sweden.

B. Wahlberg (1991). System identification using Laguerre models. *IEEE Trans. Automat. Contr., AC-36*, 551-562.

B. Wahlberg (1994). System identification using Kautz models. To be published in *IEEE Trans. Autom. Control.*

Selected Topics in Identification, Modelling and Control
Vol. 6, December 1993

Test for local structural identifiability of high order, non-linearly parametrized state space models

Hans G.M. Dötsch and Paul M.J. Van den Hof

Mechanical Engineering Systems and Control Group
Delft University of Technology, Mekelweg 2, 2628 CD Delft, The Netherlands

Abstract. When a model is to be determined by use of system identification where the model parametrization is non-canonical, existence of a unique model (i.e. unique parameter values) not only depends on the excitation properties of the input signal but also on the model parametrization. The latter is referred to as structural identifiability of a model parametrization. In this paper a method is proposed to investigate local structural identifiability of high order state space models with non-linear parametrizations. The method is based on rank evaluation of an information matrix. A gradient computation algorithm, based on a dynamic programming formulation and normally used in an identification framework, enables computation of an analytical expression for the information matrix.

Keywords. system identification, identifiability, state space model structures, gradient computation

1 Introduction

The issue addressed in this paper concerns identifiability of linear, time invariant model structures where the parametrization is based on, for example, physical a priori knowledge of the process. Since in this case the model parametrization is determined by physical laws, where the (yet unknown) parameters have physical interpretations, the parametrization usually has a non-canonical form. Whereas a canonical parametrization establishes a one-to-one relation between the input-output behaviour of the model and the parameters, this relation is not trivial in case of a non-canonical form. Now if a model is to be determined using system identification, the existence of a unique model (i.e. unique values of the parameters) is imperative for the following reasons. Firstly, if different parameter values correspond to the same input-output behaviour, the model parametrization is not capable of providing a unique description of the process. Secondly, a non-canonical model parametrization might result in an ill-posed identification problem. For these reasons investigation of the relation between input-output behaviour of the model and uniqueness of the corresponding parameter values is a necessary exercise before the actual parameter estimation procedure is carried out. The problem of investigating this relation is referred to as structural identifiability of a model parametrization and is the subject of this paper.

In literature the topic of structural identifiability has received an extensive amount of attention. Bellman and Åström (1970) stated the concept; the subject has been thoroughly studied in the field of biological and biochemical modelling (Rubinow and Winzer, 1971; Cobelli, Lepschy and Romanin Jacur, 1978; Norton, 1980; Godfrey, 1983). State space model parametrizations are analysed by Glover and Willems (1974), Grewal and Glover (1976) and Walter (1981). The problem has been treated in a stochastic framework by Rothenberg (1971) and Tse (1973). Structural identifiability of models in terms of differential-algebraic expressions

has been investigated by Ljung and Glad (1991).

We focus on the case that a priori knowledge of a process is available in the form of a large number of first order difference equations, where the coefficients are expressed in terms of physically interpretable parameters (e.g. volumes, masses, etc.). This leads to formulation of a linear, time invariant high order state space model where the model parameters usually are non-linear expressions of the physical parameters.

Investigation of local structural identifiability using existing techniques has its limitations. Since methods proposed in the field of biological modelling (Godfrey, 1983; Norton, 1980) are based on compartmental models, they can only be applied to this specific type of parametrization. Methods based on non-linearly parametrized state space models either require analytical expressions for partial derivatives of e.g. Markov parameters (to be calculated by hand) (Grewal and Glover, 1976) or they lead to calculation of matrices with dimensions equal to the square of the model order (Glover and Willems, 1974).

In this paper a method is proposed for analysis of local structural identifiability of non-linearly parametrized, high order state space model representations formulated in discrete time. The method is based on rank evaluation of the information matrix as formulated by Rothenberg (1971) and Tse (1973). A problem in their work still is the computation of the information matrix. It will be shown that use of an algorithm for gradient computation, based on a dynamic programming formulation and normally used in an identification framework, enables calculation of an analytical expression for the information matrix. The calculation requires analytical expressions for the partial derivatives of the state space matrices with respect to the argument parameters and shows very limited complexity.

Firstly we will briefly review the local structural identifiability problem. Next the computational aspects of local structural analysis based on gradient computation are elaborated in section III.

2 Local structural identifiability: mathematical formulation

We consider a linear, time invariant single-input, single-output discrete time state space model structure, parametrized in θ:

$$\begin{aligned} x(k+1) &= A(\theta)x(k) + b(\theta)u(k) \\ y(k) &= c(\theta)x(k) \end{aligned} \qquad (1)$$

where $x(k) \in \mathbb{R}^n$, $u(k) \in \mathbb{R}$, $y(k) \in \mathbb{R}$ and $\theta \in \Theta \subset \mathbb{R}^q$. There is no direct feedthrough $d(\theta)$. The elements of $A(\theta)$, $b(\theta)$, $c(\theta)$ are supposed to be algebraic functions of the elements of θ.
For a definition of local structural identifiability we adopt the formulation by Glover and Willems (1974):

Definition 2.1 *A model structure* (1) *is said to be locally identifiable from the transfer function at the point* $\hat{\theta} \in \Theta$ *if there exists* $\epsilon > 0$ *such that the following conditions*

1. $\|\theta_1 - \hat{\theta}\| < \epsilon, \quad \|\theta_2 - \hat{\theta}\| < \epsilon$ *and*

2. $c(\theta_1)(zI - A(\theta_1))^{-1}b(\theta_1) = c(\theta_2)(zI - A(\theta_2))^{-1}b(\theta_2)$
   for all $z \in \mathbb{C}\backslash\{\lambda(A(\theta_1)), \lambda(A(\theta_2))\}$ *where* $\lambda(.)$ *indicates the eigenvalues of a matrix*

imply that $\theta_1 = \theta_2$. □

In words, in a neighbourhood of $\hat{\theta}$ there are no two models with distinct parameters which have the same transfer function.

In definition 2.1 equality of the transfer functions is related to equality of the parameters. To mould this in a mathematical framework the following lemma on injective maps is presented (Glover and Willems, 1974):

Lemma 2.2 *Let* Ω *be an open set in* $\mathbb{R}^n$ *and* $f : \Omega \rightarrow \mathbb{R}^m$ *be a k-times continuously differentiable map with* $k \geq 1$. *Then if* $\partial f(x)/\partial x$ *has constant rank* r *in a neighbourhood of* $\hat{x}$, f *is locally injective at* $\hat{x}$ *if and only if* $r = n$.

Now definition 2.1 together with lemma 2.2 lead to the following proposition (see also Grewal and Glover, 1976, and Norton, 1980).

Proposition 2.3 *Consider the map* $S : \Theta \subset \mathbb{R}^q \rightarrow \mathbb{R}^{2n}$ *defined by:*

$$S(\theta) := [h(1,\theta)\ h(2,\theta)\ \ldots\ h(2n,\theta)]^T \qquad (2)$$

where $h(k,\theta) = c(\theta)A^{k-1}(\theta)b(\theta)$ $(k = 1, 2, \ldots, 2n)$ *are the first* $2n$ *Markov parameters of the model. Then the model* (1) *is locally structural identifiable in* $\theta = \theta_0$ *if* $rank(\partial S/\partial\theta) = q$ *in* $\theta = \theta_0$. □

So analysis of local structural identifiability of (1) amounts to evaluation of the rank of

$$\left.\frac{\partial S(\theta)}{\partial \theta}\right|_{\theta=\theta_0} = \left[\begin{array}{cccc} \frac{\partial h(1)}{\partial \theta_1} & \frac{\partial h(1)}{\partial \theta_2} & \cdots & \frac{\partial h(1)}{\partial \theta_q} \\ \frac{\partial h(2)}{\partial \theta_1} & \cdot & \cdots & \cdot \\ \cdot & \cdot & \cdots & \cdot \\ \vdots & & & \vdots \\ \frac{\partial h(2n)}{\partial \theta_1} & \cdot & \cdots & \frac{\partial h(2n)}{\partial \theta_q} \end{array}\right]_{\theta=\theta_0} \tag{3}$$

with dimensions $2n \times q$.

It is obvious that calculation of (3) is a non-trivial, if not impossible exercise in case of a high order, complex model parametrization. Nevertheless it is possible to perform structural analysis by rank evaluation using a specific algorithm for computation of the gradient of a quadratic loss-function; in this algorithm explicit use is made of analytical expressions for the partial derivatives of $A(\theta), b(\theta)$ and $c(\theta)$ with respect to θ_r $(r = 1, \ldots, q)$. This will be shown in the next section.

3 Structural identifiability analysis using gradient computation

In this section the relation between rank evaluation of (3) and gradient computation in an identification framework is established. Next it is shown how this relation enables calculation of the rank of (3) using a specific algorithm for gradient computation.

3.1 Gradient computation in identification

Consider the following identification problem.

Let there be given a linear, time invariant system that generates input-output data $\{u(k), y(k)\}_{k=1,\cdots,N}$, determined by

$$\begin{aligned} z(k+1) &= A_0 z(k) + b_0 u(k) \\ y(k) &= c_0 z(k) + e(k) \end{aligned} \tag{4}$$

where state $z(k) \in \mathbb{R}^n$, input $u(k) \in \mathbb{R}$, output $y(k) \in \mathbb{R}$ and $\{e(k)\}$ a sequence of independent, identically distributed random variables (white noise) with unit variance.

When identifying a model on the basis of measurement data obtained from this data generating system, we consider a state space model structure

$$\begin{aligned} x(k+1) &= A(\theta)x(k) + b(\theta)u(k) \\ \varepsilon(k,\theta) &= y(k) - c(\theta)x(k) \end{aligned} \tag{5}$$

where $A(\theta), b(\theta), c(\theta)$ is a parametrized state space model with $\theta \in \Theta \subset \mathbb{R}^q$ and $\varepsilon(k,\theta)$ the one-step-ahead prediction error, (Ljung, 1987). The corresponding least squares identification criterion is given by[1]

$$V_N(\theta) = \frac{1}{2}\sum_{k=1}^{N} \varepsilon^2(k,\theta). \tag{6}$$

Minimizing $V_N(\theta)$ over $\theta \in \Theta$ generally will result in a non-linear optimization procedure, for which it may be important to have available an expression for the gradient $\partial V_N(\theta)/\partial\theta$.

In Van Zee and Bosgra (1982) an algorithm has been proposed that, based on measurements $\{u(k), y(k)\}_{k=1,\cdots,N}$ and analytic expressions for the partial derivatives $\frac{\partial}{\partial\theta_r}A(\theta)$, $\frac{\partial}{\partial\theta_r}b(\theta)$ and $\frac{\partial}{\partial\theta_r}c(\theta)$ with respect to θ_r $(r = 1, \ldots, q)$, generates the gradient $\partial V_N(\theta)/\partial\theta_r$ for a prechosen value of θ.

This algorithm that is based on a dynamic programming formulation, is characterized by the following relations.

Given $\frac{\partial}{\partial\theta_r}A(\theta)$, $\frac{\partial}{\partial\theta_r}b(\theta)$ and $\frac{\partial}{\partial\theta_r}c(\theta)$, then

$$\frac{\partial V_N(\theta)}{\partial\theta_r} = \sum_{k=0}^{N-1} \frac{\partial}{\partial\theta_r} H_k(x(k), \lambda_{k+1}, \theta) \tag{7}$$

$$\begin{aligned} \text{where } \frac{\partial}{\partial\theta_r}H_k &= -\varepsilon(k,\theta)\frac{\partial}{\partial\theta_r}c(\theta) \\ &\quad + \lambda_{k+1}^T\left[\frac{\partial}{\partial\theta_r}A(\theta)x(k) + \frac{\partial}{\partial\theta_r}b(\theta)u(k)\right] \end{aligned} \tag{8}$$

$$\text{and } \lambda_k^T = \lambda_{k+1}^T A(\theta) - \varepsilon(k)c(\theta), \quad \lambda_N^T = 0. \tag{9}$$

For a given value of θ, $\{\lambda_k\}_{k=0,\cdots,N-1}$ is calculated from the data by running backwards over the time-interval (starting at $k = N-1$), while the partial derivative $\frac{\partial}{\partial\theta_r}H_k$ is constructed by running forwards over the data. A full elucidation of the dynamic programming formulation is presented in appendix A.

3.2 Rephrasing the identifiability problem

Now we raise the question whether we can employ the same dynamic programming mechanism as present in this gradient algorithm of Van Zee and Bosgra (1982) in order to obtain information about (the rank of) the Jacobi matrix (3) of a parametrized model structure $(A(\theta), b(\theta), c(\theta))$.

To this end the following Proposition will be fruitful.

Proposition 3.1 *Consider a parametrized model structure* (5)*, and any* $\theta_0 \in \Theta$*. Let a data generating system* $(A(\theta_0), b(\theta_0), c(\theta_0))$ *generate input-output data with* $u(k)$ *being a pulse signal, i.e.*

[1] For reasons that will become clear later on, we will not consider a factor $\frac{1}{N}$ in $V_N(\theta)$.

$u(k) = 1, k = 0$, $u(k) = 0, k \neq 0$ *and let* $e(k,\theta)$ *be a white noise with unit variance. Then*

$$E\left(\frac{\partial V_{2n}(\theta)}{\partial\theta}\right)\left(\frac{\partial V_{2n}(\theta)}{\partial\theta}\right)^T\Bigg|_{\theta=\theta_0} = \left(\frac{\partial S(\theta)}{\partial\theta}\right)^T \frac{\partial S(\theta)}{\partial\theta}\Bigg|_{\theta=\theta_0} \tag{10}$$

with $V_{2n}(\theta)$ *and* $\frac{\partial S(\theta)}{\partial\theta}$ *as defined in* (6),(3).

Proof: In the case of a pulse-shaped input signal with amplitude 1 the prediction error is expressed as

$$\varepsilon(k,\theta) = y(k) - h(k,\theta) \tag{11}$$

where $h(k,\theta)$ represents the k-th Markov parameter of the model: $h(k,\theta) = c(\theta)A(\theta)^{k-1}b(\theta)$. Then $V_N(\theta)$ becomes

$$V_N(\theta) = \frac{1}{2}\sum_{k=1}^{N}(y(k) - h(k,\theta))^2 \tag{12}$$

and the gradient $\partial V_N(\theta)/\partial\theta$ can be expressed as

$$\frac{\partial V_N(\theta)}{\partial\theta} = -\sum_{k=1}^{N}\varepsilon(k,\theta)\frac{\partial h(k,\theta)}{\partial\theta}. \tag{13}$$

Now consider the information matrix (Ljung, 1987) where (13) is substituted and E denotes the expectation operator:

$$E\,\frac{\partial V_N}{\partial\theta}\left(\frac{\partial V_N}{\partial\theta}\right)^T\Bigg|_{\theta=\theta_0} = E\sum_{k=1}^{N}\varepsilon(k,\theta_0)\frac{\partial h(k,\theta_0)}{\partial\theta}\sum_{l=1}^{N}\varepsilon(l,\theta_0)\left(\frac{\partial h(l,\theta_0)}{\partial\theta}\right)^T = \sum_{k=1}^{N}\sum_{l=1}^{N}\frac{\partial h(k,\theta_0)}{\partial\theta}E\varepsilon(k,\theta_0)\varepsilon(l,\theta_0)\left(\frac{\partial h(l,\theta_0)}{\partial\theta}\right)^T. \tag{14}$$

Since $\varepsilon(k,\theta_0) = e(k)$, i.e.

$$E\varepsilon(k,\theta_0)\varepsilon(l,\theta_0) = 1 \quad k = l \tag{15}$$

$$= 0 \quad k \neq l \tag{16}$$

and setting $N = 2n$, we get the following result:

$$E\,\frac{\partial V_{2n}}{\partial\theta}\left(\frac{\partial V_{2n}}{\partial\theta}\right)^T\Bigg|_{\theta=\theta_0} = \sum_{k=1}^{2n}\frac{\partial h(k,\theta_0)}{\partial\theta}\left(\frac{\partial h(k,\theta_0)}{\partial\theta}\right)^T$$

$$= \sum_{k=1}^{2n}\begin{bmatrix} \frac{\partial h(k)}{\partial\theta_1}\frac{\partial h(k)}{\partial\theta_1} & \frac{\partial h(k)}{\partial\theta_1}\frac{\partial h(k)}{\partial\theta_2} & \cdots & \frac{\partial h(k)}{\partial\theta_1}\frac{\partial h(k)}{\partial\theta_q} \\ \frac{\partial h(k)}{\partial\theta_2}\frac{\partial h(k)}{\partial\theta_1} & \cdot & & \cdot \\ \cdot & & & \cdot \\ \vdots & & & \vdots \\ \cdot & & & \cdot \\ \frac{\partial h(k)}{\partial\theta_q}\frac{\partial h(k)}{\partial\theta_1} & \cdot & \cdots & \frac{\partial h(k)}{\partial\theta_q}\frac{\partial h(k)}{\partial\theta_q} \end{bmatrix}$$

$$= \begin{bmatrix} \frac{\partial h(1)}{\partial\theta_1} & \frac{\partial h(2)}{\partial\theta_1} & \cdots & \frac{\partial h(2n)}{\partial\theta_1} \\ \frac{\partial h(1)}{\partial\theta_2} & \cdot & \cdots & \cdot \\ \cdot & & & \cdot \\ \vdots & & & \vdots \\ \cdot & & & \cdot \\ \frac{\partial h(1)}{\partial\theta_q} & \cdot & \cdots & \frac{\partial h(2n)}{\partial\theta_q} \end{bmatrix} \times \begin{bmatrix} \frac{\partial h(1)}{\partial\theta_1} & \frac{\partial h(1)}{\partial\theta_2} & \cdots & \frac{\partial h(1)}{\partial\theta_q} \\ \frac{\partial h(2)}{\partial\theta_1} & \cdot & \cdots & \cdot \\ \cdot & & & \cdot \\ \vdots & & & \vdots \\ \cdot & & & \cdot \\ \frac{\partial h(2n)}{\partial\theta_1} & \cdot & \cdots & \frac{\partial h(2n)}{\partial\theta_q} \end{bmatrix}$$

$$= \left(\frac{\partial S(\theta)}{\partial\theta}\right)^T \frac{\partial S(\theta)}{\partial\theta}\Bigg|_{\theta=\theta_0} \tag{17}$$

□

Using the result of proposition 3.1 and the fact that

$$rank\left(\frac{\partial S(\theta)}{\partial\theta}\right)\Bigg|_{\theta=\theta_0} = rank\left(\left(\frac{\partial S(\theta)}{\partial\theta}\right)^T \frac{\partial S(\theta)}{\partial\theta}\right)\Bigg|_{\theta=\theta_0} \tag{18}$$

enables us to rephrase the problem of local structural identifiability in terms of rank evaluation of (3) as rank evaluation of the information matrix under the experimental conditions as specified in proposition 3.1.

In the next subsection it is shown that, using the expression for the gradient according to the dynamic programming formulation (7), (8), (9) and with complete knowledge of the experimental conditions, it is possible to find an analytical expression for the information matrix only requiring analytical expressions for $\frac{\partial}{\partial\theta}A(\theta)$, $\frac{\partial}{\partial\theta}b(\theta)$ and $\frac{\partial}{\partial\theta}c(\theta)$.

3.3 An analytical expression for the information matrix

If we consider the gradient expressions (7), (8) and (9) and the experimental conditions as specified in proposition 3.1,

1. $u(k)$ is a pulse-signal with amplitude 1: $u(0) = 1$ and $u(k) = 0$ for $k = 1,\ldots,2n$;
2. $x(k) = A^{k-1}b$ for $k = 1,\ldots,2n$;
3. $e(k)$ is a standard white noise, i.e. $E\,e(i)e(j) = 1$ if $i = j$ and 0 if $i \neq j$,

we arrive at the following expression for $\frac{\partial V_{2n}(\theta)}{\partial \theta_r}$ (see appendix B):

$$\begin{aligned}\frac{\partial V_{2n}(\theta)}{\partial \theta_r} &= -\varepsilon(2n-1)\frac{\partial c}{\partial \theta_r}A^{2n-2}b \\ &\quad - \sum_{i=1}^{2n-1} \varepsilon(2n-i)cA^{2n-1-i}\frac{\partial b}{\partial \theta_r} \\ &\quad - \sum_{k=1}^{2n-2} \varepsilon(k)\frac{\partial c}{\partial \theta_r}A^{k-1}b \\ &\quad - \sum_{k=1}^{2n-2}\sum_{i=1}^{2n-k-1} \varepsilon(2n-i)cA^{2n-k-1-i}\frac{\partial A}{\partial \theta_r}A^{k-1}b. \end{aligned} \tag{19}$$

The information matrix is calculated element-wise by multiplying (19) with a similar expression for $\frac{\partial V_{2n}}{\partial \theta_s}$ and taking the expectation. As a consequence of the third experimental condition the terms of this product containing $E\,\varepsilon(i)\varepsilon(j)$ where $i \neq j$ will disappear. The exact elaboration is quite technical and is presented in appendix B. Here we only state the result.

Before we do so, some notational conventions are introduced:

1. the extended controllability matrix W_c is defined as
$$W_c := \begin{bmatrix} b & Ab & A^2b & \dots & A^{2n-2}b \end{bmatrix}; \tag{20}$$
2. the extended observability matrix W_o is defined as
$$W_o := \begin{bmatrix} c^T & A^Tc^T & \dots & (A^T)^{2n-2}c^T \end{bmatrix}^T; \tag{21}$$
3. for $i \leq j$, $E_c(i,j) \in \mathbb{R}^{2n-1 \times j-i+1}$ is defined as the matrix that selects the i-th up to the j-th column of a matrix with $2n-1$ columns by post-multiplication:
$$E_c(i,j) := \begin{bmatrix} 0_{(i-1)\times(j-i+1)} \\ I_{(j-i+1)\times(j-i+1)} \\ 0_{(2n-1-j)\times(j-i+1)} \end{bmatrix} \tag{22}$$
where $i,j = 1,\dots,2n-1$. $0_{p\times r}$ denotes the $(p\times r)$ 0-matrix; $I_{p\times p}$ denotes the $(p \times p)$ identity matrix;
4. for $i \leq j$, $E_o(i,j) \in \mathbb{R}^{j-i+1 \times 2n-1}$ is defined as the matrix that selects the i-th up to the j-th row of a matrix with $2n-1$ rows by pre-multiplication:
$$E_o(i,j) := \begin{bmatrix} 0_{(j-i+1)\times(i-1)} & I_{(j-i+1)\times(j-i+1)} & 0_{(j-i+1)\times(2n-1-j)} \end{bmatrix} \tag{23}$$
where $i,j = 1,\dots,2n-1$.

With these notational conventions we state the following result:

Proposition 3.2 *Under the conditions stated in proposition 3.1 and using the notational conventions* (20), (21), (22) *and* (23) *the* (r,s)*-element of the information matrix is expressed as:*

$$\begin{aligned} E\left(\frac{\partial V_{2n}}{\partial \theta_r}\right)\left(\frac{\partial V_{2n}}{\partial \theta_s}\right)^T = \\ &\left(W_o\frac{\partial b}{\partial \theta_r}\right)^T\left(W_o\frac{\partial b}{\partial \theta_s}\right) + \left(W_o\frac{\partial b}{\partial \theta_r}\right)^T\left(\frac{\partial c}{\partial \theta_s}W_c\right)^T + \\ &\left(W_o\frac{\partial b}{\partial \theta_s}\right)^T\left(\frac{\partial c}{\partial \theta_r}W_c\right)^T + \left(\frac{\partial c}{\partial \theta_r}W_c\right)\left(\frac{\partial c}{\partial \theta_s}W_c\right)^T + \\ &\sum_{k=1}^{2n-2}\left(W_o\frac{\partial b}{\partial \theta_r}\right)^T E_o^T(k+1,2n-3)\times \\ &\quad E_o(1,2n-3-k)\left(W_o\frac{\partial A}{\partial \theta_s}W_c\right)E_c(k,k) + \\ &\sum_{k=1}^{2n-2}\left(W_o\frac{\partial b}{\partial \theta_s}\right)^T E_o^T(k+1,2n-3)\times \\ &\quad E_o(1,2n-3-k)\left(W_o\frac{\partial A}{\partial \theta_r}W_c\right)E_c(k,k) + \\ &\sum_{k=1}^{2n-2}\left(\frac{\partial c}{\partial \theta_r}W_c\right)E_c^T(k+1,2n-3)\times \\ &\quad E_o(1,2n-3-k)\left(W_o\frac{\partial A}{\partial \theta_s}W_c\right)E_c(k,k) + \\ &\sum_{k=1}^{2n-2}\left(\frac{\partial c}{\partial \theta_s}W_c\right)E_c^T(k+1,2n-3)\times \\ &\quad E_o(1,2n-3-k)\left(W_o\frac{\partial A}{\partial \theta_r}W_c\right)E_c(k,k) + \\ &\sum_{k=1}^{2n-2}\sum_{l=1}^{k}E_c^T(k,k)\left(W_o\frac{\partial A}{\partial \theta_r}W_c\right)^T\times \\ &E_o^T(1,2n-3-k)E_o(k-l+1,2n-3-l)\times \\ &\qquad\left(W_o\frac{\partial A}{\partial \theta_s}W_c\right)E_c(l,l) + \\ &\sum_{k=1}^{2n-2}\sum_{l=k+1}^{2n-2}E_c^T(k,k)\left(W_o\frac{\partial A}{\partial \theta_r}W_c\right)^T\times \\ &E_o^T(l-k+1,2n-3-k)E_o(1,2n-3-l)\times \\ &\qquad\left(W_o\frac{\partial A}{\partial \theta_s}W_c\right)E_c(l,l). \end{aligned} \tag{24}$$

□

Although the analytical expression (24) seems quite elaborate, the calculation is straightforward. Note that using the notation based on row- and column-selection the (r,s)-element of the information ma-

trix contains the following expressions:

$$\left(W_o\frac{\partial A}{\partial\theta_i}W_c\right),\left(\frac{\partial b}{\partial\theta_i}W_c\right),\left(W_o\frac{\partial c}{\partial\theta_i}\right) \qquad (25)$$

for $i = r, s$.

Computation of the partial derivatives of the state space matrices $(A(\theta), b(\theta), c(\theta))$ with respect to θ_i $(i = 1, \ldots, q)$ for $\theta = \theta_0$ is done by hand and the extended controllability and observability matrices are calculated straightforwardly. The expression (24) therefore states an attractive formulation from a computational point of view, since the main computation effort consists of calculation of summarized matrix products of reasonable dimensions. Another feature is that the expressions (25) state a very nice intuitive result, since parameter identifiability is expressed in terms of controllability and observability properties of the model and the sensitivity of the state space matrices with respect to the elements of the argument parameter vector θ.

4 Conclusions

When a unique linear, time invariant model is to be determined using system identification techniques and the model parametrization is based on physical a priori knowledge of the process, there is no guarantee that a unique model exists as a result of the model parametrization. Structural identifiability should therefore be investigated before the parameters are actually estimated.

In this paper a method is presented to analyse local structural identifiability of SISO, non-linearly parametrized state space models of high order. The method implies rank evaluation of the information matrix under specific experimental conditions. It is shown that use of an algorithm for gradient computation, based on a dynamic programming formulation as formulated by Van Zee and Bosgra (1982), enables computation of an analytical expression for the information matrix.

Appendix A

Here the algorithm for gradient computation according to the dynamic programming formulation as formulated by Van Zee and Bosgra (1982) is elucidated. Consider a SISO state space model, parametrized in θ,

$$\begin{aligned} x(k+1) &= A(\theta)x(k) + b(\theta)u(k) \\ y(k) &= c(\theta)x(k) + e(k) \end{aligned} \qquad (26)$$

then the parameter vector θ is found as the minimizing argument of

$$V_N(\theta) = \frac{1}{2}\sum_{k=1}^{N}\varepsilon^2(k,\theta) \qquad (27)$$

in which $\varepsilon(k,\theta)$ is the prediction error $y(k) - \hat{y}(k)$.

A one-step ahead prediction $\hat{y}(k)$ is obtained as:

$$\begin{aligned} \hat{x}(k+1) &= A\hat{x}(k) + bu(k) \\ \hat{y}(k) &= c\hat{x}(k) \end{aligned} \qquad (28)$$

The prediction error $\varepsilon(k)$ can then be expressed as:

$$\begin{aligned} \hat{x}(k+1) &= A\hat{x}(k) + bu(k) \\ \varepsilon(k) &= -c\hat{x}(k) + y(k) \end{aligned} \qquad (29)$$

Dynamic programming formulation is based on definition of a partial criterion function:

$$V_i(\hat{x}(i),\theta) \equiv \frac{1}{2}\sum_{k=i}^{N-1}\varepsilon^2(k) \qquad (30)$$

and derivation of the partial derivatives of $V_i(\hat{x}(i),\theta)$ to $\hat{x}(i)$ and θ on the given trajectory $\hat{x}(i)$, where $V_i(\hat{x}(i),\theta)$ is expressed as

$$V_i(\hat{x}(i),\theta) = \frac{1}{2}\varepsilon^2(i) + V_{i+1}(\hat{x}(i+1),\theta). \qquad (31)$$

This leads to

$$\begin{aligned} \frac{\partial}{\partial\hat{x}(i)}V_i(\hat{x}(i),\theta) &= \frac{1}{2}\frac{\partial}{\partial\hat{x}(i)}\varepsilon^2(i) \\ &\quad + \frac{\partial}{\partial\hat{x}(i+1)}V_{i+1}(\hat{x}(i+1),\theta)\frac{\partial\hat{x}(i+1)}{\partial\hat{x}(i)} \\ &= -\varepsilon(i)c(\theta) + \frac{\partial}{\partial\hat{x}(i+1)}V_{i+1}(\hat{x}(i+1),\theta)A(\theta); \end{aligned} \qquad (32)$$

$$\begin{aligned} &\frac{\partial}{\partial\theta}V_i(\hat{x}(i),\theta) = \\ &\quad \frac{1}{2}\frac{\partial}{\partial\theta}\varepsilon^2(i) + \frac{\partial}{\partial\hat{x}(i+1)}V_{i+1}(\hat{x}(i+1),\theta)\frac{\partial\hat{x}(i+1)}{\partial\theta} \\ &\qquad + \frac{\partial}{\partial\theta}V_{i+1}(\hat{x}(i+1),\theta). \end{aligned} \qquad (33)$$

Adopting the following notations:

$$\lambda_i^T \equiv \frac{\partial}{\partial\hat{x}(i)}V_i(\hat{x}(i),\theta) \qquad (34)$$

$$H_i(\hat{x}(i),\lambda_{i+1},\theta) \equiv \frac{1}{2}\varepsilon^2(i) + \lambda_{i+1}^T[A\hat{x}(i) + bu(i)] \qquad (35)$$

calculation of the gradient $\frac{\partial}{\partial\theta}V_N(\theta)$ is carried out in the following two steps.

1. λ_{i+1} is computed for $i = 0, 1, \ldots, N-1$ from

$$\lambda_i^T = \lambda_{i+1}^T A(\theta) - \varepsilon(i)c(\theta), \quad \lambda_N^T = 0. \quad (36)$$

This implies a backward run on the error-sequence $\varepsilon(i)$;

2. $\frac{\partial}{\partial\theta}H_k$ is calculated for $k = 0, ..., N-1$ as

$$\frac{\partial}{\partial\theta}H_k = -\varepsilon(i)\frac{\partial}{\partial\theta}c(\theta) + \lambda_{i+1}^T[\frac{\partial}{\partial\theta}A(\theta)\hat{x}(i) + \frac{\partial}{\partial\theta}b(\theta)u(i)] \quad (37)$$

where $\frac{\partial}{\partial\theta}A(\theta)$, $\frac{\partial}{\partial\theta}b(\theta)$ and $\frac{\partial}{\partial\theta}c(\theta)$ are determined analytically.

The gradient $\frac{\partial V_N(\theta)}{\partial\theta}$ is finally found as:

$$\frac{\partial V_N(\theta)}{\partial\theta} = \sum_{k=0}^{N-1}\frac{\partial}{\partial\theta}H_k(\hat{x}(k), \lambda_{k+1}, \theta). \quad (38)$$

Appendix B

The analytical expression of the information matrix (14) as stated in proposition 3.2 is elaborated using the results of the dynamic programming formulation algorithm as described in appendix A. Notations used are adopted from appendix A and the argument parameter θ is left out for brevity.

First an explicit expression is derived for λ_l^T which follows from (9) in a straightforward way:

$$\lambda_l^T = -\sum_{i=1}^{2n-l}\varepsilon(2n-i)cA^{2n-l-i} \quad (39)$$

where $l = 1, \ldots, 2n-1$ and $\lambda_{2n}^T = 0$.

In the elaboration of expression (38) the following experimental conditions are taken into account:

1. $u(k)$ is a pulse-signal with amplitude 1: $u(0) = 1$ and $u(k) = 0$ for $k = 1, \ldots, 2n$;
2. $x(k) = A^{k-1}b$ for $k = 1, \ldots, 2n$;
3. $e(k)$ is a standard white noise, i.e. $E\, e(i)e(j) = 1$ if $i = j$ and 0 if $i \neq j$.

Substitution of the conditions 1, 2 and the explicit expression for λ_l^T in (38) gives expression (19):

$$\begin{aligned}\frac{\partial V_{2n}}{\partial\theta_r} = &-\varepsilon(2n-1)\frac{\partial c}{\partial\theta_r}A^{2n-2}b \\ &-\sum_{i=1}^{2n-1}\varepsilon(2n-i)cA^{2n-1-i}\frac{\partial b}{\partial\theta_r} \\ &-\sum_{k=1}^{2n-2}\varepsilon(k)\frac{\partial c}{\partial\theta_r}A^{k-1}b \\ &-\sum_{k=1}^{2n-2}\sum_{i=1}^{2n-k-1}\varepsilon(2n-i)cA^{2n-k-1-i}\frac{\partial A}{\partial\theta_r}A^{k-1}b.\end{aligned}$$

As stated in subsection 3.3 calculation of the information matrix (14) is carried out element-wise; multiplying $\frac{\partial V_{2n}}{\partial\theta_r}$ and $\frac{\partial V_{2n}}{\partial\theta_s}$ expressed as (19) and taking the expectation, where all terms containing $E\varepsilon(i)\varepsilon(j)$ for $i \neq j$ become 0 as a consequence of condition 3, the (r,s)-element of (14) is found as the sum of the following expressions:

$$\sum_{i=1}^{2n-1}\left(cA^{2n-i-1}\frac{\partial b}{\partial\theta_r}\right)\left(cA^{2n-i-1}\frac{\partial b}{\partial\theta_s}\right) \quad (40)$$

$$\left(cA^{2n-2}\frac{\partial b}{\partial\theta_r}\right)\left(\frac{\partial c}{\partial\theta_s}A^{2n-2}b\right) \quad (41)$$

$$\sum_{k=1}^{2n-2}\left(cA^{k-2}\frac{\partial b}{\partial\theta_r}\right)\left(\frac{\partial c}{\partial\theta_s}A^{k-2}b\right) \quad (42)$$

$$\left(cA^{2n-2}\frac{\partial b}{\partial\theta_s}\right)\left(\frac{\partial c}{\partial\theta_r}A^{2n-2}b\right) \quad (43)$$

$$\sum_{k=1}^{2n-2}\left(cA^{k-2}\frac{\partial b}{\partial\theta_s}\right)\left(\frac{\partial c}{\partial\theta_r}A^{k-2}b\right) \quad (44)$$

$$\left(\frac{\partial c}{\partial\theta_r}A^{2n-2}b\right)\left(\frac{\partial c}{\partial\theta_s}A^{2n-2}b\right) \quad (45)$$

$$\sum_{k=1}^{2n-2}\left(\frac{\partial c}{\partial\theta_r}A^{k-2}b\right)\left(\frac{\partial c}{\partial\theta_s}A^{k-2}b\right) \quad (46)$$

$$\sum_{k=1}^{2n-2}\sum_{i=1}^{2n-k-1}\left(cA^{2n-i-1}\frac{\partial b}{\partial\theta_r}\right)\times\left(cA^{2n-k-i-1}\frac{\partial A}{\partial\theta_s}A^{k-1}b\right) \quad (47)$$

$$\sum_{k=1}^{2n-2}\sum_{i=1}^{2n-k-1}\left(cA^{2n-i-1}\frac{\partial b}{\partial\theta_s}\right)\times\left(cA^{2n-k-i-1}\frac{\partial A}{\partial\theta_r}A^{k-1}b\right) \quad (48)$$

$$\sum_{k=1}^{2n-2}\left(\frac{\partial c}{\partial\theta_r}A^{2n-2}b\right)\left(cA^{2n-k-2}\frac{\partial A}{\partial\theta_s}A^{k-1}b\right) \quad (49)$$

$$\sum_{l=1}^{2n-2}\left\{\sum_{p=l+1}^{2n-2}\left(\frac{\partial c}{\partial\theta_r}A^{p-1}b\right)\times\left(cA^{p-l-1}\frac{\partial A}{\partial\theta_s}A^{l-1}b\right)\right\} \quad (50)$$

$$\sum_{k=1}^{2n-2}\left(\frac{\partial c}{\partial\theta_s}A^{2n-2}b\right)\left(cA^{2n-k-2}\frac{\partial A}{\partial\theta_r}A^{k-1}b\right) \quad (51)$$

$$\sum_{l=1}^{2n-2}\left\{\sum_{p=l+1}^{2n-2}\left(\frac{\partial c}{\partial\theta_s}A^{p-1}b\right)\times\left(cA^{p-l-1}\frac{\partial A}{\partial\theta_r}A^{l-1}b\right)\right\} \quad (52)$$

$$\sum_{k=1}^{2n-2}\sum_{l=1}^{2n-2}\left\{\sum_{i=1}^{2n-1-max(k,l)}\left(cA^{2n-k-1-i}\frac{\partial A}{\partial\theta_r}A^{k-1}b\right)\right.$$

$$\times \left(cA^{2n-l-1-i} \frac{\partial A}{\partial \theta_s} A^{l-1} b \right) \Bigg\} \quad (53)$$

To gain a better insight in these expressions the summations are reordered and rewritten in a matrix notation as follows.

Expression (40) and the summations of (41) and (42), (43) and (44), (45) and (46) give the first 4 terms of (24), using the notational conventions for the extended controllability and extended observability matrix. Expression (47) can be written as:

$$\sum_{k=1}^{2n-2} \frac{\partial b}{\partial \theta_r} \left[(A^T)^k c^T \;\; (A^T)^{k+1} c^T \;\; \ldots \right. \\ \left. \ldots \;\; (A^T)^{2n-2} c^T \right] \begin{bmatrix} c \\ cA \\ cA^2 \\ \vdots \\ cA^{2n-k-2} \end{bmatrix} \frac{\partial A}{\partial \theta_s} A^{k-1} b. \quad (54)$$

Similar expressions are found for (48), the summation of expressions (49) and (50) and the summation of expressions (51) and (52). This results in terms 5 up to 8 in (24).

Expression (53) requires more elaboration. The two summation signs are rewritten as follows:

$$\sum_{k=1}^{2n-2} \sum_{l=1}^{2n-2} = \sum_{k=1}^{2n-2} \left\{ \sum_{l=1}^{k} + \sum_{l=k+1}^{2n-2} \right\}.$$

Splitting up (53) according to this summation expression gives the following expression:

$$\sum_{k=1}^{2n-2} \sum_{l=1}^{k} \left\{ b^T (A^T)^{k-1} \left(\frac{\partial A}{\partial \theta_r} \right)^T \times \right. \\ \left[c^T \;\; A^T c^T \;\; \ldots \;\; (A^T)^{2n-k-2} c^T \right] \begin{bmatrix} cA^{k-l} \\ cA^{k-l+1} \\ \vdots \\ cA^{2n-l-2} \end{bmatrix} \times \\ \left. \frac{\partial A}{\partial \theta_s} A^{l-1} b \right\} \; + \\ \sum_{k=1}^{2n-2} \sum_{l=k+1}^{2n-2} \left\{ b^T (A^T)^{k-1} \left(\frac{\partial A}{\partial \theta_r} \right)^T \times \right. \\ \left[(A^T)^{l-k} c^T \;\; (A^T)^{l-k+1} c^T \ldots \;\; (A^T)^{2n-k-2} c^T \right] \times \\ \left. \begin{bmatrix} c \\ cA \\ \vdots \\ cA^{2n-l-2} \end{bmatrix} \frac{\partial A}{\partial \theta_s} A^{l-1} b \right\}. \quad (55)$$

Using the notational conventions (20), (21), (22) and (23) this results in the last two terms of (24).

References

Bellman, R. and K.J. Åström (1970). On structural identifiability. *Mathematical Biosciences 7*, pp. 329-339.

Cobelli, C., A. Lepschy and G. Romanin Jacur (1979). Identifiability of compartmental systems and related structural properties. *Mathematical Biosciences 44*, pp. 1-18.

Glover, K. and J.C. Willems (1974). Parametrizations of linear dynamical systems: canonical forms and identifiability. *IEEE Trans. Autom. Control, AC-19*, pp. 640-645.

Godfrey, K. (1983). *Compartmental Models and their Application.* Academic Press, London.

Grewal, M.S. and K. Glover (1976). Identifiability of linear and nonlinear dynamical systems. *IEEE Trans. Autom. Control, Short Papers*, pp. 833-837.

Ho, B.L. and R.E. Kalman (1966). Effective construction of linear state-variable models from input-output functions. *Regelungstechnik, Heft 12*, pp. 545-548.

Ljung, L. (1987). *System Identification: Theory for the User.* Prentice Hall, Englewood Cliffs, N.J.

Ljung, L. and T. Glad (1991). *On Global Identifiability for Arbitrary Model Parametrizations.* Report LiTH-ISY-I-1308, Dept. of Electrical Engineering, Linköping University.

Norton, J.P. (1980). Normal-mode identifiability analysis of linear compartmental systems in linear stages. *Mathematical Biosciences 50*, pp. 95-115.

Rothenberg, T.J. (1971). Identification in parametric models. *Econometrica*, Vol. 39, No. 3, pp. 577-591.

Rubinow, S.I. and A. Winzer (1971). Compartment analysis: an inverse problem. *Mathematical Biosciences 11*, pp. 203-247.

Tse, E. (1973). Information Matrix and Local Identifiability of Parameters. *Proc. Joint Automatic Control Conf.*, pp. 611-619.

Van Zee, G.A. and O.H. Bosgra (1982). Gradient computation in prediction error identification of linear, discrete-time systems. *IEEE Trans. Autom. Control, AC-27*, pp. 738-739.

Walter, E. (1981). Identifiability of State Space Models. *Lecture Notes in Biomathematics, vol. 46, Springer Verlag, Berlin.*

Selected Topics in Identification, Modelling and Control
Vol. 6, December 1993

Application of estimated error bounds in robust control of a wind energy conversion system

Douwe K. de Vries and Peter M.M. Bongers

Mechanical Engineering Systems and Control Group
Delft University of Technology, Mekelweg 2, 2628 CD Delft, The Netherlands.

Abstract. In this paper a robust controller will be designed to reduce fatigue load in variable speed wind energy conversion systems. The applied design methodology consist of the following steps, which will be discussed in this paper. First a model has been estimated using measured data. Based on this nominal model a stable controller has been designed such that the rotor shaft torque variations, quantifying fatigue loading, are minimized. Using a bound on the model error, estimated on the measured data, it is shown that the controller will at least robustly stabilize the real system. Experimental verification of these results showed the same amount of reduction of rotor shaft torque variations for the experimental closed loop, as for the designed closed loop.

Keywords. estimated error bounds, control design & implementation, wind turbine system.

1 Introduction

In times of growing environmental concern the need for clean and renewable energy sources is increasing. Wind power plants, being a renewable energy source, have become an acceptable alternative for electrical energy generation by fossile or nuclear power plants. In order to make wind turbine systems economically more attractive they have to be *designed* and *controlled* in a proper way. The design of well controlled flexible wind turbines seems to be attractive for commercial applications because lighter and less costly construction elements can be used, a more efficient energy conversion can be achieved, and a longer lifetime can be obtained.

In this paper we will focus on the role of control system design. The purpose of a control system is to increase the efficiency of energy conversion and reduce the dynamic loading, implying a longer life time.

On a simulation level, a number of results on control design for variable speed wind turbines are obtained. In Steinbuch (1989) a controller has been designed to reduce the rotor shaft torque for a rigid wind turbine, using the Linear Quadratic Output Feedback method (LQOFB, see Mäkilä and Toivonen (1987)). Robustness of the controller against model uncertainties (sensor noise, actuator dynamics, non-linearities) is checked using a complex μ analysis (see Doyle (1982,1984)). In Bongers and Dijkstra (1988,1992) and Bongers and Schrama (1991) LQ design methods, both LQG as well as LQOFB, are applied to flexible wind turbines. In that work the controller requirements are increased from not only rotor shaft torque reduction but also blade load reduction. At the application side little has been done. Although in Bongers *et al.* (1989) experimental results are presented, rotor shaft torque reduction is not obtained, due to limitations in the control computer.

In this paper we will design a robust controller for a laboratory set-up of a wind turbine system (the IRFLET test-rig, see Engelen *et al.* (1993)) operating in full load conditions. The main control

objective is the reduction of rotor shaft torque variations, even under the existence of model uncertainties. In the design of mechanical components a load factor, larger than one, multiplying the design stresses is used to determine the admissible strain of the component. For the transmission, the load factor is mainly determined by the damping of the mechanical resonance frequencies. Therefore it is natural to apply an $\mathcal{H}_\infty$ control design method, by reasoning that reduction of the $\mathcal{H}_\infty$-norm will increase the damping of the resonance frequencies. Thereby a smaller load factor allows a reduction in the construction costs.
In order to design a high performance controller a model of the complete test-rig is necessary. In this model all dynamics of the test-rig in the frequency range of interest have to be described quite accurately. To this end a model of the test-rig will be derived out of the measured data using standard system identification techniques.
Furthermore, besides a nominal model, an upper bound on the modelling error for the estimated transfer function is needed. This error bound will be obtained from the measured data.

Facing the task to estimate an upper bound on the modelling error arising in the IRFLET test-rig models we find ourselves posing the following question: is it possible to specify a realistic bound on the model uncertainty in a situation where undermodelling seems inevitable, and where colored noise with an unknown distribution acts on the system ? The classical identification literature, see e.g. the accounts given by Ljung (1987), Söderström and Stoica (1989), Brillinger (1981) and Priestley (1981), does not provide a satisfactory answer to the above question. These methods fall short in two important aspects:

Bias. In parametric identification a bias error due to undermodelling seems inevitable: the system will in general be far too complex to be modelled exactly. In spectral analysis a bias error is introduced due to windowing. Moreover, the best results are obtained in system identification when the bias and variance errors are approximately of the same size. This implies that the bias error can be considerable, and is as important as the variance contribution to the identification error. However, the available expressions for the bias error are implicit or require knowledge of the true system. In addition, these expressions are asymptotic in the number of data points.

Variance. Reliable confidence intervals for the variance error of the estimated transfer function cannot be provided. The variance expressions are asymptotic in both the number of data points, as well as the model order or the inverse window width. Furthermore, they contain the unknown true spectrum of the noise.

Regarding the recent literature on model uncertainty estimation, see the Special Issue on System Identification for Robust Control Design (1992) of the IEEE Transactions on Automatic Control, we have the following remarks. We are of the opinion that in an amazingly large number of cases the noise really is "noisy". That is, the noise can and should be modelled as a stochastic process. The unknown-but-bounded noise approach, which has recently become popular in model uncertainty estimation, will, as a rule, introduce considerable conservatism when the noise is random. On the other hand, the bias due to undermodelling is by definition a deterministic quantity. The combination of stochastic (averaging) noise with a deterministic (worst case) bias due to undermodelling does however not appear in the literature on model uncertainty estimation, although this setting is quite common in the classical identification literature, see e.g. Ljung (1987) and Brillinger (1981). We will apply a model uncertainty estimation procedure which does employ this combination, and which solves the problems outlined above for the classical identification techniques. A further discussion on these issues, and a detailed description of the proposed model uncertainty estimation techniques, can be found in (De Vries and Van den Hof (1993), De Vries (1994)).

This paper is organized as follows: The nominal modeling procedure will be described in Section 2. Secondly, based upon this nominal model, a controller has to be designed such that the controlled test-rig satisfies the control objectives. As argued before an $\mathcal{H}_\infty$ control design method will be used, this procedure is discussed in Section 3. The data used to determine the control design model is also used to estimate additive model error bounds. This procedure is outlined in Section 4. After the verification that the controller will stabilize the true system, the designed controller will be used on the test-rig. In Section 5 the experimental results are given and compared with the nominal model predictions.

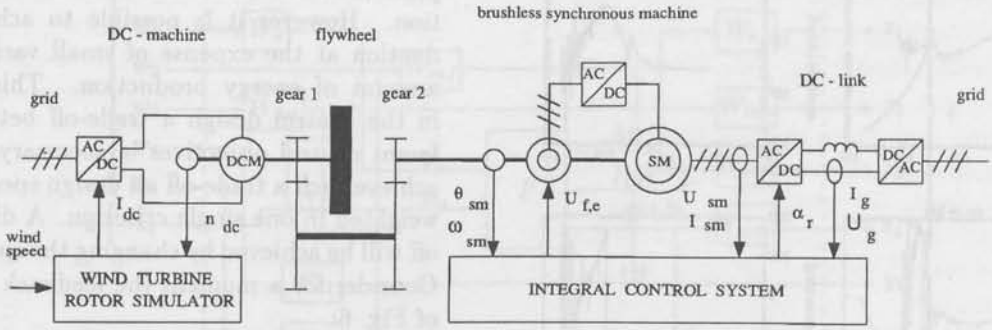

Fig. 1: IRFLET test-rig (Engelen *et al.* (1993))

2 Wind Energy Conversion System

The layout of the wind energy conversion system under consideration is given in Fig. 1. The controlled DC-machine on the left part of Fig. 1 emulates the rotor part of a small wind turbine. This enables experimentations under user definable conditions.
The test-rig (Fig. 1) is schematically represented in Fig. 2, including the input and output variables:

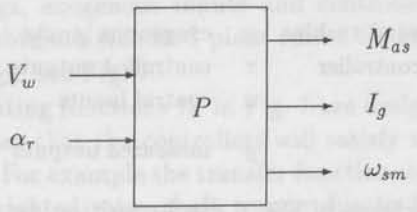

Fig. 2: Wind turbine

with[1]

vw	V_w	wind velocity	$[m/s]$
alf	α_r	delay angle rectifier	$[rad]$
Mas	M_{as}	rotor shaft torque	$[Nm]$
Idc	I_g	direct current	$[\ A\ ]$
omg	ω_{sm}	generator speed	$[rpm]$

In order to derive a model of this test-rig, standard system identification techniques (see Ljung and Söderström (1983), Ljung (1987)) are used on measured data to calculate parametric models.

Experimental results

Experiments are carried out in one operating condition of the test-rig, where the following operating condition has been chosen:

wind velocity	**12**	m/s
field excitation voltage	**22**	V
delay angle rectifier	**0.47**	rad

In Figs. (3,4,5) the transfer functions of the individual channels are shown. For each channel the empirical transfer function estimate (ETFE, see Ljung (1987)) and the estimated parametric model is given. A discussion on how the parametric models have been obtained can be found in Bongers (1993) and Bongers *et al.* (1993).

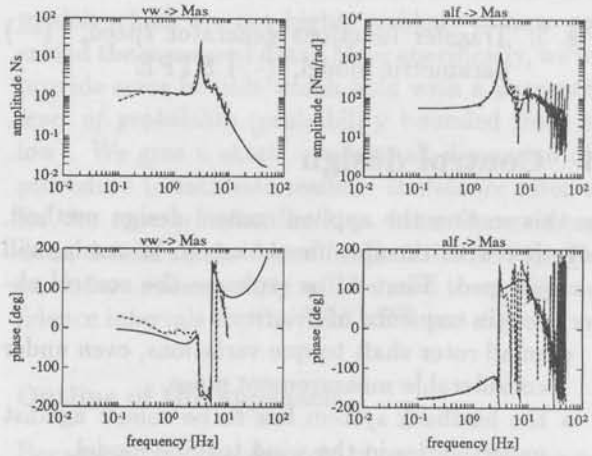

Fig. 3: Transfer functions rotor shaft torque, (—) parametric model, (- -) ETFE

It can be seen in the figures (3,4,5) that there exists a close resemblance between the parametric models and the ETFE. This holds for both the amplitude as well as the phase.

[1]The symbols in the first column refer to the labels used in the figures.

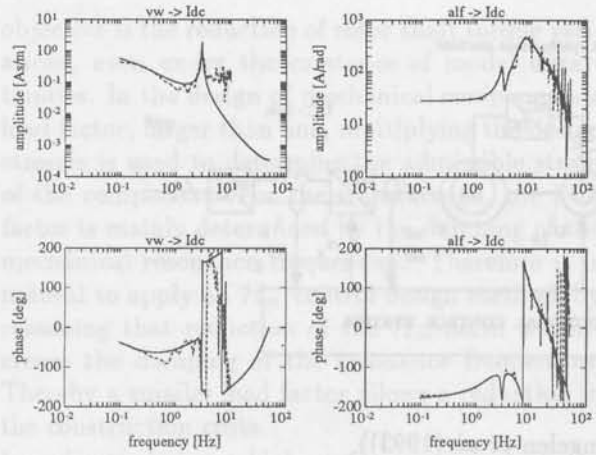

Fig. 4: Transfer functions DC-current, (—) parametric model, (- -) ETFE

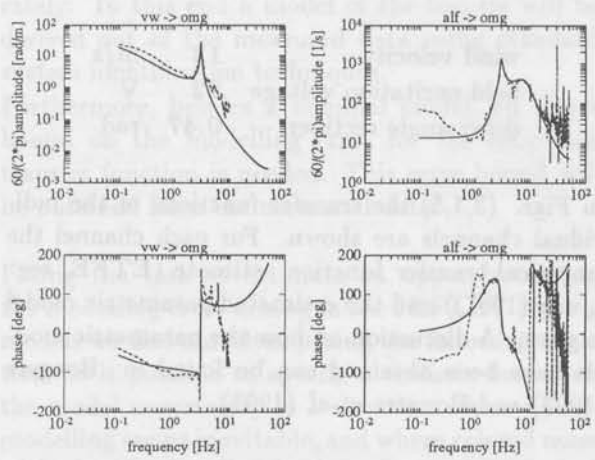

Fig. 5: Transfer functions generator speed, (—) parametric model, (- -) ETFE

3 Control design

In this section the applied control design method, together with the specific choices to be made, will be discussed. First let us rephrase the control objectives (in sequence of priority):

- small rotor shaft torque variations, even under considerable measurement noise.
- the feedback system has to be robust against uncertainties in the wind turbine model.
- the controller itself has to be stable, to make the implementation of the controller acceptable for future industrial users.
- small control effort.
- constant amount of produced electrical energy, in order to prevent off-design loads.

The control objectives are conflicting, for example it is impossible to independently achieve complete load reduction and constant energy production. However it is possible to achieve load reduction at the expense of small variations in the amount of energy production. This means that in the control design a trade-off between the different control objectives is necessary. In order to achieve such a trade-off all design specifications are weighted in one single criterion. A different trade-off will be achieved by changing the specific weights. Consider for a moment the feedback configuration of Fig. 6:

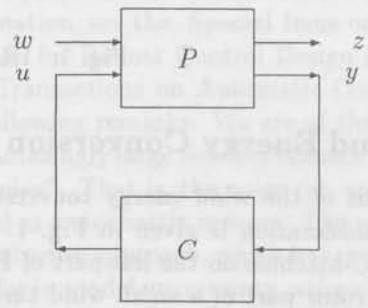

Fig. 6: Feedback configuration

with

P	wind turbine	w	exogenous inputs	=	V_w
C	controller	z	controlled outputs	=	M_{as}
		u	control inputs	=	α_r
		y	measured outputs	=	$\begin{pmatrix} I_g \\ \omega_{sm} \end{pmatrix}$

The scheme of Fig. 6 can be written as:

$$\begin{pmatrix} z \\ y \end{pmatrix} = P \begin{pmatrix} w \\ u \end{pmatrix}$$

where P is partitioned as $\begin{bmatrix} P_{11} & P_{12} \\ P_{21} & P_{22} \end{bmatrix}$, with P_{ij} having the appropriate dimensions. The closed loop transfer function from w to z will be written as a lower linear fractional transformation on the plant and controller:

$$\mathcal{F}_l(P, C) = P_{11} + P_{12} C \left(I - P_{22} C\right)^{-1} P_{21}$$

The $\mathcal{H}_\infty$ optimal control problem is to find a controller C, such that $\mathcal{F}_l(P, C)$ is stable and $\|\mathcal{F}_l(P, C)\|_\infty$ is minimal. Note that $\|\mathcal{F}_l(P, C)\|_\infty$ is a scalar criterion representing the trade-off of all control specifications.

In Doyle *et al.* (1989) and Glover and Doyle (1988) it is shown that two Riccati equations need to be solved, in order to calculate the central controller. The order of the controller equals the order of

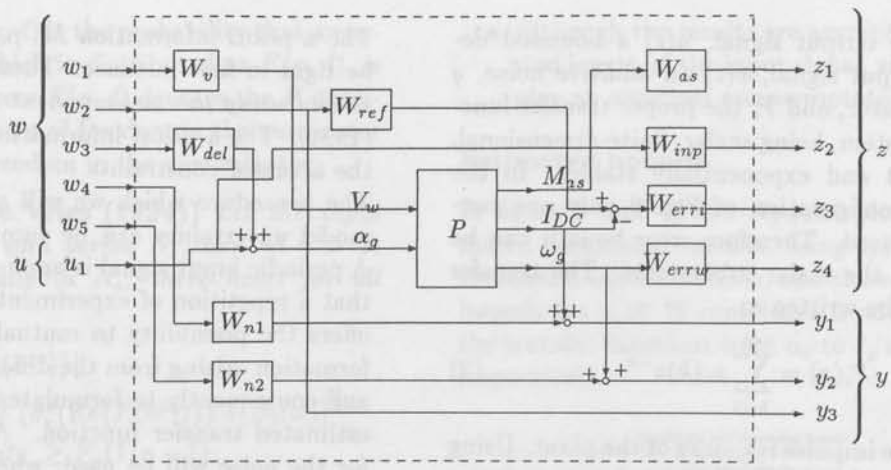

Fig. 7: Weighted wind turbine model

the plant, including the order of possible weighting functions.

In order to design a controller for the test-rig, such that the control objectives are satisfied, we need to translate the control objectives to properties that can be used in the $\mathcal{H}_\infty$-controller design. For this purpose the wind turbine model is extended with weightings, exogenous inputs and controlled outputs to obtain a standard plant suited for the control design, see Fig. 7.

All weighting functions W in Fig. 7 are designed in such a way that the controllers will satisfy the objectives. For example the transfer function $w_1 \rightarrow z_1$ is the weighted rotor shaft torque due to filtered wind velocity disturbances. A more detailed discussion on the design of the weighting functions can be found in Bongers (1993,1993a).

Based on this extended model, a controller has been calculated using MATLAB MUSYN toolbox (Balas *et al.* (1991)), the controller has 37 states. The process computer constrains the maximum allowable size of the controller to 25 states. Using a standard Hankel norm reduction technique (see Glover (1984)) a 25^{th} order controller has been obtained.

As an example of the designed closed loop, in Fig. 8 the rotor shaft torque reduction is given. It can be seen that the first control objective has been met.

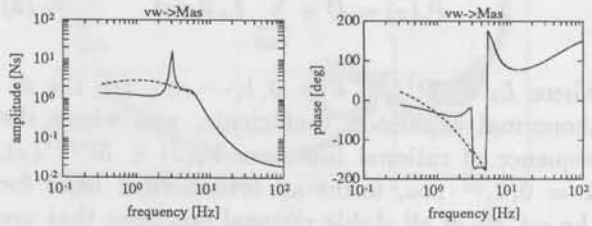

Fig. 8: Transfer functions, (—) open loop, (- -) designed closed loop

4 Error bound Estimation

The aim of this section is to find a *realistic* reflection of the uncertainty about the model – as a description of the system – which is present in the data, considering the situation where the available data about the system is incomplete and corrupt. That is, we want to find a description of the set of all models which are not highly unlikely to have generated the measured data. More specifically, we will provide error bounds which hold with a *guaranteed level of probability* (probability bounded from below). We give a short, conceptual, discussion of a procedure to estimate realistic confidence intervals for the true transfer function from the measured data; details can be found in De Vries (1994). This procedure subsequently will be used to specify confidence intervals for the IRFLET test-rig.

Outline of the approach

Because of the decisive role played by the assumptions and prior information in model uncertainty estimation, we will start by listing the ones that we use. Next, we will shortly discuss the main points of the estimation procedure.

It is assumed that the plant, and the measurement data that is obtained from this plant, allow a description

$$y(t) = P_o(q)u(t) + v(t) \qquad (1)$$

with $y(t)$ the output signal, $u(t)$ a bounded deterministic input signal, $v(t)$ an additive noise, q the shift operator, and P_o the proper transfer function of the system, being scalar, finite-dimensional, time-invariant and exponentially stable. In the closed loop configuration of Fig. 6 only one control input is used. Therefore error bounds can be calculated on the scalar subsystems. The transfer function can be written as

$$P_o(z) = \sum_{k=0}^{\infty} p_o(k) z^{-k} \tag{2}$$

with $p_o(k)$ the impulse response of the plant. Using the system based orthonormal basis functions introduced by Heuberger (1991) and Heuberger *et al.* (1993) the transfer function can also be written as

$$P_o(z) = D + \sum_{k=0}^{\infty} L_k \mathcal{V}_k(z) \tag{3}$$

where $L_k \in \mathbb{R}^{1 \times n_b}$, $k = 0, 1, \cdots, \infty$, are the orthonormal expansion coefficients, and where the sequence of rational functions $\mathcal{V}_k(z) \in \mathbb{R}^{n_b \times 1}(z)$, $k = 0, 1, \cdots, \infty$, forms an orthonormal basis for the set $\mathcal{H}_2$ of all stable rational functions that are squared integrable on the unit circle. Employing system based orthonormal basis functions has the important advantage that prior knowledge, which may be inaccurate or approximate (e.g. resulting from identification or physical modelling), can be taken into account, so that a *good low order approximation* of the system can be obtained.
The output disturbance $v(t)$ is represented as

$$v(t) = H_o(q) e(t) \tag{4}$$

where $e(t)$ is a sequence of independent identically distributed random variables, of which all moments exist, with zero mean values and variance σ_e^2, and where H_o is a stable proper transfer function.
We assume to have available the following a prior information on the past input signal and the system.

Assumption 4.1 *We have as a priori information that*

i. *there exists a finite and known* $\bar{u}^p \in \mathbb{R}$, *such that* $|u(t)| \leq \bar{u}^p$ *for all* $t < 0$

ii. *there exist finite and known* $M, \rho \in \mathbb{R}$, *with* $\rho > 1$, *such that* $|p_o(k)| \leq M\rho^{-k}$, *for all* $k \in \mathbb{N}$.

iii. *there exist finite and known* $\mathcal{K} \in \mathbb{R}^{1 \times n_b}, \eta \in \mathbb{R}$, *with* $\eta < 1$, *such that* $|L_k| \leq \mathcal{K}\eta^k$, *for all* $k \in \mathbb{N}$.

The a priori information M, ρ, $\mathcal{K}$ and η need not be tight in first instance. These priors *can be improved using the measurement data*, see De Vries (1994). The a priori information on $\bar{u}^p$ is given by the actuator constraints.
The procedure which we will apply to bound the model uncertainty can be summarized as follows. A periodic input signal is applied to the system, so that a repetition of experiments is obtained. This offers the possibility to mutually compare the information arising from the different data segments, and consequently to formulate the statistics of the estimated transfer function. A stochastic setting for the noise will be used, whereas the errors due to undermodelling and unknown initial conditions will be considered to be deterministic.
More specifically, let the input signal contain r periods of length N_o. A frequency domain least squares estimate of a finite number of orthonormal expansion coefficients L_k is made over each period of the input signal

$$\hat{\theta}_i = \underset{\theta}{\operatorname{argmin}} \frac{1}{N_o} \sum_{k=1}^{N_o} \left| \hat{P}_i(e^{j\omega_k}) - \phi(e^{j\omega_k})\theta \right|^2 \qquad i = 1, \cdots, r$$

where $\hat{P}_i(e^{j\omega_k})$ is the ETFE (see Ljung (1987)) over the i-th data segment, and

$$\begin{aligned} \theta_o &= [D \;\; L_0 \;\; \cdots \;\; L_{n-1}]^T \\ \phi(e^{j\omega_k}) &= \left[1 \;\; \mathcal{V}_0^T(e^{j\omega_k}) \;\; \cdots \;\; \mathcal{V}_{n-1}^T(e^{j\omega_k})\right] \\ \omega_k &= \frac{2\pi k}{N_o} \qquad k = 0, 1, \cdots, N_o - 1 \end{aligned}$$

This results in a set of transfer function estimates $P_i(e^{j\omega})$ of the system $P_o(e^{j\omega})$

$$P_i(e^{j\omega}) = \phi(e^{j\omega})\hat{\theta}_i \qquad i = 1, \cdots, r$$

Taking the average now gives the final estimate

$$P(e^{j\omega}) = \frac{1}{r} \sum_{i=1}^{r} P_i(e^{j\omega})$$

The variance of this final estimate can be estimated directly from the set of estimates $P_i(e^{j\omega})$, $i = i, \cdots, r$

$$\hat{\sigma}_r^2(P(e^{j\omega})) = \frac{1}{r(r-1)} \sum_{i=1}^{r} |P(e^{j\omega}) - P_i(e^{j\omega})|^2$$

Due to the periodicity of the input signal the estimates $P_i(e^{j\omega})$ are, asymptotically in the period length of the input signal, *independent and identically normally distributed*, which enables us to formulate a confidence interval for $P_o(e^{j\omega})$. In formulating this confidence interval, we adopt the following notation

$$F_\alpha(n, d) = \{\mathcal{P}[x \leq \alpha], \; x \in F(n, d)\}$$

meaning that $F_\alpha(n,d)$ is the probability that a random variable x, which is distributed as $F(n,d)$, is smaller than α, where $F(n,d)$ denotes the F distribution with n degrees of freedom in the numerator and d degrees of freedom in the denominator.

Theorem 4.2 (De Vries (1994)) *Let the input signal be periodic with period N_o, and let $r > 1$. Then, asymptotically in N_o, there holds for all $\omega \in [0, 2\pi)$*

$$|\mathrm{Re}\{P_o(e^{j\omega}) - P(e^{j\omega})\}| \leq B_1(\omega) + \alpha^{\frac{1}{2}} \left(\hat{\sigma}_r^2(\mathrm{Re}\{P(e^{j\omega})\}) + B_2(\omega)\right)^{\frac{1}{2}}$$

with probability $\geq F_\alpha(1, r-1)$

where the bias terms $B_1(\omega)$ and $B_2(\omega)$ can be bounded with hard error bounds using the prior information of Assumption 4.1.

The error bound of Theorem 4.2 consist of a *hard bound on the bias contributions* (due to undermodelling and unknown initial conditions), and a *confidence interval for the error due to the noise.* In establishing the confidence interval due account is taken of the fact that the variance is estimated. Similarly, a confidence interval for the imaginary part of the error can be established. The probability that $P_o(e^{j\omega})$ is contained in the rectangle in the complex plane which is obtained by combining the two confidence intervals, now can be bounded from below using the inequality

$$\mathcal{P}[x_1 \leq \alpha_1\ ,\ x_2 \leq \alpha_2] \geq 1 - (1 - \mathcal{P}[x_1 \leq \alpha_1]) - (1 - \mathcal{P}[x_2 \leq \alpha_2])$$

The important features of the procedure are the following:

- Reliable and tight error bounds can be obtained, while using only minor a priori information.
- Separate error bounds for the different sources of uncertainty (undermodelling, noise, unknown initial conditions) are obtained. This is important when the error bound is too large for the intended use of the model (robust control design). The error sources that provide a major contribution to the error bound can be isolated, so that it is known how to effectively improve the error bound. An explicit bias-variance trade-off can be made, e.g. by selecting the model order.
- A control relevant model can be used to generate the orthonormal basis functions, so that the model with respect to which the confidence interval is specified is suited for robust control design.
- Although the results are asymptotic in the period length of the input signal, simulations display an excellent nonasymptotic performance.

Estimated bounds

In figure 9 and 10 the Nyquist plots of the estimated parametric models, using system based orthonormal basis functions, and the estimated error bounds (at a 99 % confidence level) are given for the transfer functions from α_r to I_g and α_r to ω_{sm}, respectively.

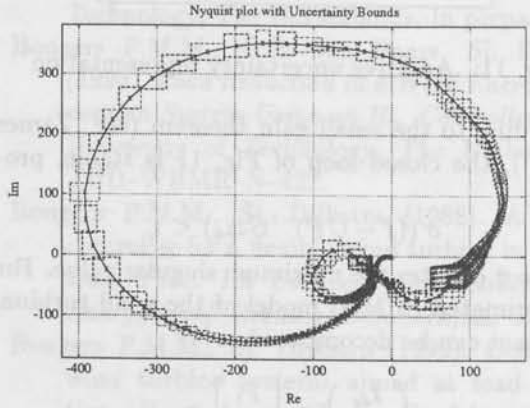

Fig. 9: Nyquist plot of the estimated transfer function `alf -> idc`, and the error bound.

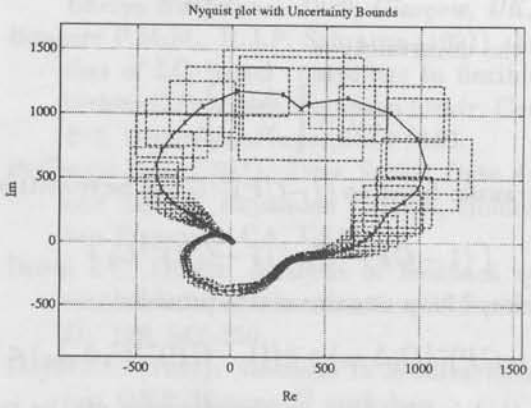

Fig. 10: Nyquist plot of the estimated transfer function `alf -> omg`, and the error bound.

Robust stability

The above estimated error bounds can be represented by an additive uncertainty model Δ_a around the estimated nominal wind turbine model P:

$$P_\Delta = P + \Delta_a$$

where $\Delta_a \leq |P_o - P|$ from the previous sections. Neglecting the external signals w,z of Fig. 6 and adding the uncertainty description, the feedback configuration is drawn in Fig. 11.

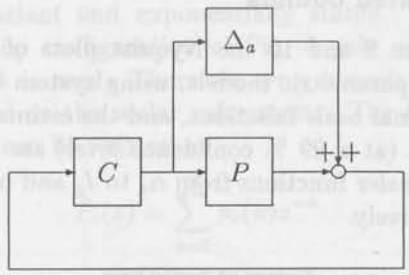

Fig. 11: Additive uncertainty representation

According to the small gain theorem (see Zames (1963)), the closed loop of Fig. 11 is stable, provided:

$$\bar{\sigma}\left((I - CP)^{-1}C\Delta_a\right) < 1$$

Where $\bar{\sigma}$ denotes the maximum singular value. For the estimated (SIMO) model of the wind turbine, the plant can be decomposed as

$$\begin{pmatrix} I_{dc} \\ \omega_g \end{pmatrix} = \begin{bmatrix} P_1 \\ P_2 \end{bmatrix} \alpha_g$$

the controller as

$$\alpha_g = \begin{bmatrix} C_1 & C_2 \end{bmatrix} \begin{pmatrix} I_{dc} \\ \omega_g \end{pmatrix}$$

while the uncertainty is

$$\Delta_a = \begin{bmatrix} \Delta_{Idc} \\ \Delta_{omg} \end{bmatrix}$$

The transfer function $(I-CP)^{-1}C$ can be rewritten as

$$\begin{bmatrix} (1-CP)^{-1}C_1 & (1-CP)^{-1}C_2 \end{bmatrix}$$

The closed loop remains stable provided:

$$\bar{\sigma}\left((1-CP)^{-1}C_1\Delta_{Idc}\right) + \bar{\sigma}\left((1-CP)^{-1}C_2\Delta_{omg}\right) < 1$$

Note that in this step conservativeness can be introduced. The estimated error bound, as measure of the perturbation, contains no phase information. Therefore the following stability condition need to be checked (without adding conservativeness to the previous step):

$$\bar{\sigma}\left((1-CP)^{-1}C_1\right)\bar{\sigma}(\Delta_{Idc}) + \bar{\sigma}\left((1-CP)^{-1}C_2\right)\bar{\sigma}(\Delta_{omg}) < 1 \qquad (5)$$

The graphical representation of the above stability condition is given in Fig. 12. Both P_1, P_2, $\bar{\sigma}(\Delta_{omg})$, $\bar{\sigma}(\Delta_{Idc})$ are taken from Figs. (9,10).

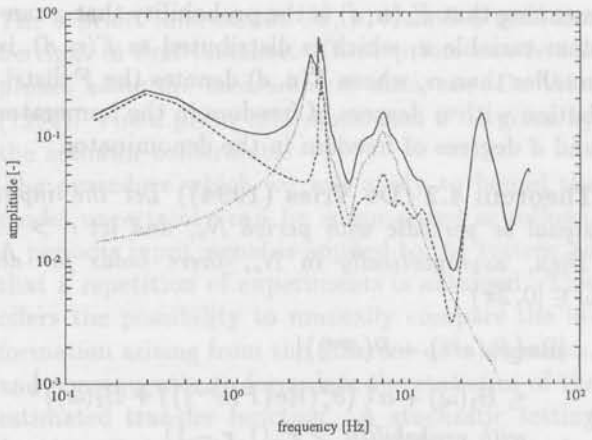

Fig. 12: Stability result w.r.t. additive uncertainty
(—) $\bar{\sigma}\left((1-CP)^{-1}C_1\Delta_{Idc}\right) + \bar{\sigma}\left((1-CP)^{-1}C_2\Delta_{omg}\right)$
(- -) $\bar{\sigma}\left((1-CP)^{-1}C_1\right)\bar{\sigma}(\Delta_{Idc})$
(...) $\bar{\sigma}\left((1-CP)^{-1}C_2\right)\bar{\sigma}(\Delta_{omg})$

It can be seen in Fig. 12 that the stability condition of (5) is fulfilled. Therefore, given the estimated error bounds, the real system will be stabilized by the controller.
Based on this result, we proceed by the actual implementation of the controller.

5 Controller implementation

In this section the predicted results of Section 3 will be verified with measurements on the test-rig. For this purpose the controller has been implemented and used to control the test-rig. The same wind velocity signal as in Section 2 has been applied. In Fig. 13 the experimentally determined closed loop transfer functions, using an ETFE, and the predicted closed loop transfer functions are given. Compared to Fig. 3 or Fig. 8 it can be seen that the maximum amplitude of rotor shaft torque variations are reduced by a factor of 10 in the frequency domain. For the resonance frequency of the rotor shaft, interpreted as a second order system, the controller increases the damping from less than 0.05 to more than 0.5. The figure also shows that the other signals: DC-current and generator speed are behaving well, the input used remains small.
It can be seen in Fig. 13 that the design model shows some spikes, which are absent in the ETFE. The reason for this is the following: in each of the individual estimated transfer functions the frequency of the resonance is calculated. This frequency differs slightly between the transfer functions. However physically it is one phenomenon. The designed controller acts on the resonance fre-

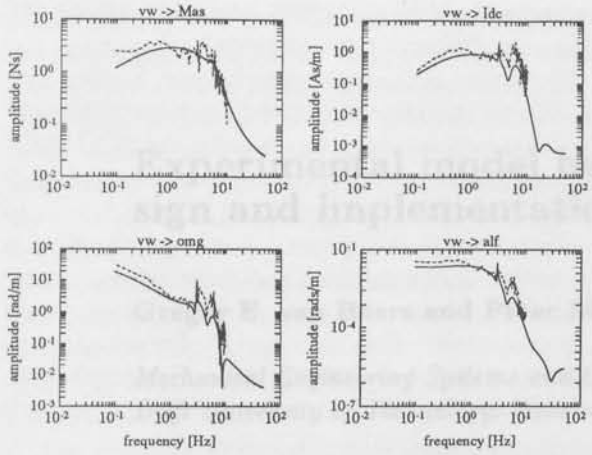

Fig. 13: Amplitude part of closed loop transfer functions, (—) designed, (- -) ETFE

quency in the $V_w \rightarrow M_{as}$ transfer function, which differs from the other transfer functions. Therefore the spikes occur in the designed transfer functions.

6 Conclusions

It has been shown that it is possible to calculate a model of the test-rig based on measured data.

Based on this model a stable robust controller has been designed such that the controlled model has small rotor shaft torque variations, without excessive variations in DC-current, generator speed or delay angle.

Additionally, uncertainty bounds are calculated with a 99% confidence interval using the measured data. Before implementing the controller, the uncertainty bounds are used to verify that the controller will stabilize the system. When the controller is applied to the test-rig it has been shown that the rotor shaft torque variations are reduced by a factor of 10. This shows that sufficient robustness is obtained by the controller, and that the actual performance is satisfactory.

Acknowledgments

The authors would like to thank explicitly Tim van Engelen of the Netherlands Energy Research Foundation for helpful discussions and his cooperation in performing the measurements. Gregor van Baars, Henk Huisman and Paul van den Hof of the Delft University of Technology are acknowledged for helpful discussions.

References

Balas G., J.C. Doyle, K. Glover, A.K. Packard, R. Smith (1991). *μ–Analysis and Synthesis Toolbox.* The MUSYN Inc. USA.

Bongers P.M.M. (1993a). Control design and implementation for a wind turbine system. *Proc. 2nd Europ. Contr. Conf.,*Groningen, The Netherlands,1956–1961.

Bongers P.M.M. (1994). *Factorizational Approach to Robust Control: Application to a Flexible Wind Turbine.* PhD Thesis, Delft University of Technology, The Netherlands, In preparation.

Bongers P.M.M., G.E. van Baars, Sj. Dijkstra (1993). *Load Reduction in a Wind Energy Conversion System Using an H_∞ Controller.* Delft University of Technology, The Netherlands, TUD–WBMR–N–422.

Bongers P.M.M., Sj. Dijkstra (1988). A filter–controller for a flexible wind turbine in partial load. *Proc. 1th European Community Wind Energy Conf.,*Herning, Denmark,320–323.

Bongers P.M.M., Sj. Dijkstra (1992). Control of wind turbine systems aimed at load reduction. *Proc. Amer. Contr. Conf.,*june 24–26, Chicago, Illinois, USA,1710–1714.

Bongers P.M.M., T.G. van Engelen, Sj. Dijkstra, Z.D.Q.P. Kock (1989). Optimal control of a wind turbine in full load. *Proc. European Wind Energy Conference 1989, Glasgow, UK,.*

Bongers P.M.M., R.J.P. Schrama (1991). Application of LQ–based controllers to flexible wind turbines. *Proc. 1st. European Contr. Conf., Jul 2–5, Grenolble, France,*2185–2189.

Brillinger D.R. (1981). *Time Series. Data Analysis and Theory.* Expanded Edition, Holden–Day, San Francisco, CA, USA.

Doyle J.C. (1982). Analysis of feedback systems with structured uncertainties. *IEE proc., part D, 129,* 242–250.

Doyle J.C. (1984). *Advances in Multivariable Control.* ONR/Honeywell workshop.

Doyle J.C., K. Glover, P.P. Khargonekar, B.A. Francis (1989). State–space solutions to standard H_2 and H_∞ problems. *IEEE Trans. Automat. Contr., AC–34,* 831–847.

Engelen, T.G. van, Bongers P.M.M., J.T.G. Pierik, G.E. van Baars (1993). Integral control for damping of mechanical resonance and protection against grid failures: results in a full load operating condition. *Proc. Europ. Community Wind Energy Conf.,*545–550.

Glover K. (1984). All optimal Hankel norm approximations of linear mutivariable systems and

their L_∞ error bounds. *Int. J. Control, 39*, 1115–1193.

Glover K., J.C. Doyle (1988). State–Space formulae for all stabilizing controllers that satisfy an H_∞ norm bound and relations to risk sensitivity. *Syst. Control Lett., 1*, 167–172.

Heuberger P.S.C. (1991). *On Approximate System Identification with System Based Orthonormal Functions.* PhD Thesis, Delft University of Technology, The Netherlands.

Heuberger, P.S.C., P.M.J. Van den Hof, O.H. Bosgra (1993). A generalized orthonormal basis for linear dynamical systems. *Proc. 32nd IEEE COnf. on Desicion and Contr.*,San Antonio, TX, USA,.

Ljung L. (1987). *System Identification: Theory for the User.* Prentice Hall Inc., Englewood Cliffs, New jersey.

Ljung L., T. Söderström (1983). *Theory and Practice of Recursive Identification.* MIT Press Cambridge, MA, USA.

Mäkilä P.M., H.T. Toivonen (1987). Computational methods for parametric LQ problems – A survey. *IEEE Trans. Automat. Contr., AC–32*, 658–671.

Priestley M.B. (1981). *Spectral Analysis and Time Series.* Academic Press, London.

Soderstrom T., P. Stoica (1989). *System Identification.* Prentice Hall Inc..

Steinbuch M. (1989). *Dynamic Modelling and Robust Control of a Wind Energy Conversion System.* PhD Thesis, Delft University of Technology, The Netherlands.

Vries D.K. de (1994). *Quantification of Model Uncertainty from Experimental Data.* PhD Thesis, Delft University of Technology, in preparation.

Vries D.K. de, P.M.J. van den Hof (1993). Quantification of model uncertainty from experimental data: a mixed deterministic–probabilistic approach. *proc. IEEE Conf. Decision and Contr.*,to appear,.

Zames G. (1963). Functional analysis applied to nonlinear feedback systems. *IEEE Trans. Circuit Theory, CT–10*, 392–404.

Special Issue on System Identification for Robust Control Design (1992). *IEEE Trans. Automat. Contr., 37*, 899–1008.

Selected Topics in Identification, Modelling and Control
Vol. 6, December 1993

Experimental model based wind turbine control design and implementation ‡

Gregor E. van Baars and Peter M.M. Bongers

Mechanical Engineering Systems and Control Group
Delft University of Technology, Mekelweg 2, 2628 CD Delft, The Netherlands.

Abstract. In this paper first results of controller design and implementation applied to the UNIWEX wind turbine system are presented. Identification experiments have been designed such that all relevant dynamics are excited. Experiments on a real life wind turbine have been carried out. Using prediction error methods experimental models with Box-Jenkins structure have been identified. Experimental models have been compared to physical models of the test turbine. Based on normalized coprime factorization of one experimental model a controller has been designed such that it robustly stabilizes all models. The implemented controller has been evaluated by means of measurements on the UNIWEX wind turbine and has proven to satisfy the design objective.

Keywords. Robust control, system identification, wind power plants

1 Introduction

The last few years wind power plants have become an acceptable alternative for electrical energy generation by fossile or nuclear power plants. In times of growing environmental conscience a clean and renewable energy source deserves more attention.

In order to make wind turbine systems more cost-effective they have to be *designed* and *controlled* in a proper way. The design of well controlled *flexible* wind turbines seems to be attractive for commercial applications because lighter and less costly construction elements can be used.

It is straightforward that an accurate mathematical dynamic model of the wind turbine system is necessary to achieve a wind turbine design that meets these high requirements. Mathematical models (such as presented Bongers *et al.* (1990)) need to be validated in practice. First results associated with this approach can be found in Bongers and van Baars (1991) .

In this paper emphasis lies on *control* of the wind turbine system. To be able to design an adequate control system for existing wind turbines also a dynamical model is needed. This model may be obtained both by mathematical and experimental modelling. This paper is involved with the experimental approach. Obviously experimental modelling requires real life measurement data.

The procedure to be exploited is as follows : Identification experiments are designed such that all relevant dynamics are excited. Experiments on a real life wind turbine are caried out. Using prediction error methods, experimental models with Box-Jenkins structure are identified. Experimental models are compared to the physical model of the test turbine. Based on normalized coprime factorization of one experimental model a controller will be designed such that it robustly stabilizes all models. The implemented controller will be evaluated by means of measurements on the wind turbine.

The power of this procedure lies in the fact that in principle it is applicable to any wind turbine system, and normal operation can proceed during the identification experiment. As such the application

‡This research was supported by the CEC under grant JOUR-0110 and the Netherlands agency for energy and environment under grant 40.35-001.10

of this procedure shows no serious practical drawbacks and can be realized within a relatively short time span.

A wind energy conversion system usually consists of a *rotor*, which absorbs the energy present in the wind, a *transmission* to gear up the rotational speed of the shaft, an *electrical conversion system* which feeds the electrical power into the public grid, and a *control system* to control the overall behaviour. The expected dynamic behaviour consists of a mix of aerodynamic phenomena, structural dynamics due to flexibilities in different construction elements, and dynamics related to the electrical energy conversion. The amount of energy absorbed by the rotor depends on the local wind speed as felt by the rotor blades and the angle of attack. Wind shear, wake of the wind turbine and the velocity of the blades determine the local wind velocity.

The operational region of a wind turbine system can be devided into two parts: *partial load* where the wind speed is below rated wind speed and power output is maximized, *full load* where wind speed is above rated but below cut-out wind speed, and power has to be limited to a fixed value. In addition to this power control the aim is also to minimize fatigue loads. In combination with the expected wind regime, this characteristic of operation and control objectives determines the design criteria for a complete wind turbine system.

An interesting feature of wind energy conversion is that a stochastic process, namely the wind speed, determines the point of operation. The wind speed simply determines the available amount of energy that can be converted into electrical power. The wind can only be measured in a few points but is not known over the complete rotor plane, and even if it were known it cannot be controlled. In other words the system is driven by noise, which makes wind turbine systems essentially different from most other systems.

As a consequence it may not be expected that operational conditions of the identification experiment and controller evaluation are the same. This motivates the need for *robust* controller design.

The procedure mentioned above is applied to the UNIWEX test facility situated in Stuttgart, Germany. The UNIWEX set up offers the possibility to emulate a wide range of (flexible) wind turbine configurations without any hardware changes (Müller (1989)) . This means, for example, that the rotor, which consists of hinged blades with computer controlled hydraulics, can be operated in such a way that it behaves like a rotor with flexible or rigid blades just by changes at software level. This setup saves the time and effort needed to mount and dismount different rotor systems.

The layout of the paper is as follows: Section 2 introduces a modular structured mathematical model which will be used to describe the UNIWEX turbine. Section 3 discusses the experimental modelling. Section 4 and Section 5 present the main contribution of this paper. Section 4 describes a controller design method and some robustness aspects. The controller synthesis and actual design are presented. Finally some implementation aspects are mentioned and results of controller experiments are presented in Section 5. The paper is closed with conclusions in Section 6.

2 Wind turbine system description

An overview of the UNIWEX test facility is given in Fig. 1.

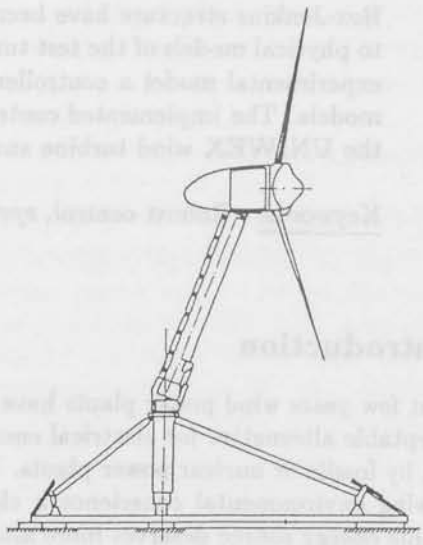

Fig. 1: Overview of UNIWEX turbine

In order to describe the wind turbine dynamics and their interactions a mathematical model has been developed (Bongers *et al.* (1990)) . The complete model consists of a description of each of the wind turbine parts and their mutual connections by interaction variables. Using this structure it is easy to describe different wind turbine configurations by connecting different submodels that are available (Bongers *et al.* (1990) and Bongers *et al.* (1989)) .

We will apply this approach to describe the dynamic behaviour of the UNIWEX turbine in particular. The mathematical model of this wind turbine consists of the interconnection of submodels having the following characteristics (more details can be found in Bongers and van Baars (1991) and

Müller (1989) : The *rotor* has two blades, without flexibility in the joints. Only pitch angle movements were allowed by the controller. In the aerodynamical model each blade is divided into 10 sections, each section has its own corde, mass, twist and profile. Based on the local wind speed and angle of attack of each section the aerodynamic loads are calculated.
The *tower* is considered to be rigid.
The *transmission* is described by the first torsional mode of the rotor shaft.
The *hydraulic generator* will be described by a spring characteristic.

The complete wind turbine system has the following input and output signals.
input signals: As mentioned in Section 1 the wind speed V_w as felt by the rotor is considered to be a *stochastic* input. The counter torque M_g generated by the hydraulic generator can be adjusted by manipulating the valve position χ_v which is the first *deterministic* input. The blade pitch angle θ can be seen as the second *deterministic* input because it directly influences the angle of attack.
output signals: In order to gain insight in the dynamic behaviour of the wind turbine the following outputs are measured: the rotor shaft speed ω_r, the rotor shaft torque M_r and blade root bending moments which form an indication for the structural loads.

3 Experimental modelling

To estimate experimental models we apply system identification methods of the well known *prediction error method* type (Ljung (1987)) . In previous studies on rigid wind turbines around one operating point (van Baars (1991), Bongers and van Baars (1991), Bongers *et al.* (1989)) this technique has shown to be successful. The application of a Box-Jenkins model structure is necessary to obtain satisfactory results. This necessity can be supported by reasoning that the influence of wind on the turbine behaviour is likely to be significantly different from the influence of deterministic inputs on the system. Therefore it can only be covered by a model structure with independently parametrized deterministic and stochastic part.

We are interested in modelling the transfer function from blade pitch angle to rotor speed and rotor shaft torque, because this transfer function offers the most direct opportunity to design and implement a controller.

During the experiments the blade pitch angle of both blades runs through a pseudo random sequence of stepwise changes between 3 and 7 degrees. An example of such a data set is given in Fig. 2. In

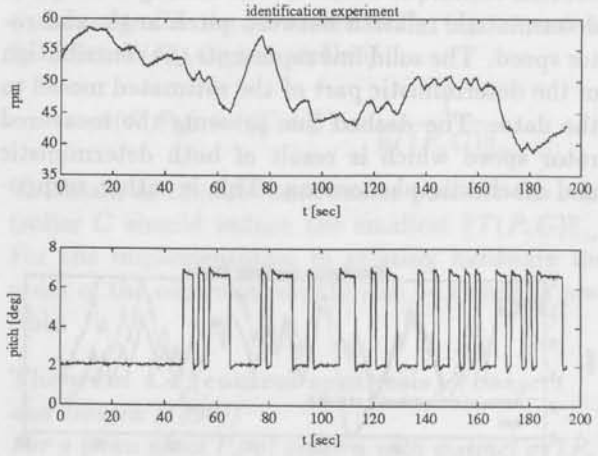

Fig. 2: experimental data identification experiment: lower part showing applied input pitch angle, upper part showing rotor speed output response

this figure it can be seen that there is no clear impact on the rotor speed due to the applied pitch steps. Therefore it is possible to apply this procedure without aborting normal operation because no rigorous excursions from the initial point of operation are introduced.

The measured signals are sampled with a sampling frequency of 50 Hz which implies that dynamics up to 25 Hz can be identified. This should be enough to cover the relevant dynamics particularly because this transfer function covers aerodynamic features which are, by nature, rather slow. Because of the ever present fluctuations in wind speed one can not expect the conditions to be constant for a long period of time. Therefore experiments have to be inspected in order to select intervals of relative constant operational conditions.

3.1 Identification results

After the data selection the experimental transfer functions from blade pitch angle to rotor shaft speed, rotor shaft torque and flap moment are estimated. Different choices of model orders have been investigated, both for the deterministic part and the stochastic part.

For deterministic orders larger than 3 and stochastic orders larger than 8 both the loss function (sum of squared residuals) and unit step responses show no significant improvement, they only differ slightly. Hence we may assume that all significant linear relations in the data are explained by the

model. Residual analysis supported this conclusion.

As shown in the upper part of Fig. 3, the identification technique succeeded in finding a clear cut deterministic relation between pitch angle and rotor speed. The solid line represents the contribution of the deterministic part of the estimated model to the data. The dashed line presents the measured rotor speed which is result of both deterministic and stochastic phenomena. This is rather surpris-

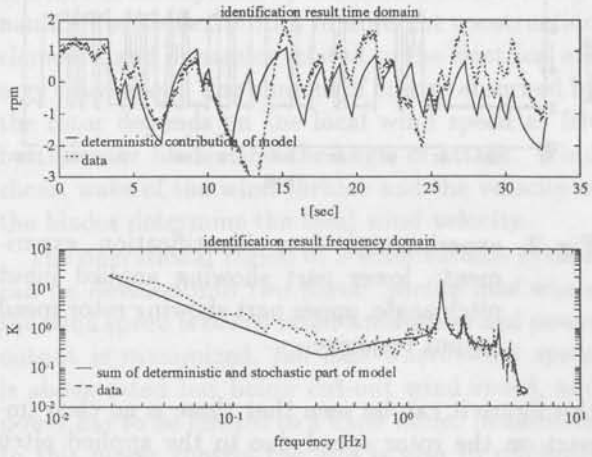

Fig. 3: Identification result time (upper part: deterministic contribution vs. data) and frequency (lower part: summed deterministic and stochastic part vs data spectrum) domain

ing because the identification data set did not show an evident correlation between pitch steps and rotor speed response. With a simple interpretation of aerodynamic behaviour in mind the deterministic response to the pitch steps seems realistic.

The accuracy of the stochastic part of the identified models cannot be judged properly in time domain. In order to investigate the validity of the stochastic part we apply the following procedure in the frequency domain. First an autospectrum of the rotor speed signal has been produced. Next the frequency response of the deterministic $(G(\theta)u)$ and stochastic part $(H(\theta)e)$ of the estimated model have been calculated. For the model to be reliable the sum of these frequency domain functions should correspond to the spectrum of the output signal (y). The lower part of Fig. 3 shows the result. Clearly there is no perfect match but no essential dynamic behaviour is missing in the experimental model so we can be quite confident about the accuracy of both the deterministic and stochastic part of the model.

4 Controller design and implementation

In this section the controller design and implementation will be discussed. A more thorough description of the applied control design method can be found in Bongers (to appear) and Bongers (1992) .

The control design objective pursued in this paper is to maintain the rotor speed as constant as possible by means of blade pitch movements. Therefore the controller has to achieve a good servo–behaviour. In general the operational conditions during the identification experiments and the controller experiments will not be the same. Therefore the wind turbine system will be approximated with a set of linear models representing the variations in operational conditions under which the controller should be able to achieve satisfactory behaviour. These models are the models estimated with the procedure described in Section 3 and the available theoretical model. The controller must not only achieve the desired servo-behaviour for the design model but also for the set of linear models. Even deviations of the designed controller have to be allowed in order to implement the controller successfully. For UNIWEX the main source of deviations in the controller is the limitations introduced by integer arithmetics of the control computer.
In this paper we will employ a controller design method based on coprime factorizations of the wind turbine model in order to achieve the desired objectives. First we need some definitions that will be used in the sequel.

Only finite dimensional linear time-invariant systems are considered. Let P be a multi-input multi-output transfer function.

Definition 4.1 (factorizations) *(Vidyasagar et al. (1982))*

A system P has a right (left) fractional representation if there exist stable $N, M(\tilde{N}, \tilde{M})$ such that:

$$P = NM^{-1} \ (= \tilde{M}^{-1}\tilde{N})$$

*The pair $M, N(\tilde{M}, \tilde{N})$ is right (left) coprime fractional representation (*rcf *or* lcf *) if it is a right (left) fractional representation and there exist stable $U, V(\tilde{U}, \tilde{V})$ such that:*

$$UN + VM = I \ (\tilde{N}\tilde{U} + \tilde{M}\tilde{V} = I)$$

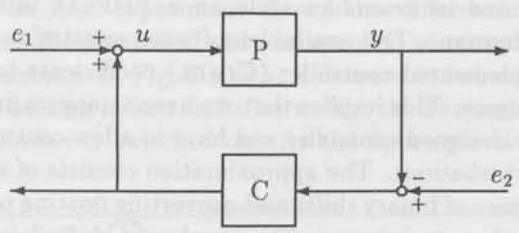

Fig. 4: Feedback configuration

*The pair $M, N(\tilde{M}, \tilde{N})$ is called normalized right (left) coprime fractional representation (*nrcf *or* nlcf *) if it is a coprime fractional representation and:*

$$M^*M + N^*N = I \ (\tilde{M}\tilde{M}^* + \tilde{N}\tilde{N}^* = I)$$

with $M^* = M^T(-s)$.

According to Meyer (1988) the graph Hankel singular values $\sigma_i^G(P)$ are defined as the Hankel singular values of the nrcf of P $\sigma_i^H(\begin{smallmatrix} M \\ N \end{smallmatrix})$

Definition 4.2 (Gap distance measure) *(El-Sakkary (1985) and Zames and El-Sakkary (1980))*

Suppose P, P_Δ are two plants with nrcf *(N, M), (N_Δ, M_Δ) respectively.*

The gap metric distance $\delta(P, P_\Delta)$ between the two plant is defined as

$$\begin{aligned} \delta(P, P_\Delta) &= \max\{\vec{\delta}(P, P_\Delta), \vec{\delta}(P_\Delta, P)\} \\ \vec{\delta}(P, P_\Delta) &= \inf_{Q \text{ stable}} \left\| \begin{bmatrix} M \\ N \end{bmatrix} - \begin{bmatrix} M_\Delta \\ N_\Delta \end{bmatrix} Q \right\|_\infty \end{aligned}$$

The feedback system considered in the sequel is given in Fig. 4, where P is the wind turbine and C the controller. The closed loop transfer function $T(P, C)$ representing the mapping between (e_1, e_2) and (u, y) is:

$$T(P,C) = \begin{bmatrix} I \\ P \end{bmatrix} (I + CP)^{-1} \begin{bmatrix} I & C \end{bmatrix} \qquad (1)$$

The (2,2)-element of the $T(P, C)$ transfer function is closely related to the servo-behaviour, the (1,1)-element is the sensitivity function. Therefore the function $T(P, C)$ represents all closed loop properties to be considered.

In the next theorem a sufficient condition for stability of the closed loop is given when uncertainties in both plant and controller are present.

Theorem 4.3 (robustness aspects) *(Georgiou and Smith (1990)))*
Suppose $T(P, C)$ is stable, and that both plant and controller are perturbed to P_Δ, C_Δ respectively. Then $T(P_\Delta, C_\Delta)$ is stable if

$$\delta(P, P_\Delta) + \delta(C, C_\Delta) < \frac{1}{\|T(P, C)\|_\infty}$$

To obtain as much robustness as possible the controller C should induce the smallest $\|T(P, C)\|_\infty$. For the implementation in existing hardware the order of the controller should also be as low as possible.

Theorem 4.4 (control synthesis) *(Bongers and Bosgra (1990))*
For a given plant P_n of order n with distinct $\sigma_i^G(P_n)$ there exists a controller C_r of order r, with $r < n$, such that $T(P_n, C_r)$ is stable and the closed loop transfer function satisfies:

$$\|T(P_n, C_r)\|_\infty \leq \frac{1}{\sqrt{1 - (\sigma_1^G + \sum_{i=r+2}^{n} \sigma_i^G)^2}}$$

Actual design

On three independent data sets experimental models have been calculated. These models are denoted by s644, s668, s669, selected from the original measurement file with corresponding experiment number. The theoretical model is also available as ST. In Fig. 5 the amplitude part of the frequency response of all these models is given. It can be seen that around the cross-over frequency these models are quite different. First a nominal model needs to be chosen. According to Theorem 4.3 we choose as nominal model, that model which generates the smallest gap (Definition 4.2) with the other models within the model set. The model P :=s669 is selected to be the nominal model. The gaps between this nominal model and the other models in the model set are: δ(s669,s644) = 0.5512, δ(s669,s668) = 0.3309, δ(s669,ST) = 0.219. This means that if the controller induces $\|T(P, C)\|_\infty < 1.81$, all models are stabilized if there are no controller perturbations.
The design bandwidth of the servo–loop will be chosen to be 1Hz. If a bandwidth larger than 0.5 Hz is achieved, the designed controller will be an improvement compared to an existing controller. A PI pre–compensator is used to obtain a zero tracking error at low frequencies. This pre–compensator can be incorporated in the nominal model to act as a weighting function (McFarlane and Glover

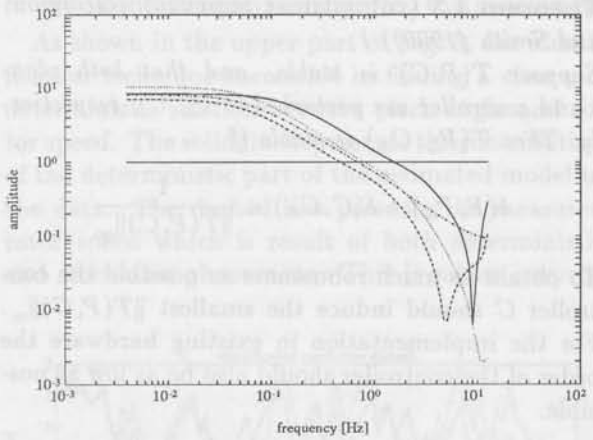

Fig. 5: Frequency response of the models in the set. (—) s644, (- -) s668, (...) s669, (-.-) ST horizontal solid line denotes 0dB

(1989)). Using the controller synthesis of Theorem 4.4 a first order controller for the weighted plant has been designed. The final controller C is composed of the controller of Theorem 4.4 and the pre–compensator. For the controller C and the nominal plant P, $\|T(P,C)\|_\infty = 1.5462$ and generates a robustness margin of 0.6467 which is large enough to incorporate the given perturbations. In Fig. 6 the amplitude plot of the frequency response of the design model with PI-pre-compensator is given, together with the obtained sensitivity and complementary sensitivity. It can be seen that the achieved bandwidth for the design model is about 0.7 Hz, hence the nominal controller design objective is satisfied. The designed controller is implemented in assembler code on a PDP 11 process computer. The available software constrains the implemented controller (CIMPL) coefficients to be integers. This implies that we have to approximate our designed controller and have to allow controller perturbations. The approximation consists of a sequence of binary shifts and converting floating point numbers to integers. The number of shifts is quite ad hoc.

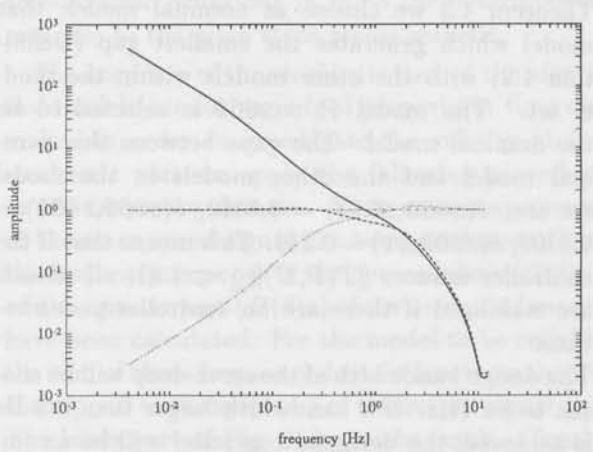

Fig. 6: Frequency response closed loop system, (—) weighted s669, (- -) Complementary Sensitivity, (...) Sensitivity

In Fig. 7 the amplitude plot of the frequency response of the theoretical controller, approximated controller and the additive error between the two controllers is given. It can be seen that the deviations are mainly at low frequencies, where they are of approximately the same amplitude as the controller. If the open loop response of both controllers

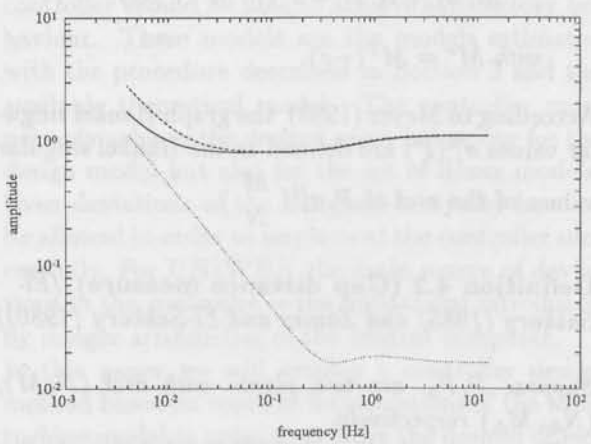

Fig. 7: Frequency response controller. (—) C, (- -) CIMPL, (...) C-CIMPL

are compared, the implemented one can easily be rejected, see Fig. 7. The gap between the two controllers is δ(C,CIMPL) = 0.008, which is surprisingly small. According to the robustness test of Theorem 4.3: $\max(\delta(P,P_i)) = 0.5512 + \delta$(C,CIMPL) = 0.008 is smaller than the allowed robustness margin of 0.6467, hence the whole model set is stabilized by CIMPL, therefore this controller will be implemented.

5 Results

After implementation a number of experiments was performed with the implemented controller. During these experiments the wind speed was smaller than during the identification experiments, which implies that the operational conditions are likely to differ significantly. As a consequence a certain performance degradation compared to the designed closed loop performance can be expected.

The first experiment shows the difference between the controlled and uncontrolled wind turbine behaviour. In Fig. 8 a clear difference in behaviour can be seen before and after t=39s, the moment the controller is switched on. As the figure shows the

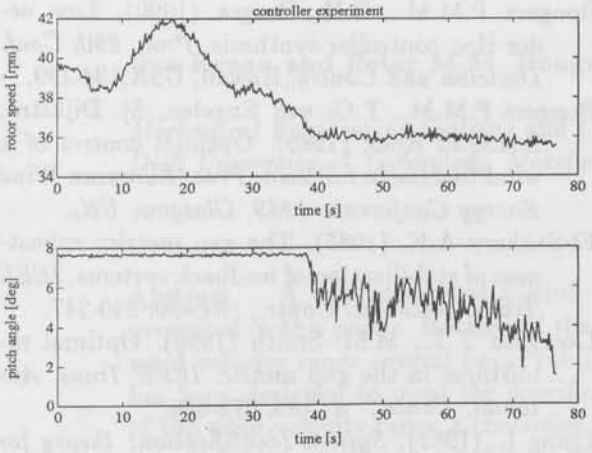

Fig. 8: Controller switching on at $t = 38s$: rotor speed response (upper part) and pitch angle contoller action (lower part)

rotor speed is controlled within a tight bound. The applied control action (the pitching of the blades) is not excessive and stays in an acceptable range. Comparing the behaviour of the rotor speed at constant pitch (no control) and active pitch (control) it is clear that the rotational speed variations due to variations of wind speed can be reduced sufficiently by this controller.

The second controller experiment investigates the tracking performance. Fig. 9 shows that the controlled system responds accurately to stepwise changes in the desired rotor speed. Considering the large rotor inertia the time span to reach the new set point (2 a 3 sec) is quite an improvement compared to previously applied controllers. The time constant of the controlled wind turbine is approximately .7 s, which implies that the designed bandwidth (1 Hz) has not been achieved. Nevertheless there is great confidence that the designed bandwidth will be achieved if the controller will be evaluated under operational conditions closer to the oprational conditions the controller has been designed for. The control actions stay within a reasonable area.

A remark has to be made concerning a large stepwise increase of desired rotor speed. This may imply that the pitch angle is steered towards negative values. This makes no sense from aerodynamic point of view and can lead to unstable behaviour.

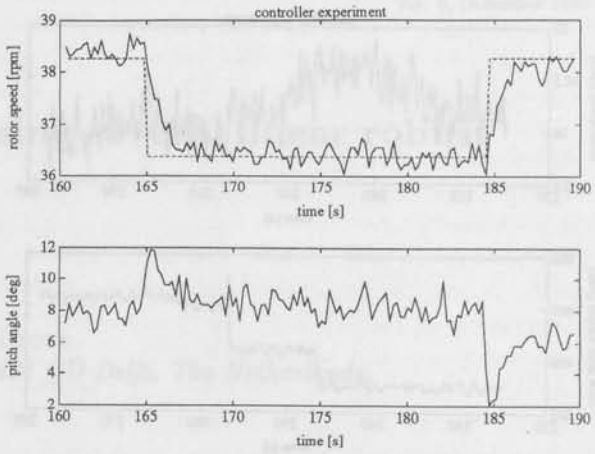

Fig. 9: servo behaviour: set point changes of desired rotor speed at $t = 165, 184$ (upper part) and pitch angle controller action (lower part)

In order to avoid this the pitch angle must be restricted to nonegative values. The consequence of this is that such rigourous setpoint changes can not be followed as fast as desired.

The final controller experiment is the most drastic one. It evaluates the performance of the controller under stepwise changes in the absorbed torque by the generator system. This can be seen as abrupt disturbances that influence the system in addition to the fluctuating wind speed. In fact there are two kinds of disturbances acting on the system: the wind stochastics which are always present and the deterministic induced variations of the counter torque. As shown in Fig. 10, the controller acts satisfactory patricularly for these drastic disturbances (the torque is doubled). The speed remains in a range of approximately .5 rpm.

6 Conclusions

A procedure consisting of identification, robust controller design and implementation has been succesfully applied to a real life wind turbine system.

An advantage of this approach is that normal operation needs not to be aborted during the identification experiments, and in principle it can be applied to almost any wind turbine system.

Since one can not expect the operational conditions during identification and controller experiments to be the same more than one experimental model has to be estimated.

A robust controller has been designed which stabilizes this set of all these experimental models. Because of implementation restrictions the designed

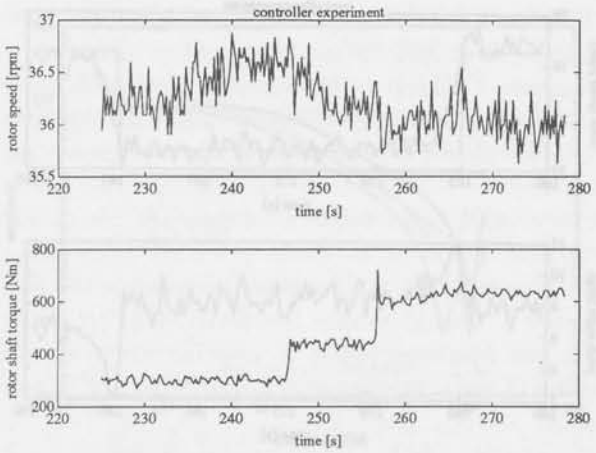

Fig. 10: response to disturbances : controlled rotor speed (upper part) and changes of absorbed rotor torque (lower part)

controller needs to be approximated and therefore controller perturbations are taken into account.

Implementation of the controller showed satisfactory behaviour with respect to the design objective both for setpoint changes and stepwise disturbances of absorbed torque.

Further research will focus on application of this procedure to more flexible wind turbine configurations.

Acknowledgements

The authors wish to thank the ICA of the universtity of Stuttgart for the possibility to experiment with the UNIWEX turbine, and in particular the people working at the test site for the pleasant cooperation during the measurement sessions.

References

Baars G.E. van (1991). *Experimental validation of the UNIWEX wind turbine* (in Dutch). Delft University of Technology, The Netherlands.

Bongers P.M.M. (). *Factorizational Approach to Robust Control: Application to a Flexible Wind Turbine.* PhD Thesis, Delft University of Technology, The Netherlands, In preparation.

Bongers P.M.M. (1992). Robust control using coprime factorizations, application to a flexible wind turbine. Proc. 31st IEEE Conf. on Decision an Control, Dec. 16-18, Tucson, AZ, 2436-2441.

Bongers P.M.M., G.E. van Baars (1991). Experimental validation of a flexible wind turbine model. *Proc. 30th IEEE Conf. on Decision and Control, Dec. 11-13, Brighton, UK,*1660-1661.

Bongers P.M.M., W.A.A.M. Bierbooms, Sj. Dijkstra, Th. van Holten (1990). *An Integrated Dynamic Model of a Flexible Wind Turbine.* Delft University of Technology, The Netherlands.

Bongers P.M.M., O.H. Bosgra (1990). Low order H∞ controller synthesis. *Proc. 29th Conf. Desicion and Control,*Hawaii, USA,194-199.

Bongers P.M.M., T.G. van Engelen, Sj. Dijkstra, Z.D.Q.P. Kock (1989). Optimal control of a wind turbine in full load. *Proc. European Wind Energy Conference 1989, Glasgow, UK,.*

El-Sakkary A.K. (1985). The gap metric: robustness of stabilization of feedback systems. *IEEE Trans. Automat. Contr., AC-30,* 240-247.

Georgiou T.T., M.M. Smith (1990). Optimal robustness in the gap metric. *IEEE Trans. Automat. Contr., AC-35,* 673-686.

Ljung L. (1987). *System Identification: theory for the user.* Prentice Hall,, Inc. Englewood Cliffs, New jersey.

McFarlane D.C., K. Glover (1989). *Robust Controller Design Using Normalized Coprime Factor Plant Descriptions.* Lecture Notes in Control and Information Sciences, vol.138, Springer Verlag, Berlin, Germany.

Meyer D.G. (1988). A fractional approach to model reduction. *Proc. Amer. Control Conf.,*1041-1047.

Müller M. (1989). Experimental investigations with the universal test wind turbine. *Proc. European Wind energy Conf. 1989.,*Glasgow, Schotland,832-836.

Vidyasagar M., H. Schneider, B.A. Francis (1982). Algebraic and topological aspects of feedback stabilization. *IEEE Trans. Automat. Contr., AC-27,* 880-893.

Zames G., A.K. El-Sakkary (1980). Unstable systems and feedback: the gap metric. *Proc. 18th Allerton Conf.,*380-385.

Selected Topics in Identification, Modelling and Control
Vol. 6, December 1993

Control of a wind turbine using several linear robust controllers

Ilya Kraan and Peter M.M. Bongers

Mechanical Engineering Systems and Control Group
Delft University of Technology, Mekelweg 2, 2628 CD Delft, The Netherlands.

Abstract. A way to control a wind turbine over a wide range of wind velocities is presented in this paper. Because of the strong non-linearity of a wind turbine along the wind velocity range several linear robust controllers are applied. Each linear controller has been designed to meet the specifications of a controlled wind turbine for the part of the wind velocity range a controller belongs to. Dependent on the wind velocity the appropriate controller is scheduled. Special attention is given to avoiding the harmful transients which arise after switching between controllers. This has been done by conditioning the linear controllers which are not in the control loop. Together with some additional specific actions a control has been synthesized which satisfies the specifications of a controlled wind turbine well for the whole range of wind velocities.

Keywords. variable speed wind turbines, robust control, controllers switching, conditioning technique

1 Introduction

The most important underlying motivation of research for large scale energy production using wind energy conversion systems is the aim to reduce the economic costs of produced electrical energy.

One single, cost effective, wind energy conversion system will then have:

(i) **low construction costs.** Low construction costs can be achieved by using lighter, and thereby more flexible, components. Allowing more flexibility in the components also introduces the possibility of reducing internal stresses. However the dynamics of each component should be designed more carefully otherwise the internal stresses are magnified.

(ii) **long lifetime.** Fatigue loads have to be kept within acceptable margins in order to guarantee a long lifetime and thereby achieve an economic attractive system.

(iii) **efficient energy conversion.** Higher energy production out of the same amount of wind implies lower costs of the produced energy.

It is evident that each of these points more or less independently reduce the costs of the generated electrical energy.

The optimal energy production for wind turbines is schematically represented in Fig. 1. Below cut-

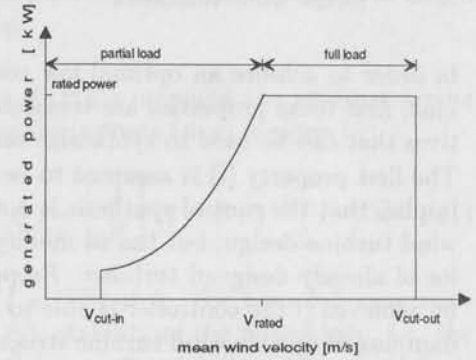

Fig. 1: Power curve

in wind velocity V_{cut-in} the maximum amount of generated energy is less than the energy dissipation

due to friction, consequently the turbine will not be operated below the cut-in wind velocity. Starting from V_{cut_in} to the "rated" wind velocity V_{rated} the turbine is operating in partial load. In this area the produced electrical energy can be optimized by controlling the rotor speed proportional to the wind velocity (optimal tip-speed ratio). It is noted that the presented power curve is only achievable if the wind turbine can operate with a variable rotational speed. Above the rated wind velocity the turbine is operating under full load conditions where the generated power has to maintain a constant level. This can be achieved by controlling the produced current. Above cut-out wind velocity $V_{cut-out}$ the turbine is taken out of operation, to prevent extremely high loads. The cut-out wind velocity is determined in a trade-off between produced energy and the loads on the construction.

The non-linear behavior of a wind turbine is explicitly shown in Fig. 2, where for a number of mean wind velocities linear model where calculated.

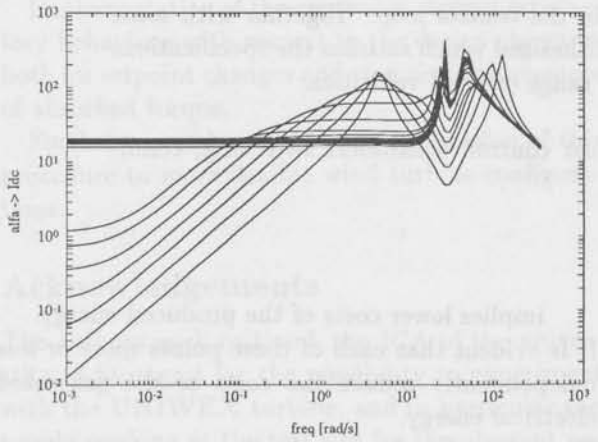

Fig. 2: Amplitude part frequency response for different wind velocities

In order to achieve an optimal low cost wind turbine, first these properties are translated to objectives that can be used to synthesize controllers:

The first property (i) is assumed to be given. This implies that the control synthesis is not part of the wind turbine design, but has to modify the behavior of already designed turbines. Property (ii) can be achieved if the controller is able to increase the damping of flexible wind turbine structure over the whole operating envelope. In order to achieve objective (iii) by a controller, the control objective can be formulated in partial load as a tracking problem on the unmeasurable wind velocity; in full load this will change to a disturbance attenuation problem.

Around one operating condition it has been shown by (Steinbuch (1989), Bongers and Dijkstra (1992)) that linear controllers can be applied to achieve objectives (ii) and (iii), experimental results can be found in (Baars and Bongers (1992), Bongers (1993)) .

Due to the variation in system behavior, with respect to the mean wind velocity, one linear controller is not able to achieve objectives (ii) and (iii) over the whole operating envelope.

In this paper, several linear controllers will be used to control the non-linear wind turbine model. For a number of appropriate wind velocities linear controller will be designed. Switching between the controllers will cause the appropriate controller to be active at the corresponding wind velocity. According to (Campo *et al.*(1989), Hanus *et al.*(1987)) a conditioning technique will be used to obtain a smooth transfer between the active and inactive controllers. This technique has been successfully applied in aerospace engineering by Hyde and Glover (1990) , whereas more details about wind turbine application can be found in Kraan (1992) .

The layout of this paper is as follows: In Section 2 the wind turbine system to be controlled is described. Backgrounds and an outline of the control design procedure are given in Section 3. The control design will be covered in Section 4. Simulation results of the controlled wind turbine will be shown in Section 5. We will end with some conclusions and recommendations in Section 6.

2 Description of the system

The experimental set-up is the IRFLET test-rig (Engelen *et al.*(1993)) , which is located at the Netherlands Energy Research Foundation, Petten, The Netherlands. In this set-up the electromechanical part of a wind turbine can be studied under predefined conditions. The test-rig is schematically represented in Fig. 3.

The test-rig consists of the following components:

- a controlled DC-motor which physically represents the torque effects created by the wind velocity acting on the rotor. In contrast to real wind turbine systems, the wind velocity can be specified.
- a flexible shaft, and a transmission for increasing the angular speed of this shaft up to a value which is appropriate for the generator;
- a synchronous generator with rectifier, DC-link and invertor which enables variable speed operation independently of the grid frequency.

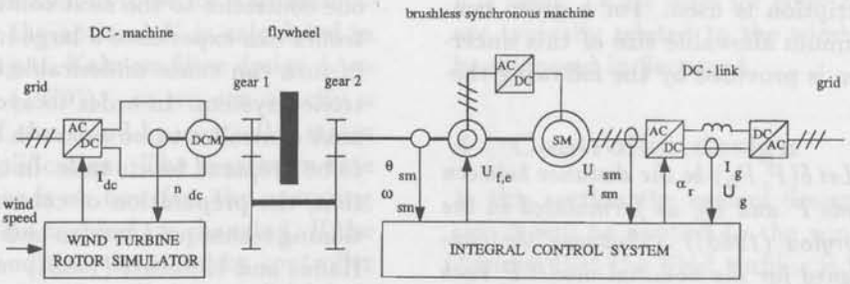

Fig. 3: IRFLET test-rig (Engelen *et al.*(1993))

The torque generated by the DC-motor represents a wind turbine configuration with a rigid tower and a rigid rotor. This permits us to direct our attention to the electro-mechanical part.

Controllable inputs are:

- the delay angle α_r of the thyristors in the rectifier, which has to be kept at a low constant value when not participating in control actions;
- the field voltage $U_{f,e}$ of the generator.

Measurable outputs are:

- the direct current I_g in the DC-link;
- the generator speed ω_{sm}.

A non-linear model of this test-rig is available in the DUWECS wind turbine simulation package (Bongers (1993a)) .

3 Backgrounds and outline of the control design method.

As argued, the aim is to control the wind turbine over the whole operating envelope by a number of linear controllers. Consequently two aspects in the control design we can be recognized:

Design of multiple linear robust controllers: Each linear controller has to satisfy the objectives (ii) and (iii) for a part of the operating envelope. The controlled wind turbine has to be robust with respect to the non-linearities involved in this part. The used design tools to achieve this will be elucidated in Section 3.1.

Minimization of switching phenomena: When a new linear controller has to substitute the one in the loop, the states and outputs of this controller are not "prepared" to the situation in the loop, which can cause very disadvantageous effects on the system. A *conditioning* technique used in this study to prepare the "stand-by" controllers will be explained in Section 3.2

3.1 H_∞ controller design

Each linear robust controller will be designed using an H_∞ design method based on coprime factor plant description (Bongers and Bosgra (1990), McFarlane and Glover (1989)) . Advantages of this design method are:

- The nominal plant P and the perturbed plant P_Δ are allowed to have a different number of unstable poles.
- The possibility to trade-off the order of the controller with robustness.
- Due to the existence of explicit solutions, fast MATLAB-compatible algorithms exist (Bongers (1993)) .

The following feedback configuration will be studied (Fig. 4), where the wind turbine model P is controlled by a controller C. The closed loop trans-

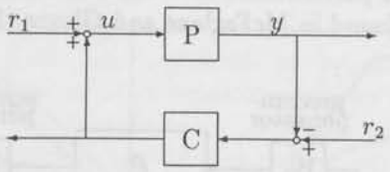

Fig. 4: controller C and wind turbine P in closed loop.

fer function $T(P,C)$ mapping the external inputs (r_1, r_2) onto the outputs (u, y) is given by:

$$T(P,C) = \begin{bmatrix} I \\ P \end{bmatrix} (I + CP)^{-1} \begin{bmatrix} I & C \end{bmatrix} \qquad (1)$$

where $det(I + CP) \neq 0$. For bounded exogenous inputs (r_1, r_2), stability of the closed loop, i.e. the controller C internally stabilizes the plant P, is guaranteed if and only if $T(P,C)$ is stable.

The purpose of the designed controller is not only to stabilize the nominal plant, but also to stabilize plants which are slightly different. To this end an

uncertainty description is used. For a given controller, the maximum allowable size of this uncertainty description is provided by the following theorem.

Theorem 3.1 *Let $\delta(P, P_\Delta)$ be the distance between two linear systems P and P_Δ as formulated in the gap-metric (Georgiou (1988)) . Suppose the controller C is designed for the nominal model P such that the feedback system $T(P,C)$ is stable. Then all $P_\Delta \in \{P_\Delta \mid \delta(P, P_\Delta) \leq \epsilon\}$ are stabilized if*

$$\|T(P,C)\|_\infty < \frac{1}{\epsilon}$$

Proof: (Georgiou and Smith (1990), Bongers and Bosgra (1990)) □

The control problem concerns the minimization of $\|T(P,C)\|_\infty$ over stabilizing C, which implies maximizing robustness ϵ. Because the four transfer functions in $T(P,C)$ represent robustness as well as performance properties, the minimization establishes a certain performance also. Control design specifications can be incorporated, using loop shaping, by means of a pre-compensator W_1 and a post-compensator W_2 (Fig. 5). Then we have the control problem of minimizing $\|T(P_T,C)\|_\infty$ over stabilizing C, where $P_T = W_2 P W_1$. The controller which has to be implemented becomes $C_T = W_1 C W_2$. For a more detailed treatment of influencing the achieved performance and robustness in this way can be found in McFarlane and Glover (1989) .

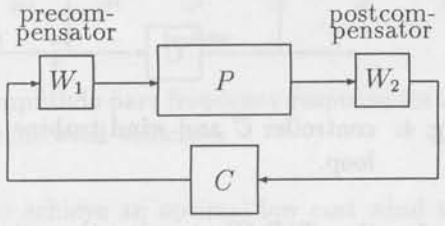

Fig. 5: manipulation of the control design by a pre-compensator W_1 and a post-compensator W_2.

3.2 Controller conditioning

Given a number of linear robust controllers, designed according to the previous section, the next step is to describe how the individual linear controllers cooperate. If one would just switch from one controller to the next controller, this next controller can experience a large initial response. This in turn can cause undesirable behavior of the controlled system. In order to avoid these effects, the next controller to be active in the control loop has to be prepared for its task. In the sequel of this section, the preparation of controllers using a conditioning technique (Åström and Wittenmark (1984), Hanus and Kinneart (1989)) will be explained.

The controlled configuration with one controller stand-by to control the wind turbine is given in Fig. 6.

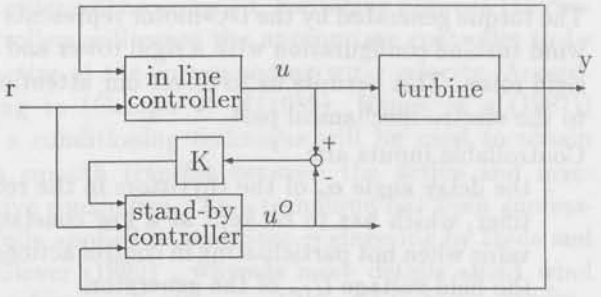

Fig. 6: Observer approach to controller conditioning

Let the state-space description of the stand-by controller be given by

$$\begin{aligned} x_{k+1} &= Ax_k + By_k + Rr_k \\ u_k^O &= Ex_k + Dy_k + Sr_k \end{aligned} \tag{2}$$

By feeding back the difference between the outputs of the in-line and the stand-by controller $u_k - u_k^O$, using a gain K, the state equation can be written as:

$$x_{k+1} = Ax_k + By_k + Rr_k + K(u_k - u_k^O)$$

Using (2) we have:

$$x_{k+1} = (A-KE)x_k + (B-KD)y_k + (R-KS)r_k + Ku_k$$

The stand-by controller states converge to a steady-state if the the eigenvalues of $A-KE$ are inside the unit disk. In this steady-state condition, the difference $U_k - u_k^O$ will be zero. Thereby, if the stand-by controller is switched into the control loop, no initial controller response will occur and a smooth transition from one controller to the next controller has been achieved.

The combination of the feed-back matrix K and the stand-by controller can be considered as an observer, which explains the name of the method, although the aim is not estimation of the in-line controller states, but conditioning the stand-by controller states. Calculation of K can be done with

methods which are related to those for state estimation. In this study the optimal K is calculated in a way corresponding to Kalman filter design (Anderson and Moore (1979)) , so we can specify a fast convergence of the stand-by controller states with low noise amplification. The maximum rate of convergence depends on how fast the operating conditions of the wind turbine are changing. If the alowable time to condition the stand-by controller not sufficient, the controller will show an initial response when it is switched in-line with the wind turbine.

This frame-work to condition controllers can also be applied in the case:

- Two consecutive controller may have a different structure or have a different state dimension. This will occur when the wind turbine operation shifts from partial load to full load and vice versa.
- An unstable controller, desired to enhance the performance of the system can be conditioned by a stable low performance controller.

The switching mechanism between conditioned controllers is illustrated in the block-scheme of Fig. 7. The vector v, consisting of variables which represent the non-linearity of the system (in this case an estimation of the wind velocity), passes a block, called 'switching logic'. This non-linear block contains several logic rules for determining the appropriate moment of linear controller transfer in dependence of the values in v. An example of such a rule is the hysteresis in the switching moment to avoid oscillations between linear controllers when v is noisy. Other rules for good controller transfer are typically related to the wind turbine and will be discussed in Section 4

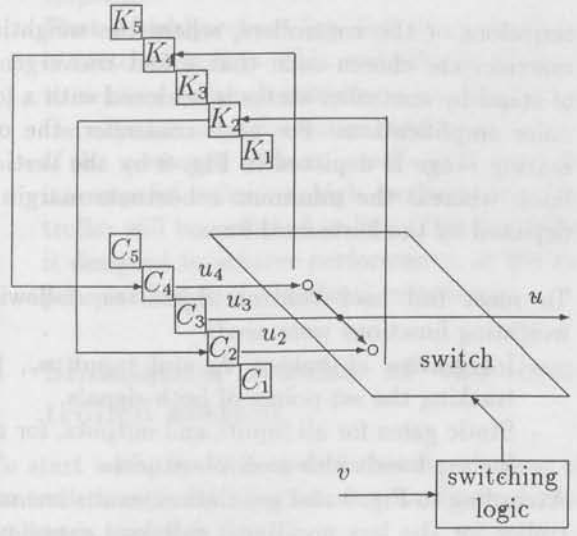

Fig. 7: blockscheme of the total control.

4 Controller design

In this section the control design method of Section 3 will be applied to the wind turbine model. Assume that the wind turbine is bound to operate on the optimal power curve of Fig. 1, then the operating condition is completely determined by the mean wind velocity. Consequently we can approximate the non-linear model, by a set of linear models parametrized by the mean wind velocity. Since one controller is not able to satisfy the desired objectives for all wind velocities, we have to determine the range of wind velocity such that one controller is able to satisfy the objectives. For this purpose the distance in gap-metric sense between the linearized models is determined. In Fig. 8 these distances between the linear models in partial load, corresponding with wind velocities between 3 and 9 m/s are represented. Fig. 9 represent the distances in full load (wind velocity from 10 to 24 m/s). In Fig. 8, for example, the dash-dotted line represents the distance between the wind turbine model linearized at 6 m/s mean wind velocity and the other linear wind turbine models. It can be seen that the distance between the two models will become larger if the wind velocities around which the models are linearized become larger.

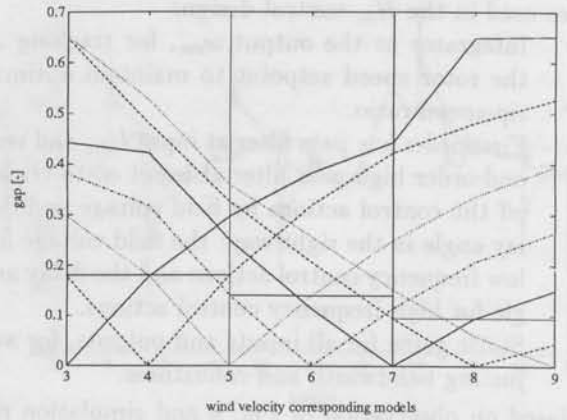

Fig. 8: Distances between linear systems corresponding to wind velocities in partial load

The determination of the wind velocity range for which the linear controllers have to be robust have to happen in an iterative way. This is caused by the fact that the controller, to be designed, determines the size of the allowable perturbations. The itera-

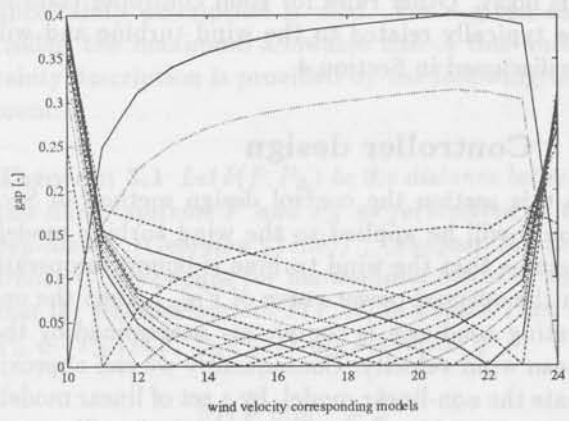

Fig. 9: Distances between linear systems corresponding to wind velocities in full load

tive character of the design procedure is illustrated by the flow diagram of Fig. 10.

Essential trade-offs, concerning the number of controllers and the robustness of each controller, are:

- much controllers cover non-linearity well, but above a certain number of controllers, performance won't be improved remarkably. Besides, enough robustness has to be left against (remaining) switching phenomena.
- few controllers imply less switching, but non-linearity is also covered less, so more robustness may be necessary and performance could get worse.

For partial load, the following weighting functions are used in the H_∞ control design:

- Integrator at the output ω_{sm}, for tracking of the rotor speed setpoint to maintain optimal tip-speed ratio.
- First order low pass filter at input $U_{f,e}$ and second order high pass filter at input α_r to trade-off the control actions by field voltage and delay angle in the right way: the field voltage for low frequency control actions and the delay angle for high frequency control actions.
- Static gains for all inputs and outputs, for adjusting bandwidth and robustness.

Based on observation of Fig. 8 and simulation results obtained with the controllers, it has been decided that three linear controllers are sufficient in the partial load range to cover non-linearity while maintaining performance. Remarkably, just the well performing controllers provide also a lot of robustness in the closed loop ($\epsilon \approx 0.6$). Three corresponding gains K_i have been designed for conditioning of the stand-by controllers. The Kalman gain design is based on balanced state-space de-

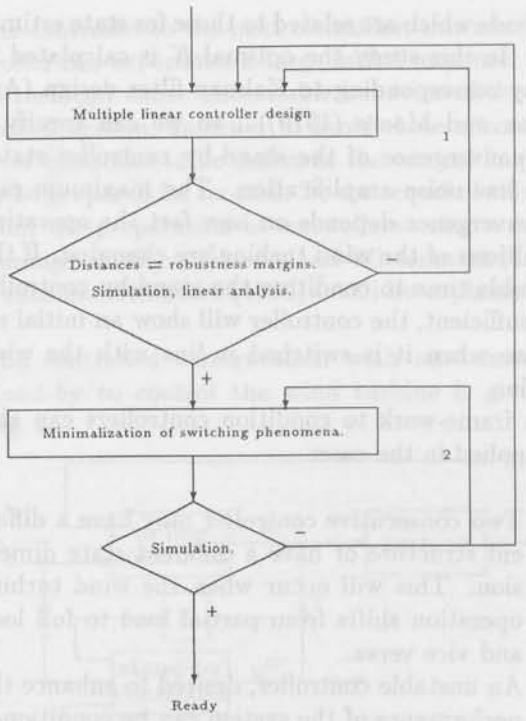

Fig. 10: flow diagram of the control design procedure. ◇ means an evaluation of design criteria, □ means a design step.

scriptions of the controllers, where the weighting matrices are chosen such that a fast convergence of stand-by controller states is achieved with a low noise amplification. For each controller, the operating range is depicted in Fig. 8 by the vertical lines, whereas the minimum robustness margin is depicted by the horizontal lines.

To meet full load control objectives, following weighting functions were used:

- Integrators at output I_g and input α_r, for tracking the set points of both signals.
- Static gains for all inputs and outputs, for adjusting bandwidth and robustness.

According to Fig. 9 and simulation results one controller for the less non-linear full load range preserves high performance while providing enough robustness ($\epsilon > 0.4$, as required by Fig. 9).

The difference between the control aims, and hence the controllers, corresponding to partial load and full load is so substantial that switching between a partial load controller and a full load controller will cause very strong and harmful effects, in spite of the controller conditioning.

To motivate the remaining control design steps, the problem with switching between partial and full

load will be considered more detail. In fact the difference between partial load and full load control aims may imply sudden changes in reference signals. For instance, let us consider a firm wind gust starting at 6 m/s (stationary value of direct current: 11 Ampere) and ending at any value belonging to the full load range ($> 9.7m/s$, stationary value of direct current: 45 Ampere). Because time is needed for acceleration of the rotating parts and consequently for reaching the stationary values of angular speed, direct current and torques, direct current will be about only 20 Ampere when switching to full load controller and control aims. This implies a sudden reference step of $45 - 20 = 25$ Ampere. In combination with tight controllers and a limited range of inputs this will be disastrous for the wind turbine. Consequently, in addition to the wind velocity, also the direct current is necessary to determine the appropriate way of switching. In order to obtain a smooth transition from partial load to full load conditions some new conditions are built in the controller. In case of switching from partial to full load:

- The difference in actual direct current and reference direct current will pass a first order filter in order to prevent a large initial controller response.
- First a highly robust (eg. low gain) controller is switched in-line. This controller is designed to achieve as much robustness as possible, at the expense of performance deterioration.
- If the measured current is sufficiently close to its setpoint value, a high performance controller will be switched in-line. This controller is designed to achieve performance, at the expense of less (but sufficient) robustness.

5 Simulation results of the controlled system

To start with, the difference between switching of controllers and switching between conditioned controllers is shown in Fig. 11.
It is obvious from Fig. 11 switching between conditioned controllers results in better system behavior in comparison with switching between non-conditioned controllers. In this special case, where the wind velocity is hardly changing and *knowing* that it won't, switching between controllers is not very sensible. One could easily design one controller for this operating envelope. The smooth transition between the conditioned controllers also holds if the wind velocity varies of a larger range.
Conditioning of the partial load controllers always

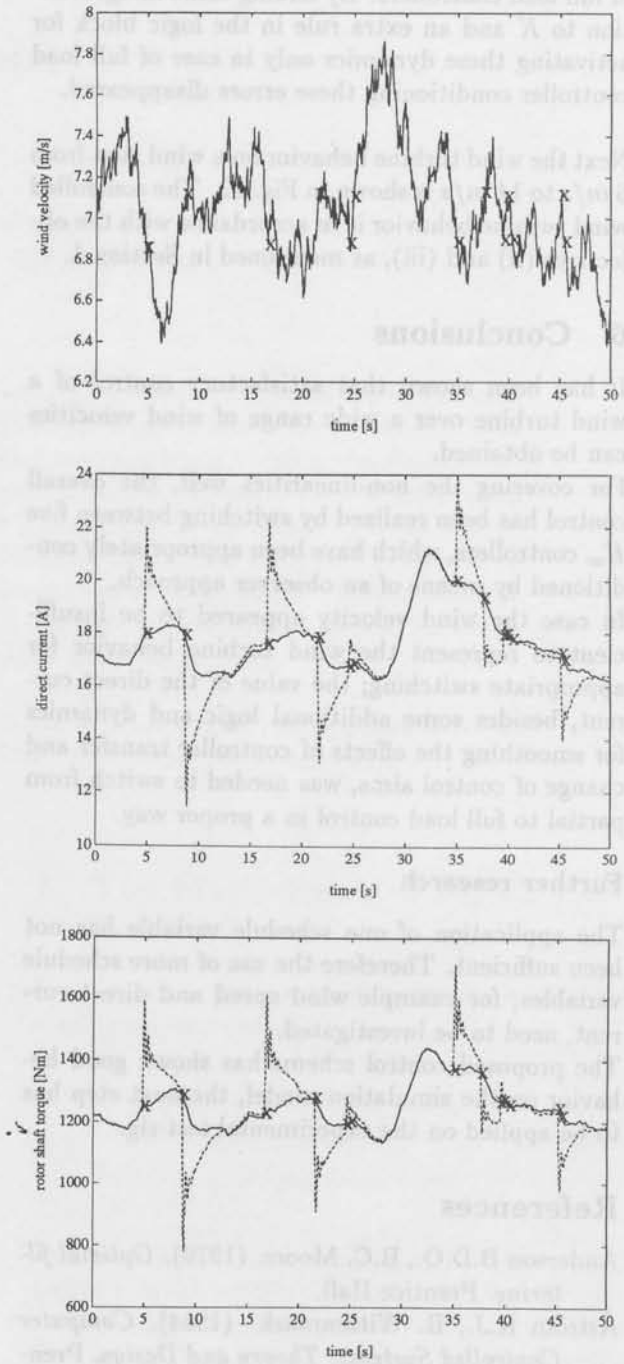

Fig. 11: Responses of direct current and moment on noisy wind while switching between conditioned controllers (——) and non-conditioned controllers (- - - -). Switching between controller is marked by X.

happened well. Although the off-line controller conditioning is robust, sometimes low frequency and even static errors happened in case of conditioning of full load controllers. By adding some integral action to K and an extra rule in the logic block for activating these dynamics only in case of full load controller conditioning these errors disappeared.

Next the wind turbine behavior on a wind gust from 6 m/s to 14 m/s is shown in Fig. 12. The controlled wind turbine behavior is in accordance with the objectives (ii) and (iii), as mentioned in Section 1.

6 Conclusions

It has been shown that satisfactory control of a wind turbine over a wide range of wind velocities can be obtained.
For covering the non-linearities well, the overall control has been realized by switching between five H_∞ controllers, which have been appropriately conditioned by means of an observer approach.
In case the wind velocity appeared to be insufficient to represent the wind turbine behavior for appropriate switching; the value of the direct current, besides some additional logic and dynamics for smoothing the effects of controller transfer and change of control aims, was needed to switch from partial to full load control in a proper way.

Further research

The application of one schedule variable has not been sufficient. Therefore the use of more schedule variables, for example wind speed and direct current, need to be investigated.
The proposed control scheme has shown good behavior on the simulation model, the next step has to be applied on the experimental test-rig.

References

Anderson B.D.O., B.C. Moore (1979). *Optimal filtering.* Prentice Hall.

Åström K.J., B. Wittenmark (1984). *Computer Controlled Systems, Theory and Design.* Prentice Hall.

Baars G.E. van, P.M.M. Bongers (1992). Wind turbine control design and implementation based on experimental models. *Proc. 31th IEEE Conf. on Decision and Control,*Tuscon, Arizona, USA,2454–2459.

Bongers P.M.M. (). *Factorizational Approach to Robust Control: Application to a Flexible Wind Turbine.* PhD Thesis, Delft University

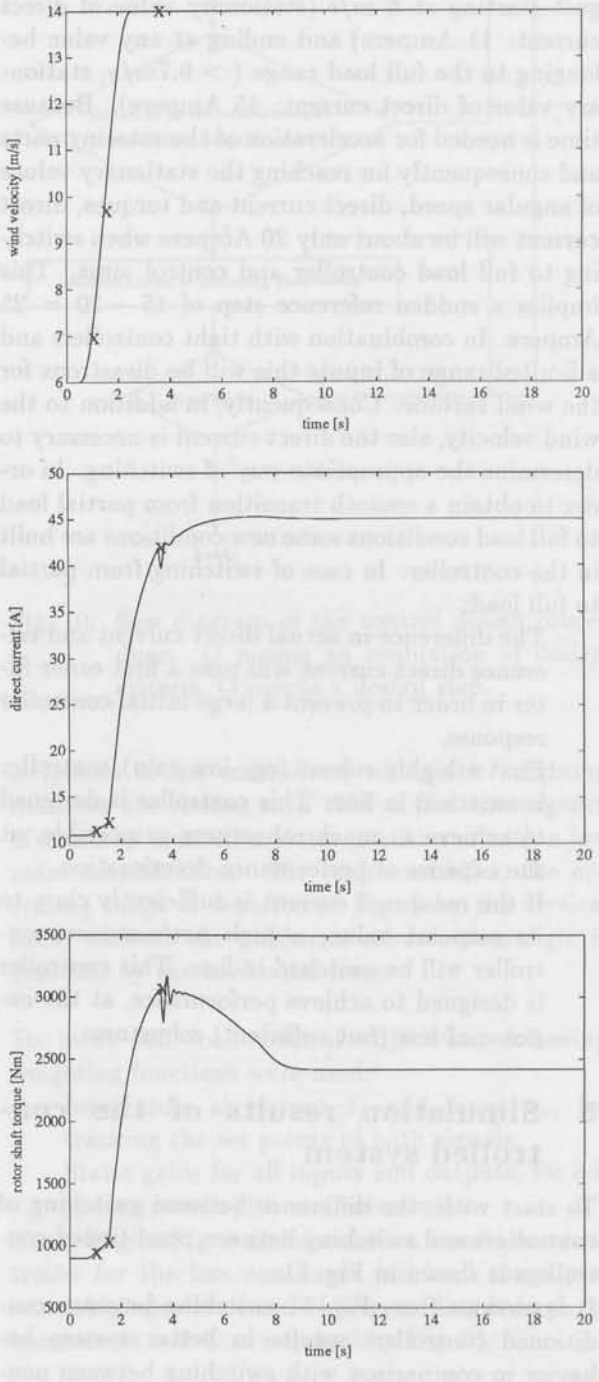

Fig. 12: responses of direct current and torque on wind gust; controller switching is marked by X.

of Technology, The Netherlands, In preparation.

Bongers P.M.M. (1993). *DUWECS V2.0 Reference Guide, Delft University Wind Energy Conversion Simulation Program.* Delft University of Technology, The Netherlands, DUT–MEMT 26, ISBN 90–370–0086–X.

Bongers P.M.M., O.H. Bosgra (1990). Low order H_∞ controller synthesis. *Proc. 29th Conf. Desicion and Control,*Hawaii, USA,194–199.

Bongers P.M.M., Sj. Dijkstra (1992). Control of wind turbine systems aimed at load reduction. *Proc. Amer. Contr. Conf.,*june 24–26, Chicago, Illinois, USA,1710–1714.

Campo P.J., M. Morari, C.N. Nett (1989). Multivariable anti–windup and bumbless transfer: a general theory. *Proc. Amer. Contr. Conf., 1989,*1706–1711.

Engelen, T.G. van, Bongers P.M.M., J.T.G. Pierik, G.E. van Baars (1993). Integral control for damping of mechanical resonance and protection against grid failures: results in a full load operating condition. *Proc. Europ. Community Wind Energy Conf.,*545–550.

Georgiou T.T. (1988). On the computation of the gap metric. *Syst. Control Lett.,* **11**, 253–257.

Georgiou T.T., M.M. Smith (1990). Optimal robustness in the gap metric. *IEEE Trans. Automat. Contr.,* **AC–35**, 673–686.

Hanus R., M. Kinnaert (1989). Control of constrained multivariable systems using the conditioning technique. *Proc. Amer. Contr. Conf., 1989,*1712–1718.

Hanus R., M. Kinnaert, J.–L. Henrotte (1987). Conditioning technique, a general anti–windup and bumbless transfer method. *Automatica,* **vol.23**, 729–739.

Hyde R.A., K. Glover (1990). VSTOL aircraft flight control system design using H_∞ controllers and switching strategy. *Proc. 29th IEEE Conf. Desicion and Control,*Honolulu, Hawaii, USA,2975–2980.

Kraan I. (1992). *Control design for a flexible wind turbine.* Delft University of Technology, TUD–WBMR–A–613.

McFarlane D.C., K. Glover (1989). *Robust Controller Design Using Normalized Coprime Factor Plant Descriptions.* Lecture Notes in Control and Information Sciences, vol.138, Springer Verlag, Berlin, Germany.

Steinbuch M. (1989). *Dynamic modelling and robust control of a wind energy conversion system.* PhD Thesis, Delft University of Technology, The Netherlands.

Selected Topics in Identification, Modelling and Control
Vol. 6, December 1993

Multiobjective H_2/H_∞ control

Carsten W. Scherer [‡]

Mechanical Engineering Systems and Control Group
Delft University of Technology, Mekelweg 2, 2628 CD Delft, The Netherlands.

Abstract. For a linear time invariant system with several disturbance input and controlled output channels defining several closed-loop transfer matrices, we show how to minimize the H_2-norm of one of these transfer matrices while keeping the H_2-norm or the H_∞-norm of the others below certain levels. This may be interpreted as minimizing the nominal performance of a system while keeping the H_2-norm or H_∞-norm performance bounded or the closed-loop system robustly stable. We show how sequences of finite dimensional convex optimization problems allow to compute the optimal value, to numerically detect the existence of a rational optimal controller, to determine its order, and to design nearly optimal rational controllers of the same order.

Keywords. Multiobjective H_2/H_∞ control, H_2 optimal control, H_∞ optimal control, minimal nominal performance, robust stabilization, constrained H_2 optimization.

Notation

$H_\infty^{p\times q}/H_2^{p\times q}$ denote the Banach/Hilbert spaces of $\mathbf{C}^{p\times q}$-valued maps F which are analytic in the open right half-plane H and satisfy $\|F\|_\infty := \sup_{s\in H}\|F(s)\| < \infty / \|F\|_2^2 := \sup_{t>0}\int_{-\infty}^{\infty} \mathrm{trace}(F(t+i\tau)^* F(t+i\tau))\, d\tau < \infty$. For any set S of functions defined on $\mathbf{C}$, RS denotes the real rational elements in S. For $Q \in RH_\infty^{p\times q}$ let the (infinite) nonincreasing sequence $\sigma_1(Q) \geq \sigma_2(Q) \geq \cdots$ denote the Hankel singular values (HSVs) of the strictly proper part of Q and recall $\sigma_j(Q) > 0$ if j is not larger than the McMillan degree of Q and $\sigma_j(Q) = 0$ for all other indices. Finally in any normed space $(X, \|.\|)$ we write $x_\nu \xrightarrow{\exp} x$ meaning that x_ν converges exponentially to x, if there exist constants $K > 0$ and $\rho > 1$ with $\|x - x_\nu\| \leq K\rho^{-\nu}$ for all indices ν.

[‡]This work is very much inspired by the helpful discussions with Prof. P.P. Khargonekar whom I would like to thank for his great hospitality during my half year visit of the University of Michigan (USA) in 1992. In addition, I would like to thank Dr. F. Allgöwer from the University of Stuttgart (Germany) for stimulating conversations about the motivations for H_2/H_∞ control.

1 The Multiobjective H_2/H_∞ Control Problem

Suppose that the underlying system admits the state-space description

$$\begin{aligned} \dot{x} &= Ax + Bu + Gd, \\ y &= Cx + Dd, \\ z &= Hx + Eu + Fd, \end{aligned}$$

with u as the control input, d as the disturbance input, y as the measured output, and z as the controlled output. A *stabilizing controller* $\mathcal{C}$ is any system $\dot{v} = Kv + Ly$, $u = Mv + Ny$ which yields $\sigma\begin{pmatrix} A+BNC & BM \\ LC & K \end{pmatrix} \subset \mathbf{C}^-$. If d and z are partitioned as $d^T = ((d^0)^T\ (d^1)^T\ \cdots\ (d^k)^T)$ and $z^T = ((z^0)^T\ (z^1)^T \cdots (z^k)^T)$, we denote by

$$\mathcal{T}_{ij}(\mathcal{C}) \in H_\infty^{q_i \times p_j}$$

the real rational transfer matrix from d^j to z^i which is defined by the closed-loop system.

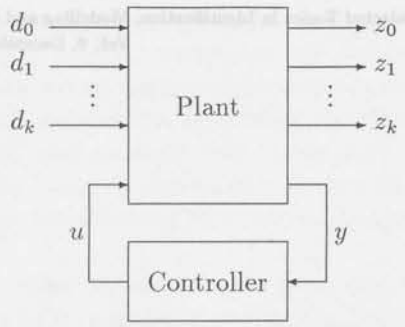

Given k positive real numbers $\gamma_1, \ldots, \gamma_k$ and some integer l with $1 \leq l \leq k$, the aim of this paper is to provide a solution technique for the optimization problem

$$\inf_{\|\mathcal{T}_{jj}(\mathcal{C})\|_2 \leq \gamma_j, j=1,\ldots,l,\ \|\mathcal{T}_{jj}(\mathcal{C})\|_\infty \leq \gamma_j, j=l+1,\ldots,k} \|\mathcal{T}_{00}(\mathcal{C})\|_2 \tag{1}$$

where the infimum is taken over all stabilizing controllers $\mathcal{C}$. Just for notational simplicity we restrict the attention to the case $k = 2$ and $l = 1$. As a first step we use the Youla parameterization to represent the set of all achievable closed-loop transfer matrices from d to z with the free $Q \in RH_\infty^{p \times q}$ as

$$\begin{pmatrix} R_1 & * & * \\ * & S_1 & * \\ * & * & T_1 \end{pmatrix} + \begin{pmatrix} R_2 \\ S_2 \\ T_2 \end{pmatrix} Q \begin{pmatrix} R_3 & S_3 & T_3 \end{pmatrix}$$

where R_j, S_j, T_j, $j = 1, 2, 3$, are easily determined real rational stable matrices. As a slight abuse of notation we call, from now on, the Youla parameter Q itself the controller. With this representation, (1) hence reads (for some $\beta, \gamma > 0$) as

$$\inf_{\|S_1 + S_2 Q S_3\|_2 \leq \beta,\ \|T_1 + T_2 Q T_3\|_\infty \leq \gamma} \|R_1 + R_2 Q R_3\|_2 \tag{2}$$

with the infimum taken over $Q \in RH_\infty^{p \times q}$.

The main control theoretic motivation for this problem has been extensively discussed recently (Bernstein and Haddad (1989), Rotea and Khargonekar (1991), Khargonekar and Rotea (1991)) and may be briefly summarized as follows: The H_2-norm of the transfer matrix $\mathcal{T}_{00}(\mathcal{C})$ is viewed as a measure for the (nominal) performance of the system. Instead of just optimizing the performance, the controller is also required to keep bounds on the H_2-norm of $\mathcal{T}_{11}(\mathcal{C})$ and on the H_∞-norm of $\mathcal{T}_{22}(\mathcal{C})$ satisfied. The channel $d^0 \to z^0$ constitutes the most important performance objective, whereas the normbounds for the channel $d^j \to z^j$ for $j = 1, 2$ may be viewed as performance constraints for less important channels expressed in the H_2 or in the H_∞ norm and resulting e.g. in desired disturbance quenching. Most importantly, however, the H_∞-norm constraints for $j = 2$ can be interpreted as keeping the system robustly stable: $\|\mathcal{T}_{22}(\mathcal{C})\|_\infty \leq \gamma$ implies that the closed-loop system remains internally stable under the action of any uncertainty $d^2 = \Delta z^2$ where Δ is an arbitrary perturbation (of suitable dimension) in the closed H_∞-ball of radius strictly larger than $\frac{1}{\gamma}$ (or even a certain finite-gain stable nonlinearity). Hence (1) describes problems in which the nominal H_2-performance is optimized while keeping other performance objectives in the H_2-norm or H_∞-norm bounded and while keeping up robust stability against a broad class of model uncertainties. In this setup we clearly assume that any required or desired frequency dependent weights are incorporated into the system description. Most importantly, our approach does not restrict the choice or even the number of the input/output channels in the system description and thus one can use *different weightings* for performance and robustness requirements in different channels. Note that (1) is formulated solely in terms of the diagonal blocks $\mathcal{T}_{jj}(\mathcal{C})$ whereas the antidiagonal blocks $\mathcal{T}_{ij}(\mathcal{C})$, $i \neq j$, are neglected (which is no restriction since bounds on such antidiagonal blocks can obviously be included by adding additional channels). This problem formulation hence reflects *structural* requirements in the design procedure as impossible in standard H_2 or H_∞ theory.

Let us briefly summarize important developments in multiobjective or mixed H_2/H_∞ control problems. In the seminal paper by Bernstein and Haddad (1989), where this problem is actually introduced, the authors replace the infimization of the H_2-norm by optimizing an upper bound of it - a problem which has been called *mixed* H_2/H_∞ control (Rotea and Khargonekar (1991a,b), Khargonekar and Rotea (1991)). The definition of the upper bound requires that the two disturbance input channels are identical. Under these modifications and restrictions, the paper by Bernstein and Haddad (1989) contains the derivation of *necessary* conditions for the existence of *optimal* controllers of an (a priori) fixed size. Although the solvability of the resulting system of highly coupled algebraic Riccati equations has shown to be sufficient for the existence of an optimal controller (Yeh et. al. (1990)), to date no reliable numerical method can handle this validation problem (Richter (1987)). Without a priori restrictions on the controller size, a major theoretical progress by Khargonekar and Rotea (1991) reveals that suboptimal controllers (arbitrarily close to the optimum) can be chosen of the same order as the plant. Indeed this is the basis for reformulating the inherently

infinite dimensional suboptimality problem to a *finite dimensional convex* validation problem, which is amenable to reliable numerical algorithms. A dual (Yeh. et. al. (1990)) situation with identical controlled output variables but possibly different disturbance inputs is discussed by Doyle et. al. (1990) and Zhou et. al. (1990). Most interestingly, this series of papers also provides system theoretic signal based motivations for mixed H_2/H_∞-design. We note that for the genuine multiobjective H_2/H_∞-problem (not to speak of (1) with multiple constraints), no helpful theoretical insights are available: There are no a priori bounds on the controller order (although simple cases might lead to the conjecture that the double plant order is a good candidate) neither does there exist any analytical solution. An interesting paper by Rotea and Khargonekar (1991b) provides sufficient conditions for the existence of a solution in the state-feedback case, again by considering an auxiliary problem which is analytically solvable - as a side-result it is shown that, although the whole state is available for control, the use of *dynamic* state-feedback cannot generally be avoided. The numerical case studies by Ridgely et. al. (1992) indicate as well the need of using dynamic controllers whose orders are larger than that of the plant. For alternative formulations of mixed H_2/H_∞ control problems we refer to Steinbuch and Bosgra (1991a,b).

Our approach is based on an approximation of a subset of all controllers by finite dimensional subspaces what has been generally proposed by Boyd and Barrat (1991). Finally, Sznaier and Sideris (1991) used approximations by truncated Laurent series to compute the optimal value of a certain multiobjective control problem (for a single input single output system in discrete time) by solving a sequence of finite dimensional convex optimization problems - this work very much inspired the present paper.

Roughly outlined, the purpose of this paper is threefold. First we slightly generalize in Section 2 scalar n-width results for unit disk function spaces as discussed by Pinkus (1985) to matrix-valued results for the open left half-plane and describe their main implication for the real rational setting as required here: The possibility to approximate (compact) sets by finite dimensional subspaces where the error bound decreases *exponentially* with the dimension of the subspaces considered. In Section 3 we briefly discuss how this allows to numerically check whether the constraint set of (1) is nonempty. In Section 4 we investigate how to compute the optimal value for (1) by a sequence of finite dimensional convex optimization problems (FCOPs). For the remaining considerations we assume the existence of a rational optimal controller and slightly restrict the system description to guarantee its uniqueness. We then describe a modification which forces the minimizers of each resulting FCOP to converge in the H_∞-norm to the optimal controller. This allows to determine the *order*, say n_*, of the optimal controller and a certain *compact* set in which it is guaranteed to be contained in. In a final step we introduce a further sequence of FOCPs in which, as an essential and to our knowledge new ingredient, the *trace norm of the Youla parameter* is minimized. Given the corresponding sequence of optima, the n_*-th order Hankel norm approximations of these optimal controllers (which are all computable) then indeed converge in the H_∞-norm to the optimal controller. Hence this technique allows to numerically design nearly optimal controllers (arbitrarily close to optimality) whose orders equal n_*. Finally, we point out how this procedure leads to numerically verifiable necessary and sufficient conditions for the existence of a rational optimal controller.

In summary, we present an algorithm to compute the optimal value, to detect the existence of a rational optimal controller, to compute its order n_*, and to design arbitrarily close to optimal controllers of the same order n_*. This could constitute the starting point for numerical studies which may indicate bounds on the order of optimal controllers and, as our final hope, may further stimulate theoretical work related to this nice and interesting problem.

2 Results from Approximation Theory

This section is devoted to transforming scalar n-width results on disks to matrix versions on half planes.

Let D be any open set in $\mathbf{C}$ and denote by $H_\infty^{p\times q}(D)$ those $p \times q$-matrix valued functions which are analytic and bounded in D. $H_\infty^{p\times q}(D)$ equipped with the standard norm $\|F\|_D = \sup_{z\in D}\|F(z)\|$ is a Banach space. As usual we denote the ball with radius R around 0 as $B_R H_\infty^{p\times q}(D) := \{F \in H_\infty^{p\times q}(D) \mid \|F\|_D \le R\}$.

For any $f = (f_1 \ \cdots \ f_\nu) \in H_\infty^\nu(D)$ let us define the complex subspace

$$\mathcal{S}(f) := \{\sum_{j=1}^{\nu} A_j f_j \mid A_j \in \mathbf{C}^{p\times q}\} \qquad (3)$$

of $H_\infty^{p\times q}(D)$ of dimension not greater than νpq. For

any open set $E \subset \mathbf{C}$ containing D we are interested in the error if trying to uniformly approximate $B_R H_\infty^{p\times q}(E)$ by subspaces of the form $\mathcal{S}(f)$ in the $H_\infty^{p\times q}(D)$-norm. Indeed, a given $F \in B_R H_\infty^{p\times q}(E)$ can be approximated by some element in $\mathcal{S}(f)$ up to the error $\inf_{X\in\mathcal{S}(f)} \|X - F\|_D$. The worst possible error for $F \in B_R H_\infty^{p\times q}(E)$, usually called the *deviation*, is hence given as

$$\sup_{F\in B_R H_\infty^{p\times q}(E)} \inf_{X\in\mathcal{S}(f)} \|X - F\|_D. \tag{4}$$

For specific choices of D and E, our aim is to find a sequence $f_1, f_2, f_3, \ldots$ such that (4) converges to zero for $\nu \to \infty$. Since we are looking for an efficient way of achieving this convergence and we even require exponential decay, it is of considerable interest to determine the *least achievable* deviation defined by

$$\inf_{f\in H_\infty^\nu(D)} \sup_{F\in B_R H_\infty^{p\times q}(E)} \inf_{X\in\mathcal{S}(f)} \|X - F\|_D.$$

In analogy to the scalar situation we call this quantity the ν-width of $B_R H_\infty^{p\times q}(E)$ in $H_\infty^{p\times q}(D)$.

Remark. Note that this is a slight abuse of notation since we only consider particular subspaces of the form (3) and not arbitrary subspaces of dimension νpq with different basis functions for each entry. The present version, however, considerably simplifies the derivation of very explicit results which suffice for our purposes.

It is most surprising and very satisfactory that the ν-width can be explicitly computed if specializing D to the unit disk and E to rD ($r \geq 1$), the disk with radius r around 0: The ν-width is then given by $\frac{R}{r^\nu}$. It is even possible to show that the functions $f_j^*(z) := z^{j-1}$ for $j = 1, \ldots, \nu$ are *optimal*: The deviation for this choice is best possible and equals $\frac{R}{r^\nu}$. For $r > 1$, we infer that $B_R H_\infty^{p\times q}(rD)$ is *compact* as a subset of $H_\infty^{p\times q}(D)$. The scalar version of this result ($p = q = 1$) for $R = 1$ is proved by Pinkus (1985) (Theorem 2.1 in Chapter VIII) and it is not difficult to extend the proof to the matrix valued setting for $R \neq 1$ as discussed here.

Using the linear fractional transformation

$$\phi(s) = \frac{s-\alpha}{s+\alpha} \text{ with inverse } \psi(z) = \alpha\frac{1+z}{1-z}$$

for some fixed $\alpha > 0$, we can easily translate these results from the open unit disk D to the half-plane $H := \{s \mid \mathrm{Re}(s) > 0\} = \phi(D)$. It is natural to choose E as $H_r := \psi(rD)$ which is the complement of the closed disk in the open left half-plane around $\alpha\frac{1+2r^2}{1-r^2}$ with radius $\alpha\frac{2r}{r^2-1}$. Then we arrive at the following result.

Theorem 1 *For $r \geq 1$ and $R > 0$, the ν-width of $B_R H_\infty^{p\times q}(H_r)$ in $H_\infty^{p\times q}$ is given as*

$$\inf_{f\in H_\infty^\nu} \sup_{F\in B_R H_\infty^{p\times q}(H_r)} \inf_{X\in\mathcal{S}(f)} \|X - F\|_\infty = \frac{R}{r^\nu}.$$

Moreover, $f^*(s) := \left(\left(\frac{s-\alpha}{s+\alpha}\right)^{j-1}\right)_{j=1,\ldots,\nu}$ is optimal in the sense of

$$\sup_{F\in B_R H_\infty^{p\times q}(H_r)} \inf_{X\in\mathcal{S}(f^*)} \|X - F\|_\infty = \frac{R}{r^\nu}.$$

Finally, if $r > 1$ then $B_R H_\infty^{p\times q}(H_r)$ is a compact subset of $H_\infty^{p\times q}$.

For our purposes the most relevant consequence for an arbitrary F in $B_R H_\infty^{p\times q}(H_r)$ may be formulated as

$$\inf_{X\in\mathcal{S}(f^*)} \|X - F\|_\infty \leq \frac{R}{r^\nu}. \tag{5}$$

In our applications, however, F is even real rational. It is not difficult to see that we can hence restrict the attention to *real* linear combinations of $f_1^*, \ldots, f_\nu^*$ and, nevertheless, obtain the same upper bound on the approximation error. With the *real* subspaces

$$\mathcal{S}_\nu := \{\sum_{j=0}^{\nu-1} A_j \phi^j \mid A_j \in \mathbf{R}^{p\times q}\}$$

for $\nu = 1, 2, \ldots$ we obtain the following easily proved corollary.

Corollary 2 *For arbitrary real rational Q in $B_R H_\infty^{p\times q}(H_r)$ one gets*

$$\min_{X\in\mathcal{S}_\nu} \|X - Q\|_\infty \leq \frac{R}{r^\nu}. \tag{6}$$

Apart from this approximation property of $\mathcal{S}_\nu$, the discussion in this section should indicate a certain efficiency if using these subspaces for reducing the original multiobjective H_2/H_∞ problem to a finite dimensional one.

As a final observation we point out that each real rational stable Q is contained in $B_R H_\infty^{p\times q}(H_r)$ if r is sufficiently close to 1 and R is chosen large enough.

3 Testing the Constraints

Let us define for any $Q \in H_\infty^{p\times q}$ the functions $\alpha(Q) := \|R_1 + R_2 Q R_3\|_2$, $\beta(Q) := \|S_1 + S_2 Q S_3\|_2$, and $\gamma(Q) := \|T_1 + T_2 Q T_3\|_\infty$. Since $\alpha(.)$ and $\beta(.)$ should be finite we assume throughout that $R_1(\infty) = 0$, $S_1(\infty) = 0$ as well as $R_2(\infty) = 0$ or $R_3(\infty) = 0$, $S_2(\infty) = 0$ or $S_3(\infty) = 0$. It is easy to see that all maps satisfy a Lipschitz condition with constants that are easily computed from the underlying data matrices.

Lemma 3
For $Q_1, Q_2 \in H_\infty^{p\times q}$ one has $|f(Q_1) - f(Q_2)| \leq L_f \|Q_1 - Q_2\|_\infty$ for $f = \alpha, \beta, \gamma$ with the Lipschitz constants $L_\alpha := \min\{\|R_2\|_2\|R_3\|_\infty, \|R_2\|_\infty\|R_3\|_2\}$, $L_\beta := \min\{\|S_2\|_2\|S_3\|_\infty, \|S_2\|_\infty\|S_3\|_2\}$, $L_\gamma := \|T_2\|_\infty\|T_3\|_\infty$.

This Lemma together with Corollary 2 lead to the following conclusion: For any $Q \in RB_R H_\infty^{p\times q}(H_r)$ there exists a $P \in \mathcal{S}_\nu$ with

$$f(P) \leq f(Q) + L_f \frac{R}{r^\nu}, \quad f = \alpha, \beta, \gamma. \tag{7}$$

For given $\beta > 0$ and $\gamma > 0$ our aim is to decide numerically whether there exists a real rational $Q \in H_\infty^{p\times q}$ with

$$\beta(Q) < \beta \text{ and } \gamma(Q) < \gamma. \tag{8}$$

Although the constraints in (2) are nonstrict, our approach requires the strict inequalities being fulfilled for some controller - the constraint set should have interior points.
If defining

$$\gamma_* := \inf_{Q\in RH_\infty^{p\times q}} \gamma(Q),$$

γ clearly has to satisfy $\gamma > \gamma_*$. Since this is just the by now standard suboptimality validation problem in H_∞ theory, there exist (good) techniques to check the inequality and to even design a real rational P_0 with $\gamma(P_0) < \gamma$. As pointed out at the end of Section 2, one can find $R_0 > 0$, $r_0 > 1$ with $P_0 \in B_{R_0} H_\infty^{p\times q}(H_{r_0})$. Let us fix P_0, R_0 and r_0. We conclude that, for large ν, there exists a $Q \in \mathcal{S}_\nu$ with $\gamma(Q) < \gamma$ - indeed this is guaranteed for

$$\nu \geq \frac{\ln(L_\gamma R_0) - \ln(\gamma - \gamma(P_0))}{\ln(r_0)}. \tag{9}$$

To determine the restrictions on β if Q satisfies $\gamma(Q) < \gamma$, one has to solve the optimization problem

$$\beta_*(\gamma) := \inf_{\{Q\in RH_\infty^{p\times q}:\ \gamma(Q)<\gamma\}} \beta(Q).$$

We reduce this problem to a sequence of FCOPs by replacing the constraint set with $\{Q \in \mathcal{S}_\nu : \gamma(Q) < \gamma\}$, a subset of the finite dimensional subspace $\mathcal{S}_\nu$. This leads to

$$\beta_\nu(\gamma) := \inf_{\{Q\in\mathcal{S}_\nu:\ \gamma(Q)<\gamma\}} \beta(Q). \tag{10}$$

For all large ν (with a guarantee if ν satisfies (9)) the optimal value of (10) is finite. Moreover, the obvious properties $\beta_\nu \geq \beta_{\nu+1} \geq \beta_*$ imply the convergence of β_ν to some (finite) value $\beta_\infty \geq \beta_*$. It is not difficult to show that β_∞ coincides with β_*.

Theorem 4 $\beta_\nu \geq \beta_{\nu+1} \overset{\nu\to\infty}{\longrightarrow} \beta_*$.

Therefore one can compute a γ_* and, by solving a sequence of FCOPs, a bounding function $\beta_*(.)$ with the following property: There exists a $Q \in RH_\infty^{p\times q}$ with (8) if and only if

$$\gamma < \gamma_* \text{ and } \beta_*(\gamma) < \beta.$$

For certain fixed γ and β with these properties it is then possible to construct a $P_1 \in \mathcal{S}_\nu$ (for some large ν) with $\beta(P_1) < \beta$ and $\gamma(P_1) < \gamma$ and one easily determines $r_1 > 1$, $R_1 > 0$ with $P_1 \in B_{R_1} H_\infty^{p\times q}(H_{r_1})$.

4 Detection and Approximation of Optimal Controllers

In this section we first describe how to compute the optimal value for the multiobjective H_2/H_∞-problem considered. We proceed by showing how to numerically *detect* the existence of a rational (small order) optimal controller and how to *design* approximations which define nearly optimal controllers of the same order as the optimal one. The proposal is based on the following idea: Suppose there exists an optimal controller which is, under certain standard properties of the plant, unique. We design a sequence of convex optimization problems whose minimizers converge to the optimal controller in the H_∞-norm. If the optimal controller has order n_*, a well-known estimation for Hankel singular values (HSVs) implies that all the HSVs of these minimizers with index greater than n_* converge to zero. This allows to detect the order of the optimal controller. To construct an n_*-th order approximation of the optimal controller one is lead to find the best Hankel norm approximant of each minimizer where the H_∞-error is known to be bounded by the sum of all HSVs with index greater than n_*. The aim is to achieve the convergence of this sum to zero such that the constructed sequence of n_*-th order controllers indeed converges to the optimal controller. The trick to enforce the convergence of the model reduction error to zero is the main new observation in this paper: One has to minimize the trace norm (the sum of all HSVs) of the controllers over a suitably defined set of constraints.
Let us use again the functions $\alpha(.)$, $\beta(.)$, $\gamma(.)$ from Section 3. We assume that, for given $\gamma > 0$ and $\beta > 0$, we have found r_1, R_1 and a real rational $P_1 \in B_{R_1} H_\infty^{p\times q}(H_{r_1})$ with $\beta(P_1) < \beta$ and $\gamma(P_1) < \gamma$. The nonempty constraint set

$$\mathcal{Q} := \{Q \in H_\infty^{p\times q} \mid \beta(Q) \leq \beta,\ \gamma(Q) \leq \gamma\} \tag{11}$$

hence *has interior points* and is a *closed subset* of $H_\infty^{p\times q}$. We now return to the multiobjective H_2/H_∞-problem

$$\alpha_* := \inf_{Q\in\mathcal{Q}} \alpha(Q). \tag{12}$$

As earlier this is reduced to a sequence of FCOPs by replacing $\mathcal{Q}$ with $\mathcal{S}_\nu \cap \mathcal{Q}$ such that we arrive at

$$\alpha_\nu := \inf_{Q\in\mathcal{S}_\nu\cap\mathcal{Q}} \alpha(Q). \tag{13}$$

As for Theorem 4 one easily proves that α_ν indeed converges to α_* - this constitutes a procedure to compute the optimal value of (12).

Theorem 5 $\alpha_\nu \geq \alpha_{\nu+1} \overset{\nu\to\infty}{\longrightarrow} \alpha_*$.

Remark. Just for numerical reasons we show that we can replace (13) by

$$\inf_{\{Q\in\mathcal{S}_\nu:\ \beta(Q)<\beta,\ \gamma(Q)<\gamma\}} \alpha(Q) \tag{14}$$

whose optimal values coincides with α_ν. Note that the strict constraint inequalities are numerically easier to handle.
For ease of reference we recall for a slightly more general situation that one can replace a convex constraint set by its interior without changing the optimal value.

Lemma 6 *Let $\mathcal{M}$ be a convex subset of the finite dimensional subspace $\mathcal{F}$ of $H_\infty^{p\times q}$, and let the interior int($\mathcal{M}$) relative to $\mathcal{F}$ be nonempty. Then*

$$\inf_{Q\in\mathcal{M}} \alpha(Q) = \inf_{Q\in\mathrm{int}(\mathcal{M})} \alpha(Q).$$

Let us now assume that there exists a rational optimal controller for (12), i.e., a $Q_* \in RH_\infty^{p\times q}$ with

$$\alpha(Q_*) = \alpha_*,\ \beta(Q_*) \leq \beta,\ \gamma(Q_*) \leq \gamma.$$

Define $r_* > 1$, $R_* > 0$, n_*, s_* with

$$\|Q_*\|_{H_{r_*}} < R_*,\ n_* = \text{ order of } Q_*,\ s_* = \sum_{j=1}^{n_*} \sigma_j(Q_*). \tag{15}$$

Without the knowledge of Q_* we will discuss in the sequel how to determine n_* and some r_*, R_* numerically. Let us first guarantee the uniqueness of Q_* by assuming that

R_2/R_3 have full normal column/row rank.

We summarize the general consequences of these assumptions in the following lemma.

Lemma 7 *If $\mathcal{M}$ is a nonempty* convex *subset of $H_\infty^{p\times q}$, there is* at most one optimal controller *for the problem*

$$\inf_{Q\in\mathcal{M}} \alpha(Q). \tag{16}$$

If $\mathcal{M}$ is, in addition, either compact in $H_\infty^{p\times q}$ or a closed subset of a finite dimensional subspace $\mathcal{F}$ of $H_\infty^{p\times q}$, the infimum is attained and there exists a unique *optimal controller $\tilde{Q}$. In the latter case if the interior int($\mathcal{M}$) relative to $\mathcal{F}$ is nonempty and if Q_ν is an infimal sequence of*

$$\inf_{Q\in\mathrm{int}(\mathcal{M})} \alpha(Q) \tag{17}$$

then $\|Q_\nu - \tilde{Q}\|_\infty \overset{\nu\to\infty}{\longrightarrow} 0$.

We infer that, for each ν with $\alpha_\nu < \infty$, there *exists a unique* Q_ν attaining the optimum in (13). However, the optimality of Q_ν for (13) does not assure that Q_ν converges in the H_∞-norm, not to speak of convergence to Q_*.
We intend to redefine (13) in order to guarantee that the resulting optima actually converge to Q_*. The trick is to restrict the attention to the compact subsets

$$\mathcal{B}(r,R) := B_R H_\infty^{p\times q}(H_r)$$

of $H_\infty^{p\times q}$ for $R > 0$ and $r > 1$. Lemma 7 reveals that

$$\alpha_*(r,R) := \inf_{Q\in\mathcal{Q}\cap\mathcal{B}(r,R)} \alpha(Q) \geq \alpha_* \tag{18}$$

is attained by a unique

$$Q_*(r,R) \in \mathcal{B}(r,R).$$

The reduction to a sequence of FCOPs leads to

$$\alpha_\nu(R,r) := \inf_{Q\in\mathcal{S}_\nu\cap\mathcal{Q}\cap\mathcal{B}(r,R)} \alpha(Q) \geq \alpha_*(r,R) \tag{19}$$

with a unique optimal

$$Q_\nu(r,R) \in \mathcal{B}(r,R).$$

In the sequel we restrict the choice of (r,R) to

$$r_1 \geq r > 1 \text{ and } R > R_1. \tag{20}$$

Then $\|P_1\|_{H_r} < R$ where we increased R to have a strict inequality. Hence P_1 is admissible for (18) which implies $\alpha_*(r,R) < \infty$. Moreover, one can compute a bound $\nu_0(r,R)$ such that we have $\mathcal{S}_\nu \cap \mathcal{Q} \cap \mathcal{B}(r,R) \neq \emptyset$ and thus $\alpha_\nu(r,R) < \infty$ for $\nu \geq \nu_0(r,R)$.
Now we can not only show that, as earlier, $\alpha_\nu(r,R)$ converges to $\alpha_*(r,R)$ but, as desired, $Q_\nu(r,R)$ indeed converges to $Q_*(r,R)$ in the H_∞-norm. There

is an additional and essential benefit of considering this modified problem. We know that the optimal Q_* is contained in $\mathcal{B}(r_*, R_*)$ for some $r_* > 1$ and $R_* > 0$ but there is presently no way to determine r_* or R_* theoretically. For later purposes, however, we require to know one such pair (r_*, R_*). Indeed, (18) or (19) actually allow to decide numerically whether or not Q_* is contained in $\mathcal{B}(r, R)$ for the particular pair (r, R): Just look whether $\alpha_*(r, R) \geq \alpha_*$ *equals* α_* or not.

Theorem 8 *For $r > 1$ and $R > 0$, $\alpha_\nu(r, R) \overset{\nu\to\infty}{\longrightarrow} \alpha_*(r, R)$ and $\|Q_\nu(r, R) - Q_*(r, R)\|_\infty \overset{\nu\to\infty}{\longrightarrow} 0$. If the optimal Q_* is contained in $\mathcal{B}(r, R)$ then $\alpha_*(r, R) = \alpha_*$ and $Q_*(r, R) = Q_*$. If Q_* is* not contained *in $\mathcal{B}(r, R)$ then $\alpha_*(r, R) > \alpha_*$.*

Without knowing Q_*, this second procedure hence allows to find (e.g. by bisection) and fix $r_* > 1$ and $R_* > 0$ as in (15).

Corollary 9 *For (r_*, R_*) one has $\alpha_\nu(r_*, R_*) \overset{\nu\to\infty}{\longrightarrow} \alpha_*$ and $\|Q_\nu(r_*, R_*) - Q_*\|_\infty \overset{\nu\to\infty}{\longrightarrow} 0$.*

Remark. Again, for numerical reasons it is advantageous to replace (19) with

$$\inf_{\{Q\in\mathcal{S}_\nu:\ \beta(Q)<\beta,\ \gamma(Q)<\gamma,\ \|Q\|_{H_r}<R\}} \alpha(Q) \qquad (21)$$

whose optimal value equals $\alpha_\nu(r, R)$ (Lemma 6) and thus still allows to determine (r_*, R_*). Moreover, if $Q_\nu \in \mathcal{S}_\nu$ is ε_ν-suboptimal for this problem (i.e. it satisfies $\beta(Q_\nu) < \beta$, $\gamma(Q_\nu) < \gamma$, $\|Q_\nu\|_{H_r} < R$ and $\alpha(Q_\nu) < \alpha_\nu(r, R) + \varepsilon_\nu$) then the choice $\varepsilon_\nu \overset{\nu\to\infty}{\longrightarrow} 0$ still implies $\|Q_\nu - Q_*(r, R)\|_\infty \overset{\nu\to\infty}{\longrightarrow} 0$.

For the multiobjective problem (12) no theoretical bounds on the order of the optimal controller Q_* are known yet. Since the order of $Q_\nu(r_*, R_*)$ grows polynomially in ν to infinity, it is strongly desirable to find criteria which allow to determine the order of Q_* out of the computable sequence $Q_\nu(r_*, R_*)$. Indeed, Corollary 9 leads to a numerically verifiable *necessary* condition for the existence of Q_* of order n_*: The $(n_* + 1)$-st Hankel singular value of $Q_\nu(r_*, R_*)$ converges to 0. This is obvious by the following well-known estimate for Hankel singular values in terms of the H_∞-norm.

Lemma 10 *For strictly proper real rational $P, Q \in H_\infty^{p\times q}$ and all $j = 1, 2, \ldots$ one has $|\sigma_j(Q) - \sigma_j(P)| \leq \|Q - P\|_\infty$.*

Theorem 11 *Let n_* be the order of the optimal controller Q_* and let Q_ν be any sequence with $\|Q_\nu - Q_*\|_\infty \overset{\nu\to\infty}{\longrightarrow} 0$. Then n_* is the smallest nonnegative integer k with $\sigma_{k+1}(Q_\nu) \overset{\nu\to\infty}{\longrightarrow} 0$. Moreover $\sigma_j(Q_\nu) \overset{\nu\to\infty}{\longrightarrow} \sigma_j(Q_*)$ for $j = 1, \ldots, n_*$ and thus $\sum_{j=1}^{n_*} \sigma_j(Q_\nu) \overset{\nu\to\infty}{\longrightarrow} s_*$. If $Q_\nu \in \mathcal{S}_\nu$ satisfies $\|Q_\nu - Q_*\|_\infty \overset{\exp}{\longrightarrow} 0$ then $\sum_{j=n_*+1}^{\infty} \sigma_j(Q_\nu) \overset{\nu\to\infty}{\longrightarrow} 0$ and thus $\sum_{j=1}^{\infty} \sigma_j(Q_\nu) \overset{\nu\to\infty}{\longrightarrow} s_*$.*

If applied to the particular sequence $Q_\nu(r_*, R_*)$, this result allows to numerically determine the order n_* of the optimal controller Q_*.

Although $Q_\nu(r_*, R_*)$ converges to Q_* and the order of Q_* is known, this seems not sufficient to determine a sequence of n_*-th order controllers which approach Q_* and could thus be used as small order nearly optimal solutions of (12). Indeed, it is natural to design such a sequence by performing a n_*-th order model reduction on each $Q_\nu(r_*, R_*)$. By using Hankel norm approximation and adjusting the direct feedthrough matrix, one can design in this way an approximant P_ν of $Q_\nu(r_*, R_*)$ up to an H_∞-norm error which is bounded by the (finite) sum of the remaining HSVs (Glover (1984)), i.e.,

$$\|Q_\nu(r_*, R_*) - P_\nu\|_\infty \leq \sum_{j=n_*+1}^{\infty} \sigma_j(Q_\nu(r_*, R_*)).$$

With the abbreviation $\delta_\nu := \|Q_* - Q_\nu(r_*, R_*)\|_\infty$ we infer from $\|Q_* - P_\nu\|_\infty \leq \delta_\nu + \|Q_\nu(r_*, R_*) - P_\nu\|_\infty$ that

$$\|Q_* - P_\nu\|_\infty \leq \delta_\nu + \sum_{j=n_*+1}^{\infty} \sigma_j(Q_\nu(r_*, R_*)). \qquad (22)$$

Hence if $\sum_{j=n_*+1}^{\infty} \sigma_j(Q_\nu(r_*, R_*)) \overset{\nu\to\infty}{\longrightarrow} 0$ then P_ν indeed constitutes a sequence of n_*-th order controllers which approach Q_*. In general, however, the convergence of the individual Hankel singular values does not imply the convergence of their sum since the order of $Q_\nu(r_*, R_*)$ and hence the number of nonzero summands (potentially) increase with ν. However, if $Q_\nu(r_*, R_*)$ converged exponentially to Q_*, Lemma 11 would yield the exponential convergence of this error bound to zero. Although it seems not possible to prove the *fast* convergence of $Q_\nu(r_*, R_*)$, this idea points into the right direction. Indeed, (2) and (15) reveal that there exists a (from now on fixed) sequence $Q_\nu \in \mathcal{S}_\nu$ with

$$\|Q_\nu\|_{H_{r_*}} < R_* \quad \text{and} \quad \|Q_\nu - Q_*\|_\infty < \frac{R_*}{r_*^\nu}. \qquad (23)$$

Since Q_ν converges *exponentially* to Q_*, we infer (Lemma 11)

$$\sum_{j=1}^{\infty} \sigma_j(Q_\nu) \overset{\nu\to\infty}{\longrightarrow} s_*. \qquad (24)$$

Our aim is to define a new sequence of FCOPs whose optimizers $\hat{Q}_\nu$ have the following two essential properties:

$$\|\hat{Q}_\nu - Q_*\|_\infty \overset{\nu}{\longrightarrow} 0, \tag{25}$$

$$\sum_{j=n_*+1}^{\infty} \sigma(\hat{Q}_\nu) \overset{\nu\to\infty}{\longrightarrow} 0. \tag{26}$$

We try to achieve (26) by relating $\hat{Q}_\nu$ to Q_ν and hence we require Q_ν being admissible for the problem to be defined. Since $\beta(Q_\nu)$ and $\gamma(Q_\nu)$ converge to but may be larger than β and γ, there is no guarantee that Q_ν is contained in $\mathcal{Q}$. If we relax $f(Q) \le f$ to $f(Q) < f + f_\nu$ with

$$f_\nu := L_f \frac{R_*}{r_*^\nu} \quad \text{for} \quad f = \alpha, \beta, \gamma, \tag{27}$$

we infer from (23) and Lemma 3 that Q_ν indeed satisfies $f(Q_\nu) < f + f_\nu$. This motivates to introduce the open convex constraint set $\hat{\mathcal{Q}}_\nu$ as all those $Q \in H_\infty^{p\times q}$ which satisfy

$$\alpha(Q) < \alpha_* + \alpha_\nu,\ \beta(Q) < \beta + \beta_\nu\ \gamma(Q) < \gamma + \gamma_\nu$$

and

$$\|Q\|_{H_{r_*}} < R_*.$$

Then $Q_\nu \in \hat{\mathcal{Q}}_\nu$ is *one* sequence in $\mathcal{S}_\nu$ converging to Q_*. Literally as for Theorem 8 one shows that *any* other sequence satisfying the constraints has this property as well.

Lemma 12 *If $\hat{Q}_\nu \in \mathcal{S}_\nu \cap \hat{\mathcal{Q}}_\nu$ for all ν, then $\|\hat{Q}_\nu - Q_*\|_\infty \overset{\nu\to\infty}{\longrightarrow} 0$.*

Hence for any such sequence $\hat{Q}_\nu$ we get from Lemma 11 that

$$\sum_{j=1}^{n_*} \sigma_j(\hat{Q}_\nu) \overset{\nu\to\infty}{\longrightarrow} s_*. \tag{28}$$

Finally, the cost functional of the optimization problem to be defined should allow to relate $\sum_{j=n_*+1}^{\infty} \sigma_j(\hat{Q}_\nu)$ to $\sum_{j=n_*+1}^{\infty} \sigma_j(Q_\nu)$ in order to enforce (26). Optimizing this sum, however, is not feasible since it is not convex in Q. Instead, the relation

$$\sum_{j=1}^{\infty} \sigma(\hat{Q}_\nu) \le \sum_{j=1}^{\infty} \sigma(Q_\nu)$$

indeed guarantees (26) by (24) and (28). Hence we are lead to use the *trace norm* $\|Q\|_{\mathrm{T}} := \sum_{j=1}^{\infty} \sigma_j(Q)$ as the *convex* cost functional. We end up with the sequence of FCOPs

$$s_\nu := \inf_{Q\in\mathcal{S}_\nu\cap\hat{\mathcal{Q}}_\nu} \|Q\|_{\mathrm{T}} \tag{29}$$

where the trace norm of Q is minimized over an open convex set in a finite dimensional space. This leads us to the central result of this paper.

Theorem 13 *Suppose (12) admits the real rational optimal controller Q_*. Determine α_*, (r_*, R_*) and n_* numerically. For some error sequence $\varepsilon_\nu > 0$ with $\varepsilon_\nu \overset{\nu\to\infty}{\longrightarrow} 0$ let $\hat{Q}_\nu$ denote any controller in $\mathcal{S}_\nu \cap \hat{\mathcal{Q}}_\nu$ with $\|\hat{Q}\|_{\mathrm{T}} < s_\nu + \varepsilon_\nu$. Then*

$$\|\hat{Q}_\nu - Q_*\|_\infty \overset{\nu\to\infty}{\longrightarrow} 0 \ \text{ and } \ \sum_{j=n_*+1}^{\infty} \sigma_j(\hat{Q}_\nu) \overset{\nu\to\infty}{\longrightarrow} 0. \tag{30}$$

If P_ν denotes an n_*-th order Hankel norm approximant of $\hat{Q}_\nu$ with $\|\hat{Q}_\nu - P_\nu\|_\infty \le \sum_{j=n_*+1}^{\infty} \sigma_j(\hat{Q}_\nu)$ then $\|P_\nu - Q_*\|_\infty \overset{\nu\to\infty}{\longrightarrow} 0$. Hence $\alpha(P_\nu) \overset{\nu\to\infty}{\longrightarrow} \alpha_*$, $\lim_{\nu\to\infty} \beta(P_\nu) \le \beta$ and $\lim_{\nu\to\infty} \gamma(P_\nu) \le \gamma$ imply that, for large ν, P_ν is a n_*-th order approximately optimal solution of problem (12).

Let us summarize the steps required for a practical implementation of the algorithm without any a priori knowledge. Most importantly, this discussion results in numerically verifiable necessary and sufficient conditions for the existence of the optimal controller Q_*.

- Compute the optimal value α_ν of (13) and the limit of α_ν for $\nu \to \infty$ which equals α_*.
- If α_ν is infinite for all ν then STOP: The intersection $\mathcal{S}_\nu \cap \mathcal{Q}$ is empty for all ν.
- Choose (r, R). Compute $\alpha_\nu(r, R)$ according to (19) or (21) and its limit $\alpha_*(r, R)$ for $\nu \to \infty$. If $\alpha_*(r, R)$ is larger than α_*, decrease $r > 1$ and increase $R > 0$ (e.g. take the half of r and double R) and repeat this step. If $\alpha_*(r, R) > \alpha_*$ holds for all $r > 1$ and $R > 0$ then STOP since a *rational Q_* does not exist.*
- If $\alpha_*(r, R) = \alpha_*$, determine the smallest integer n_* such that $\sigma_{n_*+1}(Q_\nu(r, R)) \overset{\nu\to\infty}{\longrightarrow} 0$. If n_* does not exist then STOP since Q_* *does not exist.* Otherwise fix (r_*, R_*) with $r \ge r_* > 1$ and $R_* > R$.
- Choose $\varepsilon_\nu > 0$ with $\varepsilon_\nu \overset{\nu\to\infty}{\longrightarrow} 0$. Determine $\hat{Q}_\nu$ which is admissible for (29) and satisfies $\|\hat{Q}_\nu\|_{\mathrm{T}} < s_\nu + \varepsilon_\nu$. If $\sum_{j=n_*+1}^{\infty} \sigma_j(\hat{Q}_\nu)$ does not converge to zero then STOP since Q_* *does not exist.*
- Otherwise compute P_ν, the n_*-th order Hankel norm approximant of $\hat{Q}_\nu$ as in Theorem 13. It is possible to show that P_ν converges to a real rational stable matrix which is optimal for (1). Hence we can *conclude* that Q_* exists and that, a posteriori, P_ν converges to Q_* in the H_∞-norm.

One can think of several variations of this principal procedure which are not discussed in detail. One variant might be of some interest: If one wishes to keep the poles of approximate solutions staying away from the imaginary axis and to have the controllers bounded, one may a priorily restrict the attention to (18) for some parameters r, R which are *chosen by the designer*. Then it is only required to determine $\alpha_*(r, R)$ and one can immediately proceed with (29) in order to detect the existence of rational optimal controllers for this problem. This considerably reduces the numerical complexity.

5 Reduced Order Multiobjective Control

Instead of letting the algorithm detect possible small order optimal controllers we could as well try to include an a priori constraint k on the controller order and consider, with fixed $\beta > 0$, $\gamma > 0$ the problem

$$\inf_{\{Q \in RH_\infty^{p\times q}:\ Q \text{ has order } \le k,\ \beta(Q)<\beta,\ \gamma(Q)<\gamma\}} \alpha(Q). \quad (31)$$

If, for any $\alpha > 0$, it were possible to test whether

$$\mathcal{Q} := \{Q \in RH_\infty^{p\times q} :\ f(Q) < f \ \text{ for } \ f = \alpha, \beta, \gamma\}$$

contains an element of order at most k and to construct such a Q if existing, one could clearly determine the optimal value of (31) by bisection and design a suboptimal Q arbitrarily close to optimality. The following result shows how this validation problem could be approached by a sequence of finite dimensional optimization problems. The constraint sets of these problems will turn out to be open and convex. The cost function, however, is given by

$$T_k(Q) := \sum_{j=k+1}^{\infty} \sigma_j(Q)$$

and thus, in contrast to what has been done earlier, *not convex*.

Theorem 14 *Fix $\alpha, \beta, \gamma > 0$ and some nonnegative integer k and define the sequence ε_ν by*

$$\varepsilon_\nu := \inf_{Q \in \mathcal{S}_\nu \cap \mathcal{Q}} T_k(Q).$$

If there exists a $Q \in \mathcal{Q}$ of order at most k then $\varepsilon_\nu \overset{\nu\to\infty}{\longrightarrow} 0$. On the other hand, suppose $\varepsilon_\nu \overset{\nu\to\infty}{\longrightarrow} 0$ and choose an arbitrarily small $\varepsilon > 0$. Then there exists a ν with $\varepsilon_\nu < \varepsilon$ and a $Q \in \mathcal{S}_\nu \cap \mathcal{Q}$ with $T_k(Q) < \varepsilon$. A k-th order Hankel norm approximant P of Q with $\|Q - P\|_\infty \le T_k(Q)$ then satisfies $f(P) \le f(Q) + L_f\varepsilon$ for $f = \alpha, \beta, \gamma$.

This may be viewed as a suboptimality approach to optimization problems with reduced order controllers and constitutes an alternative to those techniques in which the existence of an optimal controller has to be assumed (Bernstein and Haddad (1989)). However, it is presently unclear how to globally solve the nonconvex optimization problems involved which once again exhibits the inherent difficulties in reduced order optimal control problems.

References

Bernstein D.S., Haddad W.M. (1989). LQG control with an H_∞ performance bound: A Riccati equation approach. *IEEE Trans. Automat. Control*, Vol. *AC-34*, pp. 293–305.

Bernstein D.S., Haddad W.M. (1989). Steady-state Kalman filtering with an H_∞ error bound. *Systems Control Lett.*, Vol. *12*, pp. 9–16.

Boyd S.P., Barratt C. (1991). *Linear Controller Design.* Prentice Hall, Englewood Cliffs.

Dorato P. (1991). A survey of multiobjective design techniques. *Proceedings of the International Workshop on Robust Control*, San Antonio, TX.

Doyle J., Glover K., Khargonekar P., Francis B. (1989). State-space solutions to standard H_∞ and H_2 control problems. *IEEE Trans. Automat. Control*, Vol. *AC-34*, pp. 831–847.

Doyle J., Zhou K., Bodenheimer B. (1989). Optimal control with mixed $\mathcal{H}_2$ and $\mathcal{H}_\infty$ performance objectives. *Proc. American Control Conference*, pp. 2065-2070.

Francis B.A. (1987). *A Course in H_∞ Control Theory.* Lecture Notes in Control and Information Sciences No. 88, New York: Springer-Verlag.

Francis B.A., Doyle J.C. (1987). Linear control theory with an H_∞ optimality criterion. *SIAM J. Contr. Optimiz.*, Vol. *25*, pp. 815–844.

Glover K. (1984). All optimal Hankel-norm approximations of linear multivariable systems and their L_∞-error bounds. *Int. J. Control*, Vol. *39*, pp. 1115–1193.

Haddad W.M., Bernstein D.S., Mustafa D. (1991). Mixed-norm $\mathcal{H}_2/\mathcal{H}_\infty$ regulation and estimation: The discrete time case. *Systems Control Lett.*, Vol. *16*, pp. 235–247.

Iwasaki T., Skelton R.E. (1993). All Controllers for the General $\mathcal{H}_\infty$ Control Problem: LMI Existence Conditions and State Space Formulas. Preprint.

Khargonekar P.P., Rotea M.A. (1991). Mixed $\mathcal{H}_2/\mathcal{H}_\infty$ control: a convex optimization approach. *IEEE Trans. Automat. Control*, Vol. *AC-36*, pp. 824–837.

Mustafa D. (1989). *Minimum Entropy $\mathcal{H}_\infty$ Control.* Ph.D. Thesis, St. John's College, Cambridge, UK.

Pinkus A. (1985). *n-Widths in Approximation Theory.* Ergebnisse der Mathematik und ihrer Grenzgebiete, Band 7, Berlin: Springer-Verlag.

Ridgely D.B., Mracek C.P., Valavani L. (1992). Numerical solution of the general mixed H_2/H_∞ optimization problem. *Proc. American Control Conference*, pp. 1353–1357.

Richter S. (1987). A homotopy algorithm for solving the optimal projection equations for fixed-order dynamic compensation: Existence, convergence and global optimality. *Proc. American Control Conference*, pp. 1527-1531.

Rotea M.A., Khargonekar P.P. (1991a). H^2-optimal control with an H^∞ constraint: The state feedback case. *Automatica*, Vol. *27*, pp. 307–316.

Rotea M.A., Khargonekar P.P. (1991b). Generalized $\mathcal{H}_2/\mathcal{H}_\infty$ control via convex optimization. *Proc. 30th IEEE Conf. Decision and Control*, Brighton, UK, pp. 2719–2720.

Scherer C. (1992). H_∞-optimization without assumptions on finite or infinite zeros. *SIAM J. Control Optim.*, Vol. *30*, pp. 143–166.

Steinbuch M., Bosgra O.H. (1991a). Necessary Conditions for Static and Fixed Order Dynamic Mixed H_2/H_∞ Optimal Control. *Proc. American Control Conference*, pp. 1137-1143.

Steinbuch M., Bosgra O.H. (1991b). Robust performance in H_2/H_∞ optimal control. *Proc. 30th IEEE Conf. Decision and Control*, Brighton, UK, pp. 539-550.

Stoorvogel A.A. (1990). *The H_∞ control problem: A state space approach.* Ph.D. Thesis, Eindhoven University of Technology, The Netherlands.

Sznaier M., Sideris A. (1991). Suboptimal Norm Based Robust Control of Constrained Systems with an H_∞ Cost. *Proc. 30th IEEE Conf. Decision and Control*, Brighton, UK, pp. 2280–2286.

Yeh H., Banda S., Chang B. (1990). Necessary and sufficient conditions for mixed $\mathcal{H}_2$ and $\mathcal{H}_\infty$ control. *Proc. 29th IEEE Conf. Decision and Control*, Honolulu, HI, pp. 1013–1017.

Zhou K., Doyle J., Glover K., Bodenheimer B. (1990). Mixed $\mathcal{H}_2$ and $\mathcal{H}_\infty$ control. *Proc. 29th IEEE Conf. Decision and Control*, Honolulu, HI, pp. 1013–1017.

Selected Topics in Identification, Modelling and Control
Vol. 6, December 1993

Design of an integrated autopilot/autothrottle using μ – synthesis

Samir Bennani[‡], Bob J.A. Mulder[‡] and Ton J.J.vd Weiden[§] [♭]

[‡]*Sec. Stability and Control, Fac. Aerospace Eng.,*
Delft University of Technology, Kluyverweg 1, 2629 HS Delft, The Netherlands.
[§]*Mechanical Engineering Systems and Control Group*
Delft University of Technology, Mekelweg 2, 2628 CD Delft, The Netherlands.

Abstract. This paper demonstrates the use of H_∞ and μ-synthesis methods to develop control laws for the longitudinal motion of an aircraft. The objective is to design a controller that provides independent control of altitude and speed, while maintaining stability and performance robustness throughout different flight conditions.

Keywords. H_∞ and μ controller synthesis, uncertainty modelling and weighting function choice.

1 Introduction

A preliminary study towards the application of robust controller synthesis techniques, such as μ–synthesis, for the design of an integrated autopilot-autothrottle of the laboratory aircraft of Delft University of Technology is presented. Following on this study, the results developped by these techniques are to be used in the very near future in the fly-by-wire configured Cessna Citation II of the Delft University of Technology and the Dutch National Aerospace Laboratory (NLR). A two degree of freedom controller as proposed by Kaminer (1990) is shown in Fig. 1. The feedback loop consists of a μ-synthesis controller to comply with the feedback requirements, while the feedforward loop consists of an ideal command response model, reflecting the desired flying quality requirements.
The desired commands that can be generated from the pilots inputs are actually the aircraft's speed and altitude. These modes can be engaged simultaneously, giving rise to a multivariable control problem. The actuators used are the aircraft elevator and engine which have to provide coordinated commands similar to the way a pilot would fly a prescribed trajectory. Besides the multivariable character of the problem it is important to notice that the open loop aircraft has a strong interaction in speed command response and altitude command response. This can be ratified from an energetical viewpoint of the aircraft motion. Roughly speaking, a demand in speed causes a demand in the kinetic enery level, which has to be furnished by the avail-

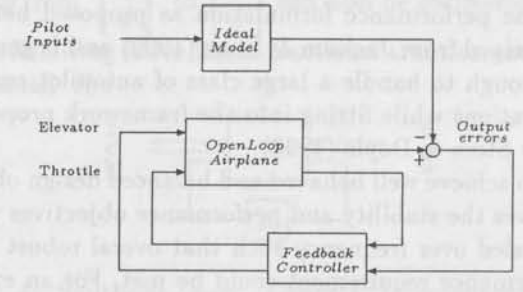

Fig. 1: The two loop control structure.

[♭]The authors would like to thank Isaac Kaminer, Paul Lambrechts and the reviewers for their suggestions and critical comments. The real-complex μ calculations have been made possible thanks to John Doyle, Andy Packard and Gary Balas. Further, we would like to thank the Dutch National Aerospace Laboratory NLR for the financial support of this research.

able potential energy if the total system's energy is supposed to remain constant. Finally, the aerodynamics vary over the operational flight conditions, in our case both velocity and altitude are allowed to vary substantially.
These two considerations about the aircraft's dynamics over a wide range of operational conditions give rise to the formulation of three design goals that are to be met by the feedback controller.

1. achieve decoupled error free tracking of the pilot's commands of speed and altitude; this objective is be called the *nominal performance* specification and is related to one design model.

2. ensure stability robustness in presence of modelling uncertainty and varying operational conditions; this objective represents the *robust stability* specification.

3. ensure decoupled error free tracking of altitude and speed commands in presence of a set of possible linear time invariant models that capture the model variations for varying flight conditions; this objective forms the *robust performance* objective.

The performance formulation as proposed here is derived from Jackson & Enns (1990) and is general enough to handle a large class of autopilot configurations while fitting into the framework proposed by Stein & Doyle (1990)
To achieve well behaved and balanced design objectives the stability and performance objectives were scaled over frequency such that overal robust performance requirement could be met. For an excellent reference on how optimality trade-offs have to be made we refer to Boyd & Barrat (1991). This is the hardest part of the design, having achieved this point it is not difficult to push the design in the direction of more performance or more stability robustness to find the required robust performance level. Nevertheless, in order to play this game in a behaved way the whole problem formulation as stated above has to be absorbed into a special structure, the general interconnection structure as proposed by Stein & Doyle (1990), having the feature that with some key results on matrix norms it provides the designer information about the closeness to the proposed stability and performance objectives. These analysis results together with some synthesis results are shortly reviewed in section in section 2. Then, in section 3 the set of design models together with the specifications as initially given are presented. In section 4 the requirements are translated into a suitable form, this consist in real uncertainty modelling in order to obtain a state space representation for a set of models that describe the various operational flight condition and the choice of weighting functions representing the desired performance characteristics. Next, are given in section 5 the analysis considerations that provided clear design guidelines during the controller synthesis phase described in section 6. We conclude with a brief discussion of the results and review the experience obtained in applying the method.

2 μ-Synthesis Methodology in a General Framework

A general controller synthesis and analysis problem description as proposed by Stein & Doyle (1990) is shown in Fig. 2. Associated to this representation

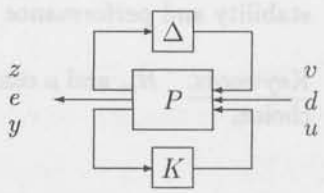

Fig. 2: General Analysis and Synthesis framework.

of the problem description is a suitable measure of magnitude for matrix transfer functions and some key analysis and synthesis results, these define a framework for controller synthesis and analysis.
The problem description consists of a generalized system P with three pairs of input/output variables. The first pair consists of the measured outputs $y(t)$, and control inputs $u(t)$. The second pair consists of performance variables $e(t)$, and external input signals $d(t)$, and the third pair consists of output signals $z(t)$, and $v(t)$ through which unit-norm perturbations are fed back into the system.
Any linear interconnection of inputs, outputs and commands along with the perturbations and a controller can be viewed in this context and can be rearranged to match this diagram so that P can be chosen to reflect many different problem specifications.

2.1 Analysis Review

Within this framework a non-conservative necessary and sufficient condition for robust performance can be formulated (Stein & Doyle (1990)). To obtain this condition the compensator feedback-loop

in Fig. 2 has to be closed to get the loop in Fig. 3. The system $M(P,K)$ in this figure has a 2×2 block-structured transfer function $M(s)$ whose blocks are defined in terms of the original 3×3 partition of $P(s)$ as follows:

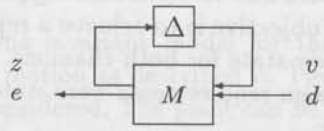

Fig. 3: Analysis part General interconnection structure

$$M_{ij}(s) = P_{ij}(s) + P_{i3}(s)\,[I - K(s)P_{33}(s)]^{-1} K(s)P_{3j}(s) \quad i,j = 1,2 \tag{1}$$

(1) represents a linear fractional transformation of the system P through K, therefore the notation $M(P,K)$.

When this system is stable, then the following results apply (Stein & Doyle (1990)):

1. **Nominal performance is satisfied if and only if**

$$\|M_{22}(j\omega)\|_\infty < 1 \tag{2}$$

2. **Robust stability is satisfied if and only if**

$$\|M_{11}(j\omega)\|_\infty < 1 \tag{3}$$

3. **Robust performance is satisfied if and only if**

$$\mu[M(j\omega)] < 1 \quad \forall\,\omega \tag{4}$$

where μ is a function to be defined shortly.

Robust performance is equivalent to robust stability in presence of two perturbations Δ and Δ_p connected around the system $M(P,K)$. The latter stability is assured, if and only if the function $\det(I - diag(\Delta,\Delta_p)M(j\omega))$ remains nonzero along the imaginary axis.

This observation gives rise to the function μ. This function was defined in Doyle (1982) to test this kind of determinant conditions.

Its full definition for complex matrices is the following:

$$\mu[M] \triangleq \left[\min\left\{\epsilon \;\middle|\; \begin{array}{l}\det[I-\epsilon XM]=0 \\ \text{for some } X = diag(\Delta_1,\ldots,\Delta_m) \\ \text{with } \|\Delta_i\|_\infty < 1 \text{, for all } i\end{array}\right\}\right]^{-1} \tag{5}$$

In words, μ is the reciprocal of the smallest value of scalar ϵ which makes the matrix $I-\epsilon XM$ singular for some X in a block-diagonal perturbation set. If no such ϵ exists, μ is taken to be zero.

This is a tight condition for robust stability with respect to two perturbation blocks, and equivalently a tight condition for robust performance. Note that the definition is not limited to 2×2 block structures, so that it can be used to test stability with respect to *any number of diagonal blocks*. This permits to establish robust stability with respect to plant sets characterized by *several unstructured perturbations*, and simultaneously, to establish robust performance.

For practical use, the function $\mu[M]$ has to be evaluated. This is done across frequency, providing a Bode-like plot to analyze robust stability/performance of any given design. It should be clear from the argument of the function μ which kind of test is carried out.

2.2 Synthesis Review - H_∞ Optimization

For the purpose of synthesis, the perturbation can be normalized properly to unity so that the normalizing factor can be absorbed into P. This results in the synthesis problem as shown in Fig. 4. The synthesis problem involves finding a controller K such that performance requirements are satisfied under prescribed uncertainties. The interconnection structure P can be partitioned so that the input-output map from $\begin{bmatrix} v \\ d \end{bmatrix}$ to $\begin{bmatrix} z \\ e \end{bmatrix}$ can also be expressed as the following lower linear fractional transformation denoted F_l:

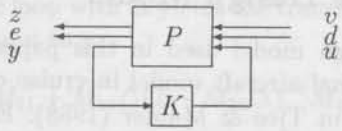

Fig. 4: Synthesis part General interconnection structure

$$\begin{bmatrix} z \\ e \end{bmatrix} = F_l(P,K)\begin{bmatrix} v \\ d \end{bmatrix} = M(P,K)\begin{bmatrix} v \\ d \end{bmatrix}$$

For the H_∞ optimal problem, the objective is to find a stabilizing controller K which minimizes $\|F_l(P,K)\|_\infty$. Thus find a controller K such that

$$\|F_l(P,K)\|_\infty < \gamma \tag{6}$$

where $\frac{1}{\gamma}$ is the minimum norm of the perturbation that destabilizes the closed-loop system. An excellent reference on this matter is Francis (1987), while the algorithms used to obtain H_∞ controllers come from Doyle, Glover, Khargonekar & Francis (1988) and are implemented in the μ-Analysis and Synthesis Toolbox by Balas, Doyle, Glover, Packard & Smith (1990).

2.3 μ-Synthesis Methodology

The μ-synthesis methodology emerges as a practical approach for the design of control systems with robust performance objectives. This technique essentially integrates two powerfull theories for synthesis and analysis into a systematic design technique involving H_∞ optimization methods for synthesis and the structured singular value μ for analysis. The problem of robust controller design becomes that of finding a stabilizing controller K and scaling matrix D such that the quantity $\| DF_l(P,K)D^{-1} \|_\infty$ is minimized.

One approach for solving this problem is that of alternaly minimizing the above expression for either K or D while holding the other constant. For fixed D, it becomes an H_∞ optimal control problem and can be solved using the well-known state-space method of Doyle, Glover, Khargonekar & Francis (1988). On the other hand, with fixed K, the above quantity can be minimized at each frequency as a convex optimization in $\ln(D)$. The resulting data of D can be fit with an invertible, stable, minimum-phase, real-rational transfer function. This proces is carried on until a satisfactory controller is constructed. For a deaper treatement of this procedure, the reader is refered to Stein & Doyle (1990) and Balas, Doyle, Glover, Packard & Smith (1990).

3 The Design Model

The design model used in this paper consists of longitudinal aircraft model in cruise configuration as given in Tjee & Mulder (1988). From the full non-linear aircraft model linear models for trimmed cruise configuration are generated in varying operating conditions. The velocity is allowed to vary

Flight Condition	Airspeed [m/s]	Altitude [ft]
CRUISE	40, 45, 50, 55, 60	2000
	40, 45, 50, 55, 60	4000
	40, 45, 50, 55, 60	6000
	40, 45, 50, 55, 60	8000
	40, 45, 50, 55, 60	10000

Table 1: The set of design points

between 40 and 60 m/s while altitude may vary between 2000 and 10000 ft.

In addition to the aircraft model, we assume that the elevator and engine dynamics are not well defined to some extend.

To reflect handling quality requirements, two second order ideal command response models for the altitude and the speed are included. The filters have a natural frequency of $\omega_n = 0.3\, rad/sec$ and damping $\zeta = 0.7$.

Output errors due to command signals have to be small. The objective is to achieve a rejection factor of 100 steady-state for both channels.

Further design requirements were stated in the following way:

1. All eigenvalues should have relative damping better than 0.4.
2. Phugoid eigenvalues should have relative damping better than 0.7.
3. Loop gain should satisfy $10dB$ gain margin and 45 deg phase margin.
4. The closed loop bandwidth frequency for the altitude and speed loop should be about $1\, rad/sec$. High frequency loop gain should be less than $10\, dB$ at $10\, rad/sec$ rolling off at a rate of $-40\, dB/dec$ beyond $10\, rad/sec$.
5. The commanded throttle values for the manifold pressure should be less than ± 5" Hg around trim value.
6. The maximum elevator deflection has to remain within $\pm 5\, deg$ around trim.
7. The maximum elevator deflection rate should be less that $30\, deg/sec$.

and should hold for the set of prescribed models.

4 Application of μ-Synthesis to a Flight Control System design.

4.1 Introduction

This section deals with the application of the in section 2 presented theory for the synthesis of a flight control system (FCS). To make practical design possible all design models as given in section 3 and objectives have to be absorbed into the general interconnection structure presented in section 2. First a description of the linear aircraft model is given which represents the longitudinal part of the dynamical motion of a rigid body aircraft. To capture a whole set of models describing the aircraft motion in cruise configuration for the range of operating conditions as given in section 3 the modelling principle following Morton (1985) is adopted. Then the set of objectives as presented in section

1 and section 3 are translated into suitable weighting functions. Together the last two steps are combined to form the general interconnection structure for this design problem.

4.2 Description of the aircraft model

A linear time invariant model for the longitudinal aircraft motion as described in Tjee & Mulder (1988). is considered. The plant can be represented in state space form as:

$$\begin{aligned} \dot{x} &= Ax + Bu \\ y &= Cx + Du \end{aligned} \tag{7}$$

where x represents state vector, u the input vector and y the output vector (it should be clear from the context when is refered to the control vector or the forward speed).

$$x = \begin{bmatrix} u \\ \alpha \\ \theta \\ q \\ h \end{bmatrix} \begin{matrix} (m/s) & \text{forward speed} \\ (rad) & \text{angle of attack} \\ (rad) & \text{attitude angle} \\ (rad/s) & \text{pitch rate} \\ (m) & \text{altitude} \end{matrix}$$

$$u = \begin{bmatrix} pz & \delta_e \end{bmatrix} \begin{matrix} (Pa) & \text{manifold pressure} \\ (rad) & \text{elevator deflection} \end{matrix}$$

$$y = \begin{bmatrix} u \\ h \\ \dot{u} \\ \dot{h} \\ q \end{bmatrix} \begin{matrix} (m/s) & \text{forward speed} \\ (m) & \text{altitude} \\ (m/s^2) & \text{forward acceleration} \\ (m/s) & \text{climb rate} \\ (deg/s) & \text{pitch rate} \end{matrix}$$

Having defined the states, inputs and available measurements, the modelling of the variations of this model throughout different operating conditions is in first instance carried out. Further the selection of the weights is presented, for a clear treatment of this subject we refer to Maciejowsky (1989).

4.3 Uncertainty modelling and choice of weighting functions

In the following a motivation for the choice of the distinct design variables will be given.

1. Variation aerodynamic coefficients.

   To reflect the variation of the aerodynamic model through the flight envelope, linear uncertainty modelling following Morton has been adopted.

   Starting from the fact that the set of linearized aircraft models over the whole flight envelope for the cruise configuration can be modelled by the following uncertain equation:

$$\begin{aligned} \dot{x} &= A + \sum_{i=1}^{k} \delta_i A_i x + B + \sum_{i=1}^{k} \delta_i B_i u \\ y &= C + \sum_{i=1}^{k} \delta_i C_i x + D + \sum_{i=1}^{k} \delta_i D_i u \end{aligned} \tag{8}$$

   where the nominal system description is given by (A, B, C, D) and the pertubed part is parametrized by k uncertain parameters where δ_i, corresponds in this case to speed and altitude variations δ_u and δ_h that occur over the different operating conditions. The information of model variation is contained in the 2 scalar operators δ_u and δ_h which are assumed to be LTI operators.

   For purpose of synthesis and analysis the pertubed model is required to be formulated in such a way that the variations enter the model in a linear fractional way. This can be done in the following way:

$$\begin{aligned} \dot{x} &= Ax + Bu + B_2 v \\ y &= Cx + Du + D_{12} v \\ z &= C_2 x + D_{21} u + D_{22} v \\ v &= \Delta z = \operatorname{diag}(\delta_u I_{qu}, \delta_h I_{qh}) z \end{aligned} \tag{9}$$

   where additional inputs v and outputs z will be defined. Further, $B_2, C_2, D_{12}, D_{21}, D_{22}$ have dimensions according to qu and qh representing the dimension of the pertubation block. Closing the loop with Δ yields the transfer function relating u to y:

$$M_{11} + M_{12}\Delta(I - M_{22}\Delta)^{-1} M_{21} \tag{10}$$

   In this case the uncertainty is modelled such that it affects the plant in an affine manner such that $M_{22} = 0$. This assumption permits to obtain in a simple way by singular value decomposition the uncertainty that affects the model in a linear fractional way. Therefore, $\forall i$ with, $1 \leq i \leq k$, let q_i denote the rank of the matrix :

$$P_i = \begin{bmatrix} A_i & B_i \\ C_i & D_i \end{bmatrix} \tag{11}$$

   with $P_i \in R^{(n+n_y)\times(n+n_u)}$.

   Then P_i can be writen as:

$$\begin{bmatrix} L_r \\ W_i \end{bmatrix} \begin{bmatrix} R_i \\ Z_i \end{bmatrix}^T \tag{12}$$

   Where, $L_i \in R^{n\times q_i}$, $R_i \in R^{n\times q_i}$, $W_i \in R^{n_y \times q_i}$, $Z_i \in R^{n_u \times q_i}$.

$$\delta_i P_i = \begin{bmatrix} L_r \\ W_i \end{bmatrix} [\, \delta_i I_{qi} \,] \begin{bmatrix} R_i \\ Z_i \end{bmatrix}^T \qquad (13)$$

And therefore $M_{11} + M_{12}\Delta M_{21}$ which is,

$$\begin{bmatrix} A + \sum_{i=1}^{k} \delta_i A_i & B + \sum_{i=1}^{k} \delta_i B_i \\ C + \sum_{i=1}^{k} \delta_i C_i & D + \sum_{i=1}^{k} \delta_i D_i \end{bmatrix}$$

and looks in fact like:

$$\begin{bmatrix} A & B \\ C & D \end{bmatrix} + \begin{bmatrix} L_i & \cdots & L_k \\ W_i & \cdots & W_k \end{bmatrix} \begin{bmatrix} \delta_i I_{q1} & \cdots & \cdots \\ \cdots & \cdots & \cdots \\ \cdots & \cdots & \delta_k I_{qk} \end{bmatrix} \begin{bmatrix} {R_1}^T & {Z_1}^T \\ \cdots & \cdots \\ {R_k}^T & {Z_k}^T \end{bmatrix}$$

Therefore the matrices B_2, C_2, D_{12}, D_{21} and D_{22} are given by: $B_2 = [L_1, \cdots, L_k]$, $C_2 = [R_1, \cdots, R_k]$, $D_{12} = [W_1, \cdots, W_k]$, $D_{21} = [Z_1, \cdots, Z_k]$, and $D_{22} = 0$. The uncertainty is contained in the block diagonal matrix Δ. Define the block structure associated with the system as :

$$\mathbf{\Delta} = \{\text{diag}\ [\delta_u I_{qu}\ \delta_h I_{qh}]\ \ \delta_i \in R\} \qquad (14)$$

and,

$$\mathbf{B\Delta} = \{\Delta \in \mathbf{\Delta} \text{ with } \sigma(\Delta) \leq 1\} \qquad (15)$$

which is the set of allowable perturbations.

To model speed and altitude perturbations around the nominal condition of $u_0 = 50\ m/s$ and $h_0 = 6000\ ft$ the perturbation matrices for speed and altitude variations P_u and P_h are first calculated.

By performing a singular value decomposition on P_u and P_h a rank 4 perturbation has been adopted for the effect of speed variations $\Delta_{u4} \in R^{4\times4}$ and rank 3 perturbation for the altitude variations $\Delta_{h3} \in R^{3\times3}$. In this way the desired matrices $B2$, $C2$, $D12$, $D21$ and $D22$ as in (9), of rank according to the dimension of the perturbation are obtained. We refer to Packard (1988) for a complete outline of the paramteric uncertainty modelling procedure.

2. Multiplicative uncertainty models.

Both actuators, the engine as well as the elevator models are not adequately known. In this study an input multiplicative uncertainty model has been adopted to capture the uncertainty in both systems. The set of models decribed by this type of uncertainty modelling is represented by:

$$G_{act}(s) = G_{act_0}(s)(1 + W_u(s)\Delta_c(s)) \qquad (16)$$

where $W_u(s)$ is a stable transfer function representing the relative variation of the system around nominal $G_{act_0}(s)$. Generally this type of uncertainty arises from unmodelled high frequency dynamics and therefore $W_u(s)$ is chosen to be small at low frequencies while increasing at high frequencies. The technical reason for this particular choice comes from the fact that this filter forces the closed loop system to roll off at a high frequencies, see Doyle Francis & Tannenbaum (1992) for a complete discussion. The shape of this filter is given by:

$$W_u(s) = a\frac{\alpha s + \beta}{\gamma s + \delta} \qquad (17)$$

and has been obtained by iteratively tuning up the design. Commonly this weighting function is taken to represent a 50% relative uncertainty level and was chosen in the initial design where the parametric uncertainty has be left out as shown in Fig. 5. In a refined design the relative uncertainty level was allowed to be only 10 % at low frequencies, because the real perturbations due to varying operating conditions already introduce the remaining uncertainty in this frequency region.

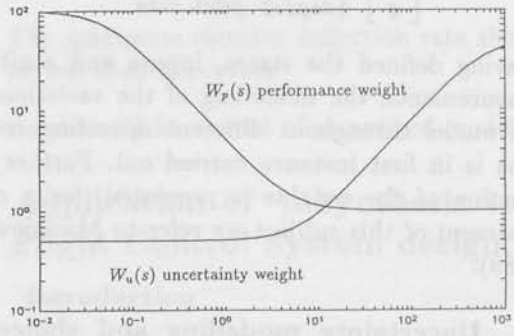

Fig. 5: Actuator uncertainty and tracking error weights.

3. Tracking error weighting functions

To reflect the requirement to keep tracking errors to commands less than 1%, $W_p(s)$ has been chosen as a first order lag-lead filter insisting on reducing errors in the lower frequencies:

$$W_p(s) = b\frac{\alpha s + \beta}{\gamma s + \delta} \qquad (18)$$

The error rejection bandwidth as shown in Fig. 5 is kept small because the command signals are low frequent and to allow the controller maintaining the required performance level over large set of operating conditions.

4. Command filter

The command filter reflects the ideal model response to speed and altitude commands, $\frac{u(s)}{u_c(s)}$ and $\frac{h(s)}{h_c(s)}$ respectively. These filters remain fixed for the design. The shape for the command filter is dictated by flying quality requirements and is shown in Fig. 6. It has been modelled as a second order filter:

$$W_c(s) = \text{diag}\left[\frac{(s^2+2\zeta\omega_1 s+\omega_1^2)(\omega_0^2)}{(\omega_1^2)(s^2+2\zeta\omega_0 s+\omega_0^2)}, \frac{(s^2+2\zeta\omega_1 s+\omega_1^2)(\omega_0^2)}{(\omega_1^2)(s^2+2\zeta\omega_0 s+\omega_0^2)}\right] \quad (19)$$

where $\omega_0 = 0.3\, rad/sec$, $\omega_1 = 10\, rad/sec$ and $\zeta = .7$. This filter is chosen to flatten out at $10 rad/sec$ with a second order numerator polynomial.

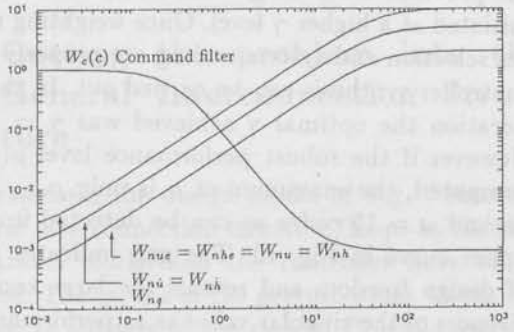

Fig. 6: Command and noise filters

5. Choice of the sensor noise filters.

Most measurements are not noise free and become sensitive to high frequency noise. The measurement noise is taken to be dynamical as a lead-lag filter. Furthermore, these filters have to be introduced to satisfy the H_∞ control problem rank conditions given in Doyle, Glover, Khargonekar & Francis (1988). As can be seen in Fig. 6 the noise filters bring in evidence the noise activity at high frequencies. Choosing the noise level to be small led to conditioning problems of the interconnection structure. These filters also permit to shape the input sensitivity of the system.

$$W_n = \text{diag}\,(W_{neu}, W_{neh}, W_{nu}, W_{nh}, W_{n\dot{u}}, W_{n\dot{h}}, W_{nq}$$

where $W_{nue} = W_{nhe} = W_{nu} = W_{nh} = 2\frac{s+0.01}{s+50}$ are the noise weights for respectively the speed and altitude error and the speed and altitude signals, $W_{n\dot{u}} = W_{n\dot{h}} = 5\frac{s+0.01}{s+50}$ for their derivatives and $W_q = 10\frac{s+0.01}{s+50}$ for the pitch rate signal.

6. Control activity weights.

Additionally to the fact that tracking errors have to be small, control activity has to remain within prescribed limits in order to prevent actuator saturation. Therefore elevator defelection, rotational rate and acceleration are limited by constant weighting function. In the same way pitch rate and forward speed were required to remain limited. The filter that limits the amplitude of all these signals is given by $W_{eff} = \text{diag}(4,\ 2/100,\ 1/1000,\ 1/1000,\ 1/500)$.

4.4 The design model

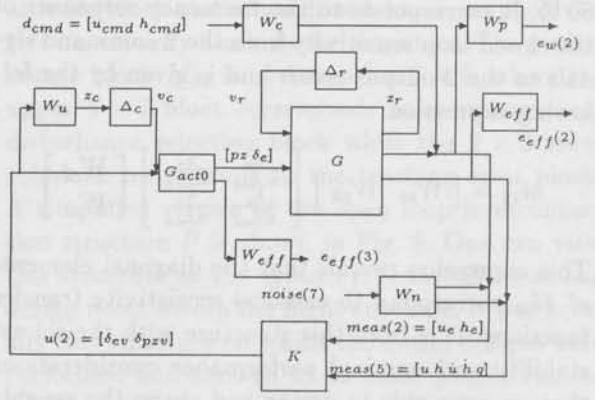

Fig. 7: Design Model.

The aforementionend considerations are stacked together leading to the design model which describes the whole set of models for which the defined performance specifications have to be met. Fig. 7 gives the block diagram of the design structure. The design model still has the same two loop control structure as Fig 1., besides the fact that uncertainties are added to the airframe to reflect the set of flight conditions and the weihgting functions to reflect the desired closed loop performance. The filter W_p represents the requirement to keep errors between the commanded signals, $d_{cmd}(2) = (u, h)$ shaped by W_c

to Fig. 9 is given by the following equation:

$$\begin{bmatrix} z \\ e_w \\ y \end{bmatrix} = \left[\begin{array}{c|c|c} O & O & W_u \\ \hline W_p G & W_p W_c & W_p G \\ \hline G & -W_c & G \end{array}\right] \begin{bmatrix} v \\ d_{cmd} \\ u \end{bmatrix} \tag{20}$$

Applying (1) on the open loop matrix P, the closed loop transfer function matrix M is obtained:

$$M = \left[\begin{array}{c|c} W_u T_i & W_u S_i K W_c \\ \hline -W_p G S_o & -W_p S_o W_c \end{array}\right] \tag{21}$$

$$= \begin{bmatrix} W_u & O \\ O & -W_p \end{bmatrix} \begin{bmatrix} T_i & S_i K \\ G S_o & S_o \end{bmatrix} \begin{bmatrix} I & O \\ O & W_c \end{bmatrix} \tag{22}$$

where S_i, S_o, T_i and T_o are respectively input/output sensitivity and complementary sensitivity transfer functions. The matrix M_{11} represents the robust stability block and reflects how the uncertainty described by W_u affects the closed loop system T_i. Scaling this block by a factor γ scales the robust stability level that we want to keep in the sense of a norm less than one. In the initial design the robust stability block M_{11} was scaled to a level of 50 % at low frequencies and becoming of increasing importance at higher frequencies. The M_{22} block representing the performance block of the closed loop system was also scaled to be about 50 %. It corresponds to the frequency responses of the closed loop sensitivity from the 2 command signals to the 2 output errors and is given by the following expression:

$$M_{22} = \begin{bmatrix} W_{p1} & W_{p2} \end{bmatrix} \begin{bmatrix} \frac{u_e}{u_{cmd}} & \frac{u_e}{h_{cmd}} \\ \frac{h_e}{u_{cmd}} & \frac{h_e}{h_{cmd}} \end{bmatrix} \begin{bmatrix} W_{c1} \\ W_{c2} \end{bmatrix}$$

This expression reveals that the diagonal elements of M_{22} correspond to classical sensistivity transfer functions. It is from this structure with the robust stability and nominal performance considerations that we were able to design and shape the weights W_p and W_u. At this stage it was decided to design a robust control system for the whole flight envelope by taking into account the parametric uncertainty of the airframe due to speed and altitude variations. This uncertainty acts mainly at low frequencies so that the complex uncertainty weighting was reduced at low frequencies such that the sum of all uncertainties remains at a level of 50 %.

6 Control Design and Results

In first instance it is required to achieve robust stability, this is done by appropriately scaling the uncertainty level of the system after a first H_∞ trial design. In this example the uncertainty level for the speed block was initially chosen to be too large. Therefore the uncertainty level has been reduced by a factor γ_1 for the speed block and γ_2 for the altitude block. Roughly speaking the philosophy adopted here was to scale the system in such a way that the nominal performance block and the robust stability block contribute in a balanced way and in the same order of magnitude to the robust performance index, in such a way that roughly the sum of the infinity norm of both indexes is about (and not larger than) 3 to 5 for the initial design. In this design, the problem frequencies for the nominal performance block are in the low frequency range which is due to the large parametric uncertainty level in this frequency range. The robust stability block gave problems in the higher frequency range starting around 10 rad/s this is where sensor noise and unmodelled high frequency dynamics have large influence on the stability of the system. It has been experienced that when the choice of sensor noise level was static and/or too small this led to badly conditioned controllers such that the results were numerically not reliable any more leading to $\gamma's$ that pop up during a $D-K$-iteration. By this we mean, that a sucessive γ iteration on the scaled system could not be started at the previous achieved gamma level, but had to be initiated at a higher γ level. Once weighting matrices selection and system scaling are properly done, controller synthesis can be carried out. In the first iteration the optimal γ achieved was $\gamma = 11.75$. However if the robust performance level $\mu(M)$ is computed, the maximum of μ is only $\mu_{max} = 1.9$ around $\omega = 15\ rad/s$ as can be detected from the upper curve in Fig. 10. The gap indicates plenty of design freedom and reveals the large conservativeness of the singular value as as performance indicator. Performing a constant D scaling and redoing a γ-iteration brings the robust performance level down to $\gamma_2 = 1.0566$. The procedure is once more applied leading to $\gamma_3 = 1.0246$. At this stage further iteration has no more sense and calculating the real-complex robust performance level μ_{rc}, shows that for this design robust performance is achieved over the whole frequency range, this corresponds to the lower curve in Fig. 10. Remark, that constant $D-$scalings are not a limiting factor for this design. Fig. 10 summarises the robust performance levels that are achieved during three three iterations. A closer look to the finally achieved system characteristics is given in Fig. 11. The upper and lower bound for the robust performance level $\mu(M)$as predicted by the real-complex μ calculation is given by the $\mu_{rc}(M)$ curves in the plot. The

and the plant G its outputs u and h, small (*number between parenthesis designate the dimension of the vector signal*). These are, as shown in Fig. 7 the weighted errors $e_w(2)$. The filter W_u imposes roll-off on the controller. The filters W_{eff} represent the requirement to keep the amplitude of actuator signals $e_{eff}(3+2) = (\delta_e, \dot{\delta}_e, \ddot{\delta}_e, u, q)$ below some level, while W_n describes the noise spectrum acting on the measurements $meas(2+5)$. The controller K then has to provide two controls, $u(2) = (\delta_{ev}, \delta_{pzv})$, these are commaded voltages resulting in an effective actuation from G_{act} i.e. elevator deflection δ_e and effective manifold pressure pz on the engine. Finally, to reflect airframe variations in speed and altitude over a set of flight conditions and actuator uncertainty, respectively real and complex uncertainties are introduced by Δ_r and Δ_c.

However, this structure is yet not suitable for the purpose of controller synthesis and analysis. It is now the task to reorder the signals in such a way that uncertainty and performance become structured at system level permitting the application of the analysis and synthesis results of section 2. In the next section we discuss the transformation process from Fig. 7 into the general interconnection structure P.

5 Getting the problem into the General Interconnection Structure

To transform the design model of Fig. 7 into the general interconnection structure, loops at the perturbations blocks and the controller have to be opened. The inputs of the perturbations blocks are viewed as outputs of the system P, while outputs of the perturbations are viewed as input of the system P. In this way the first pair of signals for P are defined, perturbations that are unstructured at component level become structured at system level. The so obtained perturbation structure is given by, $\Delta = \text{diag}(\Delta_r, \Delta_c) = \text{diag}(\Delta_{v_4}\, \Delta_{h_3}\, \Delta_{c_1}\, \Delta_{c_1})$, where $\mathbf{\Delta_{v_4}} \in \mathbf{R^{4\times4}}$, $\mathbf{\Delta_{h_3}} \in \mathbf{R^{3\times3}}$ and $\mathbf{\Delta_{c_1}} \in \mathbf{C}$ respectively represent the unit norm bounded perturbation blocks for respectively the speed, altitude and actuator uncertainty. The second pair of signals that are grouped together represent the performance variables that we want to keep small. At the input of P sensor noises are firstly grouped together and at the output the actuator activity, further we want speed and pitch rate to remain small. Secondly the commanded signals are taken at the input of P. To these inputs we associate the weighted output errors that have to remain small. Finally, the third pair of signals is for purpose of controller synthesis and are obtained by breaking the loop at the compensator.

Once the open loop interconnection structure P for the complete design problem as shown in Fig. 8 is set up, controller synthesis can be carried out with in mind to achieve the prescribed robust performance level. The complete interconnection structure is of dimension 23×20. Closing the structure P with the controller K gives the analysis structure M. The robust stability block corresponding to M_{11} is 9×9, respectively corresponding to a four dimensional real speed block, three dimensional real altitude block and a two dimensional complex relative uncertainty block on the actuators. The performance block M_{22} is of dimension 7×9, where the upper 5×7 block corresponds to a measurement disturbance rejection block while the 2×2 lower subblock corresponds to the tracking error block. A simplified version of the open loop interconnection structure P is shown in Fig. 9. One can view this structure as the system representation at one design point within the flight envelope. It was actually this structure on which the initial designs were performed and allowed us to make proper choices for the weighting functions.

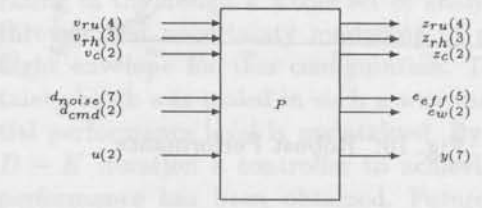

Fig. 8: Interconnection structure for the complete problem.

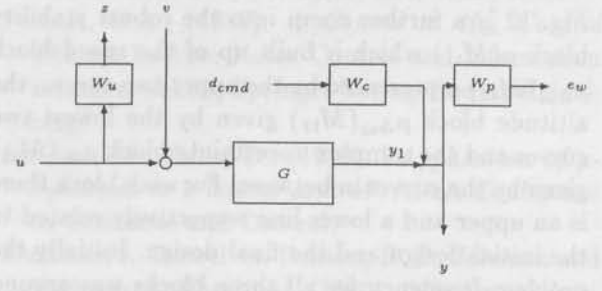

Fig. 9: Open loop interconnection structure P.

The input/output relation for P that corresponds

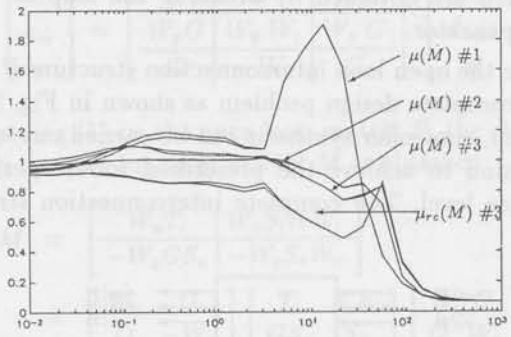

Fig. 10: Robust Performance

nominal performance level is given by $\bar{\sigma}(M_{22})$ becomes critical at low frequencies, by this we mean it tends to unity. The remaining two curves represent the upper and lower bound real complex robust stability level $\mu(M_{11})$ which is critical at higher frequencies.

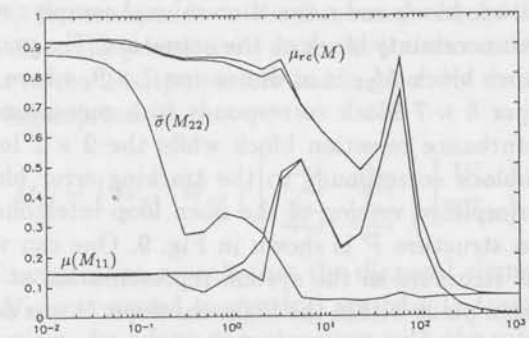

Fig. 11: Robust Performance, Nominal Performance and Robust Stability

Fig. 12 is a further zoom into the robust stability block $\mu(M_{11})$ which is built up of the speed block $\mu_{\Delta_{us}}(M_{11})$ represented by the upper two curves, the altitude block $\mu_{\Delta_{h3}}(M_{11})$ given by the lowest two curves and the complex uncertainty block $\mu_{\Delta_c}(M_{11})$ given by the curves in between. For each block there is an upper and a lower line respectively related to the initial design and the final design. Initially the problem frequency for all three blocks was around 10 rad/s. The peaks at this frequency have been succesfully eliminated for all three blocks. While the peak has been flattened out on this frequency, the complex block pops up at high frequencies. On the other hand this phenomenon gave freedom to the performance block to be reduced around 1 rad/s.

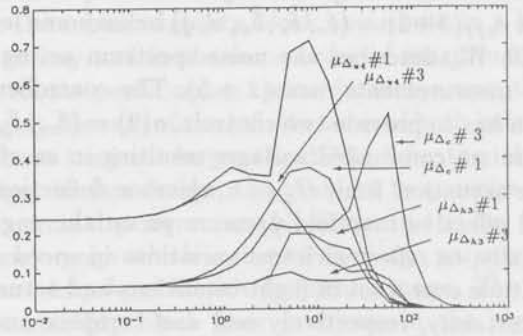

Fig. 12: Robust Stability Contributions

Zooming in at the lower 2×2 performance block, we have in Fig. 13 a Bode plot representation of the absolute tracking and interaction performance levels imposed by the upper curves. These are the boundaries imposed on the tracking error given by the diagonal terms which correspond to the classical sensitivity functions and have been imposed by the filters W_c and W_p.

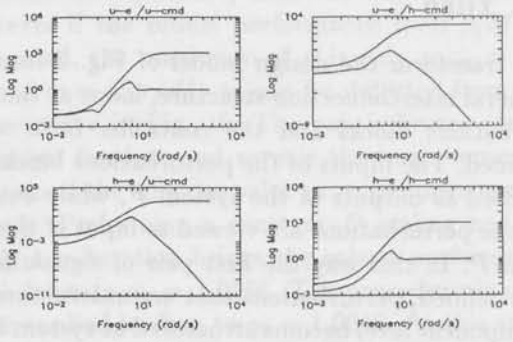

Fig. 13: Sensitivity and Interaction

Finally, in Fig. 14 command responses for both the altitude and speed channel are shown. The off diagonal plots show the interaction in the response. The plots represent command responses to the nominal system as well as all the extreme perturbed flight conditions. Remark that the interaction level does not degrade over all flight conditions. This concludes our exercise in obtaining a robustly decoupled command response to speed and altitude demands.

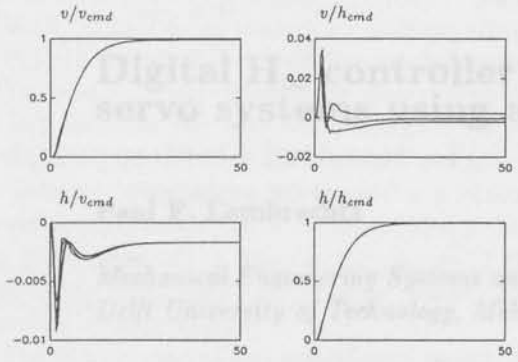

Fig. 14: Command responses, over whole flight envelope

7 Conclusion

Using μ-synthesis, a linear control law for the autothrottle/autopilot has been developed. From the time responses it can be seen that this configuration maintains the desired performance level within all operating conditions meaning that no gain scheduling is required. However, we should not be too optimistic about the results, since the time domain responses are not indicators for robustness. Recall that we have scaled the uncertainty level down by a factor γ_1, which physically means that we have shrunk the flight enveloppe by this factor. This means that the achieved robustness design design is restricted to a fourth of the initial perturbation set. So even time responses are satisfactory over the whole initial enveloppe, robustness guarantees are excluded for a wide operating range, which means that a switching or gain scheduling scheme for this control system is still required. The primary conclusion is that μ-synthesis has been succesfully applied for the development of controllers in achieving a desired robust performance level. The general framework gives the possibility to treat problems of significant complexity, where a variety of performance goals for a large set of systems can be treated in a straightforward manner. In fact, the design method within the general framework provides the designer with all information that is needed for insight in which direction the several components of the stability and performance blocks have to be tuned such that the final requirements can be met. This feature is primarly due to the fact that the performance and stability blocks themselves, and with respect to each other, become structured when viewed in the general interconnection structure. Further, applying the structured singular value μ with respect to different quantities, provides a non conservative measure for analysis. Actually, our design was set up in two stages. The first stage was the a robust performance design for one flight condition which provided insight in the choice of the filters W_p and W_c. This structure was the starting point for the robustification of the design over a wide set of operating conditions. This has been done by incorporating in the design a whole set of analysis points through real uncertainty modelling to reflect the flight envelope for this configuration. The uncertainty block was scaled in such a way that the initial performance level is maintained. By means of $D-K$ iteration a controller to achieving robust performance has been obtained. Future research will be conducted towards the development of a robust integrated autothrottle/autpilot design for the Cessna Citation II Laboratory Aircraft of the Delft University of Technology and the Dutch National Aerospace Laboratory NLR.

References

Balas, G.J., Doyle, J.C., Glover, K., Packard, A.K., Smith, R., (1990). $\mu-$Analysis and Synthesis Toolbox, (Musyn Toolbox). Matlab Functions for the Analysis and Design of Robust Control Systems. Sept, 1990.

Boyd S.P., Barratt C. (1991). *Linear Controller Design.* Prentice Hall, Englewood Cliffs.

Doyle, J.C., (1982). Analysis of Feedback Systems with Structured Uncertainty, *Proc. IEE,*, November, 1982.

Doyle, J.C., B.A. Francis, A. R. Tannenbaum, (1992). *Feedback Control Theory.* Macmillan.

Doyle, J.C., K. Glover, P. Khargonekar, and B.A. Francis, (1988). State-space Solutions to Standard H_2 and H_∞ Control Problems, *Proc. American Control Conf.*, Atlanta, GA, June, 1988.

Francis, B.A., (1987). *A Course in H_∞ Control Theory.* Lecture Notes Control and information Sciences, vol.88, Springer-Verlag Berlin, Heidelberg.

Jackson, M., Enns, D., (1990). "*Application of μ-Synthesis to a lateral control*" AIAA Conference on Guidance and Control.

Kaminer, I., Russel A. Benson, E. E. Coleman and Yaghoob S. Ebrahimi, (1990). "*Design of Integrated Pitch Axis for Autopilot/Autothrottle and Integrated Lateral Axis Autopilot/Yaw Damper for NASA TSRV Airplane Using Integral LQG Methodology*" NASA-CR-4268.

Packard, A., (1988). "What's new with μ". Ph.D. Thesis, Mechanical Engineering, University of California, Berkeley.

Maciejowski, J., (1989). Multivariable Feedback Design, Addison Wesley, 1989.

Morton, B. G., R. M. McAfoos, (1985). "A Mu-Test For Robustness Analysis of a Real-Parameter Variation", ACC proceedings, 1985.

Stein, G., Doyle, J.C., (1990). " Beyond Singular Values and Loop Shapes, " *A.I.A.A. Journal of Guidance and Control.*, **14**, 5-16.

Tjee, R.T.H., Mulder, J.A., (1988). Stability and Control Derivatives of the De Havilland DHC-2 'Beaver' aircraft. *Technical report LR-556*, Faculty of Aerospace Eng., Delft University of Technology, Aug 1988.

Selected Topics in Identification, Modelling and Control
Vol. 6, December 1993

Digital H_∞ controller implementation on mechanical servo systems using a DSP

Paul F. Lambrechts

Mechanical Engineering Systems and Control Group
Delft University of Technology, Mekelweg 2, 2628 CD Delft, The Netherlands.

Abstract. Recent developments in both control theory and electronical hardware provide new approaches for the solution of mechanical servo problems. The so-called 'standard plant' approach combined with H_∞ optimization theory is a method to find linear controllers that are robust and multivariable and may be used for many specific problems. However, using a detailed linear plant model, especially in combination with frequency dependent weight functions, will result in high order controllers. Implementing such controllers puts high demands on the controller hardware: mechanical servo systems often exhibit non-neglectable high frequency effects, that necessitate high sampling rates for digital controller implementation to be possible. This combination of controller complexity and high sampling rates, combined with the need for fast multivariable communication with the plant (for instance A/D and D/A conversions for measurement signals and actuator commands) can be attained by making use of a Digital Signal Processor (DSP). This paper describes the use of the TMS320C25-based control implementation environment produced by dSPACE GmbH for implementation of H_∞ controllers on two experimental setups available at the Delft Mechanical Engineering Systems and Control Group; the inverted pendulum and the three-degrees-of-freedom hydraulic positioning table. It is shown that the combination of powerful control theory and a fast, user-friendly implementation environment enables the control engineer to design high performance robust controllers.

1 Introduction

Two main problems in the practical application of modern control techniques are robustness of the closed loop system and implementation of complex controllers. The robustness problem appeared as a result of letting the controller rely on more complex plant models without accounting for the fact that even the most complex model is only an approximation of reality. Furthermore, the state-space, time-domain approach of modern control theory seemed incompatible with known 'classical' results based on frequency domain considerations (like gain and phase margins). The implementation problem was especially apparent in mechanical servo systems: although models are usually reasonably accurate, they often contain badly damped high frequency modes that should be suppressed. This then implies that controllers must be accurate up to relatively high frequencies, such that high sampling rates are necessary. Hardware solutions are mostly possible, but until the development of flexible and powerful processors like the Digital Signal Processor, or DSP, it was very hard to design and tune complex controllers.

The introduction of H_∞ control theory by Zames in 1981 was done from a highly theoretical and mathematical point of view, and it took several years to find that this concept connects very well with classical frequency domain considerations. The interpretation of frequency dependent singular values as a multivariable equivalent of gain was already known, and H_∞ theory provides a means

to shape this gain according to the wishes of the control designer: this makes it possible to improve robustness using gain margins. The first solutions to H_∞ control problems were based on an operator theoretic approach, as for instance explained by Francis (1987). They had the practical disadvantages of a complex numerical calculation and resulted in controllers of an extremely high order (ten times the order of the plant was no exception). Recently it was found that H_∞ problems can be solved as a modified LQG problem, resulting in a much simpler, more reliable numerical calculation and controllers that have the same order as the plant (Doyle and Glover, 1989). This then focuses the attention on problem formulation rather than on solution: using a general 'standard plant' framework the control designer should specify the desired result. This mostly involves the selection and/or definition of disturbance inputs, control objective functions (error signals) and weight functions, which provides a multivariable way to tune the resulting controller.

The process of tuning a multivariable controller implies that it is necessary to have a very short design-implementation cycle: based on the actual performance of the controller, the weight functions must be adjusted, after which a new controller can be calculated and implemented. Besides making use of a fast and flexible processor, it is therefore also desirable to have an implementation environment in which this entire cycle can be performed quickly and user-friendly. Although many implementation environments for DSPs are now commercially available, they are usually aimed at producing efficient code for maximal speed and necessitate low-level programming.

As we are interested in the possibilities of application of H_∞ control theory on the experimental setups available at our laboratory, for instance the inverted pendulum and the hydraulic positioning system discussed in this paper, and because for most mechanical servo problems the calculation speed of the DSP is more than sufficient, we chose the implementation environment produced by dSPACE. This provides very high-level programming possibilities, such as a direct link to PCMatLab, which enable design-implementation cycles of less than 15 minutes (for specification of new weight functions, calculation of H_∞ controller and implementation).

The next section will give a very short introduction to the standard plant approach, the interpretation of weight functions and H_∞ theory. After that, a description of the main properties of the dSPACE implementation environment will follow in section 3. Some of the results obtained by application of H_∞ controllers on the inverted pendulum setup are in section 4, followed by the results of the hydraulic positioning system in section 5. Finally some conclusions will be given in section 6.

2 The standard plant approach and H_∞ theory

The general framework used in H_∞ theory is given in figure 1. Here P is the standard plant, containing the combination of a model of the system to be controlled and several weight functions, K is the controller, z is a vector of control objectives—usually error signals—that are to be minimized, y is a vector of measurement signals, w a vector of external disturbances and u a vector of control inputs. The auxiliary signals v_1 and v_2 are added to be able to test internal stability of the closed loop system: if for any bounded v_1, v_2 and w the signals u, y and z remain bounded, the closed loop system is said to be internally stable.

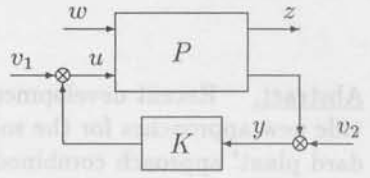

Fig. 1: The general framework for H_∞ control system design

Many control problems can be brought into this form; the control objective is to find a controller K that minimizes the transfer from w to z in some sense. We will assume that P and K are linear time invariant (LTI) systems that can be described by a finite dimensional state-space model or a real-rational transfer function matrix. A specific control design problem can be accommodated by extending the model of the physical system to be controlled, available in P, with structural properties and weight functions. The choice of this structure and the weight functions greatly influences the result of H_∞ analysis and synthesis and should therefore be set up by the control engineer who has a thorough knowledge of the control problem at hand.

In standard H_∞ problems the transfer from w to z is minimized in the sense of the infinity-norm, when searching over all allowable (i.e. internally stabilizing and real-rational) controllers:

$$\min_{K \text{allowable}} \|P_{wz} + P_{uz}(I - KP_{uy})^{-1}KP_{wy}\|_\infty \qquad (1)$$

with

$$\begin{aligned} \|P\|_\infty &= \sup_\omega \bar{\sigma}(P(j\omega)) \\ &= \sup_\omega \sqrt{\bar{\lambda}(P(j\omega)P(j\omega)^*)} \end{aligned} \quad (2)$$

$\bar{\sigma}(P(j\omega))$ denotes the largest singular value of $P(j\omega)$ and $\bar{\lambda}(P(j\omega))$ denotes its largest eigenvalue; $P(j\omega)^*$ denotes the complex conjugate transpose of $P(j\omega)$. In the case that w and z are scalar, the infinity-norm can be interpreted as a maximum power amplification factor for sinusoid signals (i.e. the peak value of the frequency response or Bode-magnitude plot), and can thus be related to the classical concept of gain.

The importance of the selection of weight functions has already been mentioned. The nature of the H_∞ design is such that a controller is synthesized in one single calculation, resulting in a trade-off between all specified signals and weight functions. It is therefore important that all available signals are made comparable with each other, for instance by scaling them in such a way that their values are expected to be between -1 and 1. The scaling factors necessary for this can be seen as weights and can be modified to put more or less emphasis on the effect of a particular signal on the resulting controller. By making these factors frequency dependent it is also possible to put emphasis on a specific frequency range of a signal: for instance if a disturbance signal has a known spectrum it is possible to use a real-rational approximation of this spectrum as a weight function. Examples of the use of weight functions can be found in sections 4 and 5.

3 The dSPACE implementation environment

As mentioned before, our intention to design and implement H_∞ controllers makes it very desirable to have an implementation environment that allows controllers calculated with PC MatLab or similar high level matrix calculation tools to be implemented quickly and efficiently without having to write low-level programming code. One of the very few DSP-based commercially available solutions for this is produced by dSPACE GmbH as the 'DSP-CITpro Control Implementation Tool'. The hardware is supplied as add-on cards for the IBM compatible PC and is built around a DSP of the Texas Instruments TMS320 line.

The main processor board (dSPACE type nr. DS1001) that was used for the experimental setups discussed in the next two paragraphs contains a fixed-point 40MHz TMS320C25 DSP with a 100ns cycle time and a 16 x 16 bit hardware multiplier for single cycle multiplication and accumulation. Communication with this processor is possible from the PC (acting as host system) via the 16-bit AT bus of the PC; programs can be downloaded to the DSP and during program execution 4K words of 16-bit true dual-port RAM is available for monitoring key variables (simultaneous DSP- and host-access). Further memory available to the DSP is 64K words of program memory and 59K words of data memory, both accessible with zero wait states and with DSP- and host-access arbitration.

The interaction with the experimental setup is performed by means of A/D and D/A converters: two DS2001 boards containing 5 A/D converters each and one DS2101 board with 5 D/A converters. Communication between processor board and interface boards is performed via the PHS-bus (Peripheral High Speed bus), a 32-bit synchronous I/O-bus with 13.3 MB/s peak transfer rate; this allows the digital controller to run completely independent of the PC. The DS2001 A/D boards each contain 5 fully parallel 16-bit A/D converters with $5\mu s$ conversion time, 14-bit linearity (typical) and Sample and Hold circuits (tracking and hold); A/D conversions can be started separately or simultaneously and ADC ready may be signalled via interrupt or flag. The DS2101 board contains 5 12-bit D/A converters with $3\mu s$ full scale settling time to 0.01%.

Equally essential to the usefulness of this control implementation environment is the implementation software package IMPAC, consisting of the Implementation Expert module IMPEX combined with the high level programming language DSPL. IMPEX is a menu-driven programming tool, independent of specific target hardware, allowing the setting up of any linear time-invariant controller. The controller parameters should be available in state-space form and given in an ASCII-file according to a prespecified format. Utilities to interface with PC MatLab are available to automatically create this file, such that any control design algorithm implemented in MatLab can be used to create a state-space controller and prepare it for IMPEX.

In general, such a controller will be continuous time and in an arbitrary state-space realization; IMPEX provides tools to convert this into a description suitable for implementation in the digital fixed-point TMS320C25 processor. First the controller may be discretized either step-invariant, ramp-invariant or bilinear, according to specific requirements. Next a transformation may be performed to reduce the number of controller parameters, the number of calculations and—most importantly—the coefficient sensitivity for instance

with respect to quantization effects. Thirdly it is possible to perform automatic or user-specified scaling of variables (input, output and state variables) to user-defined ranges; because the standard-plant approach usually makes sure that inputs and outputs are correctly scaled, this is especially important for (internal) state variables when using a fixed-point processor. The final step then is automatic code generation based on this discretized, transformed and scaled state-space model, first setting up the high level language code DSPL, followed by the compilation into TMS320C25 target processor assembly source code; after that, assembling and down-loading of object code will complete the automated implementation procedure.

Disadvantages of such a highly automated implementation procedure are of course restrictiveness of useable hardware (dSPACE products) and implementable controllers (linear time-invariant). However, it is possible to extend IMPEX with templates and drivers for user defined interface hardware or even completely different TMS320C25-based processor boards. Furthermore, IMPEX provides very well documented ASCII files of the DSPL-code and the assembly source code generated. These files can then be used as shell-files that allow a programmer to add non-linear relations, limitations, gain scheduling, start up sequences, etc. Clearly this implies a large programming effort of the user; in most cases it is sufficient to make changes to the DSPL-code, which can be seen as a high-level programming language that was tailor-made for every TMS320 processor. Only if time optimality is necessary, it may be useful to get into programming assembly code: to give an impression, a 12th order, 9 inputs, 3 outputs state-space controller for the hydraulic positioning system was automatically implemented with a calculation time of 75μs, giving a processor load of only 7.5% at the more than sufficient sampling rate of 1kHz.

This then sums up the most essential parts of the implementation environment used to obtain the results in the following sections. The extremely fast developments in this area of hardware and software, however, have already surpassed this in several respects.

- TMS320C30 and TMS320C40-based processor boards provide single-cycle floating-point multiplication/accumulation and many other improvements.
- Instead of DSPL-code it is possible to use C, which can be written by the user or automatically generated from several block oriented simulation languages: there is a direct collaboration between the manufacturers of MatLab/SimuLink and dSPACE to develop a fully automated procedure for implementation of non-linear controllers.
- Options for multiprocessing with DSPs are being developed, etc.

4 The inverted pendulum

The main parts of the inverted pendulum setup are shown in figure 2. The pendulum itself is a hollow

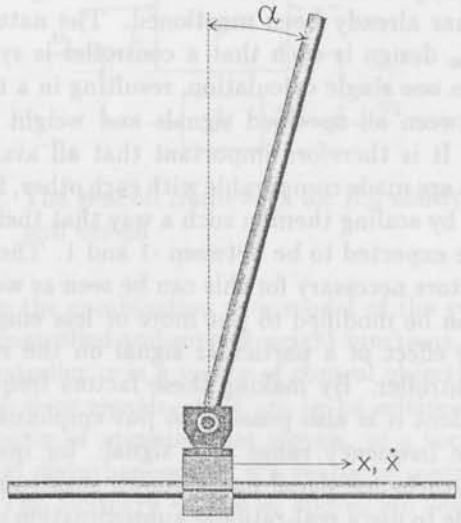

Fig. 2: The inverted pendulum setup

steel bar, weighing about 0.6 kg; it is 57 cm long, measured from rotationpoint to tip. The pendulum is connected to a cart by low friction roller bearings, giving the pendulum one degree of freedom, i.e. one rotation in the vertical plane. By means of two rubber cylinders the angular deviation from the vertical direction is limited to 15 degrees on each side. The aluminium cart can move along solid steel guiding-bars, also using roller bearings. The effective range of the cart is limited to about 1 meter. A toothed belt connected to the bottom side of the cart provides slip-free traction. The drive train consists of this toothed belt, two toothed wheels and a servomotor. The toothed belt is very stiff in longitudinal direction, but not in transversal direction. This implies that by adjusting the internal tension of the belt a trade-off must be found between the occurrence of low frequency vibrations in transversal direction and friction at the toothed wheels and the cart bearings.

This trade-off resulted in a considerable amount of (dry) friction in cart bearings and drive train,

which must be considered in the controller design. The control problem therefore was to design a controller that stabilizes the pendulum, tracks a reference signal for the cart position, attenuates torque disturbances on the pendulum and is robust against the occurrence of friction. To solve this problem the standard plant given in figure 3 was set up. The ac-

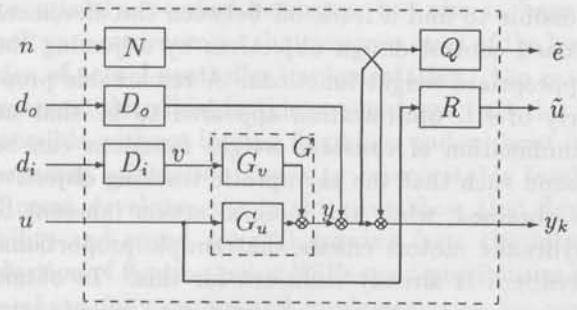

Fig. 3: Standard plant for inverted pendulum controller design

tual plant model is given as G: the combination of G_u, the transfer from control input u to measured variables y, and G_v, the transfer from disturbance inputs v to y. The vector v consists of two signals: one representing a torque disturbance on the pendulum, the other a disturbance force on the cart; the latter can be used to account for the dry friction effect in the drive train (see van der Linden (1991), and van der Linden and Lambrechts (1992,1993)).

The measured variables are pendulum angle, cart position and cart velocity; all these signals are affected by measurement noise represented by n with weight function N and result in measurements y_k that are available to the controller. Disturbance d_o with weight function D_o represent a reference signal for the cart position to accommodate the tracking demand; disturbance d_i with weight function D_i determines the effect of v on the design. The error signals $\tilde{e}$ with weight function Q are to be minimized in combination with the actuator effort $\tilde{u}$ with weight function R. In comparison with figure 1 we thus find:

$$P = \begin{bmatrix} P_{wz} & P_{uz} \\ P_{wy} & P_{uy} \end{bmatrix} = \left[\begin{array}{ccc|c} 0 & QD_o & QG_vD_i & QG_u \\ 0 & 0 & 0 & R \\ \hline N & D_o & G_vD_i & G_u \end{array}\right] \quad (3)$$

With this standard plant we are now able to completely specify a trade-off between the various control design objectives mentioned before. For instance we may design a controller without taking the effect of dry friction into account by specifying a small value for the appropriate entry of D_i. Although the resulting controller performed very well on a linear model in simulations, a limit-cycle with an amplitude of 10 cm occurs when dry friction in the cart bearings is taken into account (figure 4) and the actual implementation appeared to be unstable. This implies that it is indeed necessary to

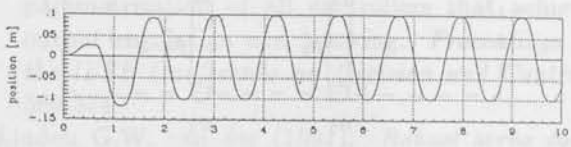

Fig. 4: Simulated limit-cycle of inverted pendulum with non-robust controller

specify a larger, more realistic value for the dry friction effect, which resulted in a controller with good performance in all respects and a limit-cycle with an amplitude of 1 mm in non-linear simulations and of 5 mm in actual implementation (figure 5): the remaining difference is probably due to unmodelled dry friction and backlash in the pendulum bearings. Note that we thus have found a linear controller us-

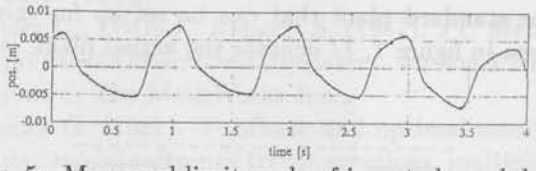

Fig. 5: Measured limit-cycle of inverted pendulum with robust controller

ing a linear control design method that is able to effectively attenuate the effect of a highly non-linear disturbance. For more information on these results see van der Linden (1991) and van der Linden and Lambrechts (1992,1993). .

5 The hydraulic positioning system

The hydraulic positioning system is given in figure 9; it consists of a steel block weighing 48 kg, supported by an air bearing on a steel table. The air bearing permits frictionless motion in the horizontal plane, allowing three degrees of freedom. Three asymmetrical hydraulic motors are attached to block and table according to the diagram in figure 6. Each motor is fitted with a linear displacement potentiometer and a piezoresistive pressure transducer (absolute pressure in first compartment of motor). The motors are actuated by means of two-stage electro-hydraulic servo valves based on a dry torque motor and a nozzle-flapper pilot stage.

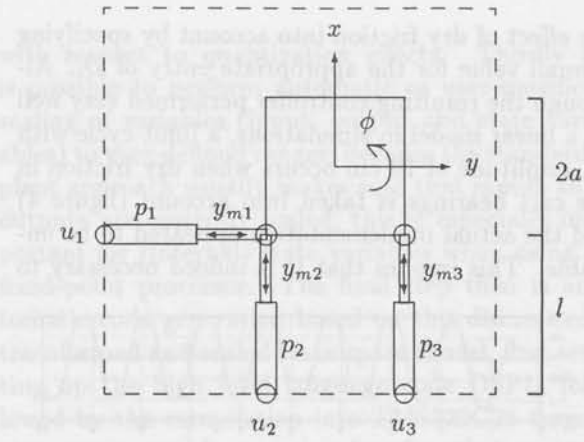

Fig. 6: Schematic representation of the hydraulic positioning system

The control problem for this setup was to find a controller with an (H_∞-) optimal trade-off between tracking performance, actuator effort, measurement noise and actuator noise. In comparison with the inverted pendulum design, also *asymptotic* tracking of position reference signals was desired. The standard plant that can be set up for this is given in figure 7. G denotes the actual plant, with

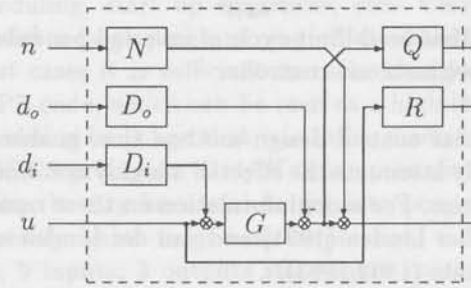

Fig. 7: Standard plant for hydraulic system controller design

control input vector u that is disturbed by actuator noise d_i acting through weight function D_i. The tracking objective is again accommodated by adding disturbance d_o and weight function D_o; measurement noise is given as n with weight function N. Objective functions to be minimized are the three position error signals given in $\tilde{e}$ and weighted by Q and the three actuator efforts $\tilde{u}$ after application of R. The measurement signals available to the controller are the three position error signals and the three pressure signals. The resulting standard plant can thus be given as:

$$P = \begin{bmatrix} P_{wz} & P_{uz} \\ P_{wy} & P_{uy} \end{bmatrix} = \left[\begin{array}{ccc|c} 0 & QD_o & QGD_i & QG \\ 0 & 0 & 0 & R \\ \hline N & D_o & GD_i & G \end{array}\right] \quad (4)$$

As in the case of the inverted pendulum, it is now possible to find a trade-off between the aforementioned control design objectives by adjusting the appropriate weight functions. A remarkable property of H_∞ optimization appeared to be that no combination of *constant* weight functions can be found such that the asymptotic tracking objective is obtained, while the integral action inherent to hydraulic motors ensure that simple proportional feedback is already sufficient for this. To obtain asymptotic tracking it is necessary to include integral action in weight function D_o, such that steady state errors result in constantly growing errors in $\tilde{e}$ (see Lambrechts and Bosgra (1991) for the general solution of this problem). With this restriction it again appeared to be possible to adjust the properties of the controlled system by means of the available weight functions. The x-direction step response of a solution with bandwidth above the hydraulic frequency, reasonable damping and asymptotic tracking is given in figure 8; step responses in other directions are similar. For a more extensive

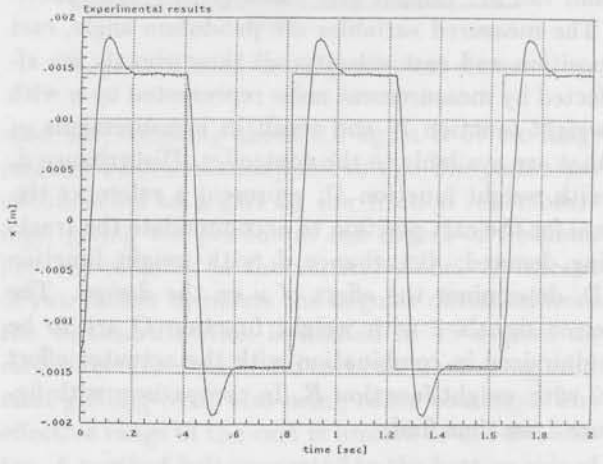

Fig. 8: x-direction step response of the hydraulic positioning system

discussion of these results see de Bruyne (1992).

6 Conclusions

Digital Signal Processor based control implementation hardware is suitable for implementation of sophisticated complex controllers for most mechanical servo control problems at sampling rates that

are extremely high. Especially for the design of multivariable controllers a single-processor solution is preferable; considering the performance of DSPs it is often unnecessary to resort to multiprocessing solutions. When one is interested in control design rather than control implementation environment design, it is not only necessary to obtain appropriately specified hardware, but also to have a software environment that removes most of the burden of actual controller implementation. The environment described in this paper shows that this is possible without loosing flexibility and without increasing calculation times to unacceptable levels. Recent developments in this area show that flexibility and speed are still growing fast: the introduction of floating point DSPs open possibilities to perform fully automated implementation for nonlinear controllers.

The advantage of automated controller implementation becomes especially clear when looking at the design examples. Modern control theory that only recently has reached the level of numerical solvability (matlababability) can quickly be tested on its practical use. Instead of bothering with hardware issues and programming low-level code, it is possible to concentrate on the setting up of a standard plant and the selection of weight functions; the implementation cycle time becomes short enough to tune the controller on the actual plant. On the other hand it is also possible to develop new methods or even theoretical concepts using an actual test setup instead of simulations.

Acknowledgements

The author wishes to thank Gert Wim van der Linden for his work on the inverted pendulum and Franky de Bruyne for his work on the hydraulic positioning system. The results given in this paper are taken from their respective graduation projects, performed at the Mechanical Engineering Systems and Control Group of the Delft University of Technology

References

DSP-CITPro (1989). *IMPEX user's guide.* document version 3.0, dSPACE GmbH, Paderborn, Germany,

Bruyne F. de (1992). *Robust servo control of a hydraulic positioning system with three degrees of freedom.* TU Delft, Mechanical Engineering Systems and Control Group, Université Catholique de Louvain, Faculté des Sciences Appliquées., Unité AUTO, ELEC 23,

Doyle J.C., Glover K., Khargonekar P.P., Francis B.A. (1989). State space solutions to standard H_2 and H_∞ control problems. *IEEE Transactions on Automatic Control, vol.34, no.8,* 831-847.

Francis B.A. (1987). *A course in H-infinity control theory.* Lecture Notes in Control and Information Sciences, vol.88, Springer Verlag, Berlin,

Lambrechts P.F., Bosgra O.H. (1991). The parametrization of all controllers that achieve output regulation and tracking. *Proceedings of the IEEE Conference on Decision and Control,* 569-574

Linden G.W. van der (1991). *Robust servo control; application to an inverted pendulum.* TU Delft, Mechanical Engineering Systems and Control Group, report nr. A-547, .

Linden G.W. van der, Lambrechts P.F. (1992). H_∞ control of an experimental inverted pendulum with dry friction. *Proceedings of the IEEE Conference on Control Applications,* 123-128.

Linden G.W. van der, Lambrechts P.F. (1993). H_∞ control of an experimental inverted pendulum with dry friction. *IEEE Control Systems, vol.13, no.4,* 44-50.

Moler C., Little J., Bangert S. (1987). *PC MatLab for MS-DOS personal computers.* version 3.2-PC, june 8, The MathWorks Inc.,

Zames G. (1981). Feedback and optimal sensitivity: model reference transformations, multiplicative seminorms, and approximate inverses. *IEEE Transactions on Automatic Control, vol.AC-26, no.2,* 301-320.

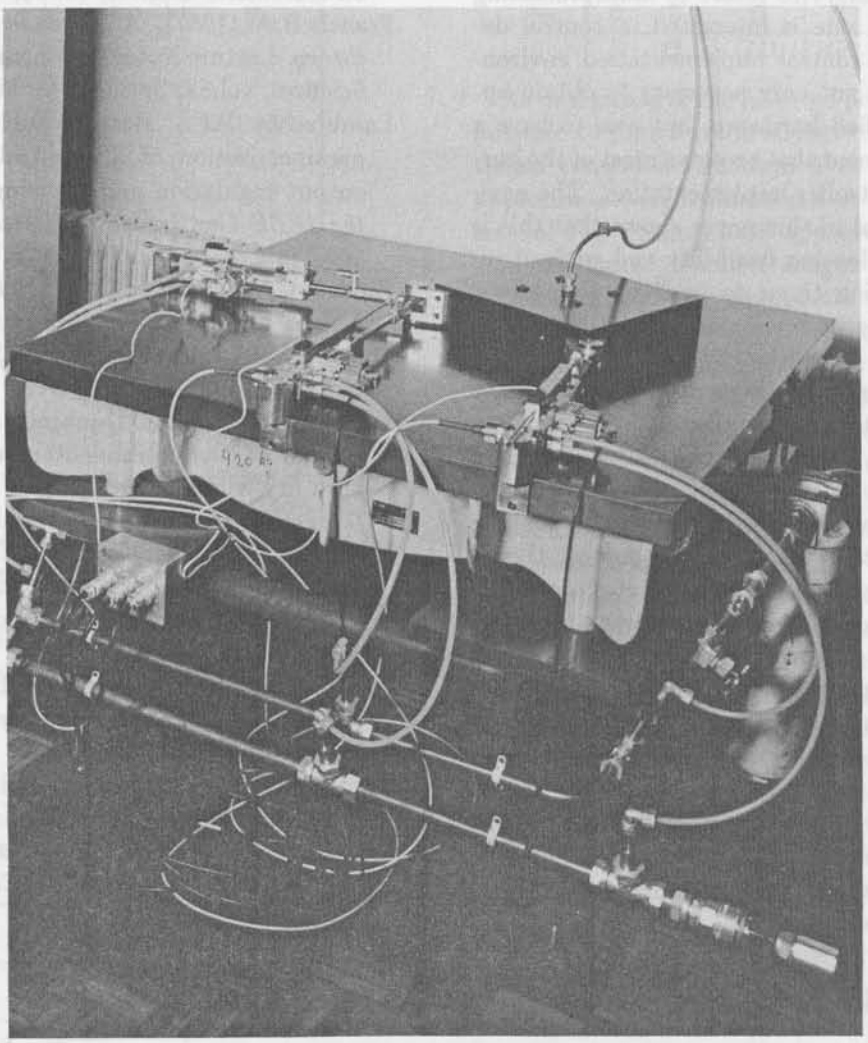

Fig. 9: The hydraulic positioning system

Selected Topics in Identification, Modelling and Control
Vol. 6, December 1993

Modeling and control of an industrial hydraulic rotary vane actuator[‡]

J. Heintze , G. v. Schothorst , A.J.J. v.d. Weiden and P.C. Teerhuis

Mechanical Engineering Systems and Control Group
Delft University of Technology, Mekelweg 2, 2628 CD Delft, The Netherlands.

Abstract. In some high performance robot applications, the use of hydraulic rotary vane actuators is preferred. The use of such (industrial) actuators mostly involves the introduction of Coulomb friction due to seals. Besides that, the connections between the actuators and the loads are often flexible. Paying attention to these phenomena during the modeling of such an actuator, results in reliable linear and nonlinear models, which are very useful for control design (linear model) and for testing of the designed controllers (nonlinear model). Implementation of the designed controllers in practice proves the validity of the followed approach.

Keywords. hydraulic rotary servo system, modeling, control design, Coulomb friction, flexible load connection.

1 Introduction

Contrary to electrical actuators, hydraulic actuators are not very common in high performance robotic applications. However, especially in applications where big loads have to be handled and where available space for construction is rare, hydraulic actuators are favorable due to their excellent rate of dimension to delivered torque. This makes hydraulic servo actuators also very suitable for direct drive applications, especially when they are provided with hydrostatic bearings, so that Coulomb friction is eliminated (Viersma, T.J. (1990)). For linear actuators, this bearing technique is widely used, but rotary actuators are not industrially available with such bearings, which implies that they contain a considerable amount of Coulomb friction. Furthermore implies the application of a rotary actuator the use of a connection shaft to the load, which in general can not be expected to be stiff, contrary to applications with linear actuators. The above mentioned phenomena (Coulomb friction and flexible shaft) have been observed from some rotary actuators, applied in a SCARA bricklaying robot as designed and developed in our laboratory (Paap, V.W. (1990)). As it is expected that the overall performance of this robot highly depends on the performance of the single actuators, we will focus on one such a rotary actuator.

The objective is to realize a controller for a hydraulic rotary vane actuator, by which a high performance is achieved, with regard to the bandwidth as well as to the positioning accuracy at low frequencies. We present an integral approach of modeling an actuator, model based control design, closed loop analysis on simulation level and experimental evaluation of results. Besides the standard actuator dynamics, we are especially focussing on the influence of Coulomb friction and flexible load connection onto the controlled system behavior.

Hydraulic components have been studied already for many years, also in view of control design or evaluation. A standard linearized third order

[‡]This paper is also presented at the 32nd IEEE Conference on Decision and Control, San Antonio, Texas, USA, December 15-17, 1993. Copyright of this paper remains with IEEE.

structure for an actuator is widely spread (Merrit, H.E. (1967), Viersma, T.J. (1990), Walters, R.B. (1991)). Known extensions include: two extra orders for the valve dynamics (e.g. Feuser, A. Von (1984), Köckemann, A., Konertz, J. and Lausch, H. (1991)); the flexible connection between actuator and load (Wierschem, T. Von (1981), Neumann, R., Engelke, W. and Moritz, W. (1991a), Neumann, R., Engelke, W. and Moritz, W. (1991b), Izawa, K. and Nakayama, Y. (1991)); and the incorporation of Coulomb friction (Köckemann, A., Konertz, J. and Lausch, H. (1991), Yun, J.S. and Cho, H.S. (1991)). In most of these studies, an experimental validation of the theoretical model is incorporated. Another way to obtain usable models is the application of standard system identification techniques (Shih, M.-C. and Chen, C.-K. (1991)).

The step which is often neglected, is to address the flexible load connection and the Coulomb friction explicitly in the system identification procedure and in the control design and analysis.

In section 2 we present an on physical relationships based model and the subsequently linearized state space model. Correct parameters for the model have been found by means of identification techniques applied on experimentally obtained data, as is shortly addressed in section 3. In section 4 the control design based on the linear model and the closed loop analysis with the use of the nonlinear model is discussed. Results of the application of the designed controllers in practice are given in section 5.

2 The modeling of a hydraulic actuator

In principle, a hydraulic actuator consists of two oil compartments, separated by a movable part. In the case of the rotary actuator, this part is the vane, which is connected to the output shaft. See figure 1. The oil flows into and out of the compartments are provided by a valve, which is the regulating element. A constant valve opening will result in a constant oil flow which will generate a rotation of constant speed. This explains the basic integrating behavior of a hydraulic actuator. Because the oil in the two compartments is compressible, the two oil columns will act as two springs. Via the vane the load is clamped between these 'springs'. This causes the second order behavior, which is always found in series with the integrating character of a hydraulic actuator.

We will examine a symmetrical rotary actuator with a symmetrical critical-center valve. For this

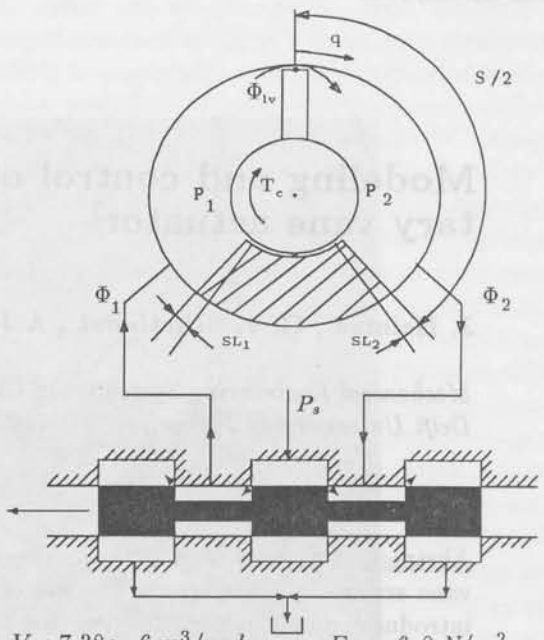

$V_r : 7.38e{-}6\ m^3/rad$ $\quad E : \approx 6e8\ N/m^2$
$S : 4.88\ rad$ $\quad J_l : 1\ kg.m^2$
$P_s : 1.4e7\ N/m^2$ $\quad T_c : 4\ Nm$
$C : 2.52e{-}6\ m^4/A\sqrt{N}s$ $\quad c_t : 1.3e4\ Nm/rad$

Natural frequency actuator: $\approx$ 7 Hz
Bandwidth valve: $\approx$ 200 Hz

Fig. 1: Schematic drawing of a rotary vane actuator with 4-way valve.

actuator, the above-mentioned dynamics are described by a number of theoretical relations.

The equations of continuity for both the compartments are:

$$\dot{P}_1 = E\frac{\Phi_1 - \Phi_{lv} - \dot{q}_a V_r}{V_r\left(\frac{S}{2}+q_a+SL_1\right)}$$
$$\dot{P}_2 = E\frac{-\Phi_2 + \Phi_{lv} + \dot{q}_a V_r}{V_r\left(\frac{S}{2}-q_a+SL_2\right)} \qquad (1)$$

with:
- P_j pressure in compartment j $[N/m^2]$, the dot means the time derivative
- E bulkmodulus of oil $[N/m^2]$
- Φ_j oil flow to compartment j $[m^3/s]$
- Φ_{lv} leakage flow across the vane $[m^3/s]$
- q_a actuator position $[rad]$
- V_r actuator volume per radian $[m^3/rad]$
- S total stroke $[rad]$
- SL_j ineffective stroke of compartment j $[rad]$

Because the bandwidth of the valve is well beyond that of the actuator, the valve dynamics were neglected. Furthermore assuming turbulent flow through the valve, the oil flows can be described

by:

$$\Phi_1 = \frac{i+|i|}{2} C\sqrt{P_s - P_1} + \frac{i-|i|}{2} C\sqrt{P_1}$$
$$\Phi_2 = \frac{i-|i|}{2} C\sqrt{P_s - P_2} + \frac{i+|i|}{2} C\sqrt{P_2} \quad (2)$$

with: i control signal $[A]$ (valve steering current)
C valve constant $[m^4/A\sqrt{N}s]$
P_s supply pressure $[N/m^2]$

For the leakage across the vane a laminar flow is assumed, giving the equation:

$$\Phi_{lv} = LPV\,(P_1 - P_2) \quad (3)$$

with LPV the leakage parameter $[m^5/Ns]$.

When the shaft which connects the load to the actuator is modeled as a torsional spring, the following two equations of motion for the 'load system' (one for the load and one for the actuator shaft) are obtained:

$$\ddot{q}_l = \frac{c_t}{J_l}(q_a - q_l) \quad (4)$$

$$\ddot{q}_a = \frac{V_r}{J_a}(P_1 - P_2) - \frac{w}{J_a}\dot{q}_a - \frac{c_t}{J_a}(q_a - q_l) + \frac{T_c}{J_a} \quad (5)$$

with: q_l position of the load $[rad]$
J_l inertia of the load $[kgm^2]$
J_a inertia of the actuator shaft $[kgm^2]$
c_t torsion stiffness of the connection shaft $[Nm/rad]$
w viscous friction coefficient $[Nms]$
T_c Coulomb friction and/or stiction torque $[Nm]$

The friction torque T_c is modeled as a constant torque during movement (opposing the movement), and a varying 'stiction torque' during standstill, similar as described in e.g. Southward, S.C., Radcliffe, C.J. and MacCluer, C.R. (1991).

Linearizing the nonlinear model

To be able to apply linear control design techniques, we have to linearize the model. Under the assumption that the mean pressure in each compartment is $\frac{1}{2}P_s$, only the pressure difference Δ_p across the vane is required to describe the dynamics of the pressures (P_1 and P_2 do not constitute two independent states). This leads to the reduction of the model order by one state, and moreover it implies that only a pressure difference transducer is required for the identification of the system dynamics from the experimental setup (section 3), instead of two absolute pressure transducers. Noting furthermore that besides the pressure difference transducer, a position transducer is mounted to the actuator shaft (so the position of the actuator and not that of the load is measured) in the given experimental setup, the equations (1) - (5) can be brought into a fifth order state space model of the following structure:

$$\begin{pmatrix} \dot{q}_l \\ \ddot{q}_l \\ \dot{q}_a \\ \ddot{q}_a \\ \dot{\Delta}_p \end{pmatrix} = \begin{bmatrix} 0 & 1 & 0 & 0 & 0 \\ -\theta_1 & 0 & \theta_1 & 0 & 0 \\ 0 & 0 & 0 & 1 & 0 \\ \theta_2 & 0 & -\theta_2 & \theta_3 & \theta_4 \\ 0 & 0 & 0 & \theta_5 & \theta_6 \end{bmatrix} \begin{pmatrix} q_l \\ \dot{q}_l \\ q_a \\ \dot{q}_a \\ \Delta_p \end{pmatrix} + \begin{bmatrix} 0 \\ 0 \\ 0 \\ 0 \\ \theta_7 \end{bmatrix} i \quad (6)$$

$$\begin{pmatrix} q_a \\ \Delta_p \end{pmatrix} = \begin{bmatrix} 0 & 0 & 1 & 0 & 0 \\ 0 & 0 & 0 & 0 & 1 \end{bmatrix} \begin{pmatrix} q_l \\ \dot{q}_l \\ q_a \\ \dot{q}_a \\ \Delta_p \end{pmatrix}$$

This model has a (2×1) transfer function vector $G(j\omega)$, in which the two transfer functions $\frac{q_a(j\omega)}{i(j\omega)}$ and $\frac{\Delta_p(j\omega)}{i(j\omega)}$ are uniquely determined by the seven parameters $\theta_1, \ldots, \theta_7$. Note that the dynamics of the flexible shaft, together with the chosen output, introduce an imaginary pair of zeros in the open loop position transfer function $\frac{q_a(j\omega)}{i(j\omega)}$, as can be deduced from (6).

It should be remarked, that the parameters in this model in principle represent nonlinear effects, as they may vary with signal amplitudes and/or operation positions of the actuator. Three nonlinearities are incorporated in this structure.

First, there is the position dependence: the parameters $\theta_{5,6,7}$ vary with the position of the actuator. At some position as an operation point, these parameters are considered to be independent of the position.

Next, the parameters θ_3 and θ_6 vary with the signal amplitude in the frequency domain. Parameter θ_3 represents the friction, which includes the nonlinear (amplitude dependent) effect of the Coulomb friction. When Coulomb friction is neglected this parameter is constant. Parameter θ_6 represents the leakage, which includes the dependence of the valve flow on the pressure difference. Assuming that the valve flow only depends on the valve steering current i, this (amplitude dependent) nonlinearity is canceled.

Taking the constant parameters as mentioned here, a linear model with model structure (6) is obtained. For a more detailed treatment of the theoretical model and the linearization procedure we refer to Schothorst, G. van (1992).

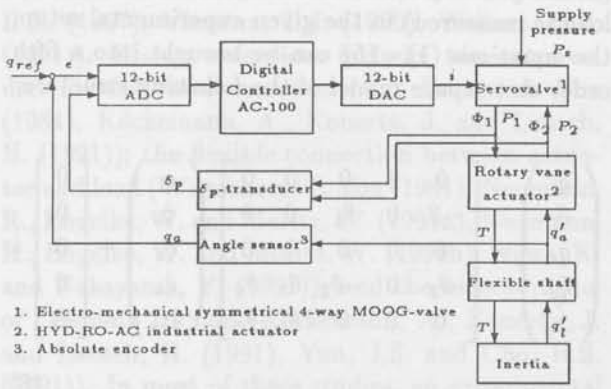

Fig. 2: Schematic drawing of the experimental setup.

Given this linear model structure, the model parameters can be estimated from experimental data by means of system identification techniques, as treated in the next section.

3 Experimental setup, parameter estimation and model validation

The experimental data, required for the parameter estimation and the model validation, were obtained with an experimental setup, which is schematically depicted in figure 2. With the use of a Hewlett Packard 3562A Dynamic Signal Analyzer, the open loop frequency response vector $G_m(j\omega)$ of this system was measured at several working points.

From one such a frequency measurement one parameter set $\theta_1, \ldots, \theta_7$ of model (6) was estimated by minimizing criterion (7):

$$J = \min_{\theta_1,\ldots,\theta_7} \sum_{k=1}^{N} \left(G_m(j\omega_k) - \hat{G}(j\omega_k) \right)^2 \qquad (7)$$

with: $\hat{G}(j\omega_k)$ estimated response at frequency point $j\omega_k$

N number of frequency points in $G_m(j\omega)$

The idea is to convert the estimated parameter set $\theta_1, \ldots, \theta_7$ back to the 'physical parameters' of the nonlinear model, given by equations (1) - (5). Due to the nonlinear properties of this model it is not possible to deduce all the physical parameters at once from one estimated parameter set.

Measurements and estimations at 3 different actuator positions q_a appeared to be imperative to discriminate between S, SL_1 and SL_2. For the friction parameter θ_3 there was a considerable amplitude dependency, while for θ_6 this dependency appeared to be negligible. Although it might be possible to separate the effects of viscous and Coulomb friction by studying the amplitude dependency, it appeared to be more accurate to estimate the friction parameters from time domain measurements, as Coulomb friction is a typical time domain phenomenon.

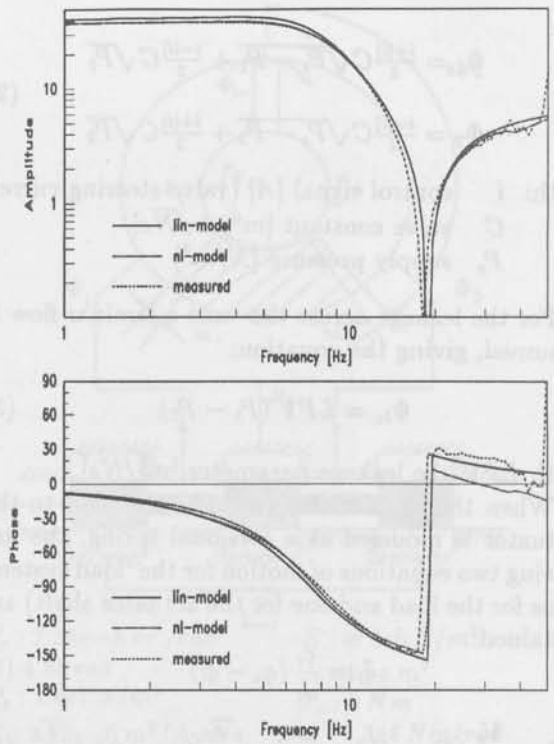

Fig. 3: Frequency response of the experimental actuator, the linear and nonlinear model, open loop transfer $\frac{\dot{q}_a(j\omega)}{i(j\omega)}$.

In figure 3 the frequency response of the linear and the nonlinear model and the measured frequency response of the open loop actuator (transfer $\frac{\dot{q}_a(j\omega)}{i(j\omega)}$) are compared. The typical dip in these responses at $\approx$ 17 Hz, which is characteristic for the imaginary pair of zeros in the transfer, was also very well observable during the measurement in practice: while the load oscillated at that frequency, the actuator did not move. Especially in the low frequency region the nonlinear model is a better description of the hydraulic actuator, due to the correct inclusion of the Coulomb friction. This observation was clearly confirmed by the model validation of time responses and of the phase plot of the open loop frequency response of the transfer $\frac{\Delta_p(j\omega)}{i(j\omega)}$. See Schothorst, G. van (1992) for a further examination

of this topic.

At this moment we can state that a satisfactory similarity between experimental and model responses is obtained, and that a reliable nonlinear model is available. The model allows physical interpretation of observed phenomena, which provides extra confidence in the model. Via a *linear* model structure and with standard optimization techniques, an effective procedure for the estimation of the parameters of the nonlinear model is developed. As a consequence, the linear model can be assumed to be a good approximation of the nonlinear system and will be suitable for linear control design techniques.

4 Control design

In common practice, the control of a hydraulic servo actuator consists of a position feedback for tracking, and mostly a pressure feedback to alter the amount of damping. However, this control is rather sensitive to Coulomb friction (causing tracking errors and static offset) due to the pressure feedback loop. Moreover, only a bandwidth of at most 7 Hz can be achieved, while a bandwidth of 12 Hz is desired. In order to achieve a higher performance we will design full order state feedback controllers, based on model (6).

The parameters used in this model are those estimated in section 3, except for one: the torsion stiffness of the flexible shaft is chosen somewhat smaller. In this way, the frequency of the zero of the system is in the same range as the desired bandwidth, so that the effect of the dynamics of the flexible shaft on the performance of the controlled system can be made clear.

From equation (6) it is clear that only Δ_p and q_a are being measured. To be able to feed back all states, a full order state estimator has been designed with the linear Kalman filter technique. The state and output noise intensity matrices which are required in this design procedure, acted as design parameters. Assuming the output noise on the Δ_p-signal to be large with respect to the q_a-signal, and assuming the state noise intensities to be related to the input noise resulted in a reasonable fast state estimator.

In order to realize the desired closed loop bandwidth, a pole-placement controller was designed. Hereby, we placed the three dominant 'actuator poles' on a circle of radius 75 in the complex plane. The remaining pair of almost imaginary poles due to the flexible shaft needed just some extra damping. For the theory of state estimation and state feedback respectively, see e.g. Chen, C.-T. (1984) and Anderson, B.D.O. and Moore, J.B. (1989).

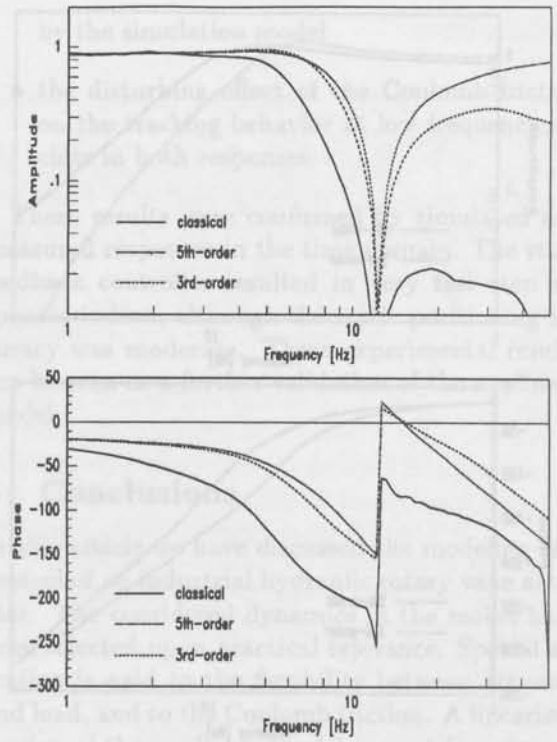

Fig. 4: Frequency response of nonlinear model, controlled by the fifth order, third order and classical controller, transfer $\frac{q_a(j\omega)}{q_{ref}(j\omega)}$.

Having obtained a satisfactory controller for the linearized model, we applied it to our nonlinear model. From these simulations we noted that: **1**] the gained dynamic performance in terms of closed loop bandwidth is not disturbed by the nonlinearities of the model, and **2**] the nonlinearities highly destroy the low-frequency tracking performance: instead of an amplitude gain of 1 in the linear case, a gain of c.a. 0.9 is found with the nonlinear model.

In order to investigate the benefit of full order state feedback, we designed a classical controller (feedback of q_a and Δ_p) and a partial state feedback plus estimator (feedback of q_a, $\dot{q}_a$ and Δ_P), based upon a model neglecting the flexible shaft dynamics. The closed loop frequency responses of the nonlinear model (transfer $\frac{q_a(j\omega)}{q_{ref}(j\omega)}$), controlled by the classical, the third order and the original fifth order controller are given in figure 4. Note that the dip in the amplitude plot is now located at $\approx$ 12 Hz instead of at $\approx$ 17 Hz. The following two remarks can be made:

- With respect to classical feedback, there is a

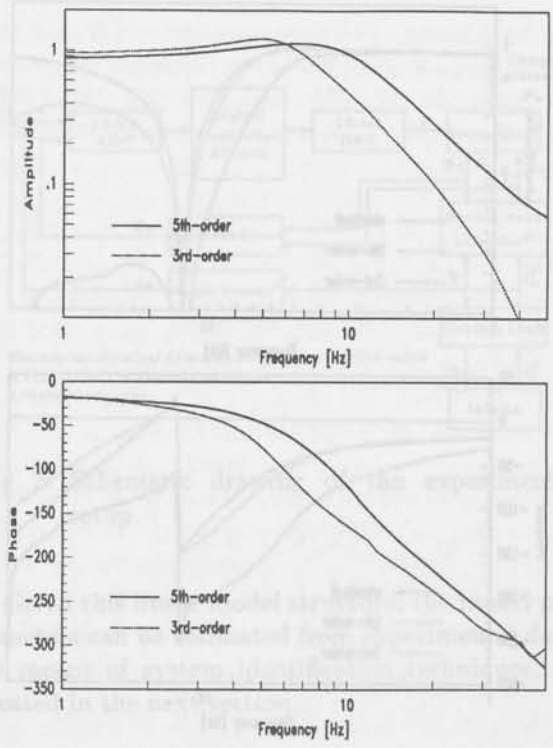

Fig. 5: Frequency response of nonlinear model, controlled by the fifth and third order controller, transfer $\frac{q_l(j\omega)}{q_{ref}(j\omega)}$.

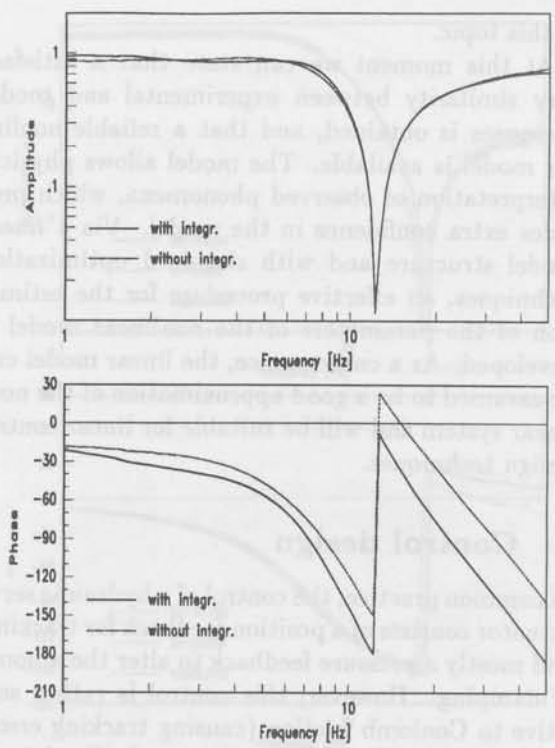

Fig. 6: Frequency response of nonlinear model, controlled by the fifth order controller with an additional integrator in the estimator, transfer $\frac{q_a(j\omega)}{q_{ref}(j\omega)}$.

considerable improvement of the bandwidth by means of state feedback. However, the aimed bandwidth of 12 Hz has not been achieved.

- The fifth order controller gives a higher bandwidth than the third order controller.

The fact that the required bandwidth is not achieved, despite the poles were placed on their desired locations, is clearly caused by the location of the zeros: they are limiting the achievable bandwidth in the transfer $\frac{q_a(j\omega)}{q_{ref}(j\omega)}$. However, while one is often interested in the positioning of the load, it may be better to look at the transfer $\frac{q_l(j\omega)}{q_{ref}(j\omega)}$. It can be seen from the linear model that no zeros are present in this transfer. And indeed, the closed loop frequency responses of the third and fifth order controlled nonlinear model (transfer $\frac{q_l(j\omega)}{q_{ref}(j\omega)}$) in figure 5, show that the bandwidth of 12 Hz has been reached. Moreover, the fifth order controller appears to give better results in terms of bandwidth once more, which justifies the inclusion of the flexibility in the model[1].

Although a good performance is achieved with regard to the bandwidth by the designed controllers, this is not the case for the low frequency tracking behavior cq. positioning accuracy. This appears to be caused by the Coulomb friction; this strongly nonlinear phenomenon highly disturbs the Δ_p-signal at low frequencies. This again disturbs the linear state estimation of the Kalman filter at low frequencies. So disturbed estimated states are fed back by the control law, which results in bad tracking performance. In order to reduce the last effect, an integrator has been included in the *estimator* feedback path of the estimated position-state. Thus, the estimated pressure state may differ from the measured, disturbed Δ_p-signal at low frequencies, but the position-state estimation error is reduced at low frequencies by the integrator. In this way, the low frequency tracking behavior has been improved at simulation level as shown in figure 6.

An experimental verification of the control de-

[1] At the investigation of an equivalent system in Izawa, K. and Nakayama, Y. (1991) (without Coulomb friction), the transfer $\frac{q_l(j\omega)}{q_{ref}(j\omega)}$ has been used. Although they validated the model and showed the influence of the shaft stiffness and load inertia on the behavior, it became not clear how this would affect the choice of a specific control structure and the accompanying performance results.

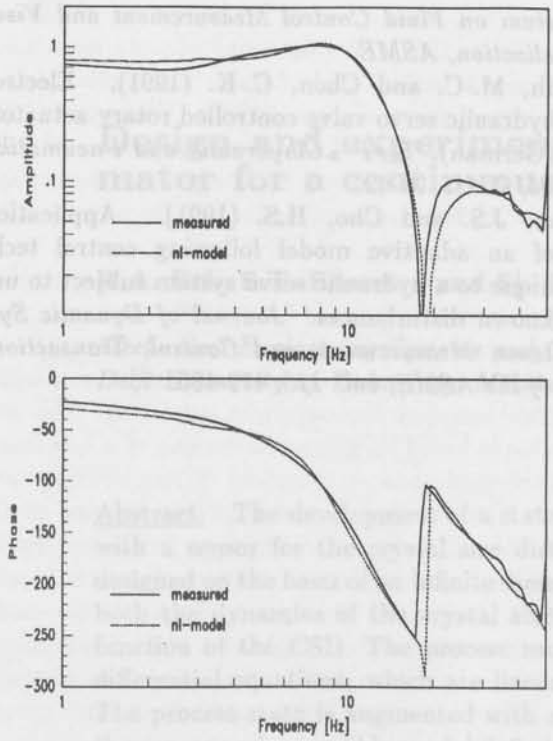

Fig. 7: Measured and simulated (nonlinear model) closed loop frequency response, fifth order controller, transfer $\frac{q_a(j\omega)}{q_{ref}(j\omega)}$.

sign, will be the final subject of this paper in section 5.

5 Experimental results

As the simulation model was build in exactly the same configuration as the experimental setup, including scaling factors et cetera, the designed controller which was tested on the simulation model (with the correct parameter for the torsion stiffness of the flexible shaft), could be used directly for implementation in practice. After an automated discretization with a sample time interval $\Delta t = 1\ ms$ by Matrix$_x$, the controller was implemented automatically in the AC-100 digital controller (figure 2).

For different designed controllers, the responses were measured in practice and compared with the simulated responses. A representative response is given in figure 7. In this figure, the simulated as well as the measured closed loop frequency responses (transfer $\frac{q_a(j\omega)}{q_{ref}(j\omega)}$) are given for the fifth order dynamic compensator (without integrator in the estimator). The given responses show a good agreement between simulated and measured response, especially at two points:

- the achieved bandwidth is predicted correctly by the simulation model
- the disturbing effect of the Coulomb friction on the tracking behavior at low frequencies is clear in both responses.

These results were confirmed by simulated and measured responses in the time domain. The state feedback controller resulted in very fast step responses indeed, although the static positioning accuracy was moderate. These experimental results can be seen as a further validation of the nonlinear model.

6 Conclusions

In this article we have discussed the modeling and control of an industrial hydraulic rotary vane actuator. The considered dynamics in the model have been selected upon practical relevance. Special attention is paid to the flexibility between actuator and load, and to the Coulomb friction. A linearized version of the nonlinear model is used for parameter estimation on the basis of measured data, and for control design. The results of practical application of the designed controllers were conform the expectation from simulation studies. Model based control design proved to be capable of achieving high performance specifications for the controlled system. Specifically the following three items became clear:

- Via a linear model structure and standard optimization techniques, one can effectively estimate the parameters of the nonlinear model description.
- If the frequency of a zero, caused by the dynamics of a flexible connection between the actuator and the load, approaches the desired bandwidth, it is essential to include the concerned dynamics in the model used for control design.
- The closed loop behavior of a state feedback controlled system (including a state estimator) is considerably affected by Coulomb friction, with regard to tracking behavior at low frequencies and to static positioning accuracy.

As these type of rotary vane actuators have been used in an experimental SCARA-type robot build in our laboratory, above mentioned results will be important issues in the modeling and control research of the complete robot.

References

Merrit, H.E. (1967). *Hydraulic control systems.* John Wiley & Sons, Inc.

Viersma, T.J. (1990). *Analysis, Synthesis and Design of Hydraulic Servosystems and Pipelines.* Delft University of Technology, Faculty of Mechanical Engineering, 2nd edition.

Walters, R.B. (1991). *Hydraulic and electro-hydraulic control systems.* Elsevier applied science.

Paap, V.W. (1990). *Modeling and design of an industrial robot.* (Dutch). Mechanical Engineering Systems and Control Group, Delft University of Technology, report number A-552.

Chen, C.-T. (1984). *Linear System Theory and Design.* Holt-Saunders International Editions.

Anderson, B.D.O. and Moore, J.B. (1989). *Optimal Control, linear quadratic methods.* Prentice-Hall International, Inc.

Schothorst, G. van (1992). *Modeling and control of a hydraulic rotary vane actuator.* Mechanical Engineering Systems and Control Group, Delft University of Technology, report number A-575.

Southward, S.C., Radcliffe, C.J. and MacCluer, C.R. (1991). Robust nonlinear stick-slip friction compensation. *Journal of Dynamic Systems, Measurement, and Control, Transactions of the ASME, vol. 113,* 639-645.

Wierschem, T. Von (1981). Position control of weakly-damped drives by state feedback. (German). *Regelungstechnik 29, Heft 1,* 11-19.

Feuser, A. Von (1984). Design of state controllers in the time and frequency domain for position control of a valve-controlled servo-hydraulic linear drive. (German). *Regelungstechnik 32, Heft 9,* 309-316.

Köckemann, A., Konertz, J. and Lausch, H. (1991). Control algorithms for electro-hydraulic servo drives based on industrial marginal conditions. (German). *Automatisierungstechnik 39, Nr. 6,* 187-196.

Neumann, R., Engelke, W. and Moritz, W. (1991a). Digital path control for a hydraulic portal robot. (German). *O+P »Ölhydraulik und Pneumatik« 35, Nr. 3,* 206-216.

Neumann, R., Engelke, W. and Moritz, W. (1991b). Robust simultaneous controller/observer design by parameter optimization for a hydraulic portal robot. (German). *Automatisierungstechnik 39, Nr. 5,* 151-157.

Izawa, K. and Nakayama, Y. (1991). Matching between servo drive and load structure of a servo system. *Third Triennial International Symposium on Fluid Control Measurement and Visualization, ASME.*

Shih, M.-C. and Chen, C.-K. (1991). Electro-hydraulic servo valve controlled rotary actuator. (German). *O+P »Ölhydraulik und Pneumatik« 35, Nr. 1,* 39-42.

Yun, J.S. and Cho, H.S. (1991). Application of an adaptive model following control technique to a hydraulic servo system subject to unknown disturbances. *Journal of Dynamic Systems, Measurement, and Control, Transactions of the ASME, vol. 113,* 479-486.

Selected Topics in Identification, Modelling and Control
Vol. 6, December 1993

Design and experimental evaluation of a state estimator for a continuous crystallization process

R.A. Eek, S.T. Boerstra and Sj. Dijkstra

Mechanical Engineering Systems and Control Group
Delft University of Technology, Mekelweg 2, 2628 CD Delft, The Netherlands.

Abstract. The development of a state estimator for a crystallization process, equipped with a sensor for the crystal size distribution (CSD), is discussed. The estimator is designed on the basis of an infinite dimensional non-linear process model, which describes both the dynamics of the crystal size distribution and the output of the sensor as a function of the CSD. The process model is lumped to a set of non-linear first order differential equations, which are linearized leading to a high order state-space model. The process state is augmented with a single term to correct for background errors of the sensor and a possible model deficit in the small crystal size range. With this model a constant error feedback gain is designed using Kalman filter theory. Estimates are used for the measurement and process noise covariance matrices. The designed gain is implemented in the non-linear lumped process model. The resulting state estimator is customised with raw data from a pilot crystallizer, equipped with an on-line CSD sensor. For different sets of output data the designed estimator is able to track the process output signal trend, while reconstructing the CSD, the supersaturation level, and a set of related variables. The estimator designed at one specific steady-state process condition has sufficient performance at other conditions. Moreover sufficient robustness is demonstrated for sensor failure, an unfitted initial state and process disturbances.

Keywords. process control; crystallization; observability; state estimation; distributed parameter system

1 Introduction

The dynamic behaviour of continuous industrial crystallizers is often characterized by badly dampened or even oscillatory behaviour in time (Eek, 1993). The performance of a suspension crystallizer is mainly determined by the size, the purity and the morphology of the produced crystals. Although crystal purity and morphology aspects are relatively new and active areas of present academic and industrial research, the size of crystals expressed by the crystal size distribution (CSD) is often considered as the most important process parameter to be optimized. Subsequently the supersaturation of the solution which enables crystal growth is seen as an important parameter since it strongly influences crystal nucleation and growth kinetics which determine the crystal size, the purity and morphology of particles.

In industrial practice undesired dynamics of the CSD and supersaturation limit the marketability and transportability of crystals and put a constraint on the performance of the downstream crystal handling processes like thickeners, centrifuges and dryers. Therefore a demand exists for control systems which increase the overall performance of crystallizers and downstream processes.

A basic requirement for the implementation of a control system is the availability of accurate and reliable information on the relevant process dynamics.

For on-line measurement of the CSD and supersaturation in crystallizers different sensors have been developed which, however, still have severe shortcomings for application. On-line measurement of supersaturation is usually extremely difficult as the relative level of supersaturation is often not more than 1 percent. CSD measurement is difficult as most CSD sensors are indirect, i.e. reconstruction scheme's are required to obtain a proper estimate of the CSD based on the output of the sensor. Solutions which are often applied to this estimation problem are direct inversion algorithms which estimate the CSD based on the estimated inverse of the sensor model. This inversion procedure is however ill conditioned and as a consequence sensitive to measurement noise. In addition, the resolution is limited and the inversion algorithms do not take into account the evolution in time of the measured signal trend which is governed by the process dynamics.

Another approach to the CSD estimation problem is the use of dynamic process information to reconstruct the distributions. This can be achieved with state estimators and observers, which were introduced in the 1960's by Kalman and Luenberger. State estimators and observers are derived from a process model which is used to estimate the state of a process from available (limited) input and output measurements. Basically a state estimator is a dynamic system, which runs on a computer and operates sequentially on the raw sensor data as they become available. An optimal designed estimator will give the best compromise between sensitivity for measurement noise and rapid convergence to the real process. In contrast with state estimators, observers are mostly designed for deterministic systems with insignificant process or sensor disturbances.

The purpose of this article is to present a practical state estimator for a crystallization process, based on a first principles process model. This estimator should primarily reconstruct the CSD and the supersaturation level for control purposes, and secondly serve as a process monitor to facilitate the operator task in making decisions with respect to manual control actions.

Most observer applications reported in the literature deal with space systems or navigation systems. Unfortunately the number of applications in the chemical process industry is still limited, due to severe modelling limitations and sometimes to the absence of accurate and robust on-line measurement systems. Some successful implementations in polymerization reactors are reported by Dimitratos (1989) and in monitoring for hazardous conditions by Gilles (1981). Applications of state estimation techniques in the field of industrial crystallization are reported by Cooper (1986), Hashemi (1982), Myerson(1987) and Tsuruoka (1987). Most of these applications lack robust on-line process sensors and are often based on simple (MSMPR) process models.

In this paper an experimental 970 litre pilot crystallizer equipped with a robust CSD sensor was used to generate process data. The CSD measurement system comprises a continuous slurry diluter and a sensor based on forward light scattering. The estimator is based on a lumped version of a non-linear distributed parameter model of the CSD dynamics. This lumped model is chosen instead of the distributed model as it strongly facilitates the filter design and implementation (Anderson & Moore, 1979). A detailed description of the process model and the estimation of unknown model parameters is given by Eek (1993). Step response analysis, based on a linearized version of the model around its steady-state, indicates that the crystallizer can be considered as a sufficiently linear process. For this reason we applied linear Kalman filter theory to design the constant Kalman gain matrix. The resulting filter is tuned and evaluated on experimental data obtained from the pilot crystallizer. Several robustness features like sensitivity of the estimator for sensor failure and process disturbances are outlined.

The approach we follow is applicable to other crystallization processes equipped with different sensors provided that sufficient accurate models for their behaviour are available.

2 Process description

The crystallizer studied here is an evaporative isothermal continuous draft-tube baffled crystallizer equipped with an annular zone around the crystallizer vessel in which classified removal of the fine particles is established.

An elementary process flow sheet with the process inputs, outputs and the constant controlled internal variables is depicted in Fig. 1.

PI control loops are present to maintain the slurry temperature (T), the pressure in the crystallizer (Pr), the crystallizer volume (V), the fines (Q_f) and product (Q_p) removal flows, the temperature of the dissolved fines (T_r) and the total heat input (P_{tot}), at prescribed set-point values. Effective actuators for the process dynamics are the fines removal rate, the total heat input to the system de-

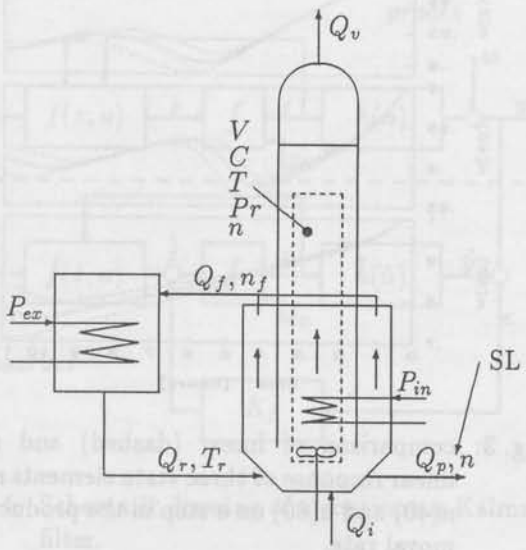

Fig. 1: Schematic drawing of an evaporative Draft tube baffled crystallizer, equipped with a fines removal system.

fined by: $P_{tot} = P_{in} + P_{ex}$ and the product removal rate. CSD measurements are performed at sample location SL (Fig. 1), where the CSD of unclassified removed product crystals is measured.
The CSD is characterised by the population density function $n(x,t)$, defined by:

$$n(x,t) \triangleq \lim_{\Delta x \to 0} \frac{\Delta N(x,t)}{\Delta x}, \qquad (1)$$

with $N(x,t)$ the cumulative number function describing the number of crystals per unit volume, with a size equal or lower than x.

3 Process modelling

A widely accepted framework for the modelling of crystallization processes is a population balance model in which CSD dynamics are described by a first order hyperbolic partial differential equation:

$$\frac{\partial n(x,t)}{\partial t} = -\frac{\partial G_c(x,t)n(x,t)}{\partial x} - \frac{Q_p(t) + h_f(x,t)Q_f(t)}{V} n(x,t), \qquad (2)$$

with a boundary condition $n(x = x_0, t)$ and an initial condition: $n_s(x, t = t_0)$.
With this equation CSD dynamics are described by crystal growth and birth rates and fines and product crystal removal. The crystal birth rate is included in the model as a boundary condition. The crystal growth rate, G_c, is determined by the supersaturation which is described by:

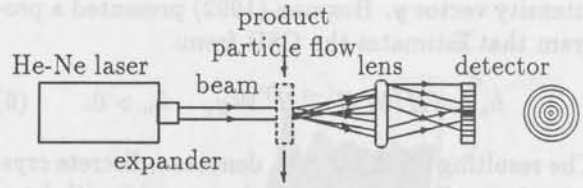

Fig. 2: Principle of forward light scattering.

$$\frac{\Delta C}{dt} = f_{\Delta C}(u(t), z(x,t)). \qquad (3)$$

With $u(t)$ the input vector which is given by: $u(t) = \{Q_p(t), Q_f(t), P_{tot}(t)\}$, and the infinite process state z, given by: $z(x,t) = \{n(x,t), \Delta C(t)\}$. Empirical relations for the crystal growth and birth kinetics, the separation efficiency of fine and product crystal removal systems and the initial state are included. The crystal birth rate B is assumed to be dependent on the supersaturation level and the presence of other crystals:

$$B(t) = f_b(n(x,t), \Delta C(t)). \qquad (4)$$

The empirical relationships contain a set of unknown parameters θ, which are estimated from process data resulting in optimal parameter values $\hat{\theta}$. A detailed description of the population balance model is given by Eek (1993) and de Wolf (1990).
The crystallizer model is extended with a sensor model to describe the output of a Malvern™ particle sizer as a function of the CSD that passes through an optical cell. The working principle is outlined in Fig. 2. Measurement of particle size distributions with light scattering techniques is well known and often applied (Hecht, 1987). The main advantages are the relatively wide range of crystal sizes that is covered, the speed of performance and the good detectibility of error sources. Fraunhofer theory was used to develop a model for the particle sizer. The discretized version of this model is written as:

$$y = H(\alpha)n, \qquad (5)$$

with H the sensor model matrix, y the light intensity vector measured on the detector rings and n a discrete population density function.
Inversion of the model given by Eqn. 5 can be used to calculate the size distribution from an averaged

intensity vector y. Boxman (1992) presented a program that estimates the CSD from:

$$\hat{n}_v = (H^T W H)^{-1} H^T W y, \quad \hat{n}_v > 0. \qquad (6)$$

The resulting CSD: $\hat{n}_v(x,t)$, denotes a discrete crystal volume distribution based on a grid with logarithmically equidistant size classes. From this distribution characterizing quantities like a median or spread can be calculated. The non-negativity constraint is added to avoid physically impossible solutions. The weighting matrix W is the noise covariance matrix that corresponds to the averaged light intensity vector y. We will compare the outcome of this direct inversion approach with the observer approach.

4 Model lumping and linearization

The process model is lumped to a finite non-linear state space model. For this purpose a second order accurate method-of-lines scheme is used (de Wolf, 1990). Subsequently the model equations are linearized by considering small disturbances around the stationary solution. The steady-state solution is calculated from the right hand side of Eqns. 2 and 3 and the expression for the boundary condition from Eqn. 4. As these equations do not represent an explicit solution, an iteration scheme is applied to find the stationary solution.
The linearized equations constitute a high order linear state-space structured model which is given by:

$$\begin{aligned} \Delta\dot{z} &= F\Delta z + G\Delta u, \qquad z_0 = z_s, \\ \Delta y &= H\Delta z. \end{aligned}$$

where Δ denotes a small perturbation around the stationary solution. To improve the numerical condition, this model is scaled by transforming the process state with a diagonal transformation matrix, which has the inverse of the stationary process state on its diagonal. The transformed linear state-space model has 99 states and is used for further analysis of the process behaviour and the design of a filter. In Fig. 3 the step response of the linear model on a positive step of 10 percent in the product removal rate was compared to the positive and inverse negative non-linear model response. For a model with negligible non-linearities the positive response should equal the inverse negative response. The product removal flow induces a proportional change in the main dynamic response time period. Disturbing the product removal rate can be considered as a worst case, because the responses on fines

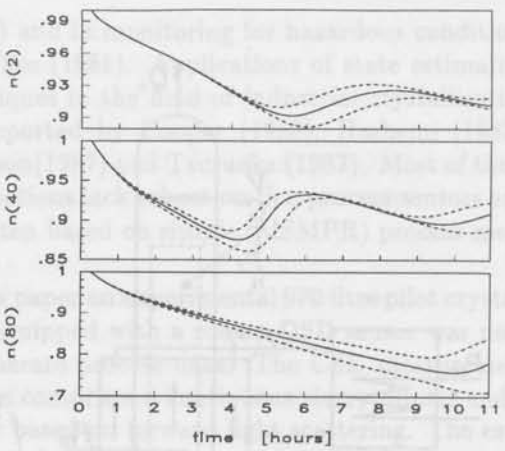

Fig. 3: comparison of linear (dashed) and non-linear response of three state elements n(2), n(40) and n(80) on a step in the product removal rate.

and heat input disturbances were found to be quasi-linear. Therefore it is asumed that the population balance model has only limited non-linearities which can be approximated by linear models with sufficient accuracy.

5 Process observability

The state space model $\{F, G, H\}$ enables the estimation of observability properties. An important tool to study observability properties of a process is the observability Gramian Q which is defined as:

$$Q = \int_0^\infty e^{Ft} H H^T e^{Ft} dt. \qquad (7)$$

An interpretation of the observability Gramian can be given in terms of energy. The amount of energy measured at output of the system from $t = 0$ to $t = \infty$ due to an initial condition x_0 at $t = 0$ with zero inputs is:

$$\int_0^\infty y(t)^T y(t) dt = x_0^T Q x_0. \qquad (8)$$

If Q is singular an unobservable initial condition will exist that will not contribute to the output signal energy. In addition Q will provide information about well or weakly observable states.

6 Kalman filter design

With Kalman filtering theory a state estimator can be devised which takes into account the stochastic nature of model and process information in a systematic way. The working principle of a Kalman

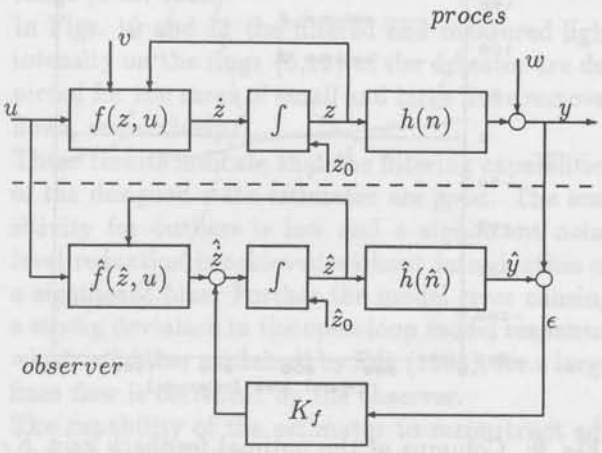

Fig. 4: Schematic drawing of a continuous Kalman filter.

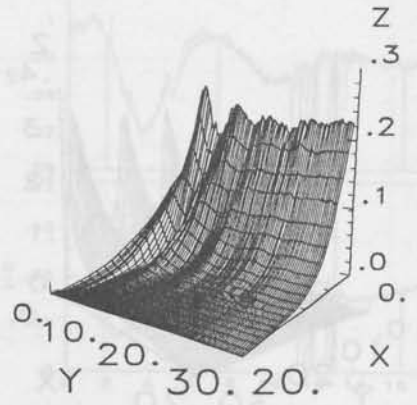

Fig. 5: Experimental time response of scaled light intensity on first 20 detector rings (fines removal rate 1.0 l/s).

filter is depicted in Fig. 4. The error ϵ between the actual process output y and the model output $\hat{y}$ is calculated and amplified with the so called Kalman gain K_f. This results in a correction signal which is used as an additional input that forces the model in a way that the estimated state converges to the real process state.

For linear time-invariant state-space models the solution for the optimal filter gain is given by the solution of an algebraic Ricatti equation (Anderson & Moore, 1979). Extending the model described by Eqn. 7 with uncorrelated random process and sensor noise inputs gives:

$$\begin{aligned} \dot{z}(t) &= Fz(t) + Gu + w(t), \\ y(t) &= Hz(t) + v(t). \end{aligned} \tag{9}$$

The corresponding covariance matrices for the sensor and process noise are given by:

$$E\{v^T v\} = V, \tag{10}$$

$$E\{w^T w\} = W. \tag{11}$$

Based on this model the filter gain matrix K_f is given by:

$$K_f = P_f H^T V^{-1}, \tag{12}$$

where P_f satisfies an algebraic Riccati equation:

$$P_f F^T + F P_f - P_f H^T V^{-1} H P_f + W = 0. \tag{13}$$

This solution indicates that an accurate process and sensor model and good estimates for the covariance matrices for the different noise sources play a decisive role in the filter design procedure. This can be seen as a disadvantage as it is often difficult or even impossible to obtain a sufficiently accurate model representation of the process and the corresponding noise sources. However in many practical situations it suffices to treat the noise covariance matrices as free design parameters that are adapted to achieve a satisfactory filter response based on an imperfect model.

7 Results

The results of two free-run experiments (described by Eek, 1993), measured on the product output (SL in Fig. 1) of the pilot plant, at different process conditions, were used to optimize and evaluate the designed state estimator. Figs. 5 and 6 show the raw light intensity patterns measured on the inner 20 detector rings of the Malvern instrument, over 30 hours for a fines removal rate of 1.0 l/s and 3.4 l/s respectively. The measured signal trends are corrected for outliers by linear interpolation.

In Fig. 7 the corresponding experimental time response is given for the median crystal size X_{50} which was obtained from volume based distributions calculated by direct inversion (Eqn. 6). In this plot all outliers caused by tube blockage or other process disturbances are present.

From inspection of the singular values of the observability Gramians, depicted in Fig. 8, it is concluded that the system is weakly observable. Because only a limited number of modes (< 6) are well observable, a lot of redundancy is present in the 31 process outputs. To improved the numerical condition and to reduce the influence of measurement noise the measurements and the model output matrix H

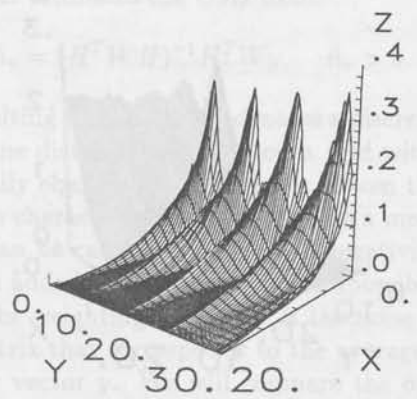

Fig. 6: Experimental time response of scaled light intensity on first 20 detector rings (fines removal rate 3.4 l/s).

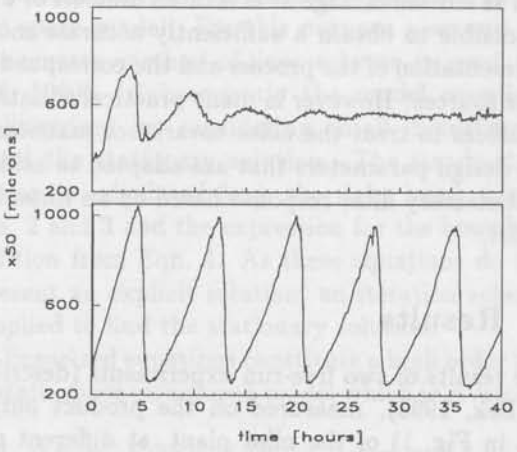

Fig. 7: Experimental time response of X_{50} (fines removal rate 1.0 and 2.2 l/s respectively).

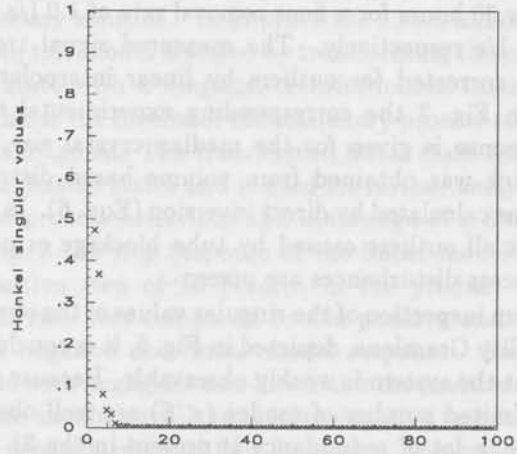

Fig. 8: Singular values of the observability Gramian.

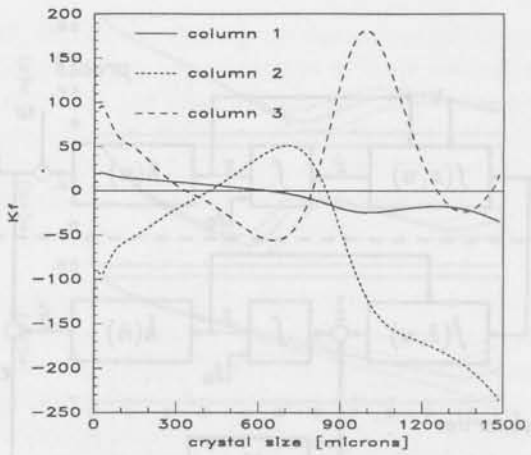

Fig. 9: Columns of the optimal feedback gain K_f scaled by the stationary crystal size distribution.

are transformed by a matrix U_{sr}. This matrix is obtained from the singular value decomposition of the output matrix given by: $H = U_s \Sigma_s V_s^T$, where Σ_s contains the 31 singular values of H and U_s and V_s are unitary matrices containing the right and left singular vectors. The matrix U_{sr} now contains the first n_r left singular vectors corresponding to the largest singular values. The reduced output matrix H_r is now calculated with: $H_r = U_{sr}^T H$. Good results are obtained when only three modes ($n_r = 3$) are taken into account.

The Kalman filter gain is calculated from the solution of the Ricatti Equation 13 for the model $\{F, G, H_r, V, W\}$. Diagonal structured matrices are used for the noise covariance matrices V and W. The matrix W could easily be estimated from noise present in the experimental data. A rough estimate of the process noise covariance matrix V was obtained by first perturbing the physical parameters θ of the model randomly within their estimated confidence bounds and calculating the corresponding stationary crystal size distributions. From the resulting large set of stationary crystal size distributions an estimate is obtained for the variance of each state variable.

The calculated Kalman gain is implemented to the non-linear model as depicted in Fig. 4. Fig. 9 shows the columns of the (scaled) optimal gain K_f. The final filter is adapted to achieve a satisfactory filter response by amplifying the designed filter gain by a constant factor α_f. To reduce the sensitivity of the filter for outliers the gain K_f is reduced to zero when strong signal outliers occur. Further the state to be estimated is augmented with one element to correct for model deficit in the small crystal size

range (Eek, 1993).
In Figs. 10 and 11 the filtered and measured light intensity on the rings {5,10} of the detector are depicted for the cases of small and large fines removal flows, respectively.
These results indicate that the filtering capabilities of the designed state-estimator are good. The sensitivity for outliers is low and a significant noise level reduction is achieved without introduction of a significant bias. Further the model error causing a strong deviation in the open-loop model response, which is further explained by Eek (1993), for a large fines flow is corrected by the observer.
The capability of the estimator to reconstruct additional process information which is relevant for operators or engineers is depicted in Fig. 12 which shows reconstructed trends of the median crystal size X_{50}, the nucleation rate B and the supersaturation ΔC corresponding to plant start-up conditions with a low fines removal rate. The median crystal size obtained from the direct inversion approach is added as a dotted line in the first strip of these plots.
In Fig. 13 the same trends are depicted but the estimator reconstruction is deliberately biased by selecting the steady-state CSD as the initial CSD. In addition it is assumed that sensor measurements were not available between 6 and 11 hours after start-up. In this period the estimator generates an uncorrected open-loop estimate of the process state variables. It appears that although these large disturbances bias the estimates the model still follows the signal trends reasonably well.
In Fig. 14 the observer reconstruction of a certain relative volume distribution at four different time instants corresponding to the time points of the trends depicted in Fig. 12 are given. In Fig. 15 the same distributions obtained from direct inversion are depicted. It can be seen that the resolution of the estimated CSD is much larger then the resolution of the CSD obtained by direct inversion. It should be noted, however, that the error between the model and the measured output signals, as can be seen in Figs. 10 and 11, is not uncorrelated white noise. Because no strong process disturbances have ocured this indicates that a model error exist which bias the estimates.

8 Discussion and conclusions

With the application of a state estimator dynamic process information stored implicitly in a dynamic model is combined with on-line process information to reconstruct quantities that cannot be measured

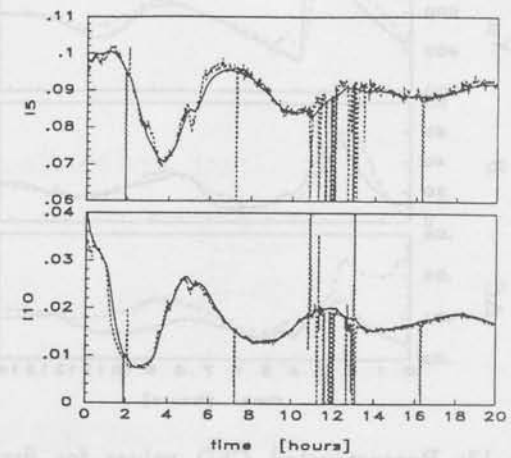

Fig. 10: Filtered (drawn) and measured (dotted) response of ring $\{5, 10\}$ after start-up (fines flow 1.0 l/s).

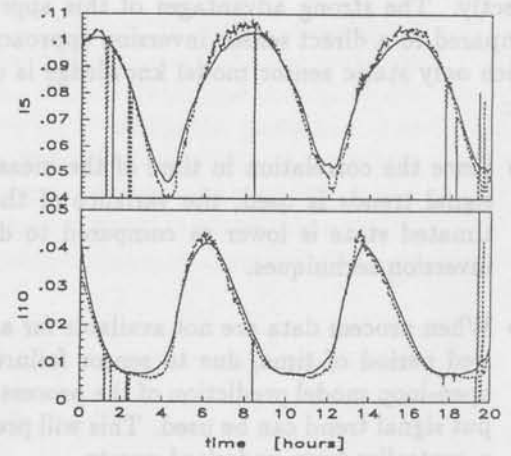

Fig. 11: Filtered (drawn) and measured (dotted) of ring $\{5, 10\}$ after start-up (fines flow 3.4 l/s).

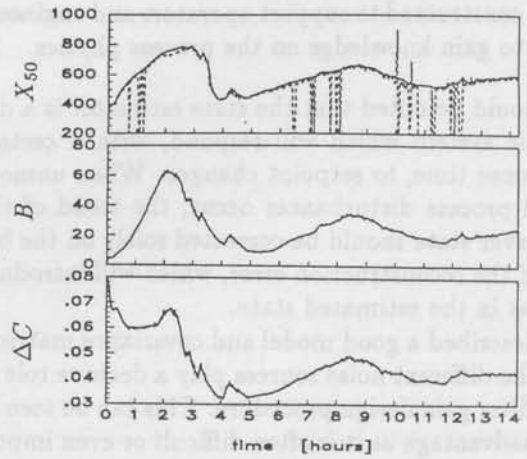

Fig. 12: Reconstructed CSD values for first 14 hours compared to X_{50} from inversion (dashed) for start-up (fines flow 1.0 l/s).

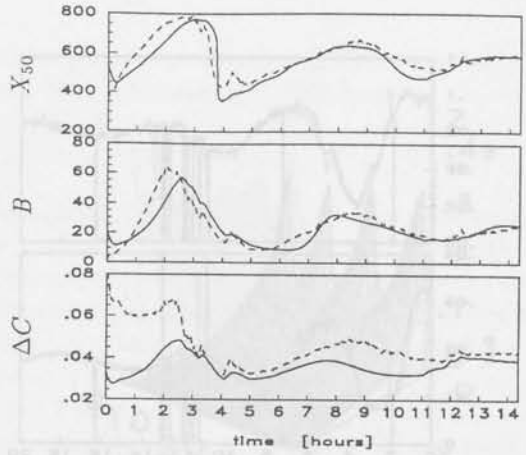

Fig. 13: Reconstructed CSD values for first 14 hours compared to X_{50} from inversion (dashed) for start-up (fines flow 1.0 l/s).

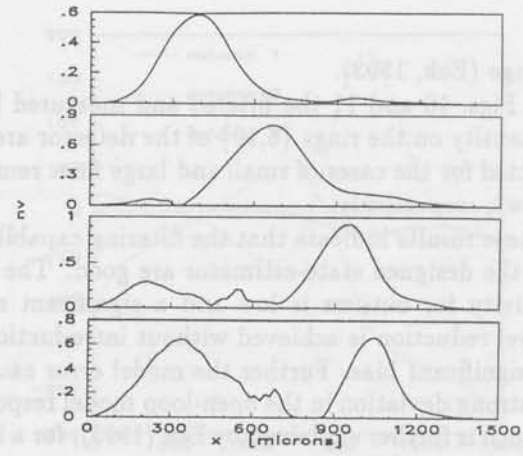

Fig. 14: Volume based CSD reconstructed with estimator at 0.5, 2, 4 and 4.5 hrs. after start-up (fines flow 1.0 l/s).

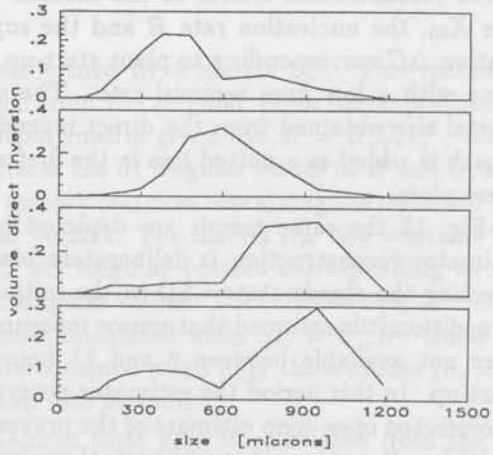

Fig. 15: Volume based CSD reconstructed with inversion at 0.5, 2, 4 and 4.5 hrs. after start-up (fines flow of 1.0 l/s).

directly. The strong advantages of this approach compared to a direct sensor inversion approach, in which only static sensor model knowledge is used, are:

- Since the correlation in time of the measured signal trends is used, the variance of the estimated state is lower as compared to direct inversion techniques.
- When process data are not available for a limited period of time, due to sensor failure, an open-loop model prediction of the process output signal trend can be used. This will prevent a controller from undesired upsets.
- Physical quantities like the supersaturation, the crystal birth rate and the crystal growth rate, that cannot be measured directly, are reconstructed to support operators and engineers to gain knowledge on the process physics.

It should be noted that the state estimator is a dynamic system which will respond, with a certain response time, to setpoint changes. When unmodelled process disturbances occur, the trend of the observer state should be corrected solely on the basis of the reconstruction error, which will introduce a bias in the estimated state.
As described a good model and covariance matrices for the different noise sources play a decisive role in the filter gain design procedure. This can be seen as a disadvantage as it is often difficult or even impossible to obtain sufficiently accurate representations of the nominal model and the corresponding noise models. However when a model is available it will enhance the quality of reconstructed distributions as compared to the direct inversion approach.
This paper has indicated how a state estimator for a crystallization process that is based on an simplified high order model can be applied for reconstruction of the CSD and related quantities from raw plant data. This approach forms a good basis for observer applications for industrial crystallization. Future work will be focused on the topic of observer robustness and the search for simple dynamic models which still enhance the quality of reconstructed process states as compared to direct inversion.

Acknowledgement

The authors would like to express their gratitude to the Dutch Foundation of Technology (STW),

AKZO, DOW Chemicals, ICI, DSM, E.I. Dupont de Nemours, and Eastman Chemical Company for their financial support of the UNIAK project.

References

Anderson B.D.O., Moore J.B. (1979) Optimal Filtering. *Prentice-Hall Inc., Englewood Cliffs.*

Boxman A. (1992) Particle Size Measurement for the Control of Industrial crystallizers. *PhD Thesis Delft University of Technology.*

Cooper D.J., Clough D.E. (1986). Real time estimation of dynamic particle-size distributions in a fluidized bed: theoretical foundation. *AIChE Journal, Vol. 31, No. 7, pp. 1202-1136.*

Dimitratos J, Georgakis C, El-Asser M S. (1989). Dynamic modelling and state estimation for an emulsion copolymerization reactor. *Computers and Chem. Eng., vol. 13, no. 1-2, pp. 21-33.*

Eek R.A., Dijkstra Sj. Rosmalen, G.M. van (1993). Dynamic modelling of a suspension crystallizer using experimental pilot plant start-up data. *Submitted for publication.*

Frank, P.M. (1987), Advanced Fault Detection and Isolation Schemes Using Non-linear and Robust Observers, *Proc. 10th IFAC World Congress, Munich, vol. 3, pp. 63-68.*

Gilles E D, Schuler H. (1981). Zur fruhzeitigen Erkennung gefahrlicher Reaktionszustande in chemischen reaktoren. *Chemie Ingenieur Technik, Bd. 53, H. 9, pp. 673-682.*

Hashemi R, Epstein M A F (1982). Observability and Controllability Considerations in Crystallization Process Design *AIChE Symposium series, No. 215, Vol. 78, pp. 81-89*

Hecht, E (1987). Applied Optics. *Adison-Wesley Publishing Company, second edition.*

Myerson A S, Rush S, Schork F J, Johnson J L (1987). Control of Crystallization processes. *Proc. Techn. Proc., 6. Industrial Crystallization 87, pp. 407-410.*

Tsuruoka S., Randolph, A. (1987). State Space representations of the dynamic crystallizer population balance: application to CSD controller design. *AIChE Symp. Series Vol. 83, No. 253, pp. 104-109.*

Wolf S. de. (1990). Modelling, System Identification and Control of an Evaporative Continuous Crystallizer. *PhD thesis, Delft University of Technology.*

Wortelboer, P.M.R. (1992). Generalized frequency weighted balanced reduction. *Select Topics in Identification, Modelling and Control*, Delft Univ. Press, Vol. 5.

Fig. 12. Reconstructed CSD values for first 14 hours compared to X_{ss} from inversion (dashed) for startup (feed flow 1.0 l/s).

directly. The strong advantages of this approach compared to a direct sensor inversion approach, in which only static sensor model knowledge is used, are:

- Since the correlation in time of the measured signal trends is used, the variance of the estimated state is lower as compared to direct inversion techniques.
- When process data are not available for a limited period of time, due to sensor failure, an open loop model prediction of the process output signal trend can be used. This will prevent a controller from undesired upsets.
- Physical quantities like the supersaturation, the crystal birth rate and the crystal growth rate, that cannot be measured directly, are reconstructed to support operators and engineers to gain knowledge on the process physics.

It should be noted that the state estimator is a dynamic system, which will respond, with a certain response time, to setpoint changes. When unmodelled process disturbances occur, the trend of the observer state should be corrected solely on the basis of the reconstruction error, which will introduce a bias in the estimated state.

As described a good model and covariance matrices for the different noise sources play a decisive role in the filter gain design procedure. This can be seen as a disadvantage as it is often difficult or even impossible to obtain sufficiently accurate representations of the physical model and the corresponding noise models. However when a model is available it will

Selected Topics in Identification, Modelling and Control
Vol. 6, December 1993

Frequency-weighted balanced reduction in closed-loop systems

Pepijn M.R. Wortelboer[‡], Okko H. Bosgra[§], and Carel Ceton[♯]

[‡]*Philips Research Laboratories, Prof. Holstlaan 4, 5656 AA Eindhoven, The Netherlands.*
[§]*Mechanical Engineering Systems and Control Group*
Delft University of Technology, Mekelweg 2, 2628 CD Delft, The Netherlands.
[♯]*Agrotechnological Research Institute (ATO-DLO)*
P.O. Box 17, 6700 AA Wageningen, The Netherlands.

Abstract. A recent extension of balanced reduction to a specific frequency-weighted closed-loop configuration is reformulated to fit into the more general controller synthesis configuration using linear fractional transformations. Both system and controller are written in a feedback loop of an interconnection system of which the performance is specified. The order-reduction scheme is as simple as balanced reduction and facilitates interactive step-by-step solution of the low-order controller design problem. High-order models encountered in structural dynamics control can be reduced safely within a few iterations. New properties of the method are derived and two examples show the efficiency of the method.

Keywords. order-reduction, controller design, balancing, linear fractional transformations, structural dynamics, computer-aided design.

1 Introduction

In high-performance control of mechanical servo systems, one of the hardest problems is to find an appropriate linear model of the system to be controlled. A model of the mechanical part is often derived using finite element techniques. These models of the structural dynamics can only be accurate for a bounded set of input and disturbance signals. Knowlegde about the control signal(s) however is very limited in the early stage of servo-system design. This forces one to model in great detail which leads to high-order models. The servo-controllers are preferred as simple as possible in practice. Since the controller complexity roughly equals the complexity of the controller design model, order reduction of either the system model or the controller is indispensable. If the model of the mechanical system is of very high order, the controller synthesis will generally fail to generate reliable results. Model reduction is often the only way to start the controller design process. The evaluation of the final performance of any controller should always be done using the most accurate (high-order) model of the mechanics. For mechanical servo-systems we can say that high performance with low-order controllers requires some type of iteration: in each step a better understanding of the essential system dynamics can be obtained and the impact of the performance wishes on the controller complexity becomes clearer. In the light of this it is important to have easy manageable reduction schemes for reduction 'in-the-loop' that apply both to the mechanical model and the controller.

To make things more clear, let G represent the mechanical model, K a controller, and M a collection of frequency weighting functions that are involved in the performance specification of the servo-system. The iteration can be performed at different levels

1 *model structural dynamics*
→ high-order model G_m (A)

2 *define performance*
→ criterion for the attenuation of
$\mathcal{I}(M, G_m, K_{\text{unknown}})$ (B)

3 *reduce model*
→ reduced model G_n (C)

4 *make controller synthesis configuration*
→ $\mathcal{I}(M, G_n, K_{\text{computable}})$ (D)

5 *compute controller*
→ controller K_{n_K} (E)

6 *reduce controller*
→ implementable controller K_r (F)

7 *evaluate performance*
→ $\mathcal{I}(M, G_m, K_r)$ OK, or go back (G)

The convergence is better if we take advantage of the knowledge gained in previous steps. For step 3 this means that the unknown controller may be replaced by a preliminary one to reflect the closed-loop in which G_m operates better. The order reductions in step 3 and 6 should be performed in such a way that convergence of the iteration does not break down. The reduction method for step 3 should be very efficient and robust to avoid numerical problems. Iterative controller design requires many steps of adjusting weighting functions, order reduction, and controller synthesis.

This paper focusses on order reduction within the above scheme. The strategy is to use balanced reduction in a closed-loop configuration (Ceton, Wortelboer & Bosgra, 1993) which is relatively simple, and to adjust the results if necessary by introducing frequency weighting functions; these can be created efficiently based on the frequency-dependent reduction error (Wortelboer & Bosgra, 1992).

Balanced reduction in closed-loop can be applied to model and controller. It only requires the closed-loop system to be stable. It is a straightforward extension of balanced reduction to systems in a feedback connection in the same way as frequency-weighted balanced reduction is an extension of balanced reduction to systems in a series connection (Enns, 1984a, 1984b). Frequency-weighted balanced reduction can be used for reduction in closed-loop systems as Enns showed, but system and controller have to be stable. The creation of closed-loop relevant weighting functions may be difficult and high-order functions may be needed to emphasize specific frequency regions.

Other reduction techniques that take the controlled system into account are LQG-balanced reduction (Jonckheere & Silverman, 1983), and H_∞-balanced reduction (Mustafa 1989). The implicit assumption in these methods is that a normalized full-order LQG (or H_∞) controller closes the loop. These controllers can be computed and reduced in the same manner. Considering the scheme above, these methods are situated in steps 5 and 6 provided we have an unweighted performance specification in LQG or H_∞ sense. For fixed-order LQG controller design, Hyland & Bernstein (1984) formulated the optimal projection equations to satisfy the first-order necessary conditions for quadratic optimality. Due to the numerical complexity of the equations, this method cannot (yet) be applied directly after step 2 in the above scheme.

Once a controller has been computed, controller reduction can be applied. Closed-loop controller reduction can and has to take full advantage of the knowledge of the full-order closed-loop system. Many strong results have been reported on this issue. The factorization theory largely stimulated these results: see Anderson & Liu (1989) for an overview. Fractional balanced reduction, an extension of balanced reduction to possibly unstable systems is closely related to LQG-balanced reduction; see Meyer (1988). Bongers & Bosgra (1991) propose frequency-weighted optimal Hankel-norm reduction with weightings based on the factors of the system and the full-order controller, and they derive an a priori controller order that is sufficient for closed-loop stability. De Villemagne and Skelton (1988) proposed a controller reduction method based on "controller canonical correlation coordinates" to force reduced-order stability while retaining important closed-loop system parameters.

This paper describes an alternative approach that tries to perform closed-loop relevant reduction in a configuration that is also used for controller synthesis. The incorporation of frequency weighting functions is given special attention. It is shown how simple extensions of the famous balance and truncate procedure can be used to achieve fast and accurate order reduction within a general controller design configuration. Iterations on the modelling method or the controller design method are not discussed. We concentrate on continuous time linear systems with performance specifications in the frequency domain. The organisation of this paper is as follows.

First the general *controller synthesis configuration* (CSC) will be introduced and adopted for combined system and controller reduction. Secondly the principles of balanced reduction will be formu-

lated in terms that opens up the way for the extension of balanced reduction of a system interconnected with any set of other systems. Frequency-weighted and closed-loop balanced reduction are special cases. Finally the effectiveness of the proposed method is shown in a standard example introduced by Enns (1984), and in CD-player model reduction.

2 A general feedback structure

In order to be able to do *system* and *controller* reduction in any stage of design, the system and controller have to be isolated from the controller design configuration. The general interconnection structure proposed is given in Fig. 1. This interconnection structure was first used to define the robust controller design problem (Doyle, 1982). The performance is the attenuation that is achieved between signals w and z. G is the system model, and K is the controller. M will be referred to as the connector system or connector and incorporates any selection of weighting functions.

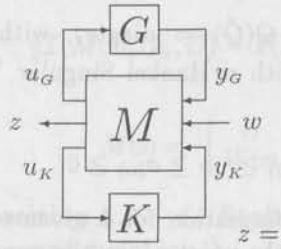

$$z = \mathcal{I}(M, G, K)w.$$

Fig. 1: Interconnection with weights in M and system G and controller K in feedback loops

2.1 Open-loop frequency-weighted model reduction

In the early stage of design we only have a very high-order model and some idea of the required performance specification. Sometimes a preliminary controller is available. Here we assume we do not know any controller that achieves closed-loop stability. We discern two different approaches in adapting the general controller design configuration. *i)* the controller is set to zero, and *ii)* the controller is omittted.

i: The controller is set to zero. This means the controller inputs and outputs are assumed to contribute only weakly. The equivalent feedback scheme then is

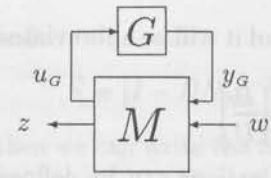

$$z = \mathcal{I}(M, G, O)w$$

ii: The controller is empty: $K = [\,]$. This means the controller input channels are considered relevant outputs in the model reduction step, and the controller output channels are used for inputs in model reduction. The equivalent feedback scheme then is

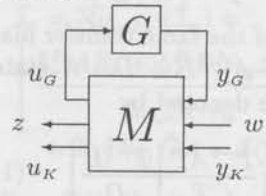

$$\begin{bmatrix} z \\ u_K \end{bmatrix} = \mathcal{I}(M, G, [\,]) \begin{bmatrix} w \\ y_K \end{bmatrix}$$

2.2 Controller Synthesis Configuration (CSC)

In the controller synthesis step, the model is already of an order amenable to controller synthesis. The aim is to find a controller $K(s)$ that achieves sufficient attenuation of the following system

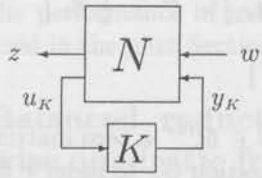

$$z = \mathcal{F}_l(N, K)w$$
$$N = \mathcal{F}_u(M, G)$$

Fig. 2: Controller synthesis configuration

The model used in controller synthesis is of limited order n.

2.3 Controller reduction configuration

The controller reduction configuration is the same as the controller synthesis configuration with the difference that the model behind N might be of the original order m.

3 Reduction based on Transform & Truncate

Continuous-time finite-dimensional time-invariant linear systems can be written in state-space as

$$G: \quad \begin{aligned} \dot{x} &= Ax + Bu \\ y &= Cx + Du \end{aligned}$$

G is a specific realization, and it will be abbreviated as

$$G = \left[\begin{array}{c|c} A & B \\ \hline C & D \end{array}\right]$$

Using $\tilde{x} = T^{-1}x$ other realizations can be defined for the same input-output system:

$$\tilde{G}: \begin{array}{rcl} \dot{\tilde{x}} & = & T^{-1}AT\tilde{x} + T^{-1}Bu \\ y & = & CT\tilde{x} + Du \end{array}$$

$$\tilde{G} = \left[\begin{array}{c|c} T^{-1}AT & T^{-1}B \\ \hline CT & D \end{array}\right] = \left[\begin{array}{c|c} \tilde{A} & \tilde{B} \\ \hline \tilde{C} & D \end{array}\right]$$

and G are two realizations of the same transfer matrix $G(s) = \tilde{G}(s) = C(sI-A)^{-1}B + D$. A state transformation on G will be denoted by

$$\tilde{G} = \mathcal{R}_{[T^{-H},T]}(G) \stackrel{\text{def}}{=} \left[\begin{array}{c|c} T^{-1}AT & T^{-1}B \\ \hline CT & D \end{array}\right] \quad (1)$$

A subscript n as in $G_n(s)$ means that the transfer matrix has McMillan degree n. G_n is an n^{th}-order realization. In the sequel n will always be the full order, r is the reduced-order, and $t = n - r$ represents the reduction in order. State-space matrices of the full-order system are partitioned as follows

$$A = \begin{bmatrix} A_r & A_{rt} \\ A_{tr} & A_t \end{bmatrix}, \quad B = \begin{bmatrix} B_r \\ B_t \end{bmatrix}$$

$$C = \begin{bmatrix} C_r & C_t \end{bmatrix}$$

Let $\Gamma_r = \begin{bmatrix} I_r \\ O \end{bmatrix}$ with $O \in \mathbb{R}^{t\times r}$ a zero matrix, then the truncation of realization G_n to order r is:

$$G_r = \mathcal{R}_{[\Gamma_r^T,\Gamma_r]}(G_n) \stackrel{\text{def}}{=} \left[\begin{array}{c|c} \Gamma_r^T A\Gamma_r & \Gamma_r^T B \\ \hline C\Gamma_r & D \end{array}\right]$$

$$= \left[\begin{array}{c|c} A_r & B_r \\ \hline C_r & D \end{array}\right] \stackrel{\text{def}}{=} \mathcal{R}_{r-n}(G_n)$$

Note that this formulation is consistent with (1).

Order reduction of G_n by Transform & Truncate discerns two steps:

$$\tilde{G}_n = \mathcal{R}_{[T^{-H},T]}(G_n)$$

$$\tilde{G}_r = \mathcal{R}_{[\Gamma_r^T,\Gamma_r]}(\tilde{G}_n)$$

and this can be merged into the equivalent projection-based operation

$$\tilde{G}_r = \mathcal{R}_{[L_r,R_r]}(G_n)$$

with

$$R_r = T\Gamma_r \ , \ L_r = T^{-H}\Gamma_r$$

satisfying $L_r^H R_r = I_r$. This means L_r and R_r form a projection matrix $\Pi_r = R_r L_r^H$ of rank r.

4 Balanced reduction

Balanced reduction is the truncation of a balanced realization (Moore, 1981). Transformation to a balanced realization hinges on the controllability and observability Gramians (P and Q) of the original realization. For $G_n(s)$ stable with realization

$$G_n = \left[\begin{array}{c|c} A & B \\ \hline C & D \end{array}\right]$$

P and Q are solved from

$$\begin{array}{rcl} AP + PA^H + BB^H & = & O \\ A^HQ + QA + C^HC & = & O \end{array}$$

and these Lyapunov equations have unique positive definite solutions denoted by $\mathcal{P}(G_n)$, $\mathcal{Q}(G_n)$. P and Q are realization-dependent: for $\tilde{G}_n = \mathcal{R}_{[T^{-H},T]}(G_n)$ we have

$$\mathcal{P}(\tilde{G}_n) = T^{-1}\mathcal{P}(G_n)T^{-H}, \quad \mathcal{Q}(\tilde{G}_n) = T^H\mathcal{Q}(G_n)T$$

Balancing is the transformation to a realization

$$\breve{G}_n = \left[\begin{array}{c|c} \breve{A} & \breve{B} \\ \hline \breve{C} & D \end{array}\right]$$

for which $\mathcal{P}(\breve{G}) = \mathcal{Q}(\breve{Q}) = \text{diag}(\sigma)$, with $\sigma = \sqrt{\lambda(PQ)}$ a vector with n Hankel Singular Values (HSVs) satisfying

$$\sigma_{(1)} \geq \sigma_{(2)} \geq \cdots \geq \sigma_{(n)} \geq 0$$

The balancing transformation for a given realization G_n is not strictly unique. In the sequel we will use a pair of matrices to describe the balancing operation:

$$[\breve{T}^{-H}, \breve{T}] \stackrel{\text{def}}{=} [\breve{L}_n, \breve{R}_n] =$$
$$\mathcal{T}(P,Q) = \mathcal{T}(\mathcal{P}(G_n), \mathcal{Q}(G_n))$$

We call also write $[\breve{L}_n, \breve{R}_n] = \mathcal{T}(G_n)$.

With $\breve{R}_r = \breve{T}_{(:,1:r)}$, $\breve{L}_r = [\breve{T}^{-H}]_{(:,1:r)}$, the balanced reduction can be formulated as:

$$\breve{G}_r = \mathcal{R}_{r-n}(\breve{G}_n) = \mathcal{R}_{[\breve{L}_r,\breve{R}_r]}(G_n) \stackrel{\text{def}}{=} \text{bal}\mathcal{R}_{r-n}(G_n)$$

5 Balanced reduction in the general feedback interconnection

To define balanced reduction within a general interconnection structure we need to analyse the realizations of the interconnected system $\mathcal{I}(M,G,K)$. From linear fractional transformation theory (Doyle *et al.*, 1991, Zhou *et al.*, 1993) we know that

$$\mathcal{I}(M,G,K) = \mathcal{F}_l(\mathcal{F}_u(M,G),K) = \mathcal{F}_u(\mathcal{F}_l(M,K),G)$$

The key point for our scheme is that we make a realization of $\mathcal{I}(M,G,K)$ with a state vector that is built from G-states, M-states, and K-states in that precise order: $x_I^T = \left[\begin{array}{ccc} x_G^T & x_M^T & x_K^T \end{array}\right]$. Balanced reduction of G within $\mathcal{I}$ follows the standard balanced reduction procedure with the difference that instead of P, Q parts of the Gramians of $\mathcal{I}(M,G_n,K)$ are used. The scheme for G reduction then is:

$$
\begin{aligned}
&P_G = \mathcal{P}(\mathcal{I}(M,\underline{G_n},K)) \stackrel{\text{def}}{=} [\mathcal{P}(\mathcal{I}(M,G_n,K))]_{(1:n,1:n)}\\
&Q_G = \mathcal{Q}(\mathcal{I}(M,\underline{G_n},K)) \stackrel{\text{def}}{=} [\mathcal{Q}(\mathcal{I}(M,G_n,K))]_{(1:n,1:n)}\\
&[\tilde{L}_n,\tilde{R}_n] = \mathcal{T}(P_G,Q_G)\\
&\tilde{G}_r = \text{bal}\mathcal{R}_{r-n}(\mathcal{I}(M,\underline{G_n},K)) \stackrel{\text{def}}{=} \mathcal{R}_{[\tilde{L}_r,\tilde{R}_r]}(G_n)
\end{aligned}
$$

For K reduction we have

$$\tilde{K}_r = \text{bal}\mathcal{R}_{r-n}(\mathcal{I}(M,G,\underline{K_n}))$$

Order reduction of both the system and controller can be performed, the weightings involved remain unreduced.

Remark 5.1 (Frequency-weighted balanced reduction) *In frequency-weighted reduction the aim is to minimize $\|W(s)(G_n - G_r)V(s)\|$. This is equivalent with minimizing*

$$\|\mathcal{I}(M(s),G_n,O) - \mathcal{I}(M(s),G_r,O)\|$$

for

$$M(s) = \left[\begin{array}{cc} O & V(s) \\ W(s) & O \end{array}\right]$$

Proposition 5.2 (Stability of reduced-order configuration) *Let G_n be stabilized in $\mathcal{I}(M_0,G_n,K_0)$ by a constant controller K_0 and let M_0 be constant too. Then model reduction within $\mathcal{I}(M_0,G_n,K_0)$*

$$\tilde{G}_r = \text{bal}\mathcal{R}_{r-n}(\mathcal{I}(M_0,\underline{G_n},K_0)) = \mathcal{R}_{[L_r,R_r]}(G_n) \quad (2)$$

yields a stable $\mathcal{I}(M_0,G_r,K_0)$

Proof: Since M_0 and K_0 have order zero,

$$
\begin{aligned}
P_G = \mathcal{P}(\mathcal{I}(M_0,\underline{G_n},K_0)) &= \mathcal{P}(\mathcal{I}_n)\\
Q_G = \mathcal{Q}(\mathcal{I}(M_0,\underline{G_n},K_0)) &= \mathcal{Q}(\mathcal{I}_n)
\end{aligned}
$$

and

$$[L_n,R_n] = \mathcal{T}(P_G,Q_G)$$

balances both the closed-loop system $\mathcal{I}$ and G_n within $\mathcal{I}(M_0,G_n,K_0)$. Next we prove that

$$\mathcal{I}_r = \mathcal{R}_{[L_r,R_r]}(\mathcal{I}_n) = \mathcal{I}(M_0,\tilde{G}_r,K_0) \quad (3)$$

Let

$$N_0 = \mathcal{F}_l(M_0,K_0) = \left[\begin{array}{cc} N_{0g} & N_{0v} \\ N_{0w} & N_{0e} \end{array}\right]$$

and

$$\check{S} = [I - DN_{0g}]^{-1}, \quad \hat{S} = [I - N_{0g}D]^{-1}$$

then we can write the full-order closed-loop system as

$$
\begin{aligned}
\mathcal{I}_n &= \mathcal{I}(M_0,G_n,K_0)) = \mathcal{F}_u(N_0,G_n)\\
&= \left[\begin{array}{c|c} A + BN_{0g}\check{S}C & B\hat{S}N_{0v} \\ \hline N_{0w}\check{S}C & N_{0e} + N_{0w}D\hat{S}N_{0v} \end{array}\right]
\end{aligned}
$$

The reduced-order closed-loop system is

$$
\begin{aligned}
&\mathcal{I}_r = \mathcal{R}_{[L_r,R_r]}(\mathcal{I}_n) =\\
&\left[\begin{array}{c|c} L_r^H AR_r + L_r^H BN_{0g}\check{S}CR_r & L_r^H B\hat{S}N_{0v} \\ \hline N_{0w}\check{S}CR_r & N_{0e} + N_{0w}D\hat{S}N_{0v} \end{array}\right]\\
&= F_u(N_0,\tilde{G}_r) = \mathcal{I}(M_0,\tilde{G}_r,K_0)
\end{aligned}
$$

Since $\mathcal{I}_r$ is the balanced approximation of $\mathcal{I}_n$ which is stable, $\mathcal{I}_r$ is also stable. Note that $\tilde{G}_r$ need not be stable. □

For dynamic controllers, the procedure still lacks a priori stability conditions, but using generalized frequency-weighted balanced reduction (Wortelboer & Bosgra, 1992) in an iterative fashion, a good trade-off can be found between the controller order and the performance in most cases. This will be discussed in the next Section.

6 Balanced reduction with piecewise quadratic frequency weights

The full procedure consists of closed-loop balanced reduction with inputs w and/or outputs z weighted by scalar interval-based frequency functions (Wortelboer & Bosgra, 1992). These frequency functions can be interpreted as filters on the inputs w or on the outputs z, and are very effective in emphasizing specific frequency regions in which a better fit is required compared to the unit-weighted case. Let $\psi(\omega)$ be a positive symmetric frequency function which built from interval parts with quadratic weighting

$$
\begin{aligned}
(m + \acute{m}|\omega| + \acute{\acute{m}}\omega^2)\,\eta(\omega,[\![\underline{\omega},\overline{\omega}]\!]) &\stackrel{\text{def}}{=}\\
m - \acute{m}\omega + \acute{\acute{m}}\omega^2 &\quad \text{for} \quad \omega \in [-\overline{\omega},-\underline{\omega}]\\
m + \acute{m}\omega + \acute{\acute{m}}\omega^2 &\quad \text{for} \quad \omega \in [\underline{\omega},\overline{\omega}]
\end{aligned}
$$

and from pulse parts

$$\hat{m}\,\delta(\omega,[\![\hat{\omega}]\!]) \stackrel{\text{def}}{=} \hat{m}(\delta(-\hat{\omega}) + \delta(\hat{\omega}))$$

The frequency pulse $\delta(\omega,[\![\hat{\omega}]\!])$ originates from

$$\lim_{\underline{\omega}\to\overline{\omega}} \eta(\omega,[\![\underline{\omega},\overline{\omega}]\!])/(\overline{\omega} - \underline{\omega})$$

Each input or output can be weighted individually by such interval-based scalar frequency functions. A direct solution exists for the $\psi_w(\omega)$-weighted controllability of a system $\mathcal{I}$, and the $\psi_z(\omega)$-weighted observability of $\mathcal{I}$. We simply write $\mathcal{P}(\mathcal{I}\cdot\psi_w)$ and $\mathcal{Q}(\psi_z\cdot\mathcal{I})$. The computation involves the standard Lyapunov equation solution and the computation of matrix logarithms. The parts of the frequency weighted Gramians $\mathcal{P}(\mathcal{I}\cdot\psi_w)$ and $\mathcal{Q}(\psi_z\cdot\mathcal{I})$ that are due to the states of G_n are used to transform and truncate the system:

$$\dot{G}_r = \mathrm{bal}\mathcal{R}_{r-n}(\psi_z\cdot\mathcal{I}(M,\underline{G_n},K)\cdot\psi_w)$$

The same can be defined for controller reduction. The fruitful use of the method heavily depends on an adequate implementation. The result of order reduction should be visualized in relevant performance terms. In the current MATLAB4 implementation these are attenuation measures (H_2, H_∞) and frequency-magnitude plots. These plots are the clue to making scalar frequency functions (mouse driven) that can improve the approximation for certain frequency ranges while allowing worse fits outside these ranges.

7 Examples

The proposed procedure will be illustrated by applying it to two controller design problems. The first is the four-disk problem of Enns (1984b). This example is often used in literature to illustrate the effectiveness of new controller reduction methods. We do the same.

The second example focusses on the reduction of a 120^{th}-order model of a CD-player servo-system for controller design purposes.

7.1 4-disk system

Enns (1984b) treats the problem of controlling the angle of a disk that is mounted with three other disks on a flexible shaft. The actuation is on the third disk (Fig. 3). All parameters (disk inertia,

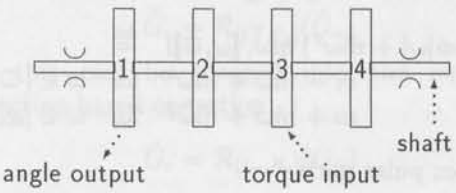

Fig. 3: Four disk system

spring constants) are equal to one. Two poles are in the origin. The vibration modes are damped by introducing 2% modal damping. This non-collocated configuration leads to a non-minimum phase system. The system is described by the following equations

$$\begin{aligned}\dot{x} &= Ax + Bu + v_x\\ y &= Cx + w\end{aligned}$$

with white noise disturbance signals v_x and w having intensities

$$\begin{aligned}V_x &= q_2 BB^H\\ V_w &= 1\end{aligned}$$

and the performance objective is to minimize

$$\mathcal{J} = \int_0^\infty (x^H R_x x + u^H R_u u)\,\mathrm{d}t$$

with

$$\begin{aligned}R_u &= 1\\ R_x &= r^H r\\ r &= [\,0\;0\;0\;0\;0.55\;11\;1.32\;18.0\,]*10^{-3}\end{aligned}$$

for specific values of q_2 and for small controller orders. The matrices A, B, C, D are taken from Greeley & Hyland (1988)

$$A = \begin{bmatrix} -p & I_7 \\ 0 & O \end{bmatrix},\quad p = \begin{bmatrix} 0.161\\ 6.004\\ 0.5822\\ 9.9835\\ 0.4073\\ 3.982\\ 0 \end{bmatrix},\quad B = \begin{bmatrix} 0\\ 0\\ 0.0064\\ 0.00235\\ 0.0713\\ 1.0002\\ 0.1045\\ 0.9955 \end{bmatrix}$$

$$C = [\,1\;0\;0\;0\;0\;0\;0\;0\,],\qquad D = 0$$

By setting

$$\begin{aligned}z &= rx\\ v_x &= \sqrt{q_2}Bv\end{aligned}$$

we have

$$\begin{aligned}\dot{x} &= Ax + B(u+\sqrt{q_2}v)\\ y &= Cx + w\\ z &= rx\end{aligned}$$

with v, w unit intensity white noise, and the performance index

$$\mathcal{J} = \int_0^\infty (z^H z + u^H u)\,\mathrm{d}t = \int_0^\infty \begin{bmatrix} u^H & z^H \end{bmatrix}\begin{bmatrix} u\\ z\end{bmatrix}\,\mathrm{d}t$$

We introduce a new input variable:

$$u_G = u + \sqrt{q_2}v$$

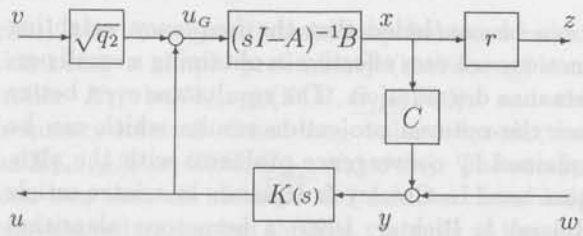

Fig. 4: controller synthesis configuration

Figure 4 gives the controller synthesis configuration. To state the general H_2 control problem in terms of the interconnection $\mathcal{I}(M,G,K)$, we have to define $G(s)$ such that it has no direct connection to the 'world', i.e. the regulation variable z has to be fed back to $M(s)$:

$$\begin{bmatrix} y-w \\ z \end{bmatrix} = \begin{bmatrix} C \\ r \end{bmatrix} (sI-A)^{-1}B\,(u+\sqrt{q_2}v) = G(s)u_G$$

resulting in a non-square system transfer matrix $G(s)$. M is non-square too, it only contains the weighting parameter q_2 and thus has no dynamics of its own:

$$\left|\begin{array}{c} u_G \\ \cdots\cdots \\ u \\ z \\ \cdots\cdots \\ y \end{array}\right| = \left|\begin{array}{cc:cc:c} 0 & 0 & \sqrt{q_2} & 0 & 1 \\ \cdots & \cdots & \cdots & \cdots & \cdots \\ 0 & 0 & 0 & 0 & 1 \\ 0 & 1 & 0 & 0 & 0 \\ \cdots & \cdots & \cdots & \cdots & \cdots \\ 1 & 0 & 0 & 1 & 0 \end{array}\right| \left|\begin{array}{c} y-w \\ z \\ \cdots\cdots \\ v \\ w \\ \cdots\cdots \\ u \end{array}\right|$$

The purpose is to minimize $\|\mathcal{I}(M,G,K)\|_2$ over

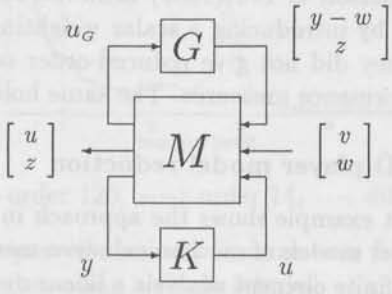

Fig. 5: Signals in the four-disk problem

$K(s)$ for different values of q_2 and for different controller orders. For the full-order case optimal solutions exist that can be computed by solving Riccati equations. These controllers will be denoted by K_8 (they depend on q_2). Greeley & Hyland have shown that the difficulty with obtaining reduced-order controllers that yield a stable closed-loop system can be resolved by directly synthesizing a low-order controller using the optimal projection equations. They compared their method in 42 cases with indirect methods that first design a full-order optimal controller and then reduce this controller by a specific method. 7 values for the disturbance noise intensity parameter q_2 were examined:

0.01 0.1 1 10 100 1000 2000

and the controller order r was fixed to:

2 3 4 5 6 7

The original method of Enns only failed to give stable closed-loop systems in 4 cases, as did the fractional balanced reduction method of Liu & Anderson (1986). Closed-loop balanced controller reduction as developed in this paper yields 6 unstable cases as shown in Table 1. Three of them are due to an almost hidden unstable pole in the controller, and the stable part of the controller achieved closed-loop stability. The remaining three cases are clearly the most critical ones: the disturbance levels are high and the controller order is limited to 2. The advantage of closed-loop balanced controller reduction is that it is extremely

Enns (1984d)

	0.01	0.1	1	10	100	1000	2000
7							
6							
5							
4							■
3							
2					■	■	■

Liu & Anderson (1986)

	0.01	0.1	1	10	100	1000	2000
7							
6							■
5							■
4							
3						■	■
2							

bal$\mathcal{R}(\mathcal{I}(M,G,\underline{K_8}))$

	0.01	0.1	1	10	100	1000	2000
7							
6							
5				=			
4							
3			=				=
2					■	■	■

□ : stable, ■ : unstable, [=] : stable with stable part of unstable controller

Table 1: Stability of $\mathcal{I}(M,G,K_r)$ for different q_2 (horiz.) and r (vert.)

simple and that the results can be manipulated afterwards by adding scalar frequency functions. It proved to be relatively simple to force *stability* by adding frequency functions in regions where unstable poles occured. Also it was revealed that better *performance* was possible by highlighting the frequency regions that contribute most to the H_2 norm of the closed-loop system. Thereto we compare normalized H_2-norms. Since Greeley & Hyland only give the controllers of 9 cases we only treat those cases. For $q_2 \leq 1$ the reduction results are almost the same which means that by a simple method as closed-loop balanced controller reduction, controller states that are spurious can be discarded. For $q_2 > 1$ differences occur especially for small r. Figure 6 compares the optimal $\|\mathcal{I}(M,G,K_8)\|_2/\sqrt{q_2}$ with $\|\mathcal{I}(M,G,K_2)\|_2/\sqrt{q_2}$ for K_2 either from optimal projection, fractional balanced reduction, or frequency weighted closed-loop balanced controller reduction. The frequency functions used to achieve the reduction in performance degradation are very simple: each channel has a unit weight over all frequencies and pulses and/or intervals are added to both inputs and/or both outputs. For the $q_2 = 100$ case the frequency functions were

H_2-norms of closed-loop system divided by $\sqrt{q_2}$ for different values of q_2

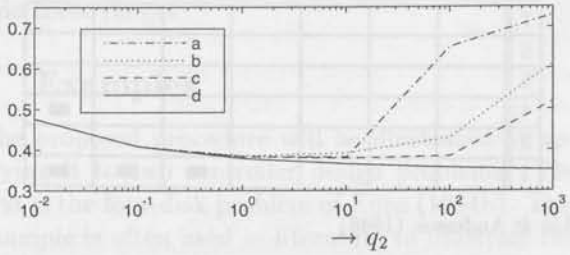

a) K_2 by optimal projection
b) K_2 by fractional balanced reduction
c) $\text{bal}\mathcal{R}_{-6}(\psi_{u,z}(\omega)\cdot\mathcal{I}(M,G,\underline{K_8})\cdot\psi_{w,v}(\omega))$
d) optimal controller K_8

Fig. 6: Performance degradation with second-order controller

$$\begin{aligned}\psi_{v,w}(\omega) &= 1 + 0.05\ \delta(\omega,[\![0.05]\!])\\ \psi_{u,z}(\omega) &= 1 + 1000\ \delta(\omega,[\![0.246]\!])\end{aligned}$$

For $q_2 = 10$ it was sufficient to use one additional frequency pulse:

$$\begin{aligned}\psi_{v,w}(\omega) &= 1\\ \psi_{u,z}(\omega) &= 1 + 35\ \delta(\omega,[\![0.17]\!])\end{aligned}$$

It can be concluded that the frequency weighting functions are very effective in obtaining a small performance degradation. The results are even better than the optimal projection results which can be explained by convergence problems with the algorithm used in Greeley & Hyland: in a later article (Hyland & Richter, 1990) a homotopy algorithm is used and results for $q_2 = 2000$, $r = 2$ are very close to the optimal full-order result as is shown in Table 2). Hyland & Richter do not provide

r	A	a	b	c
8	15.60			
4	16.2	16.99	30.10	16.92
	$\psi_{v,w} = 1{+}12.79\delta(\omega,[\![0.0917]\!])$			
	$\psi_{u,z} = 1{+}75.23\delta(\omega,[\![0.0637]\!]){+}$			
	$(-9.875{+}40.01\omega{-}18.33\omega^2)\eta(\omega,[\![0.6804,1.4953]\!])$			
2	16.8	30.02	42.36	18.06
	$\psi_{v,w} = 1{+}250\eta(\omega,[\![0.0003,0.03]\!])$			
	$\psi_{u,z} = 1{+}60\eta(\omega,[\![0.03,0.6]\!])$			

A) K_r as in Hyland & Richter (1990)
a) K_r as in Greeley & Hyland (1988)
b) K_r by fractional balanced reduction
c) $\text{bal}\mathcal{R}_{r-8}(\psi_{u,z}(\omega)\cdot\mathcal{I}(M,G,\underline{K_8})\cdot\psi_{v,w}(\omega))$

Table 2: H_2 norms of closed-loop system for the $q_2 = 2000$ case

reduced-order controller data for the other values of q_2. Other solutions for Finally it should be noticed that Anderson & Liu (1989) achieved stability in all cases by introducing a scalar weighting parameter. They did not give reduced-order controllers nor performance measures. The same holds for

7.2 CD-player model reduction

The next example shows the approach in reducing high-order models of mechanical servo-mechanisms.

From finite element analysis a linear model of order 120 has been derived for the servo-mechanism of a CD-player. It has inputs for in-plane tracking and out-of-plane focussing. The outputs are the tracking and focussing errors. The vibration modes are lightly damped. Balanced reduction is appropriate for $r \geq 32$. For smaller r balanced reduction yields bad results in the desired cross-over frequency range. Ceton (1993) compares a number of methods to do closed-loop relevant reduction to 14^{th} order. These includes LQG-balanced reduction, H_∞-balanced reduction, the open-loop frequency-interval balanced reduction $\text{bal}\mathcal{R}_{14-120}(\psi(\omega)\cdot G_{120}\cdot$

$\psi(\omega)$), the unweighted closed-loop balanced reduction using a simple preliminary (stabilizing) controller K_4, bal$\mathcal{R}_{14-120}(\mathcal{I}(M, \underline{G_{120}}, K_4))$, and the frequency-interval closed-loop balanced reduction bal$\mathcal{R}_{14-120}(\psi(\omega)\cdot\mathcal{I}(M, \underline{G_{120}}, K_4)\cdot\psi(\omega))$. The conclusion was that all methods did achieve closed-loop relevant reduction, but the first two only at the cost of solving 120^{th}-order Riccati equations. The frequency interval weighting $\psi(\omega)$ was applied at all channels simultaneously. Here we focus on open-loop reduction with only input shaping to emphasize the cross-over frequency region in which normal balanced reduction failed to fit the mechanical modes. Figure 7 compares unweighted balanced reduction bal$\mathcal{R}_{14-120}(G_{120})$ with interval-balanced reduction bal$\mathcal{R}_{14-120}(G_{120}\cdot\psi_w(\omega))$ with

$$\psi_w(\omega) = (1.5616 - 7.5825/10^5|\omega| + 1.8790/10^9\omega^2)\cdot \eta(\omega, [\![10^4, 3\,10^4]\!])$$

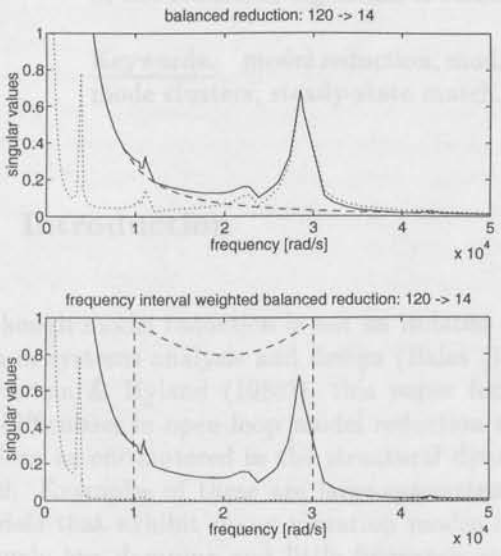

—: order 120, −−: order 14, $\cdots$: difference

Fig. 7: Improved accuracy in cross-over frequency region using a single interval

8 Conclusion

Simple extensions of frequency weighted balanced reduction are very suitable for application of order reduction within controlled systems. Model and controller reduction can be used in conjunction with model-based control design, since the same configuration is used. Flexible computer implementation using MATLAB4 facilitates the interactive design of systems with relatively low-order controllers.

9 References

Anderson B.D.O. and Y. Liu, (1989). Controller reduction: concepts and approaches, *IEEE Trans. Automat. Contr.*, vol.34, 802–812.

Balas G.J., J.C. Doyle, K. Glover, and A.K. Packard (1991). *μ-Analysis and Synthesis Toolbox*, MUSYN Inc., Minneapolis.

Bongers P.M.M., and O.H. Bosgra, (1991). Controller reduction with closed-loop stability margins, *Selected Topics in Identification, Modelling and Control, vol.3,* Delft Univ. Press, 35–41.

Ceton C., P. Wortelboer, and O. Bosgra, (1993). Frequency weighted closed-loop balanced reduction, *Proc. 2^{nd} European Control Conference,*, Groningen June 26- July 1, 1993, 697–701.

Ceton C., (1993). Closed-loop model and controller reduction: An application to a CD-player system. *Philips Unclassified Report 007/93.*

Doyle J.C. (1982). Analysis of feedback systems with structured uncertainties. *IEE Proc., Part D, Conmtrol Theory and Applicatinos, vol.129, no.6,* 242–250.

Doyle J.C., A. Packard, and K. Zhou, (1991). Review of LFTs, LMIs, and μ, *Proc. 30^{th} IEEE Conf. Dec. & Contr.,* 1227–1232.

Enns D.F. (1984a). Model reduction with balanced realization: an error bound and a frequency weighted generalization, *Proc. 23^{rd} IEEE Conf. Dec. & Contr.,* 127–132.

Enns D.F. (1984b). *Model reduction for control system design,* Ph.D. Thesis, Dept. Aeronautics and Astronautics, Stanford University, Stanford, CA, USA.

Gawronski W., and J-N Juang, (1990). Model Reduction for Flexible Structures, *Control and Dynamic Systems,* vol.36, 143–222.

Greeley S.W., and D.C. Hyland (1988). Reduced-order compensation: Linear-Quadratic Reduction versus optimal projection. *AIAA Journal of Guidance, Control and Dynamics,* vol.11, 328–335.

Hyland, D.C. and D.S. Bernstein, (1984). The optimal projection equations for fixed-order dynamic compensation, *IEEE Trans. Automat. Contr.*, vol.AC-29, no.11, 1034–1037.

Hyland, D.C. and S. Richter, (1990). On direct versus indirect methods for reduced-order controller design, *IEEE Trans. Automat. Contr.*, vol.35, no.3, 377–379.

Jonckheere E.A., and L.M. Silverman (1983). A new set of invariants for linear systems-application to reduced order compensator design,

IEEE Trans. Automat. Contr., vol.AC-28, 953–964.

Liu Y., and B.D.O. Anderson, (1986). Controller reduction via stable factorization and balancing, *Int. J. Control,* vol.44, no.2, 507–531.

Meyer D.G. (1988). A fractional approach to model reduction, *Proc. American Control Conf.*, 1041–1047.

Moore B.C. (1981). Principal component analysis in linear systems: controllability, observability, and model reduction, *IEEE Trans. Automat. Contr.*, AC-26, 17–32.

Mustafa D. (1989). $\mathcal{H}_\infty$-Characteristic values, *Proc. 28th IEEE Conf. Dec. & Contr.* , 1483–1487.

Villemagne, C. de, and R.E. Skelton, (1988). Controller reduction using canonical interactions, *IEEE Trans. Automat. Contr.*, vol.33, no.8, 740–750.

Wortelboer P.M.R., and O.H. Bosgra, (1992a). Generalized frequency weighted balanced reduction, *Proc. 31st IEEE Conf. Dec. & Contr.* , 2848–2849.

Wortelboer P.M.R., and O.H. Bosgra, (1992b). Generalized frequency weighted balanced reduction, *Selected Topics in Identification, Modelling and Control, vol.5,* Delft Univ. Press, 29–36.

Wortelboer P.M.R., and O.H. Bosgra, (1994). Order reduction in the control design configuration, *IMACS Symposium on Mathematical Modelling,* Vienna, Febr.2–4, 1994, to appear

Wortelboer P.M.R., (1994). *Frequency-Weighted Balanced Reduction of Closed-Loop Mechanical Servo-Systems: Theory and Tools,* Dr. Dissertation, Delft University of Technology, to appear.

Zhou K., J. Doyle, and K. Glover, (1993). *Robust and Optimal Control, preprint*

Selected Topics in Identification, Modelling and Control
Vol. 6, December 1993

Mixed forms of modal and balanced reduction

Pepijn M.R. Wortelboer [‡] **and Okko H. Bosgra**[§]

[‡]*Philips Research Laboratories, Prof. Holstlaan 4, 5656 AA Eindhoven, The Netherlands.*
[§]*Mechanical Engineering Systems and Control Group*
Delft University of Technology, Mekelweg 2, 2628 CD Delft, The Netherlands.

Abstract. In this paper it is shown that modal reduction and balanced reduction each have difficulties with specific reduction problems, whereas a combination of both can solve these reduction problems. High-order models with lightly damped and/or closely spaced eigenvalues are well-known examples of difficult reduction problems and require a reduction strategy based on such a combination. It is shown that a minor adjustment of the reduction algorithm is sufficient to preserve gains both at $\omega = 0$ and for $\omega \to \infty$.

Keywords. model reduction; modal reduction; balanced reduction; structural dynamics; mode clusters; steady-state match.

1 Introduction

Although model reduction is not an isolated problem in systems analysis and design (Balas (1982), Bernstein & Hyland (1988)), this paper focusses on difficulties in open-loop model reduction applications as encountered in the structural dynamics field. Examples of these are large-space-structure models that exhibit many vibration modes of extremely low damping and little frequency separation, and fast mechanical servo systems of which many high-frequency modes may deteriorate the closed-loop behaviour.

Models of such systems are often in modal form. In specific applications not all vibration modes are equally important: the placement of actuators and sensors determines an input-output-importance ranking of the vibration modes that may deviate from the natural frequency ranking of the vibration modes. Irrespective of their natural frequency, vibration modes may be almost hidden, and extraction of these modes from the mechanical model (often called modal reduction) is a straightforward procedure to obtain a lower-order and accurate input-ouput description of the mechanical system. [1] Other order reduction techniques, such as balanced reduction and optimal Hankel-norm reduction (Glover, 1984), that are designed for reducing input-output systems, are not used much in structural dynamics modelling: they are more elaborate and tend to minimize the frequency response mismatch over all frequencies, while in mechanical systems it is often more appropriate to minimize the *relative* frequency response mismatch due to the inherent roll-off. The reason for using other methods than modal reduction, is that modal reduction of systems with closely-spaced eigenvalues can be very difficult. Balanced reduction can be applied to high-order models if all modes are damped. It will be shown that balanced reduction sometimes outperforms modal reduction and that modal reduction handles almost cancelling modes much better than balanced reduction. This paper sketches a reduction strategy including modal and balanced reduction, that can safely solve reduction problems in structural dynamics.

Besides, a general procedure is developed to mod-

[1] Note that modal reduction in system theory is based on the assumption that some modes with the highest frequencies are infinitely fast and can be described statically by a singular perturbation approach.

ify the reduction such that the steady state gain is preserved. This is important in mechanical systems in case the static deformation due to external forces has to be described accurately. The common approach to achieving a perfect match at zero frequency is residualization. The advantage of the new method is that it does not introduce (or change) the direct feedthrough term D.

The organisation of this paper is as follows. After some preliminaries the modelling approach in structural dynamics is explained, then the reduction principle behind modal and balanced reduction is described and modal and balanced reduction are reviewed in an 'algorithmic' way. Some illustrative difficult reduction problems are introduced to show the weaknesses of balanced and modal reduction. The reduction strategy to solve these problems is exposed thereafter. Finally the modification for matching the steady state is developed and applied to one of the examples.

2 Preliminaries

The systems discussed in this paper are linear time-invariant and finite-dimensional. A system of order n with n_u inputs and n_y outputs is represented in state-space coordinates as follows:

$$G: \quad \begin{array}{rcl} \dot{x}(t) & = & Ax(t) + Bu(t) \\ y(t) & = & Cx(t) + Du(t) \end{array}$$

$x(t) \in \mathbb{R}^{n\times 1}$, $u(t) \in \mathbb{R}^{n_u\times 1}$, and $y(t) \in \mathbb{R}^{n_y\times 1}$. Matrices A, B, C, D have compatible sizes.

$$G = \left[\begin{array}{c|c} A & B \\ \hline C & D \end{array}\right]$$

is a specific realization of the transfer matrix $G(s) = C(sI - A)^{-1}B + D$.

$$\tilde{G} = \left[\begin{array}{c|c} T^{-1}AT & T^{-1}B \\ \hline CT & D \end{array}\right] \qquad T \in \mathbb{R}^{n\times n} \text{non-singular}$$

represents other realizations of $G(s) = \tilde{G}(s)$.

System norms that are frequently used to measure the reduction error $G_r - G_n$ are the infinity norm

$$\|F\|_\infty \stackrel{\text{def}}{=} \sup_{\omega\in\mathbb{R}} \varsigma_{\max}(F(j\omega)) \qquad (1)$$

with $\varsigma(A)$ the singular values of a constant matrix A, and the two-norm

$$\|F\|_2 \stackrel{\text{def}}{=} \frac{1}{2\pi}\int_{-\infty}^{\infty} \text{tr}\,[F^H(j\omega)F(j\omega)]\,\mathrm{d}\omega \qquad (2)$$

3 Structural dynamics and modal reduction

In structural dynamics (see Bathe (1982), and Argyris (1991)) it is common practice to model mechanical systems using finite-element techniques: the distributed inertia of each element is lumped to its nodal points (corners of the element), and the (distributed) flexibility is translated to flexibilities between nodal points. The resulting inertia and stiffness matrix (M and K) together state the undamped eigendynamics of the mechanical system:

$$A = \begin{bmatrix} O & I \\ -M^{-1}K & O \end{bmatrix}.$$

To model all vibration modes with an undamped frequency below a specific threshold frequency accurately, it may be necessary to use many elements and this leads to high-dimensional A matrices. The highest-frequency vibration modes are less accurate than the lower-frequency vibration modes and therefore only the lower-frequency modes are actually computed. To model a specific input-output behaviour only the structural points on which actuation forces or disturbances enter, and structural points of which the motion is measured (controlled), are relevant: they state the input matrix B and output matrix C. Damping is hard to quantify, but very small in most cases. This explains why it is often neglected in the finite-element-modelling stage and specified afterwards by adding a small modal damping factor to the modes. Next we look at the modal system description from a more general point of view. Recall that each linear system has a partial fraction expansion (see Skelton, 1988) of which most fractions are of the $r/(s-\lambda)$-form, with r the residue and λ the eigenvalue or pole. In case λ is complex, we often write

$$\lambda = -\beta\omega_0 + j\omega_0\sqrt{1-\beta^2}$$

with ω_0 the undamped frequency and β the damping ratio. In this case it is convenient to build a second-order modal fraction with real parameters by taking the complex conjugate pair of first-order fractions together:

$$\begin{aligned} \frac{r}{s-\lambda} + \frac{\bar{r}}{s-\bar{\lambda}} &= 2\,\frac{\text{Re}(r)\,s + \text{Re}(r\bar{\lambda})}{s^2 - 2\text{Re}(\lambda)\,s + \lambda\bar{\lambda}} \\ &= 2\,\frac{\text{Re}(r)\,s + \text{Re}(r\bar{\lambda})}{s^2 + 2\beta\omega_0\,s + \omega_0^2} \end{aligned}$$

In structural dynamics, a 'mode' means a vibration mode, and deleting a mode means neglecting a

second-order modal fraction. Candidates for deletion are modes with large β and ω_0 and small $|r|$. The problem is that modes may have strong interaction. One often resorts to frequency-response-based mode selection; if the poles are lightly damped and well separated, the contribution of each mode to the frequency response of the system can be easily traced back, but in case modes have poles that are well-damped or close to each other, the selection process is less obvious and reduction is often hardly possible.

In modal reduction it is possible to make approximations that are better in one frequency range than in the other.

4 Reduction by projection

First we define a projection matrix (Villemagne & Skelton, 1987)

Definition 4.1 (Projection matrix) *A projection matrix Π_r is a square matrix $(n \times n)$, that can be written as*

$$\Pi_r = R_r L_r^H$$

with $R_r, L_r \in \mathbb{R}^{n\times r}$ satisfying

$$L_r^H R_r = I_r$$

Π_r has the following properties: $\Pi_r^2 = \Pi_r$, $\text{rank}(\Pi_r) = r$, it has r eigenvalues equal to 1 and $t = n - r$ eigenvalues equal to 0, and there exist $R_t, L_t \in \mathbb{R}^{n\times t}$ such that $\Pi_t = R_t L_t^H = I_n - \Pi_r$ is a projection matrix of rank t. If $\Pi_s = \Pi_s^T$ the projection is called 'orthogonal', otherwise it is 'oblique'. A subspace $S \subseteq \mathbb{R}^n$ is often characterized by an orthogonal projection matrix (Golub & van Loan, 1989): $S = \text{range}(\Pi_s)$, and for the distance between two subspaces S and T we have

$$\text{dist}(S,T) = \|\Pi_s - \Pi_t\|_2$$

where Π_s, Π_t are orthogonal projections onto S and T respectively.

Next we analyse the role of projections in model reduction. In the sequel a subscript as in G_r means that the realization is of order r. The original model is of order n, but we often write G instead of G_n. Order reduction is basically achieved by neglecting states with the highest index: this amounts to truncating a state-space realization. Let $\Gamma_r = \left[\begin{smallmatrix} I_r \\ O \end{smallmatrix}\right]$ with $O \in \mathbb{R}^{t\times r}$ a zero matrix, then the truncation of realization G_n to order r is:

$$G_r = \left[\begin{array}{c|c} \Gamma_r^T A \Gamma_r & \Gamma_r^T B \\ \hline C\Gamma_r & D \end{array}\right] = \left[\begin{array}{c|c} A_{(1:r,1:r)} & B_{(1:r,:)} \\ \hline C_{(:,1:r)} & D \end{array}\right] \quad (3)$$

In the projection of dynamics formulation, the truncation is induced by the projection matrix

$$\Pi_r = \Gamma_r \Gamma_r^T = \left[\begin{smallmatrix} I_r & O \\ O & O \end{smallmatrix}\right]$$

4.1 Modal reduction

The type of realization prior to truncation states the reduction type. Modal reduction is the truncation of a modal realization. The ordering of the modal states in a modal realization is free and the procedure for modal reduction then is:

1) compute modal realization
2) arrange modal states in decreasing order of importance
3) truncate the new modal realization

In case of vibration modes, the complex conjugate pairs of modal states should be kept together. As all truncation methods modal reduction preserves the transfer matrix 'at infinity': D does not change. The steady-state however changes in general. Residualization of the least important modal fractions:

$$\frac{r}{s-\lambda} \rightarrow \frac{r}{-\lambda} \quad (4)$$

restores the steady-state gain, but the new constants of (4) add to the D-term.

4.2 Balanced reduction

Balanced reduction was first described by Moore (1981). A short summary is given in terms of the balancing algorithm for a stable linear finite-dimensional system. First the controllability Gramian P and observability Gramian Q are solved from two Lyapunov equations

$$\begin{aligned} AP + PA^H + BB^H &= 0 \\ A^H Q + QA + C^H C &= 0. \end{aligned}$$

$\sigma = \sqrt{\lambda(PQ)}$ are realization independent Hankel singular values (HSVs) arranged in decreasing order. Relatively small HSVs point to the existence of states that contribute little to the input-output behaviour of the system. These states can be found be applying a balancing transformation $\breve{T}$ that achieves equal and diagonal Gramians of the transformed (balanced) realization

$$\breve{G} = \left[\begin{array}{c|c} \breve{A} & \breve{B} \\ \hline \breve{C} & D \end{array}\right] = \left[\begin{array}{c|c} \breve{T}^{-1} A \breve{T} & \breve{T}^{-1} B \\ \hline C\breve{T} & D \end{array}\right]$$

with

$$\breve{T}^{-1} P \breve{T}^{-H} = \breve{T}^H Q \breve{T} = \Sigma = \text{diag}(\sigma)$$

Balanced reduction is the truncation of a balanced realization. After partitioning of $\breve{T}$,

$$\begin{aligned} \breve{T} &= \left[\begin{array}{cc} \breve{R}_r & \breve{R}_t \end{array} \right] \qquad (\breve{R}_r = \breve{T}\Gamma) \\ \breve{T}^{-H} &= \left[\begin{array}{cc} \breve{L}_r & \breve{L}_t \end{array} \right] \qquad (\breve{L}_r = \breve{T}^{-H}\Gamma) \end{aligned}$$

we can write

$$\breve{G}_r = \left[\begin{array}{c|c} \breve{L}_r^H A \breve{R}_r & \breve{L}_r^H B \\ \hline C\breve{R}_r & D \end{array} \right]$$

The balanced approximation is still stable and balanced. The steady-state changes in general. Similarly as a modal realization the balanced realization can be truncated and residualized. The balanced residualization leads to preservation of the steady-state gain and to a change in the D-term.

The choice of the order r is based on the HSVs: as shown by Enns (1984), and Glover (1984), we can derive an a priori H_∞ reduction error bound based on the HSVs associated with the truncated balanced states

$$\|G_n(j\omega) - \breve{G}_r(j\omega)\|_\infty \leq 2(\sigma_{(r+1)} + \ldots + \sigma_{(n)})$$

Balanced reduction is not optimal in H_∞-norm nor in H_2-norm, but the experience is that balanced reduction is a nice compromise between H_∞-norm and H_2-norm optimal reduction in most cases (see Hakvoort (1993) for computation of the H_∞-norm optimal reduction).

Remark 4.2 *The link between modal and balanced reduction that has been established for lightly damped systems disappears for systems with closely spaced eigenvalues (Gregory, 1984).*

5 Difficult reduction problems

Here we consider a siso system with some lightly damped and close eigenvalues.

$$\begin{aligned} G_{12}(s) &= \sum_{i=1}^{6} G_{pi}(s) \\ G_{pi}(s) &= G_{ci}(s) + \mathrm{conj}(G_{ci}(s)) \qquad i = 1, \ldots, 6 \end{aligned}$$

Each second-order real-valued modal fraction $G_{pi}(s)$ is completely defined by a complex-valued first-order modal fraction:

$$\begin{aligned} G_{c1}(s) &= \frac{7.62080 + 0.04598j}{s + 10.000 - 0.082960j} \\ G_{c2}(s) &= \frac{-2.01979 + 1.13666j}{s + 0.0015324 - 0.314136j} \\ G_{c3}(s) &= \frac{2.00633 - 1.13571j}{s + 0.0015243 - 0.314140j} \\ G_{c4}(s) &= \frac{0.61072 + 1.56996j}{s + 0.0098736 - 0.999430j} \\ G_{c5}(s) &= \frac{-0.69828 - 1.55806j}{s + 0.0100070 - 0.999930j} \\ G_{c6}(s) &= \frac{-8.92875 - 6.55249j}{s + 3.0000 - 9.539200j} \end{aligned}$$

Inspection reveals that G_{p2} and G_{p3} almost cancel each other, and modal reduction to order 8 seems natural:

$$\dot{G}_8(s) = G_{p1}(s) + G_{p4}(s) + G_{p5}(s) + G_{p6}(s)$$

The approximation is visualized in Fig. 1. The frequency response plots of the full-order and reduced-order model lie on top of the other. Next the 8^{th}-

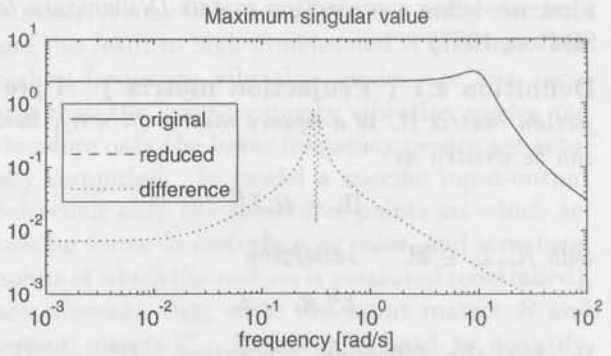

Fig. 1: Modal reduction of G_{12} to order 8 by truncating almost cancelling modes: $\dot{G}_8$

order balanced approximation $\breve{G}_8$ is shown in Fig. 2. It is clear that balanced reduction suffers from these

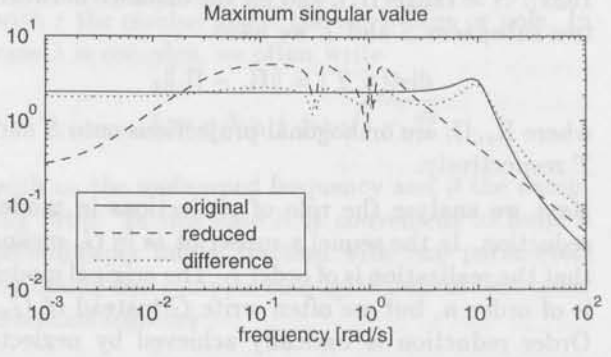

Fig. 2: Balanced reduction of G_{12} to order 8: $\breve{G}_8$

nearly cancelling modes. This is a common phenomenon in mechanical systems, and shows that modal reduction can help in avoiding unpredictable reduction results.

The second example is meant to stress that balanced reduction *can* cope with modes of nearly equal eigenfrequencies. Consider

$$K_{12} = G_{p1} - G_{p2} + G_{p3} + G_{p4} + G_{p5} + G_{p6}$$

and let

$$\breve{K}_8 = \breve{K}_{p3} + \breve{K}_{p4} + \breve{K}_{p5} + \breve{K}_{p6}$$

be the 8^{th}-order balanced approximation (Fig. 3). The frequency function of the reduction error does not show any peaks which is confirmed by $\|K_{12} - \breve{K}_8\|_\infty = 0.4001$. Loosely speaking, the G_{p1} dynamics is lost, and $-G_{p2}$ and G_{p3} are substituted by a new $\breve{K}_{p3}$ with poles $-0.0015291 \pm 0.031414j$ very close to the original pairs. Modal reduction can-

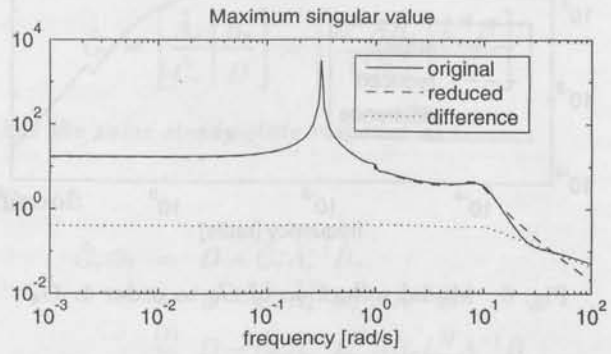

Fig. 3: Balanced reduction of K_{12} to order 8: $\breve{K}_8$

not merge $-G_{p2}$ and G_{p3}, we have to select one of them or both. If we choose both we can approximate the main peak very well, but only at the cost of less accuracy at other frequencies.

$$\grave{K}_8 = -G_{p2} + G_{p3} + G_{p4} + G_{p5}$$

The reduction error, $\|K_{12} - \grave{K}_8\|_\infty = \|G_{p1} + G_{p6}\|_\infty = 3.0985$, is clearly larger than 0.4001. This

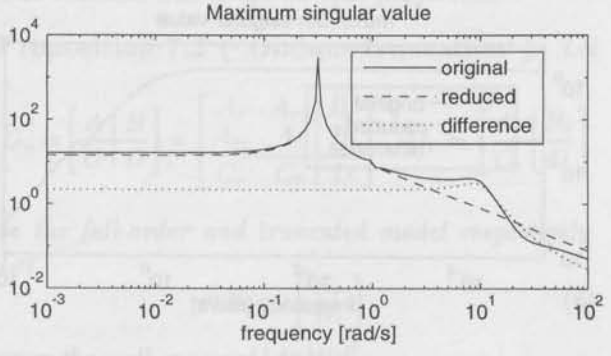

Fig. 4: Modal reduction of K_{12} to order 8: $\grave{K}_8$

is shown in Fig. 4. Truncating $G_{p1} - G_{p2}$, $G_{p1} + G_{p3}$, $G_{p2} + G_{p6}$, or $G_{p3} + G_{p6}$ all yield extremely bad H_∞-norm errors (> 1500).

Next we summarize the strong and weak points of modal reduction:

+ computationally straightforward
+ recursive
+ direct frequency dependent approximation
– restricted for strongly coupled modes
– iterations required

and balanced reduction

+ computationally straightforward
+ recursive
– restricted for nearly cancelling modes
– no direct frequency dependent approximation
+ only iterations on order required

It seems that depending on the type of coupling between modes, either modal or balanced reduction is required.

6 Reduction strategy using both modal and balanced reduction

Starting point is a modal realization as mechanical system analysis usually provides. Frequency response calculations are extremely simple, even for very large models. This enables fast graphical evaluation in the frequency domain.

The main idea is to use clusters of modes. Modes within a cluster have eigenvalues close to each other, but clearly different from the eigenvalues of all modes out of the cluster. Each cluster can be reduced separately by balanced reduction. This includes truncating the entire cluster in case the modes in the cluster are nearly cancelling each other. Each time we reduce, we compare the resulting model with the full-order model by inspecting both frequency responses. If the reduction error increases dramatically, we go one step back and try less severe reduction within the cluster. It may well be necessary to keep the cluster entirely. Having found a satisfactory cluster approximation, we proceed with another cluster. The procedure assumes that a system can be divided in parallel subsystems that have little coupling seen from input to output. Instead of balanced reduction other reduction methods can be applied to the clusters too. The freedom in clustering and in choosing the reduced order per cluster, can be exploited to force the approximation to be more accurate in specific frequency regions than in others. A drawback is that many choices are to be made which makes com-

puter graphics indispensable.

A priori error bounds cannot be given in general. In case we reduce each cluster only once, an H_∞-norm error bound can be derived straighforwardly and the method is recursive in this special case. The procedure unifies modal reduction and balanced reduction. Summarizing:

+ computationally straightforward
+ direct frequency dependent approximation
+ no problems with strongly coupled modes
+ modal and balanced reduction are special cases
- iterations on cluster selection required
- iterations on order required

The next example was used by Hung & Muzlifah (1990) to illustrate their optimal Hankel-norm reduction method that can retain specific poles. The purpose was to force a good approximation near specific resonant poles.

Example 6.1 (Hung & Muzlifah, 1990) *Let*

$$
\begin{aligned}
G_6(s) &= R_2(s) + I_2(s) + J_2(s) \\
R_2(s) &= \frac{8.4693}{s+1} - \frac{8.7211}{s+1.5} \\
I_2(s) &= 0.0080014\,\frac{s+0.055805}{s^2+0.1\,s+1} \\
J_2(s) &= 0.25380\,\frac{s+4.3278}{s^2+3\,s+100}
\end{aligned}
$$

The purpose is to reduce G_6 from order 6 to order 4 while retaining the poles of J_2. In Hung & Muzlifah (1990) the optimal Hankel-norm solution is given. This

$$
\begin{aligned}
H_4(s) &= 0.1510\,\frac{s+20.616}{s^2+3\,s+100} \\
&- 0.6937\,\frac{s-6.7534}{s^2+2.9131\,s+1.8241} \\
&+ 0.0336
\end{aligned}
$$

is compared with

a) Modal reduction: $\grave{G}_4(s) = R_2(s) + J_2(s)$

b) Balanced reduction: $\breve{G}_4(s)$

c) Cluster-based balanced reduction: $\hat{G}_4(s) = \breve{F}_2(s) + J_2(s)$ with $\breve{F}_2(s)$ the second-order balanced approximation of $F_4(s) = R_2(s) + I_2(s)$

i.e.

$$
\begin{aligned}
\hat{G}_4(s) &= 0.2538\,\frac{s+4.3278}{s^2+3\,s+100} \\
&- 0.2457\,\frac{s-16.341}{s^2+2.5092\,s+1.5153}
\end{aligned}
$$

From Figures 5, 6, 7, 8 it can be concluded that the high-frequency approximation of balanced reduction and optimal Hankel-norm reduction with fixed poles is worse than the high-frequency approximation of modal reduction and cluster-based balanced reduction.

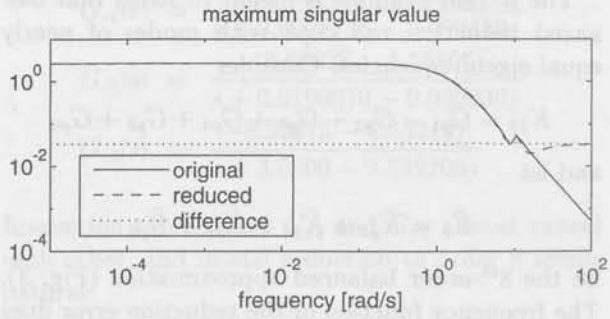

Fig. 5: Optimal Hankel-norm reduction of G_6 to order 4 with fixed poles: H_4

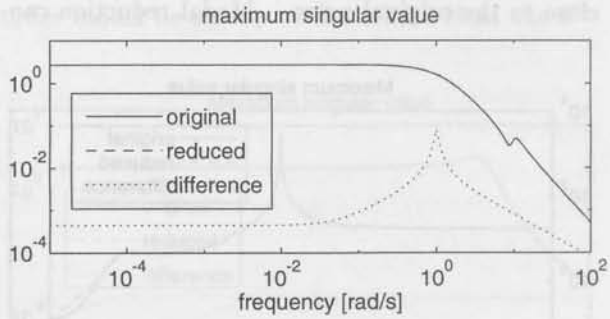

Fig. 6: Modal reduction of G_6 to order 4: $\grave{G}_4$

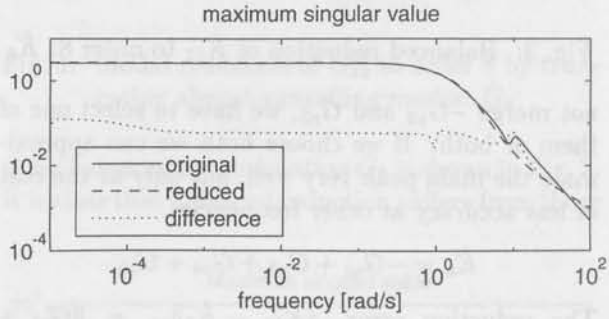

Fig. 7: Balanced reduction of G_6 to order 4: $\breve{G}_4$

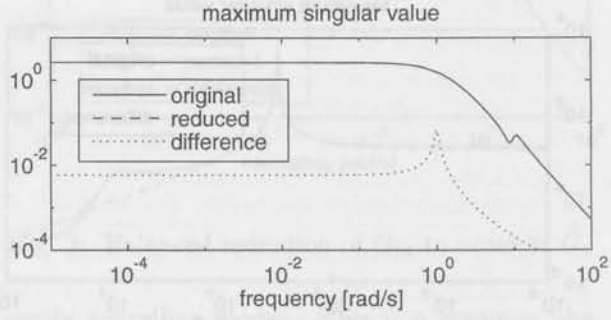

Fig. 8: Cluster-based balanced reduction of G_6 to order 4: $\hat{G}_4$

7 Matching the steady-state

Here a projection-based modification is worked out to ensure that the steady-state response remains the same after reduction. From Villemagne & Skelton (1987) we have the following result.

Proposition 7.1 (Projection of dynamics for steady-state matching) *Let*

$$G = \left[\begin{array}{c|c} A & B \\ \hline C & D \end{array}\right]$$

and the projection matrix $\Pi_r = R_r L_r^H$ *such that*

$$\Pi_r A^{-1} B = A^{-1} B \tag{5}$$

then

$$\hat{G}_r = \left[\begin{array}{c|c} \hat{A}_r & \hat{B}_r \\ \hline \hat{C}_r & D \end{array}\right] = \left[\begin{array}{c|c} L_r^H A R_r & L_r^H B \\ \hline C R_r & D \end{array}\right]$$

has the same steady-state response as G.

Proof:

$$\begin{aligned} \hat{G}_r(0) &= D - \hat{C}_r \hat{A}_r^{-1} \hat{B}_r \\ &= D - \hat{C}_r \hat{A}_r^{-1} L_r^H A A^{-1} B \\ &\overset{(5)}{=} D - \hat{C}_r \hat{A}_r^{-1} L_r^H A R_r L_r^H A^{-1} B \\ &= D - \hat{C}_r L_r^H A^{-1} B \\ &= D - C R_r L_r^H A^{-1} B \\ &\overset{(5)}{=} D - C A^{-1} B = G(0) \end{aligned}$$

□

Without loss of generality we only consider reduction by truncation. It is the purpose to adjust the truncation process such that $G_n(0) = \hat{G}_r(0)$. The truncation is governed by $L_r^H = R_r^H = [I_r \;\; O]$, i.e. an orthogonal projection. The idea is to apply a minor adjustment to the projection to satisfy (5). The solution will be an oblique projection.

Proposition 7.2 ('Oblique truncation') *Let*

$$G_n = \left[\begin{array}{c|c} A & B \\ \hline C & D \end{array}\right] = \left[\begin{array}{cc|c} A_r & A_{rt} & B_r \\ A_{tr} & A_t & B_t \\ \hline C_r & C_t & D \end{array}\right], \quad G_r = \left[\begin{array}{c|c} A_r & B_r \\ \hline C_r & D \end{array}\right]$$

be the full-order and truncated model respectively. Let

$$N = \left[\begin{array}{c} N_r \\ N_t \end{array}\right] \tag{6}$$

span the null space of $[A^{-1}B]^H$*:*

$$N^H A^{-1} B = 0 \tag{7}$$

and define the orthogonal projection matrix $\Pi_N = NN^H$*. Let*

$$X = -(N_t N_t^H)^{-1} N_t N_r^H$$

then

$$\hat{R}_r = \left[\begin{array}{c} I_r \\ X \end{array}\right], \quad L_r = \left[\begin{array}{c} I_r \\ O \end{array}\right]$$

define a projection to an r^{th}*-order realization*

$$\hat{G}_r = \left[\begin{array}{c|c} A_r + A_{rt} X & B_r \\ \hline C_r + C_t X & D \end{array}\right]$$

with $G_n(0) = \hat{G}_r(0)$

Proof:

$$\Pi_r = \left[\begin{array}{cc} I_r & O \\ X & O \end{array}\right]$$

and

$$\begin{aligned} \Pi_t &= I_n - \Pi_r = R_t L_t^H \\ L_t &= N N_t^H \\ R_t &= \left[\begin{array}{c} O \\ [N_t N_t^H]^{-1} \end{array}\right] \end{aligned}$$

Condition (5) is identical to $\Pi_t A^{-1} B = 0$, and this follows from

$$L_t^H A^{-1} B = N_t N^H A^{-1} B \overset{(7)}{=} 0$$

□

For $A_{rt} = O$ stability of $G_n(s)$ implies stability of $\hat{G}_r(s)$. Thus the modification can be applied to any modal realization without the risk of destabilizing the model.

A similar result can be derived based on $CA^{-1}\Pi_r = CA^{-1}$. Matching of the steady-state gain requires r to be larger than or equal to $\min(n_u, n_y)$.

Example 7.3 (Hung's example cont'd) *The steady-state modification is applied to Hung's example. The 'oblique truncation' of the balanced realization yields a fourth-order model (8) that approximates the full-order system better than the normal balanced approximation for most frequencies, see Fig. 9. In Fig. 10 a similar improvement is shown for the modification of the cluster-based balanced reduction (9).*

$$\begin{aligned} \hat{G}_4^o(s) &= -2.7972 \frac{s + 2.4213}{s^2 + 3.7962\,s + 6.0786} \\ &\quad + \; 2.9004 \frac{s + 0.01283}{s^2 + 0.7775\,s + 0.009842} \end{aligned} \tag{8}$$

$$\begin{aligned} \hat{G}_4^o(s) &= 0.2538 \frac{s + 4.3283}{s^2 + 3\,s + 100} \\ &\quad - \; 0.2493 \frac{s - 16.1962}{s^2 + 2.5289\,s + 1.5202} \end{aligned} \tag{9}$$

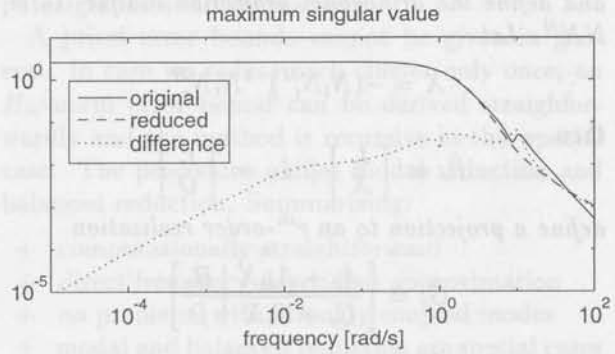

Fig. 9: balanced reduction of G_6 to order 4 with steady-state match: $\check{G}_4^{to}(s)$

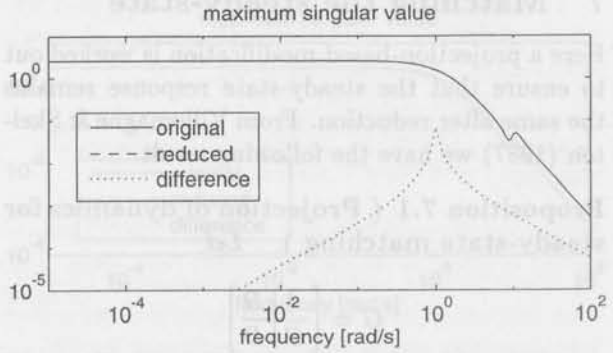

Fig. 10: Cluster-based balanced reduction of G_6 to order 4 with steady-state match: $\hat{G}_4^{to}(s)$

8 Conclusion

Both modal reduction and balanced reduction can have difficulties with reducing systems that have modes with close eigenvalues. A reduction strategy based on iterative reduction of separate mode clusters is proposed. On a number of example problems the new method shows best results. A new method for exact matching of the steady state response has been introduced, that can be applied to all truncation-based reduction methods such as modal and balanced reduction.

9 References

Argyris, J., and H-P. Mlejnek, (1991). *Dynamics of structures.* vol.5 in 'Texts on Computational Mechanics', North-Holland, Amsterdam.

Balas, M., (1982). Trends in large space structure control theory: fondest hopes, wildest dreams. *IEEE Trans. Automat. Contr.*, vol.AC-27, no.3, 522–535.

Bathe, K-J., (1982). *Finite element procedures in engineering analysis.* Prentice-Hall.

Bernstein, D.S., and D.C, Hyland, (1988). Optimal pro
fied theory of reduced-order, robust control design. *Large Space Structures (Eds Atluri, Amos),* Springer-Verlag, 263–302.

Enns, D.F. (1984). Model reduction with balanced realization: an error bound and a frequency weighted generalization. *Proc. 23rd IEEE Conf. Dec. & Contr.,* 127–132.

Glover, K. (1984). All optimal Hankel-norm approximations of linear multivariable systems and their L_∞-error bounds. *Int. J. Contr.*, vol. 39, 1115–1193.

Golub, G.H., and C.F. van Loan, (1989). *Matrix computations,* 2nd edition, The Johns Hopkins University Press, Baltimore.

Gregory C.Z. Jr., (1984). Reduction of large flexible spacecraft models using internal balancing theory. *AIAA Journal of Guidance, Control and Dynamics,* vol.7, 725–732.

Hakvoort, R.G. (1993). Frequency domain curve fitting with maximum amplitude criterion and guaranteed stability, *Proc. 2nd-European Control Conference,* 252–257.

Hung, Y.S. and M.A. Muzlifah, (1990). Hankel-Norm Model Reduction with Fixed Modes, *IEEE Tr. Automat. Contr.*, vol.35, 373–377.

Moore B.C. (1981). Principal component analysis in linear systems: controllability, observability, and model reduction, *IEEE Trans. Automat. Contr.*, AC-26, 17–32.

Skelton, R.E. (1988). *Dynamic Systems Control,* New York: John Wiley & Sons.

Villemagne, C. de, and R. E. Skelton, (1987). Model reductions using a projection formulation, *Int. J. Control,* vol.46, 2141–2169.

Wortelboer P.M.R., (1994). *Frequency-weighted balanced reduction of closed-loop mechanical servo-systems: theory and tools,* Dr. Dissertation, Delft University of Technology, 1994.

Selected Topics in Identification, Modelling and Control
Vol. 6, December 1993

Control of a series-resonant converter with a new topology and a reduced number of thyristors

Henk Huisman

Mechanical Engineering Systems and Control Group
Delft University of Technology, Mekelweg 2, 2628 CD Delft, The Netherlands.

Abstract. Multiphase series-resonant (SR) power converters provide a flexible way to transform power between a utility grid and a multiphase load or source. The current implementations all suffer from a high component count, which makes the use of these converters unattractive from an economical point of view.
A new topology for multiphase SR converters has been proposed in De Beer, 1991 in a simulation context. This topology uses half the number of power semiconductors compared to the existing multiphase SR converters.
The present paper addresses the implementation of the new topology in a prototype converter. Simulation data and measured waveforms are shown, and a comparison is made between the new and the existing topologies. It is shown that the reduction in component count is offset by a lower power rating.

Keywords. Power electronics; Control systems; inverters; series resonant converters; three-phase; AC-to-AC power converter; reversible power flow; thyristors; reactive power generation

1 Introduction

Series-resonant (SR) techniques have been used for a long time to attain low switching losses in DC-DC power converters. The low switching losses make it possible to use high switching frequencies while keeping, at the same time, the conversion efficiency high.

During the last decade the use of series-resonant (SR) techniques has spread out into the field of multiphase applications (Schwarz,1979; Huisman,1985;1988b;1992). The converters which have been presented in the literature feature several interesting properties, including:

- Smooth input- and output voltages and -currents,
- adjustable power factor at the input of the converter, including unity,
- absence of low-frequency filters, thus reducing weight,
- common grounds for inputs and outputs, thus reducing high-frequency interference, and facilitating 'clean' measurements,
- easy parallel operation of multiple modules, and
- expandability to any number of inputs or outputs.

In these applications one resonant L-C tank is time-shared between the input- and output terminals of the converter. The topology of the power circuit which is often used makes it necessary to connect both sides of the resonant tank to the terminals of the converter. For AC operation, we need to achieve current flow in two directions, and therefore the number of semiconductor switches needed for multiphase AC applications equals four times the total number of terminals. For a three-phase to

three-phase converter 24 switches would be needed. Clearly, this number compares badly to the number of active devices which is needed to build a PWM bridge.

In this paper we will present a modified multiphase series-resonant converter topology, in which only one side of the resonant circuit can, by means of a switch matrix, be connected to the input- and output terminals of the converter. The other side of the resonant tank is connected to a common neutral. The number of active semiconductors (SCR thyristors in our case) in this topology reduces to 12, which clearly is an advantage as compared to the 24-thyristor alternative.

In section 2 we will introduce both the 'classic' and the 'new' power circuit topology. The following section discusses the intended operation of the new circuit. The resonant circuit is grounded at one side. It is shown that this topology severely restricts the freedom to choose active terminals. This topic is further dealt with in section 4.

Before committing our ideas to hardware, a simulation was set up. In section 5 the simulated converter is shown to be running smoothly. Section 6 shows measurement results of a prototype converter.

2 Circuit topologies

The 'new' circuit topology can be thought to be derived from the 'classic' topology which has been presented in (Huisman,1988a;1988b). Simplified schematics of both the 'old' and the new power circuit topology have been depicted in figure 1.

In figure 1 every switch represents the combination of two antiparallel thyristors and their snubber circuits. The operation of the circuit in figure 1a has been verified in (Huisman,1987;1988a;1988b;1992). A slightly different version of the circuit in figure 1b has been presented in a simulation context in (De Beer,1991).

The symmetry of the circuits in both figures 1a and 1b gives rise to two classes of power converters with these two basic topologies. Table 1 gives an indication of possible applications of converters for different numbers of terminals.

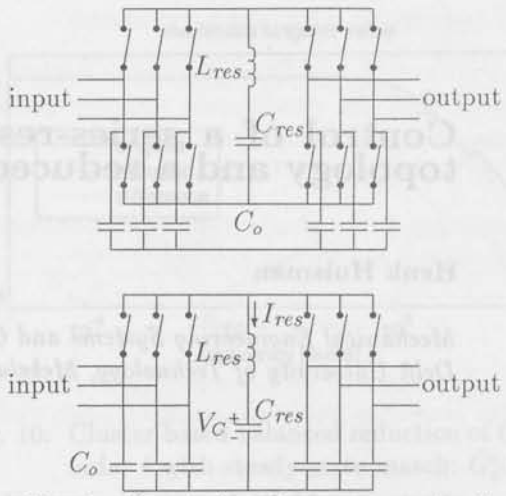

Fig. 1: Topologies of two power circuits
a: (left) The 'old' circuit
b: (right) The new circuit

3 Operation during one resonant pulse

3.1 State-plane description

The operation of the power circuit of figure 1b is most easily demonstrated starting from the situation where the voltage across the resonant capacitor (V_C) is at its maximum value. We will assume that the magnitude of this peak capacitor voltage is larger than any of the input- or output voltages. Furthermore we will assume that the value of the filter capacitors (C_o) is much larger than the value of C_{res}, which implies that the source and load of the converter can be modeled as ideal voltage sources.

Current flow in the circuit starts with the closing of one of the six switches. With the assumptions above, the direction of the resonant current is dictated by the sign of V_C, i.e. I_{res} will become positive if V_C was negative and vice versa. For brevity, we will only consider the case of a negative initial value for V_C in the following. The case for positive V_C can be treated in a completely analogous way.

Without further intervention, the resonant current I_{res} will develop as a positive sinewave. At the moment this current becomes zero again, the thyristor switch will turn off, and V_C will have been mirrored in the voltage of the terminal whose switch has been closed.

Figures 2 a) and b) show the development of the resonant current (I_{res}) and capacitor voltage (V_C) against time. When these two variables are plotted against each other in the so-called state-plane

N	applications
3	One-phase DC-DC converter (see Tilgenkamp(87))
	Three-phase reactive power controller (see Melse(88))
4	idem with starpoint connection
	DC-DC to DC/DC converter
5	Three-phase to DC (+/-) converter or vice-versa
6	Three-phase to three-phase converter
7	idem with neutral connection
9	Three-phase in, three-phase out uninterruptible power supply with $+/-/0$ battery connection

Table 1: Applications of SR converters for a number N of terminals

(Oruganti,1985) the trajectory shows up as an ellipse, or, with proper scaling, as a circle. This circle has been depicted in fig. 2c. The centre of this circle is located at (V_{LC},0), where V_{LC} indicates the voltage applied to the resonant circuit. Geometrically the "mirroring" of the capacitor voltage in V_{LC} is quite obvious.

3.2 Energy considerations

For continuous operation of a multiphase resonant converter, it has been argued in (Huisman,1987) that V_C should be exactly inverted after every resonant half cycle. In this way it is guaranteed that the initial conditions for the next resonant half cycle are (apart from a trivial inversion) identical to those of the cycle which has just been finished.

If the capacitor voltage is exactly inverted after every resonant half cycle, the net energy supplied to the resonant circuit needs to be zero. This implies that we need to apply two voltages of opposite polarity in sequence to the resonant circuit. The reader may want to compare this need to the situation in the well-known buck-boost converter, where two voltage polarities are used to constrain the energy in the main inductance.

The moment of turnover (t_1) from the 'first' to the 'second' terminal voltage serves to control the final value of V_C. If the two terminal voltages involved satisfy some auxiliary constraints, the reachable range for V_C at $I_{res} = 0$ includes the inverse of the initial value of V_C. Figure 3 shows the influence of a varying moment of turnover from the

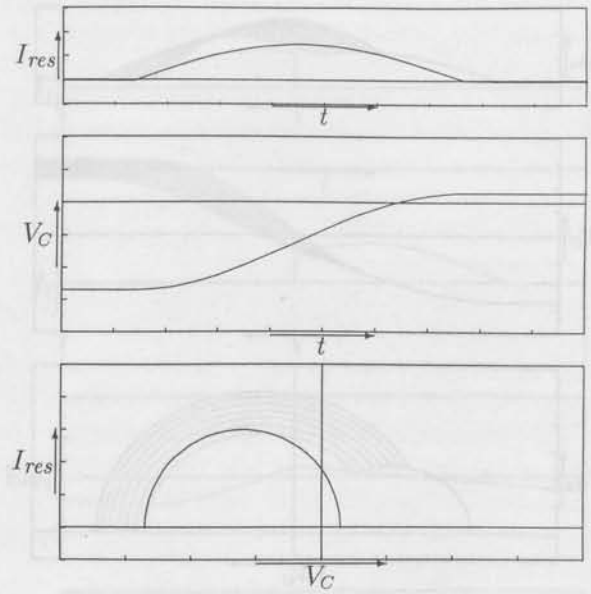

Fig. 2: Signal shapes for one resonant sine wave
a: (left) I_{res}: Current through L_{res}
b: (middle) V_C: Voltage across C_{res}
c: (right) I_{res} vs. V_C

first to the second current segment on the shape of the resonant current (fig. 3a) and on the capacitor voltage (fig. 3b). The state-plane portrait of the operation of the converter for this case has been drawn in figure 3c.

The trajectories in fig. 3c are each composed of two circle segments. The first circle is centred around the first voltage (V_{LC1}) applied to the resonant tank, and the second segment is centred around V_{LC2}. If the values for V_{C0}, V_{C2}, V_{LC1}, and V_{LC2} are supplied, the construction of the trajectory is straightforward. Clearly, the proper moment for turnover is indicated by the intersection of the two circles.

3.3 Predictor circuit

For the real-time control of the peak capacitor voltage (V_{C2}) we need to determine the instant in time where the two circles of the state plane trajectory intersect. In this converter we have used the following method.

The value of the capacitor voltage at the instant of turnover (V_{C1}) can be derived analytically from the equations describing the circuit behaviour. Skipping the derivation, which can be found in

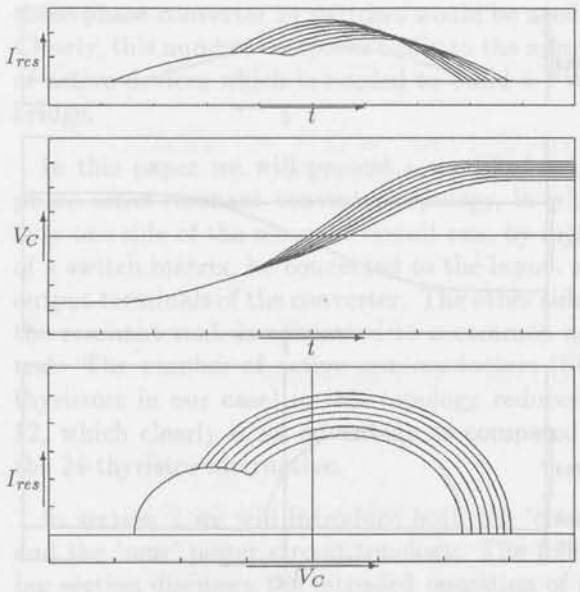

Fig. 3: Signal shapes for a resonant sine wave composed of two current segments for varying turnover time t_1
a: (left) I_{res}: Current through L_{res}
b: (middle) V_C: Voltage across C_{res}
c: (right) I_{res} vs. V_C

(Huisman,1992), this value is given by:

$$V_{C1} = \frac{V_{C2}(V_{C2} - 2V_{LC2}) - V_{C0}(V_{C0} - 2V_{LC1})}{2(V_{LC1} - V_{LC2})} \quad (1)$$

where V_{C0} equals the initial value of the capacitor voltage, and V_{LC1} and V_{LC2} indicate the voltages applied to the resonant circuit during the first and second current segment, respectively. Note that if no disturbances are present, then

$$V_{C0} + V_{C2} = 0 \quad (2)$$

which simplifies equation 1 somewhat. However, we have used the complete equation for our control setup.

The value of V_{C1} in equation 1 can be computed in real-time, and compared to the actual (measured) value of the capacitor voltage. As soon as the latter crosses the value of V_{C1}, the turnover to the second current segment is initiated.

3.4 Commutation

For the duration of one resonant half cycle, the active part of the circuit of figure 1b can be drawn as in figure 4. For convenience, in figure 4 the

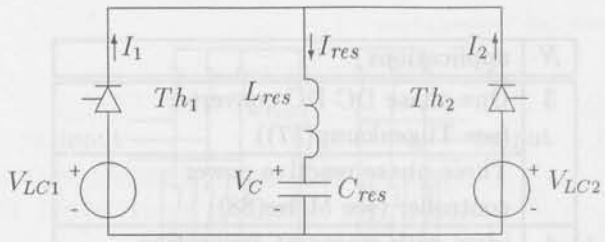

Fig. 4: The part of the power circuit of figure 1 which is active during one resonant half cycle

first voltage (V_{LC1}) applied to the resonant circuit has been drawn at the left, and the second voltage (V_{LC2}) at the right. However, these voltages can correspond to *any* of the terminals (input or output) in figure 1b.

If SCR thyristors are used for the power semiconductors, the sequence of voltages applied to the resonant circuit is subject to the laws which govern the commutation of current from one thyristor (Th_1 in figure 4) to the other (Th_2). Inspection of the circuit shows that if I_{res} is positive, V_{LC2} needs to be more positive than V_{LC1}, in order to be able to turn off Th_1.

An example of the currents in the circuit branches of figure 4 has been depicted in figure 5.

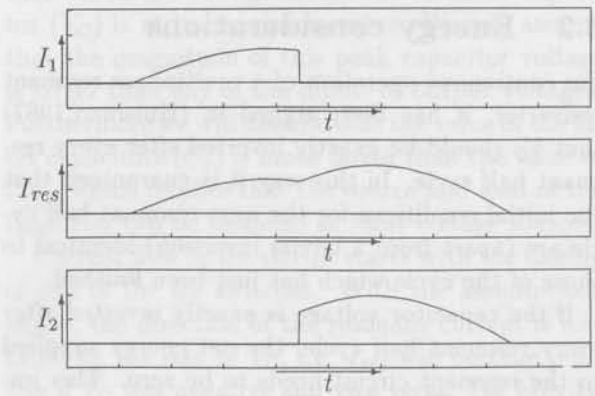

Fig. 5: Currents in the branches of figure 4

The currents in the two voltage sources show infinitely steep transients at the instant of turnover. For physical thyristors, these steep current slopes would lead to high turn-on and turn-off losses. Also, high levels of EMI (electromagnetic interference) may be expected. Therefore, in the real circuit commutation inductances are placed in series with the thyristors in order to smoothen the current transients somewhat. It needs to be noted that

these inductances have not been incorporated in the circuit model on which the predictor operation has been based. As a consequence, deviations in the peak capacitor voltage can occur.

3.5 Current control

The signals in figure 5 show that the currents in both voltage sources (with the sign conventions of figure 4) flow in the same direction as I_{res}. Clearly, during the next resonant half cycle I_{res} will flow in the opposite direction. This implies that at least two (other) terminals should be available which can handle this direction of current flow. We will come back to that matter in the following section.

Figure 5 shows that a finite amount of charge has been transported to two out of the six terminals of the converter. For the next current pulse other terminals can be chosen, which implies that in time every terminal can be supplied with the desired amount of charge. A control loop is needed to adjust the charge transfer process in order to arrive at the desired current flow in every terminal.

The control system which we have used consists of a modified ASDTIC controller (Schwarz,1969; Huisman,1985) for every terminal of the power circuit. In this controller, every terminal is associated with an ASDTIC error signal which is defined as follows:

$$\mathrm{Err} = \int (i - i_{ref})dt \qquad (3)$$

The sum of the rectified ASDTIC errors, which can be interpreted as an overall error signal, is used to trigger the generation of a new current pulse.

Some signals in the modified ASDTIC control system have been shown in figure 6. The upper traces show the currents in the two voltage sources of fig. 4. The lower traces show the corresponding ASDTIC error signals. The figure shows that due to the displaced charge of the current pulse the two ASDTIC signals are restored to a position closer to zero.

4 Selection of terminals

The flow of current in the resonant circuit is initiated when the overall error signal, composed from the individual terminal error signals, crosses a certain bound. However, in *which* terminals the current is going to flow is still to be decided. From the previous discussion two items are of special importance here:

- The currents in both terminals which will be serviced during this particular resonant current pulse will flow in the same direction as the resonant current, and
- In order to be able to keep the peak capacitor voltage at a predictable level, the voltages on these two terminals need to oppose each other.

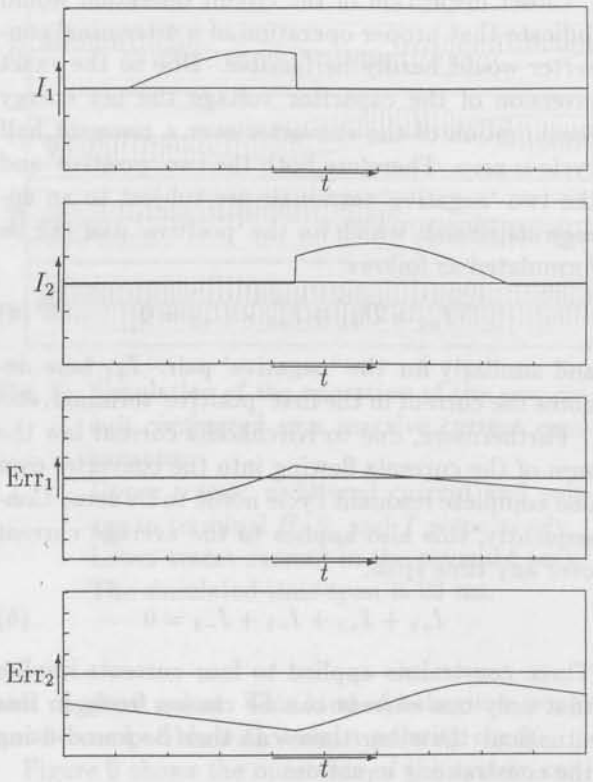

Fig. 6: Signals in the control system

Of course, the charge transported by a resonant current pulse needs to be used to lower the overall error signal. Therefore a selection of terminals according to the sign and magnitude of their individual error signals is appropriate.

4.1 Strict polarity check

For the situation depicted in figure 6, it obviously would be wise to service those terminals with the most negative error signal first.

If we were to adhere strictly to this polarity criterion, the minimum number of terminals for a converter would appear to be 4. Two out of these terminals would operate with positive current flow, and be serviced during the positive resonant half cycles, and the other two would be serviced during the negative half cycles.

Closer inspection of the circuit operation would indicate that proper operation of a 4-terminal converter would hardly be feasible. Due to the exact inversion of the capacitor voltage the net energy consumption of the converter over a resonant half cycle is zero. Therefore both the two 'positive' and the two 'negative' terminals are subject to an energy constraint, which for the 'positive' pair can be formulated as follows:

$$I_{+1} \times U_{+1} + I_{+2} \times U_{+2} = 0 \qquad (4)$$

and similarly for the 'negative' pair. I_{+1} here denotes the current in the first 'positive' terminal, etc.

Furthermore, due to Kirchhoff's current law the sum of the currents flowing into the converter over one complete resonant cycle needs to be zero. Consequently, this also applies to the average current over any time span:

$$I_{+1} + I_{+2} + I_{-1} + I_{-2} = 0 \qquad (5)$$

Three constraints applied to four currents implies that only one current can be chosen freely in this situation: the other three can then be found using the constraining equations.

In the (more interesting) case of a three-phase to three-phase converter, we would expect to have three degrees of freedom (six terminals - three constraints). These three degrees can be used to select the wave shapes of the three output currents, the input currents would then be defined by the constraints. It follows that in this situation we are not able to select the shape of the input currents: the system has too many constraints to achieve this. This conclusion was confirmed by a simulation of this system: although the output currents conformed reasonably well to their prescribed (sine) wave shapes, the input currents showed a ragged appearance. The reader may want to compare this result with the simulation data given in (De Beer,1991, fig. 7).

4.2 Loose polarity check

Inspection of the operation of the simulated converter revealed that as a consequence of the strict polarity check the control system spent a large percentage of time waiting for one of the terminal voltages or -current references to pass through zero. For the controller with a strict polarity check, a signal being at +1 or -1mV makes a large difference. However, a human observer would interpret both values to be 'close to zero'.

Trying to mimic this observation in the control system, it was decided to loosen the polarity check. For example, for a positive half wave of the resonant current, we would first select the terminal with the most negative or least positive error signal. Then, on the remaining terminals with opposite polarity of the voltage, we would again perform a similar selection. In some instances this schedule could for example lead to positive current flow in a terminal with an already positive error signal, thus in fact worsening the situation for this individual terminal. However, for the complete converter system the total error is still lowered. Contrary to the setup with a strict polarity check, the operation of the complete system does not stall any more because we might for example have only one terminal with positive current flow. Simulation of this setup showed superior performance. It was even shown to be possible to operate a three-terminal converter in this way.

4.3 Algorithm

Similarly to the system which has been discussed in (Huisman,1992), we have used a sequential two-pass selection circuit here. During the *first pass*, the terminal with the most positive (least negative) or most negative (least positive) error signal, depending on the direction of the resonant current (polarity of V_C), is selected. The *second pass* is used to select a second terminal from the remaining terminals with an opposing voltage.

After the selection process, the thyristor which is going to conduct during the first current segment can be fired. Turnover to the second current segment is initiated when the Vcpeak-predictor circuit indicates that the cross-over point between the two trajectories of figure 3 has been reached. The second current segment is terminated when the resonant current again reaches zero. After an appropriate turn-off time, the circuit is ready for the next current pulse.

5 Simulation

In order to test the intended operation of the power circuit and its control, a simulation needed to be set up. Due to the similarity of the 'new' circuit to its 'old' counterpart, it was decided to re-use the software which had been written for that circuit (Huisman,1992). It was found that only minor modifications were needed in the analog sections of the simulation. However, the new selection algorithm made it necessary to reprogram the digital part of the circuit.

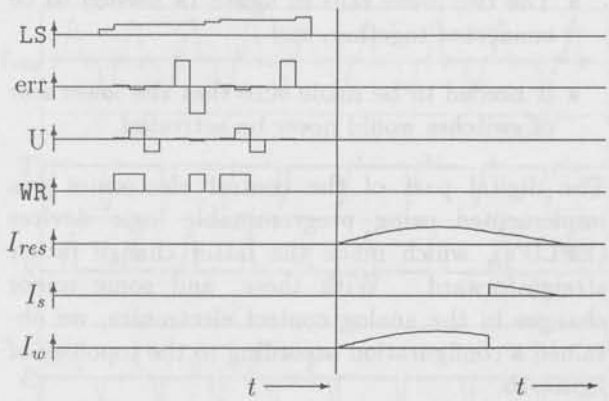

Fig. 7: Simulated operation of the terminal selector and start of current flow.

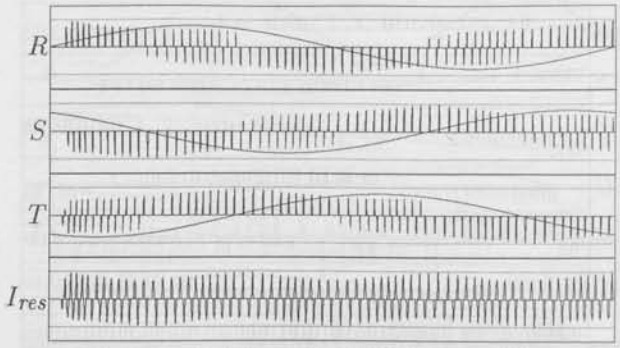

Fig. 8: Simulation of the operation of the new circuit configured as a reactive current compensator.
Upper traces: unfiltered current and voltage in terminal R, S, and T respectively,
Lower trace: current in the resonant tank.
The simulated time span is 20 ms.

Figure 7 shows the algorithm for the terminal selection doing its job. For clarity, the left-hand part of the figure is plotted with a stretched time scale. During a first pass, indicated by the second step on the staircase-like signal LS, all six terminals (R,S,T,U,V,W) are checked in order to find the one with the worst error signal. The signal WR indicates whether a terminal has been temporarily selected. The last terminal for which signal WR is high, is included in the final selection. In the figure, this is terminal W. Also, during the first pass, the sign of the voltage on the selected terminal is stored for use during the second pass.

In the second pass, indicated by the fourth step on signal LS, the remaining five terminals are checked for the proper polarity of their voltages. If more candidates are available, the one with (again) the worst error signal is taken. Figure 7 shows that finally terminal S remains selected in this pass.

The right-hand part of figure 7 shows the development in time of the currents in the resonant circuit and in two of the six terminals of the power circuit on a much longer time scale. The current flow is initiated in terminal W, because during the first current segment energy needs to be transported out of the converter.

On a much larger time scale, the operation of the circuit starting at zero initial conditions has been depicted in figure 8. In figure 8, the converter is configured as a three-phase reactive current compensator. The upper traces show the current pulses flowing in the three input terminals and the associated voltages. The current pulses show a typical 90 deg. phase shift when compared to the corresponding voltage.

Figure 8 shows that around the 'zero crossings' the currents are composed of alternating positive and negative pulses. This kind of behaviour would not be compatible with a strict polarity check.

Figure 9 shows the operation of the system configured as a three-phase to three-phase converter. The simulated input frequency is 35 Hz, the frequency of the output voltages is 50 Hz. The traces in figure 9 show the division of resonant current pulses over the input (R, S, T) and output (U, V, W) terminals. Due to the larger number of degrees of freedom, the alternating pulse pattern which was shown in figure 8 is practically absent here.

In the simulation, the converter is loaded with 3 resistors of 75Ω in a star configuration. Through simulation experiments it was found that this is approximately the maximum resistive load which can be powered for this configuration. At a rated line voltage of 380 V (rms), this corresponds to an output power P of:

$$P = \frac{380^2}{75} = 1925W. \qquad (6)$$

It is interesting to note that the 'old' power circuit configuration (see figure 1a) was able to power a threefold load (25Ω in star, see (Huisman,1992)). The main reason for this difference is rooted in the fact that in the new power circuit only one side of the resonant tank is used to supply current to the terminals. Another reason lies in the handling of reactive output power. The old power circuit was able to transfer power between two terminals and supply current to the third in one resonant half cycle. The new circuit needs a complete resonant cycle to accomplish the same.

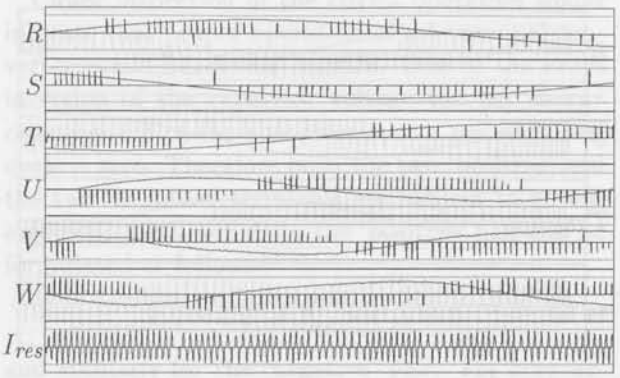

Fig. 9: Simulation of the operation of the new circuit configured as a three-phase AC to three-phase AC convertor.
Upper traces: unfiltered current and voltage in terminals R, S, and T (inputs) and U, V, and W (outputs) respectively,
Lower trace: current in the resonant tank.
The simulated time span is 20 ms

6 Measurements

For the experimental verification of the new concept, a prototype converter needed to be constructed. The primary goal of the experiments being to show the operation of the new control system on real hardware, it was decided to recuperate an existing circuit. The prototype circuit therefore does not feature the highest possible efficiency for this configuration, but in our assessment this is not a serious drawback.

Table 2 lists the most important parameters of the prototype circuit.

L_{res}	148 μH
C_{res}	2 μF
C_o	90 μF
L_c	20 μH
thyristors	SKFT60/12DT

Table 2: Parameters of the prototype circuit

As has been discussed in section 3.4, commutation inductances (L_c) were placed in series with the thyristors in order to limit the di/dt values applied to these components. A more thorough description of the power circuit can be found in (Huisman,1992).

In order to convert the old into the new topology, two major changes were called for:

- The two lower rails in figure 1a needed to be connected together, and
- it needed to be made sure that the lower row of switches would never be activated.

The digital part of the control electronics was implemented using programmable logic devices (EPLD's), which made the latter change rather straightforward. With these, and some minor changes in the analog control electronics, we obtained a configuration according to the topology of figure 1b.

6.1 Three-phase operation

Figure 10 shows the operation of the prototype converter configured as a three-phase reactive current compensator.

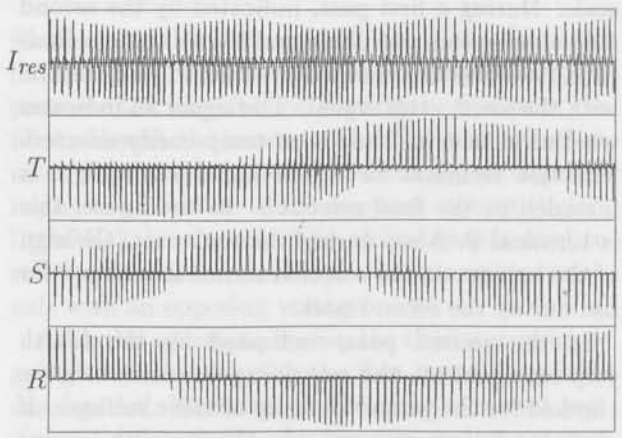

Fig. 10: Currents in the prototype of the new circuit operated as a reactive current compensator
Upper trace: current in the resonant tank.
Lower traces: unfiltered currents in terminal T, S, and R respectively.
The full range of every trace is -52.4 to 52.4 A.
The time scale covers 20 ms.

The measured signals in figure 10 show good agreement to the simulation results in figure 8. Differences lie mainly in fast transient effects, which were not modeled in the simulation which yielded figure 8. Figure 11 shows a detail of figure 10.

The currents in figure 11 show the gradual takeover of alternating current pulses from phase R to phase T. On this stretched time scale, the presence of reverse recovery spikes, which were not

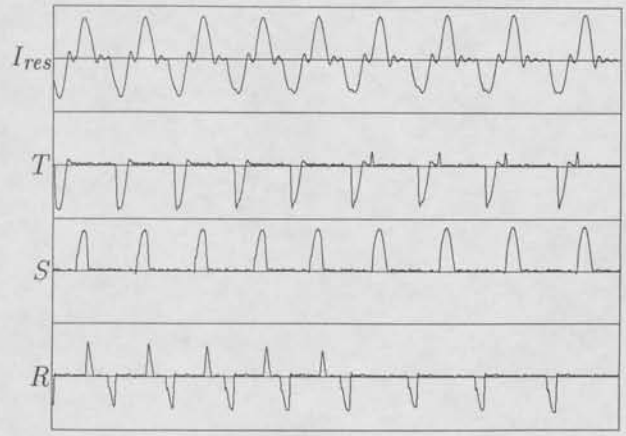

Fig. 11: Traces as in figure 10. The time scale covers 2 ms

included in the simulation model, is visible. Furthermore, it can be seen that, due to the commutation inductances, the slope of the current pulses is limited.

6.2 Three-phase to three-phase operation

Figure 12 depicts the system operating as a three-phase AC to AC converter. The input frequency is 50 Hz, the converter generates an output waveform at 25 Hz.

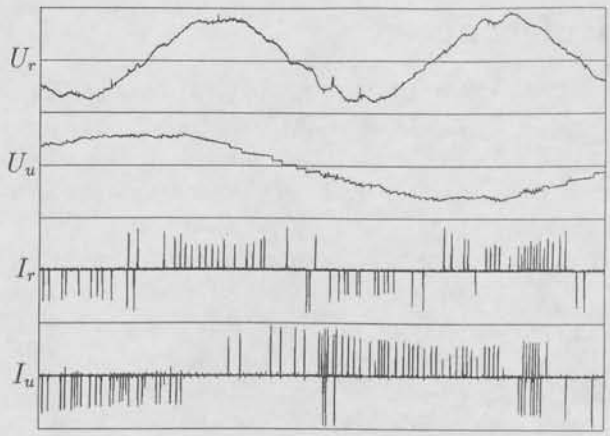

Fig. 12: The prototype of the new circuit operated as a three-phase AC to AC converter.
Traces (from high to low):
U_r: voltage on input terminal R
U_u: voltage on output terminal U
I_r: current through input terminal R (unfiltered)
I_u: current in output terminal U (unfiltered)
The full range of the voltage traces is -240 to 240 V, the current traces range from -52.4 to 52.4 A.
The time scale covers 40 ms.

7 Conclusions

The operation of a prototype of series-resonant converter with a new topology has been presented, both in a simulation context and in a prototype circuit.
The converter is based on a six-phase switch matrix. Half of the matrix is used for the three input terminals, the other half caters to the three outputs. Due to the resonant circuit, commutation of the thyristors in the matrix is guaranteed.
Inputs and outputs of the converter are all capacitively shorted to a common ground. Therefore measurements of input- and output voltages can be performed with relative ease.
The new topology uses only half the number of thyristors compared to older topologies. Therefore the new converter is an attractive candidate for the development of new, flexible power conversion equipment.
The converter topology can be applied as a flexible interface between any two multiphase grids, including DC. In the three-phase to three-phase configuration, the converter is capable to generate or consume reactive power at both input and output ports, including homopolar currents.
The state of the resonant circuit is tightly controlled with a new Vcpeak control circuit. This new controller uses only voltages to determine the instant for switch-over, and is therefore less sensitive to scaling errors than the older circuit, which uses current measurements as well.
The new topology shows a relatively low power handling capacity.

8 Acknowledgements

The author wishes to express his gratitude to Fred de Beer from the Delft Laboratory for Power Electronics for interesting discussions regarding the operation of this new converter, and to the staff of the Laboratory for Electrical Machinery and Power Electronics of Eindhoven University for the possibility to perform measurements.

References

F. de Beer, J.B. Klaassens, and G. Moekoet (1991). Novel Three-phase AC-AC Soft-Switching Series-Resonant Converter Topology with Six Switches. In *Proceedings of Intelec-91, Kyoto, Japan*, pages 587–594.

H. Huisman and S.W.H. de Haan (1985). A DC to 3-phase series-resonant converter with low harmonic distortion. *IEEE Transactions on Industrial Electronics, vol.IE-32, no.2*, pages 142–149.

H. Huisman and S.W.H. de Haan (1987). General control method for high-frequency multiphase power converters. In *Proceedings of Power Conversion International (Munich)*, pages 201–219.

H. Huisman (1988a). A three-phase to three-phase series-resonant power converter with optimal input current waveforms. Part I: control strategy. *IEEE Transactions on industrial electronics, vol. 35, no. 2*, pages 263–268.

H. Huisman (1988b). A three-phase to three-phase series-resonant power converter with optimal input current waveforms. Part II: implementation and results. *IEEE Transactions on industrial electronics, vol. 35, no.2*, pages 269–277.

H. Huisman (1992). *Design and Control of A Class of Multiphase Series-Resonant Power Converters.* PhD thesis, Delft University of Technology, Lab. for Measurement and Control.

A.L. Melse and S.W.H. de Haan (1988). Reactive power handling with series-resonant converters. *IEEE Transactions on Power Electronics, vol.3, no.1*, pages 17–25.

R. Oruganti and F.C. Lee (1985). Resonant power processors. I. State plane analysis. *IEEE Transactions on Industry Applications vol.IA-21, no.6*, pages 1453–1460.

F.C. Schwarz and W.L. Moïze de Chateleux (1979). A Multikilowatt Polyphase AC/DC Converter with Reversible Power Flow and Without Passive Low Frequency Filters. In *Proceedings of Power Electronics Specialists Conference, San Diego*, pages 448–458.

F.C. Schwarz (1969). Engineering information on an Analog Signal to Discrete Time Interval Converter (ASDTIC). *NASA Report CR-134544.*

N.V. Tilgenkamp, S.W.H. de Haan, and H. Huisman (1987). A Novel Series-Resonant Converter Topology. *IEEE Transactions on industrial electronics, vol.IE-34, no.2*, pages 240–246.

CONTENTS Volume 6, December 1993

TU Delft
Delft University of Technology